

**NON-CANONICAL ENZYMES INVOLVED IN CUTICULAR WAX BIOSYNTHESIS:
WEAVING THE COAT OF ARABIDOPSIS AND CEREAL SHOOTS**

by

Yulin Sun

B.Sc., Northwest A&F University, 2012

M.Sc., Northwest A&F University, 2015

A THESIS SUBMITTED IN PARTIAL FULFILLMENT OF
THE REQUIREMENTS FOR THE DEGREE OF

DOCTOR OF PHILOSOPHY

in

THE FACULTY OF GRADUATE AND POSTDOCTORAL STUDIES
(BOTANY)

THE UNIVERSITY OF BRITISH COLUMBIA
(Vancouver)

September 2021

© Yulin Sun, 2021

The following individuals certify that they have read, and recommend to the Faculty of Graduate and Postdoctoral Studies for acceptance, the dissertation entitled:

Non-canonical enzymes involved in cuticular wax biosynthesis: weaving the coat of Arabidopsis and cereal shoots

submitted by Yulin Sun in partial fulfillment of the requirements for

the degree of Doctor of Philosophy

in Botany

Examining Committee:

Dr. Reinhard Jetter, Botany, Chemistry, UBC

Supervisor

Dr. Lacey Samuels, Botany, UBC

Supervisory Committee Member

Dr. Simone Castellarin, Land and Food Systems, UBC

University Examiner

Dr. Katherine Ryan, Chemistry, UBC

University Examiner

Additional Supervisory Committee Members:

Dr. Abel Rosado, Botany, UBC

Supervisory Committee Member

Dr. Jörg Bohlmann, Botany, UBC

Supervisory Committee Member

Abstract

Plant cuticles play important roles in plant development, fertility, and adaptation. The cuticular waxes directly facing the environment are made mainly from derivatives of very-long-chain (VLC) aliphatics. Previous studies on cuticular waxes clarified the biosynthesis of ubiquitous wax components based on the model plant *Arabidopsis thaliana*. However, the biosynthesis and chemical structures of numerous uncommon wax components from different plant species are still unclear.

In my Ph.D. studies, I focused on wax components from both *Arabidopsis thaliana* and Poaceae crop species to identify new enzymes involved in plant cuticular wax biosynthesis and further characterize their biochemical functions.

In chapter 2, I investigated alkane biosynthesis in bread wheat. The linkage of alkane content and transcriptome data revealed a candidate gene, *TaCER1-1A*. The phenotype of corresponding nullisomic-tetrasomic substitution wheat lines and heterologous expression of *TaCER1-1A* in rice and *Arabidopsis* confirmed its function in alkane synthesis.

In chapter 3, the products associated with β -diketones in barley were profiled. New diketone homologs, the 2-alkanol ester profile and the ^{13}C isotope abundance of different wax components indicated the unique biosynthesis pathway to β -diketones. The biochemical functions of the core enzymes on this pathway, DIKETONE METABOLISM HYDROLASE (DMH) and DIKETONE METABOLISM POLYKETIDE SYNTHASE (DMP), were investigated. *In vivo* and *in vitro* assays showed the direct condensation between 3-ketoacid and fatty acyl-CoA catalyzed by DMP, thus revealing the unique character of DMP as a PKS family member and revised the model of the β -diketone synthesis pathway in barley.

In chapter 4, VLC alkenes from *Arabidopsis* young leaves were analyzed. Different from other plant species, alkenes ranging from C₃₃ to C₃₉ with predominance of 7- and 9- isomers were found in *Arabidopsis*. An acyl-CoA desaturase family member, ADS4.2, was shown to influence alkene formation. ADS4.2 was strongly expressed in young rosette leaves, especially in trichomes, and yeast expression revealed that this enzyme had ω -7 regio-specificity with high preference for acyl-CoAs longer than C₃₂. Wax-synthesis-deficient mutants were used to put the alkene-forming pathway in context with the wax synthesis. The results show that *Arabidopsis* produces characteristic alkenes through a unique elongation-desaturation pathway with the participation of ADS4.2.

Lay Summary

The above-ground organs of plants are coated by a hydrophobic layer of cuticular waxes. As the outermost layer of the plant tissue, they influence plant development, fertility, and responses to various biotic and abiotic stresses. Cuticular waxes are mixtures of compounds characteristic of each species and organ. The studies in this dissertation focused on the formation of several important wax components, including the alkanes lining wheat surfaces, the alkenes accumulating on *Arabidopsis* leaves, and the β -diketones characteristic of barley stems and spikes. This research unraveled the non-canonical enzymes responsible for formation of respective wax compounds and identified the unusual biochemical functions of these enzymes. Overall, these results enabled a fundamental revision of the mechanisms involved in forming the investigated wax components. These findings may facilitate future crop breeding to improve of plant drought tolerance through cuticle engineering.

Preface

A version of Chapter 2 has been published as a research article: Li T, Sun Y, Liu T, Wu H, An P, Shui Z, Wang J, Zhu Y, Li C, Wang Y, Jetter R, Wang Z (2019) *TaCER1-1A* is involved in cuticular wax alkane biosynthesis in hexaploid wheat and responds to plant abiotic stresses. *Plant, cell and environment* **42**: 3077-3091. Tingting Li, Yulin Sun, Chunlian Li, Yong Wang, Reinhard Jetter and Zhonghua Wang designed the experiments. Tingting Li and Yulin Sun constructed all the plasmids used in this research; Yulin Sun performed wheat organ cuticular wax profiling, wax crystal SEM, wheat nullisomic-tetrasomic substitution line wax analyses, Arabidopsis wild-type, *cer1* mutant overexpression and corresponding wax analyses; Tingting Li performed wax analyses of rice overexpression lines, drought experiments on Arabidopsis and rice overexpression lines, and drought experiments as well as cuticle integrity assays on wheat. Tianxiang Liu, Hongqi Wu, Peipei An, Zhijie Shui, Jiahuan Wang, Yidan Zhu provided assistance in this research. Tingting Li, Yulin Sun, Reinhard Jetter and Zhonghua Wang analyzed the data. Tingting Li and Yulin Sun made the figures and wrote the manuscript. Reinhard Jetter and Zhonghua Wang edited the manuscript.

A version of Chapter 3 will be submitted as a research article for peer review. Yulin Sun, Alberto Ruiz Orduna and Reinhard Jetter designed the experiments. Alberto Ruiz Orduna performed barley wax analysis and substrates chemical synthesis. Sarah J. Feakins performed the isotopic analysis on purified wax compounds. Yulin Sun constructed the plasmids used in this study, performed epicuticular wax SEM, barley mutant wax analysis, *E. coli* and yeast expression, protein purification, subcellular localization assays. Yulin Sun and Alberto Ruiz Orduna performed *in vivo* and *in vitro* assays and product analyses. Yulin Sun, Alberto Ruiz Orduna and Reinhard Jetter analyzed the data and made the figures. Yulin Sun and Alberto Ruiz Orduna

drafted parts of the manuscript (Abstract, Introduction, Methods, Results) and Reinhard Jetter edited these sections and wrote the Discussion.

A version of Chapter 4 has been published as a research article: Sun Y, Hegebarth D, Jetter R (2021) Acyl-CoA desaturase ADS4. 2 is involved in formation of characteristic wax alkenes in young *Arabidopsis* leaves. *Plant Physiology*. Yulin Sun, Daniela Hegebarth and Reinhard Jetter designed the experiments. Daniela Hegebarth performed the alkene analysis based on OsO₄-derivatization and wax-deficient mutant wax analyses. All other experiments were performed by Yulin Sun. Daniela Hegebarth analyzed the OsO₄-reaction based alkene profile and mutant wax data and made the corresponding figures. Yulin Sun, and Reinhard Jetter analyzed the rest of the data and made the figures. Yulin Sun wrote a draft of the manuscript which Reinhard Jetter edited.

Table of Contents

Abstract.....	iii
Lay Summary	v
Preface.....	v
Table of Contents	viii
List of Tables	xiv
List of Figures.....	xv
List of Abbreviations	xviii
Acknowledgements	xxiii
Dedication	xxiv
Chapter 1 : Introduction	1
1.1 The structure of cuticle.....	1
1.2 Biological functions of cuticle	2
1.2.1 Plant development	2
1.2.2 Plant reproduction	3
1.2.3 Plant adaptation	3
1.3 The ubiquitous wax components in land plants	5
1.3.1 Chemistry of ubiquitous wax components	5
1.3.2 The biosynthesis of ubiquitous wax composition	6
1.4 The specialty wax components in land plants.....	12
1.4.1 The chemistry of specialty wax components	12
1.4.2 The synthesis of specialty components.	14

1.5 The diversity of cuticular waxes in land plants.....	20
1.6 Objectives of the current study	21
Chapter 2 : Identification of the core enzyme involved in alkane biosynthesis in bread	
wheat	24
2.1 Introduction	24
2.2 MATERIALS AND METHODS	26
2.2.1 Plant materials and growth conditions	27
2.2.2 Isolation of <i>TaCER1-1A</i> gene from wheat	28
2.2.3 Sequence alignment and phylogenetic analysis	29
2.2.4 Cuticular wax extraction and chemical analysis	29
2.2.5 Scanning electron microscopy analysis.....	30
2.2.6 Overexpression of <i>TaCER1-1A</i> in rice (<i>Oryza sativa</i> L. ssp. japonica cv. Zhonghua11)	30
2.2.7 Overexpression of <i>TaCER1-1A</i> in Arabidopsis	31
2.2.8 Subcellular localization of TaCER1-1A in Arabidopsis mesophyll protoplasts	31
2.2.9 Analysis of transcript levels by qRT-PCR	31
2.2.10 Epidermal permeability analysis	32
2.3 Results	32
2.3.1 Identification of a wheat <i>CER1</i> candidate gene	33
2.3.2 Spatial expression pattern of <i>TaCER1-1A</i>	40
2.3.3 Functional characterization of <i>TaCER1-1A</i>	41

2.3.4 Testing the role of <i>TaCER1-1A</i> in stress resistance	48
2.4 DISCUSSION	56
2.4.1 <i>TaCER1-1A</i> is involved in wheat wax alkane biosynthesis	57
2.4.2 Accumulation of cuticular alkanes affects cuticle properties and leads to enhanced drought tolerance	58
2.4.3 Polyploidy of wheat and wax biosynthesis	60
Chapter 3 : Unravelling the biosynthesis of the very-long-chain β-diketones sealing barley (<i>Hordeum vulgare</i>) surfaces: a type III polyketide synthase produces cuticular β-diketones through head-to-head condensation.....	62
3.1 Introduction	62
3.2 Materials and methods	69
3.2.1 Plant materials and growth conditions	69
3.2.2 RNA isolation, reverse transcription, plasmid construction and transformation	70
3.2.3 Chemical synthesis of standards and substrates	72
3.2.4 <i>In vivo</i> assays.....	74
3.2.5 Protein purification and <i>in vitro</i> assay.....	75
3.2.6 Lipid analysis	77
3.2.7 Carbon isotope analysis.....	78
3.2.8 Barley protoplast, tobacco leaf transient expression and microscopy.....	79
3.3 Results	80
3.3.1 Homolog and isomer distributions of β -diketones	80

3.3.2 Homolog and isomer distributions of 2-alkanol ester side products of the β -diketone pathway	84
3.3.3 The core wax elongation enzyme is not required for β -diketone formation	87
3.3.4 Natural carbon isotope abundance in β -diketones and other wax compounds	88
3.3.5 Barley DMH producing a narrow range of intermediates on the β -diketone synthesis pathway	93
3.3.6 Biochemical function of the barley DMP enzyme	96
3.3.7 Chain-length specificity of DMP for fatty acyl-CoA and 3-ketoacid substrates	104
3.3.8 Subcellular compartmentation of the β -diketone-forming enzymes	109
3.4 Discussion	110
3.4.1 β -Diketones are unlikely synthesized through the elongation-decarboxylation pathway	111
3.4.2 The biochemical function and substrate specificity of DMH	114
3.4.3 The non-canonical PKS and the revised model of β -diketone biosynthesis pathway	117
Chapter 4 : The acyl-CoA desaturase ADS4.2 is required in formation of characteristic wax alkenes in young Arabidopsis leaves	123
4.1 Introduction	123
4.2 Materials and methods	128
4.2.1 Plant Material and Growth Conditions.....	129
4.2.2 Expression analysis	129
4.2.3 Plasmid construction and plant transformation	130

4.2.4 GUS histochemical staining	131
4.2.5 Transient expression in tobacco and confocal microscopy	131
4.2.6 Wax analysis	132
4.2.7 Yeast assay and lipid analysis	133
4.2.8 Site-Directed Mutagenesis	134
4.2.9 Sequence alignment and protein structure modeling	135
4.2.10 Phylogenetic analysis	135
4.2.11 Statistical analysis	135
4.2.12 Sequence information.....	136
4.3 Results	136
4.3.1 Arabidopsis wax alkenes have characteristic chain lengths and double bond positions	136
4.3.2 The acyl-CoA desaturase ADS4.2 is involved in the synthesis of the Arabidopsis wax VLC alkenes	141
4.3.3 ADS4.2 prefers the longest available fatty acyls for ω -7 desaturation	153
4.3.4 The ADS4.2 protein resides on the ER	161
4.3.5 The biosynthesis pathway to cuticular alkenes shares enzymes with pathways forming other wax components	162
4.4 Discussion	166
4.4.1 Substrate chain length preferences of the desaturase ADS4.2	166
4.4.2 Position of ADS4.2 on the biosynthetic pathway leading to alkenes.....	168

4.4.3 Role of ADS4.2 in formation of Arabidopsis leaf wax alkenes	170
Chapter 5 : Major findings and future directions	180
5.1 Major findings	180
5.1.1 The alkane biosynthesis in bread wheat	180
5.1.2 The β -diketone biosynthesis in barley	183
5.1.3 The alkene biosynthesis in Arabidopsis	185
5.2 Future directions	188
5.2.1 Specialty wax components and cuticle properties	189
5.2.2 Metabolic gene clusters, their expression regulation and wax biosynthesis	191
5.2.3 Wax composition and plant drought/pathogen resistance	192
5.2.4 The substrate specificity of wax synthesis enzymes	193
References	196

List of Tables

Table 2-1: Primers used in Chapter 2	28
Table 2-2: Cuticular wax compositions and amounts in different organs of wheat cv. W87	34
Table 2-3: Analysis of cis-acting regulatory elements in the <i>TaCER1-1A</i> promoter sequence (2 Kb)	51
Table 3-1. Primers used in Chapter 3.....	71
Table 4-1: Primers used in Chapter 4	130
Table 4-2: The wax analysis of Arabidopsis desaturase-deficient mutants	143
Table 4-3: The wax analysis of Arabidopsis <i>ads4.2</i> deficient mutants	148
Table 4-4: The wax coverages of Arabidopsis <i>ADS4.2</i> rescue plants	149
Table 4-5: Amounts of unsaturated fatty acyls in yeast expressing <i>ADS4.2</i>	155
Table 4-6: The wax analysis of Arabidopsis wax synthesis deficient mutants.....	165

List of Figures

Figure 1-1: Common wax components detected in various plant species	6
Figure 1-2: Biosynthesis of wax components	7
Figure 2-1: Composition of wax alkanes on different organs of wheat cv. W87	35
Figure 2-2: Ultrastructure of epicuticular wax crystals on different organs of wheat cv. W87 ...	36
Figure 2-3: <i>CER1</i> expression profile from different organs of wheat cv. W87.....	37
Figure 2-4: Sequence and phylogenetic position of <i>TaCER1-1A</i>	39
Figure 2-5: TaCER1-1A localized to ER.....	41
Figure 2-6: <i>TaCER1-1A</i> expression profiles and composition of wax alkanes in wheat cv. CS wild type and various nullisomic-tetrasomic lines.....	43
Figure 2-7: Composition of cuticular waxes on Arabidopsis leaves expressing <i>TaCER1-1A</i>	45
Figure 2-8: <i>TaCER1-1A</i> complementation assay in the Arabidopsis <i>cer1</i> mutant	46
Figure 2-9: Composition of cuticular waxes on rice leaves expressing <i>TaCER1-1A</i>	47
Figure 2-10: Surface permeability of rice leaves expressing <i>TaCER1-1A</i>	49
Figure 2-11: Soil water deprivation experiment of Arabidopsis overexpression lines.....	50
Figure 2-12: <i>TaCER1-1A</i> expression patterns under various abiotic stress conditions	55
Figure 2-13: <i>TaCER1-1A</i> expression levels and compositions of waxes on wheat spikes under drought stress	56
Figure 3-1: Proposed β -diketone-forming pathways in barley	67
Figure 3-2: Mass spectra of β -diketone homologs/isomers identified in barley cv. Morex spike and flag leaf sheath waxes	84
Figure 3-3: Chemical characterization of the β -diketones and associated 2-alkanol esters in the wax mixture covering barley cv. Morex spikes	86

Figure 3-4: GC-MS analysis of the TLC fraction containing β -diketones from barley cv. Morex spike wax.	87
Figure 3-5: Predicted building blocks for head-to-head condensation or elongation towards individual β -diketone homologs and isomers	89
Figure 3-6: Wax analysis of a barley mutant deficient in elongation to very-long-chain compounds	91
Figure 3-7: Characterization of the barley Diketone Metabolism Hydrolase (DMH) producing the key intermediates on the β -diketone synthesis pathway	93
Figure 3-8: MS analysis of acyls produced in <i>E. coli</i> expressing barley <i>Diketone Metabolism Hydrolase (DMH)</i>	95
Figure 3- 9: MS analysis of double bond positions in monounsaturated 2-ketones produced in <i>E. coli</i> expressing barley <i>Diketone Metabolism Hydrolase (DMH)</i>	97
Figure 3-10: Characterization of the barley Diketone Metabolism Polyketide synthase (DMP) catalyzing the condensation between 3-ketoacids and acyl-CoAs to β -diketones.....	99
Figure 3-11: GC-MS analysis of deuterium-labeled β -diketone products from yeast <i>in vivo</i> assay	100
Figure 3-12: Assessment of DMP substrate preferences	104
Figure 3- 13: Determination of DMP substrate preferences by <i>in vivo</i> assays.....	106
Figure 3-14: Subcellular localization of DMH and DMP.....	108
Figure 3- 15: Schematic representation of the proposed DMP reaction mechanism.....	110
Figure 4-1: Biosynthesis pathways to VLC unsaturated lipids in plants	127
Figure 4-2: Identification of characteristic alkenes in young Arabidopsis leaves	140

Figure 4-3: Relative abundances of wax alkene regio-isomers quantified by GC-MS analysis of OsO ₄ oxidation products	140
Figure 4-4: Screening of desaturase-deficient Arabidopsis mutants for wax alkene phenotypes	142
Figure 4-5: Analysis of wax mixtures from young leaves of Arabidopsis <i>ads4.2</i> mutant and rescue lines	145
Figure 4-6: ADS4.2-GFP expression levels in <i>ads4.2-1</i> rescue T ₂ plants	147
Figure 4-7: Transcriptome analysis of <i>ADS4.2</i> expression in different organs and cell types of Arabidopsis wild type Col-0 and mutants	151
Figure 4- 8: Expression pattern of ADS4.2 in different Arabidopsis organs.....	153
Figure 4-9: ADS4.2 activity on a broad range of VLC acyl-CoA substrates in yeast	156
Figure 4-10: Mass spectra of DMDS adducts of ω -7 and ω -9 monounsaturated FAMES.....	159
Figure 4-11: GC-MS analysis of DMDS adducts of ω -7 and ω -9 monounsaturated FAMES in different yeast lines expressing ADS4.2	160
Figure 4-12: Subcellular localization of ADS4.2	162
Figure 4-13: Coverages of characteristic alkenes in Arabidopsis mutants deficient in general wax synthesis genes.....	163
Figure 4-14: Structure analysis of ADS4.2 in comparison with other integral membrane desaturases	174
Figure 4-15: Activity of ADS4.2 histidine mutants.....	177
Figure 4-16: Phylogenetic analysis of protein sequences homologous to ADS4.2	179

List of Abbreviations

ABA: abscisic acid

ADS: acyl-CoA desaturase

ALT: acyl-lipid thioesterase

AP2/ERF: APETALA2/ethylene response factor

BiFC: bimolecular fluorescence complementation

BSTFA: *bis*-N,O-trimethylsilyltrifluoroacetamide

CaMV: cauliflower mosaic virus

CS: Chinese Spring

CURS: curcumin synthase

CUS: curcuminoid synthase

CYP: cytochrome P450

DCS: diketide-CoA synthase

DMC: diketone Metabolism CYP450

DMDS: dimethyl disulfide

DMH: diketone Metabolism Hydrolase

DMP: diketone Metabolism Polyketide Synthase

ECR: enoyl-CoA reductase

ENR: enoyl-ACP reductase

EPCS: ER-PM contact sites

ER: endoplasmic reticulum

FAE: fatty acid elongase

FAME: fatty acid methyl ester

FAR: fatty acyl-CoA reductase

FAS: fatty acid synthase

FATA: fatty acyl-acyl carrier protein thioesterase A

FATB: fatty acyl-acyl carrier protein thioesterase B

FAX1: FATTY ACID EXPORT 1

GC-FID: gas chromatography-flame ionization detector

GC-IRMS: isotope-ratio mass spectrometry

GC-MS: gas chromatography-mass spectrometry

GFP: green fluorescent protein

GPI: glycosylphosphatidylinositol

GUS: β -glucuronidase

HAD: β -hydroxyacyl-ACP dehydratase

HCD: hydroxyacyl-CoA dehydratase

Iw1, Iw2: inhibitor of WAX1, Inhibitor of WAX2

KAR: β -ketoacyl-ACP reductase

KAS: β -ketoacyl-ACP synthase

KCR: β -ketoacyl-CoA reductase

KCS: β -ketoacyl-CoA synthase

LACS: long-chain acyl-CoA synthase

LC: long-chain

LCFA: long-chain fatty acid

LPT: lipid transfer protein

LUT1: α -carotene ϵ -ring hydroxylase

MAH1: midchain alkane hydroxylase

MCMT: malonyl-CoA:acyl carrier protein malonyltransferase

MCS: membrane contact site

ME: methyl ester

MS: Murashige and Skoog

MVA: mevalonic acid

ORF: open reading frame

OSC: oxidosqualene cyclase

PEG: polyethylene glycol

PKS: polyketide synthase

PM: plasma membrane

qRT-PCR: quantitative real-time PCR

SA: salicylic acid

SAR: systemic acquired resistance

SYT: synaptotagmin

TAG: triacylglyceride

TC: tocopherol cyclase

TEM: transmission electron microscopy

TLC: thin-layer chromatography

TMS: trimethylsilyl

VAP27: vesicle-associated membrane-associated protein 27

VLC: very-long-chain

VLC: very-long-chain

VOC: volatile components

W1, W2: WAX1, WAX2

WDA1: wax-deficient anther1

WSD1: wax synthase/diacylglycerol acyltransferase

WSL5: wax crystal-sparse leaf 5

WUE: water use efficiency

γ TMT: γ -tocopherol methyltransferase

Acknowledgements

Apart from my input, many people have supported and contributed to this research, which finally led to this dissertation. I would like to express my deep gratitude to my supervisor Reinhard Jetter for his invaluable guidance on both life and research through each stage of my Ph.D. study. His insight into research, advice on experimental planning, training on critical thinking and tremendous effort to improve my writing helped me to succeed. Without his patience, supervision and motivation, this research would not be possible.

I would like to extend my gratitude to my supervisory committee Dr. Lacey Samuels, Dr. Abel Rosado and Dr. Jörg Bohlmann, who offered me constructive suggestions, helped improve my work, shared their research enthusiasm to support and encourage me during my study.

My appreciation extends to my fellow lab members, graduate students and postdocs, Daniela Hegebarth, Lucas Busta, Alberto Ruiz Orduna, Daisy Zhang, Jędrzej Gozdzik, Yanan Liu, Joyce Liu, Tongjun Sun, Meng Li, Hainan Tian, EunKyoung Lee and many more who helped me for sharing their expertise and advice, having encouraging and constructive discussions on my study.

My appreciation goes to my collaborators Alberto Ruiz Orduna, Dr. Daniela Hegebarth, and Dr. Tingting Li for their crucial contribution to this work.

I would like to acknowledge the financial support provided by the China Scholarship Council (CSC), the National Sciences and Engineering Research Council (NSERC), the University of British Columbia, and the Botany Department.

Last and most importantly, I would like to express my sincere gratitude to my family and friends, who have offered me their endless love, company and support throughout my study. Without their assistance, this work would not have been completed.

Dedication

For my beloved family and cherished friends who offered me eternal love and support throughout the journey of my life.

Chapter 1: Introduction

Terrestrial plants, sessile organisms covering the continents, are constantly suffering from stress, both biotic and abiotic, during their lifetime. For millions of years, from tiny vulnerable mosses to the giant oaks, plants have evolved graceful and sophisticated mechanisms to adapt to their environment, survive, and gradually conquer diverse habitats across the continents. The land plant traits, including the vascular transport tissue, rooting system and stomata, all contribute to land plant adaptation. Cuticle that covers the non-woody above-ground organs is one of the key mechanisms that enabled plants leave aquatic environment and initiate the long evolutionary history of land plants.

1.1 The structure of cuticle

Cuticle consists of two components. The insoluble polymerized matrix that attaches to the polysaccharide cell wall is cutin, and the organic solvent-soluble sealing that is embedded in cutin is cuticular wax. The cross-linked cutin polymer, mainly consists of oxygenated long-chain (C_{16} or C_{18}) fatty acids which contain ω -hydroxyl groups and one or more in-chain oxygenations (like hydroxyl, epoxy and sometimes oxo groups) after depolymerization (Yeats and Rose, 2013; Fich et al., 2016). The cuticular wax is a complex mixture mainly made of very-long-chain (VLC, C_{20} - C_{34}) aliphatics, and sometimes includes cyclic compounds such as triterpenoids, phenylpropanoids, and flavonoids (Samuels et al., 2008). The cuticle consists of two layers to seal the plant surface. The innermost layer of the cuticle is the cuticular layer, which is associated with the cell wall of the epidermis, contains cutin polymer, intracuticular wax and intermingled polysaccharide from the cell wall; the second layer is the cuticle proper which is made of intracuticular wax and cutin matrix. The outmost part of cuticle proper, namely the

epicuticular wax, forms wax crystals or a film covering the epidermis surface, to endow plants with a glaucous or glossy appearance, respectively (Yeats and Rose, 2013). Different layers of cuticle are hard to distinguish. Histochemical staining and transmission electron microscopy (TEM) are generally used to observe the elaborated interior arrangement of cuticle.

1.2 Biological functions of cuticle

Being the outmost layer of terrestrial plants and protecting the organism from the outside environment, cuticle is vital for land plant 1) development, 2) reproduction and 3) adaptation. In the following section, I will introduce plant cuticle function with regard to these three aspects.

1.2.1 Plant development

Cuticle is crucial for plant development in various aspects. Characterization of plant cuticle-deficient mutants suggests that proper cuticle is essential to avoid the adhesion of epidermal cells, prevent detrimental organ fusion, maintain plant normal stature and control cellular structure/differentiation. For instance, *Arabidopsis abcg11/wbc11* knock-out mutants, which had decreased cuticular wax coverages compared to wild type, exhibited reduced plant size, extensive postgenital organ fusions and deficient leaf trichomes (Bird et al., 2007).

Cuticle also plays an essential role in volatile compounds (VOC) emission. This is revealed by a recent study on flower VOCs. *Petunia (Petunia hybrida) PhABCG12* RNAi transgenic mutant lines, which exhibited decreased wax load and cuticle thickness in petals, showed reduced total VOC emission, VOC internal pool and decreased biosynthesis of phenylalanine-derived VOC and altered individual VOC cellular distribution. The thinner cuticle also perturbed the rhythmicity of VOC emission (Liao et al., 2021). These results demonstrate the hydrophobic

cuticle is not a physical barrier for VOC, instead, it balances VOC retention/emission and cellular (internal vs cuticle) distribution, thus an essential member of plant VOC network.

1.2.2 Plant reproduction

Besides development, cuticle also influences plant reproduction by controlling the male fertility of plants. In *Arabidopsis*, various cuticle-synthesis deficient mutants (*cer3*, *cer6*) showed male sterility, with shorter siliques and less seeds produced in normal growth condition, which resulted from the disrupted pollen-pistill interactions in these wax-deficient mutants (Preuss et al., 1993; Aarts et al., 1997; Millar et al., 1999). The conditional male sterility of wax-deficient mutants recovered in humid conditions further suggested the male fertility is related to cuticle integrity. In another study, rice *wax-deficient anther1* (*wda1*) mutant exhibited reduced cuticular wax coverage on anthers, retarded microspore development, disrupted pollen exine and reduced male fertility. The male sterility is likely resulted from the failure of exine development and anther dehiscence (Jung et al., 2006).

1.2.3 Plant adaptation

Cuticle maintains the fitness of plants and also influences plant-environment interactions.

As a hydrophobic layer, cuticle seals epidermal cells, strongly restricts non-stomata water loss and protects plants from desiccation, becoming one of the main factors for land plant adaptation.

The microstructure and hydrophobicity of cuticle also empowers plant self-cleaning. The epicuticular wax can form nano-scale crystals (likely containing a predominant wax compound) to minimize the plant contacting surface with water droplets and dust particles. Additionally, the hydrophobicity of cuticle prevents water droplets from sticking to plants, thus facilitating the channeling of water droplets so they wash away particles attaching to the surface (Barthlott et al.,

2017). This process also avoids wetting of plant tissues and potentially prevents pathogen infection.

Cuticles are fundamental for plants to fulfill their ecological roles. Both the physical properties and chemical compositions of cuticles influence plant-insect as well as plant-microbe interactions. Cuticles can limit the movement of insects on plant surfaces. The microstructures of epicuticular wax play the key role in this process. For instance, pitcher plants have a slippery zone in the upper part of pitcher which contains epicuticular wax crystals bearing small “stalks”. The specific structure makes the wax crystals easy to break and contaminate the adhesive pads of insects to avoid their attachment (Gorb et al., 2005). Sometimes cuticles play a major role to attract insects for plants. Different chemical compositions of cuticles are major factors that influence the interactions between insects and plants. VLC hydrocarbons are widely used as pheromones in insect intraspecific communication. VLC hydrocarbons are also the major composition of plant cuticular waxes. *Ophrys* orchids attract male insects as pollinators by sexual deception. Their flowers have not only a stripy pattern to mimic the appearance of insects, but also wax compositions that are similar to cuticle and pheromone of female insects (Schiestl et al., 1999). In this way, *Ophrys* decoy their pollinators without the cost of nectar.

The chemical compositions of cuticle influence the plant-microbe interactions. Several studies suggest that the mixed hydrocarbons with different functional groups in cuticles serve as effector molecules during pathogen infection, thus influencing plant-pathogen interaction (Reina-Pinto and Yephremov, 2009). For instance, *Arabidopsis* transgenic lines, which produce 80% more alkanes in their cuticular waxes, were more vulnerable to the bacterial pathogen *Pseudomonas syringae* pv. *Tomato* DC3000 and the fungal pathogen *Sclerotinia* compared to wild-type plants (Bourdenx et al., 2011). The physical properties of cuticle also contribute to plant pathogen

resistance. A recent study found that a deficiency in the cuticle impaired transport of the defense phytohormone salicylic acid (SA) to the symplasm and instead, plants accumulated SA in the apoplast, likely due to stronger transpiration. This sabotaged plants' systemic acquired resistance (SAR) and led to reduced pathogen resistance (Lim et al., 2020).

1.3 The ubiquitous wax components in land plants

1.3.1 Chemistry of ubiquitous wax components

Cuticular waxes are mainly very-long-chain (VLC) aliphatics, and sometimes contain cyclic compounds. There is a set of wax components widely spread among plant kingdom that are recognized as ubiquitous wax components, including fatty acids, alkanes, aldehydes, primary alcohols and acyl esters, which have been reported from plants across the entire plant kingdom (Figure 1-1A). This is different from the specialty wax components, which will be introduced later in this chapter. Ubiquitous wax components possess a fully saturated linear hydrocarbon backbone with one oxygen functional group at one terminal or no functional group at all (Busta and Jetter, 2017). Wax components bearing the same functional group form a compound class. In each compound class, the components have different carbon chain lengths usually ranging from C₂₀ to C₄₆, thus forming a series of homologs. In most cases, ubiquitous wax components are reported with two-dimensional information: the coverage of different compound classes and the homolog distribution of each compound class. In each compound class, both even-carbon-numbered and odd-carbon-numbered homologs are present, but the adjacent dominant homologs always possess total carbon numbers differing by two, thus conferring single parity to the dominant homologs in each wax compound class. Each wax compound class has different parity of major homologs (Busta and Jetter, 2018). For example, the dominant homologs of fatty acids

and primary alcohols have even carbon number parity while alkane homologs have predominantly odd carbon numbers.

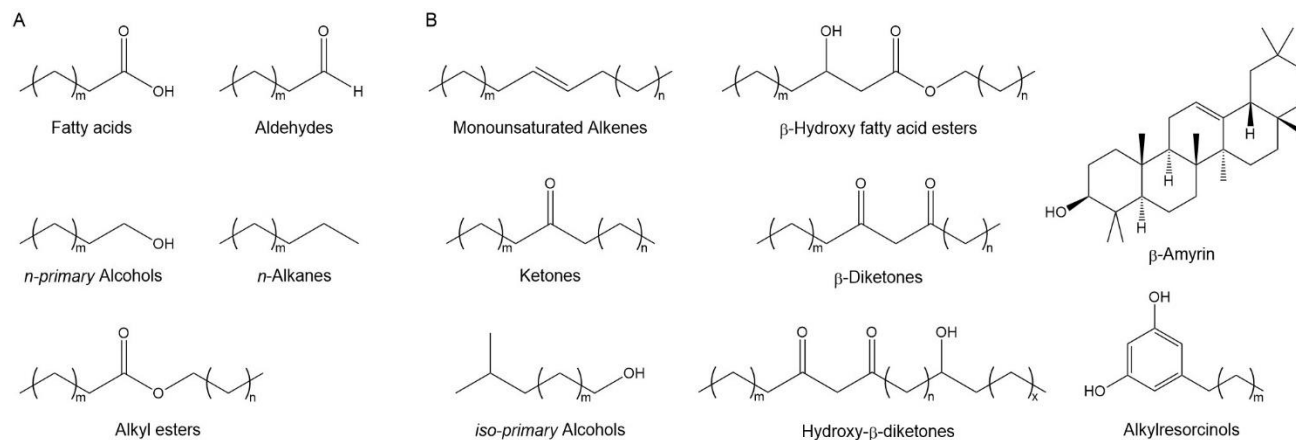


Figure 1-1: Common wax components detected in various plant species

A) Ubiquitous wax components that are detected across the entire plant kingdom. Ubiquitous wax components possess a fully saturated VLC linear hydrocarbon backbone with one oxygen functional group at one terminal or no functional group at all. B) Examples of linear and cyclic specialty wax components that are found in specific plant species or families. The specialty wax components generally have linear VLC aliphatic backbone with one or more in-chain functional groups in addition to or instead of the terminal oxygen functional group and sometimes possess cyclic, or unsaturated structures, and could have branches in their backbones. *m*, *n* and *x* = 17 to 33. The components are dominant in (A) when *m* equals an odd number.

1.3.2 The biosynthesis of ubiquitous wax composition

The synthesis of ubiquitous as well as specialty cuticular waxes requires different cellular compartments and are mainly restricted to plant epidermal cells. The synthesis of ubiquitous wax components shares core enzyme components with other synthesis pathways and contains unique machineries that specifically participate in wax formation. In the following section, I will introduce three stages in ubiquitous cuticular wax synthesis, namely i) precursor *de novo*

synthesis, ii) elongation and iii) final modification (Figure 1-2). Additionally, the transport of wax precursors/products will be described briefly here.

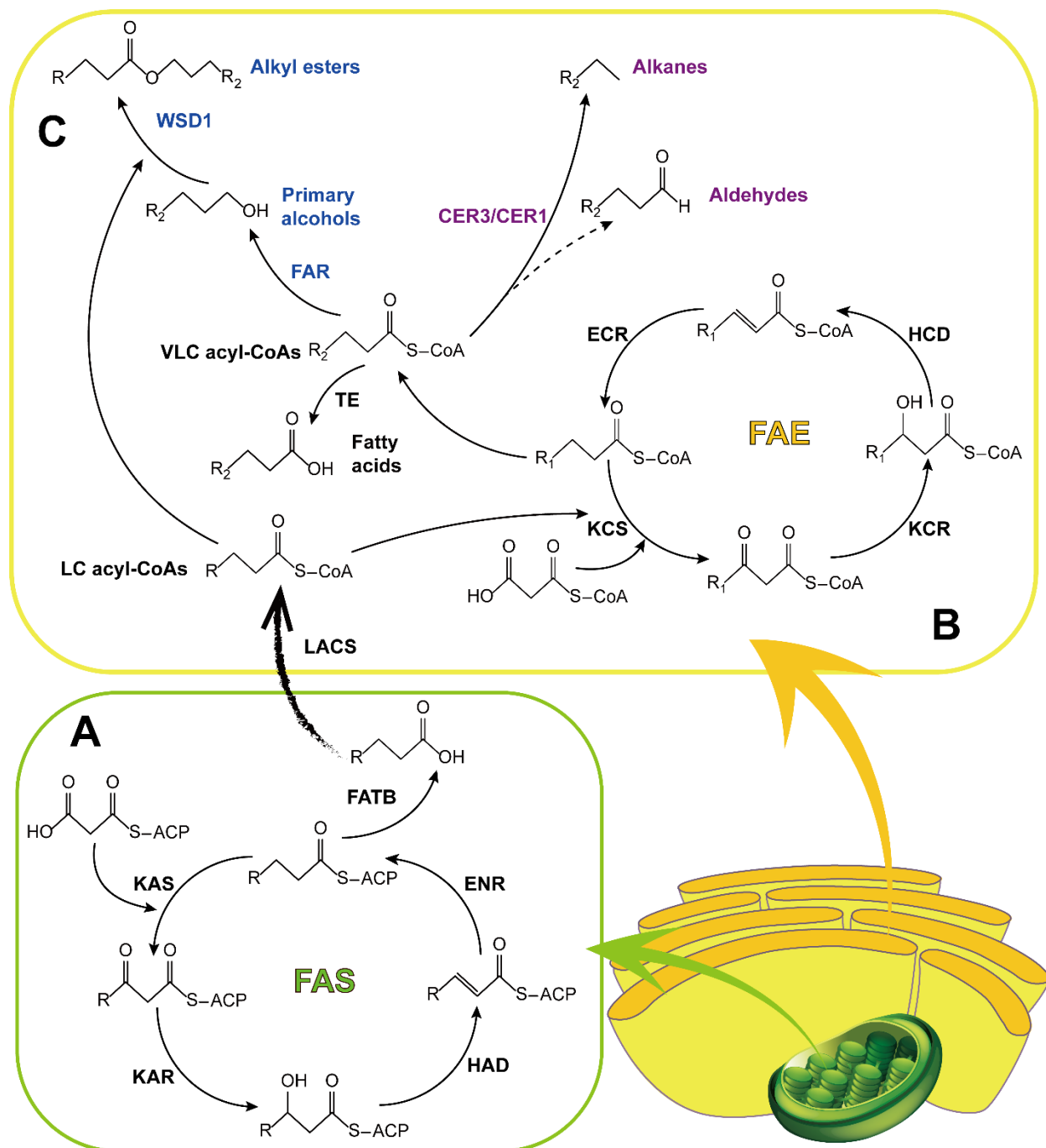


Figure 1-2: Biosynthesis of wax components

A) Fatty acid *de novo* synthesis; B) LC acyl-CoA elongation; C) Wax modification. Steps in plastids are highlighted in green box and steps in ER are highlighted in yellow box. Enzymes and

products on alcohol-forming pathway and alkane-forming pathway are labeled by blue and magenta, respectively. LC acyl-CoAs, long-chain acyl-CoAs (C_{16} - C_{18}); VLC acyl-CoAs, very-long-chain acyl-CoAs (C_{20} - C_{34}) FAS, fatty acid synthase complex; FAE, fatty acid elongase complex; KAS, β -ketoacyl-ACP synthase; KAR, β -ketoacyl-ACP reductase; HAD, β -hydroxyacyl-ACP dehydratase; ENR, enoyl-ACP reductase; FATB, fatty acyl-acyl carrier protein thioesterase B; LACS, long-chain acyl-CoA synthase; KCS, β -ketoacyl-CoA synthase; KCR, β -ketoacyl-CoA reductase; HCD, β -hydroxyacyl-CoA dehydratase; ECR, enoyl-CoA reductase; TE, thioesterase; FAR, fatty acyl-CoA reductase; WSD1, wax synthase/diacylglycerol acyltransferase; CER3, ECERIFERUM 3; CER1, ECERIFERUM 1. R, R_1 and $R_2 = C_nH_{2n+1}$ (R, $n = 1$ to 15 , R_1 , $n = 15$ to 31 , R_2 , $n = 17$ to 31)

1.3.2.1 Fatty acid *de novo* synthesis

Long-chain fatty acids (LCFAs) serve as precursors of wax lipids. While fatty acid *de novo* synthesis occurs in the cytosol of animal and fungal cells, it occurs in the plastids in plants (Ohlrogge and Browse, 1995; Li-Beisson et al., 2013). Malonyl-acyl carrier protein (ACP), which provides the C_2 moiety to fatty acid synthesis, is produced by carboxylation of acetyl-CoA by acetyl-CoA carboxylase (ACC), followed by transesterification from CoA to ACP by a malonyl-CoA:acyl carrier protein malonyltransferase (MCMT) (Li-Beisson et al., 2013). The subsequent LCFA synthesis is catalyzed by the fatty acid synthase (FAS) in the stroma (Ohlrogge and Browse, 1995; Li-Beisson et al., 2013), a dissociable complex (Brown et al., 2006) that contains four soluble enzymes and catalyzes sequential reactions to elongate the carbon chain length up to C_{16} and C_{18} . There are four steps in each sequential reaction: firstly, a β -ketoacyl-ACP synthase (KAS) drives the condensation between the C_2 moiety from the malonyl-ACP to acyl-ACP (the first condensation acceptor is acetyl-CoA) and release CO_2 ; secondly, the resulting β -ketoacyl-ACP is reduced at the carbonyl group by a β -ketoacyl-ACP reductase (KAR) with NADPH as the electron donor; the following dehydration is catalyzed by a β -hydroxyacyl-ACP dehydratase (HAD) to form the enoyl-ACP, and finally a enoyl-ACP

reductase (ENR) leads to the final acyl-ACP product with two carbons elongated (Figure 1-2A) (Ohlrogge and Browse, 1995; Samuels et al., 2008; Li-Beisson et al., 2013). KAR, HAD and ENR have no specificity and are used in all FAS complexes; in contrast, different KASs exist, with different acyl chain length specificities, thus defining different FAS complexes. KAS III catalyzes the first condensation (from C₂ to C₄) (Clough et al., 1992), KAS I catalyzes the following six condensations (from C₄ to C₁₆) and KAS II is used in the last elongation (from C₁₆ to C₁₈) (Shimakata and Stumpf, 1982).

Finally, the saturated C₁₆-ACP is hydrolyzed by the fatty acyl-acyl carrier protein thioesterase B (FATB) and released as free fatty acid (Dormann et al., 2000), while another hydrolase (FATA) has substrate preference for monounsaturated C₁₈-ACP (Li-Beisson et al., 2013). The free fatty acids are then esterified by a long-chain acyl-CoA synthase (LACS) and transported from the plastid to endoplasmic reticulum (ER) (Li-Beisson et al., 2013).

1.3.2.2 LCFA Elongation

LCFAs from plastids require further elongation, which takes place in the ER, to meet the chain length range of the wax components. The free fatty acids first need to be activated by the long-chain acyl-CoA synthetases, LACSs (LACS1/CER8, LACS2) (Schnurr et al., 2004; Lü et al., 2009). Subsequently, another heterotetrameric enzyme complex, a fatty acid elongase (FAE) consisting of a β -ketoacyl-CoA synthase (KCS), a β -ketoacyl-CoA reductase (KCR), a β -hydroxyacyl-CoA dehydratase (HCD), and an enoyl-CoA reductase (ECR), conducts further elongation rounds. It utilizes C₁₆ and C₁₈ fatty acyl-CoAs as the starting substrate and malonyl-CoA as the carbon donor, catalyzing a four-step sequential reaction to add a C₂ unit in each cycle (Kunst and Samuels, 2009; Haslam and Kunst, 2013). In this process, the acyl-CoA (carbon acceptor) is first condensed with acetyl-CoA derived from malonyl-CoA by the KCS to form β -

ketoacyl-CoA; the following reduction is driven by KCR to form β -hydroxyacyl-CoA; next, HCD converts the intermediate to trans- Δ^2 -enoyl-CoA, which finally undergoes a second reduction by ECR/CER10 to form the acyl-CoA elongated by two carbons (Kunst and Samuels, 2003; Kunst and Samuels, 2009; Li-Beisson et al., 2013). After several cycles, the acyl-CoA chain length is elongated up to C₃₄ and even C₃₈ (Figure 1-2B) (Hegebarth et al., 2016).

KCSs, which are membrane-associated proteins, have substrate chain length specificity, and thus endow the chain length specificity of FAE complexes. Twenty-one *KCS* genes have been identified in Arabidopsis genome (Joubes et al., 2008) with diverse expression profiles and various functions in plant development. For example, KCS18/FAE1 is involved in seed oil fatty acid elongation, from C_{18:1} to C_{20:1} and C_{22:1}, and from C_{18:0} to C_{20:0} (Kunst et al., 1992; James et al., 1995); while KCS2, KCS20 and KCS9 are involved in suberin synthesis and elongate the acyls up to C₂₄ (Franke et al., 2009; Lee et al., 2009; Kim et al., 2013). There are four KCSs, KCS1, KCS6/CER6/CUT1, KCS9 and KCS16, that clearly participate in cuticular lipid metabolism in Arabidopsis. *kcs1* mutants showed substantial reduction of primary alcohols and aldehydes with chain lengths from C₂₆ to C₃₀ but no obvious influences on products from alkane-forming pathway (Todd et al., 1999). In addition to suberin deficient phenotype, *kcs9* mutants also showed reduced C₂₄, C₂₆ fatty acids in their leaf cuticular waxes (Kim et al., 2013). While CER6 is the only member of the KCS family known to have a crucial role in the elongation of VLCFAs for cuticular wax; both KCS6-suppressed plants and mutants showed a waxless or glossy phenotype and conditional male sterility (Millar et al., 1999; Fiebig et al., 2000), and the suppressed lines had reduced levels of almost all wax components while C₂₂ and C₂₄ primary alcohol amounts increased, suggesting that CER6/KCS6 is responsible for the elongation of C₂₄ fatty-acyl CoA (Millar et al., 1999). Moreover, a recent study showed a strong decrease of C₃₆

and C₃₈ wax compounds in trichomes of *ksc16* mutants, suggesting that KCS16 is involved in the elongation of C₃₄ fatty-acyl CoA to C₃₆ and C₃₈ (Hegebarth et al., 2017).

Proteins belonging to BAHD acyltransferases family, the CER2-likes, are also required to further support the elongation function of FAE complexes. Arabidopsis *cer2* mutants exhibit a decrease of wax components with carbon chain lengths longer than C₂₈ (Negruk et al., 1996; Xia et al., 1996), while heterologous expression of *CER6* alone in yeast led to the synthesis of fatty acids up to C₂₈, along with trace amount of C₃₀ (Trenkamp et al., 2004; Haslam et al., 2012; Haslam and Kunst, 2020). This clearly indicates that CER2 is involved in fatty acid elongation beyond C₂₈. There are four CER2-LIKEs in Arabidopsis that function redundantly, with different abilities to extend fatty acyl chains *in planta* (Haslam et al., 2015; Haslam and Kunst, 2020). Yeast heterologous expression proved that, with CER2 association, CER6 elongation can be extended to C₃₀, with CER2-LIKE1/CER26 up to C₃₄, with CER2-LIKE2/CER26-LIKE up to C₃₂, with CER2-LIKE3 or CER2-LIKE4 up to C₃₀ (Haslam et al., 2012; Pascal et al., 2013; Haslam et al., 2015; Haslam and Kunst, 2020). BAHD acyltransferase members that are homologous to Arabidopsis CER2-LIKEs have been identified from rice (*Oryza sativa*), sacred lotus (*Nelumbo nucifera* Gaertn.), maize (*Zea mays*) and poplar (*Populus trichocarpa*), with different fatty acyl chain length extension ability when coexpressed with KCS members in yeast (Wang et al., 2017; Yang et al., 2018; Alexander et al., 2020; Gonzales-Vigil et al., 2021), indicating the conserved fatty acyl elongation mechanism that is shared by eudicots. The interaction between CER2 and specific FAE complex (CER6-associated FAE or complex) or specific KCS have been demonstrated in Arabidopsis and rice. However, the exact biochemical role that CER2-LIKEs play in fatty elongation is still far from clear (Wang et al., 2017; Haslam and Kunst, 2020).

1.3.2.3 VLCFA modification

Following elongation, VLC acyl-CoA wax precursors are further modified also in the ER of the epidermis cells. In Arabidopsis, there are mainly two pathways leading to precursor modification: the alcohol-forming pathway (also referred to as acyl reduction pathway) and the alkane-forming pathway (also referred to as decarbonylation pathway) (Kunst and Samuels, 2003; Bernard and Joubes, 2013). In the alcohol-forming pathway, CER4, a fatty acyl-CoA reductase (FAR) catalyzes the reduction of acyl-CoAs to n-primary alcohols. In the stem cuticular wax of *cer4* mutants, all the primary alcohols (C₂₄-C₃₀) are reduced severely (Rowland et al., 2006). A second enzyme in this pathway, the wax synthase/diacylglycerol acyltransferase (WSD1), condenses the primary alcohols with fatty acyl-CoAs to synthesize wax esters (Li et al., 2008). In the decarbonylation pathway, the CER3/CER1 complex (along with CYTB5s as a cofactor) first reduces acyl-CoAs to intermediate aldehydes (Goodwin et al., 2005) and then decarbonylates them to n-alkanes with one carbon released (Bernard et al., 2012). A recent study in Arabidopsis found CER1-LIKE1 also interacts with CER3 and CYTB5, and is able to form shorter VLC alkanes (Pascal et al., 2019). Similar wax modification pathways that generate ubiquitous wax components are widely shared across the plant kingdom (Figure 1-2C).

1.4 The specialty wax components in land plants

1.4.1 The chemistry of specialty wax components

In addition to the ubiquitous wax components, many plants contain specialty wax compound groups which are limited in several species or in specific plant families. They generally have linear VLC aliphatic backbone with one or more in-chain functional groups in addition to or instead of the terminal oxygen functional group and sometimes possess cyclic, or unsaturated structures, and could have branches in their backbones (Figure 1-1B) (Busta and Jetter, 2018).

Similar to ubiquitous wax components, the specialty wax components possessing the same major/first in-terminal (sometimes in-chain) functional group belong to the same compound class. The linear specialty wax components in the same compound class, usually ranging from C₂₀ to C₄₆, will again form homolog series. In addition to the primary functional group, these specialty wax components have secondary functional group that varies in type of functional group and position, which make the specialty wax homologs further group into different isomer series (Busta and Jetter, 2018). Thus, in addition to the two-dimensional information of ubiquitous wax components, at least one more dimension of information has to be provided for specialty wax components: type of the secondary functional group and the in-chain position of it. Another one dimension of information is required if the third functional group present (Busta and Jetter, 2018).

The cyclic specialty wax components can be further divided into alicyclic wax components and aromatic wax components. Instead of fatty acid *de novo* synthesis pathway, pentacyclic wax components are derived from isoprenoids synthesized via the mevalonic acid (MVA) pathway (Thimmappa et al., 2014). The various arrangement of carbon skeleton alongside the type as well as the position of functional group lead to the chemical diversity of pentacyclic wax components. The aromatic wax components could be either derivatives of the phenylpropanoid pathway or produced via the cyclization of linear VLC fatty acyls. Their chemical diversity largely relies on the oxygen functional group type as well as the position of secondary functional group.

Accompanying the ubiquitous wax components, the specialty wax compounds are minor wax components in many plant species. Sometimes they could make up the majority of wax coating and thus are the hallmark of these plant species. For example, β -diketones in various crop species in Poaceae family (wheat (*Triticum aestivum*), barley (*Hordeum vulgare*)) (Hen-Avivi et al.,

2016); and nonacosan-10-ol and its derived diols are abundant in needles of most conifers (yew (*Taxus baccata*), pine (*Pinus halepensis*)) (Matas et al., 2003; Wen et al., 2006).

Some specialty wax components are minor wax components that are hard to detect, thus are overlooked in previous studies even in model plants. Though low in abundance, they sometimes could be produced in a wide spectrum of plant species. Because of the difficulties in detection, our knowledge of minor wax components is quite limited. Iso-primary alcohols that have been recently characterized from *Arabidopsis*, iso-alkanes that have been reported from several *Brassica* species (Busta and Jetter, 2017), and monounsaturated alkenes reported from maize old leaves and *Arabidopsis* young leaves are all minor wax components (Hegebarth et al., 2016; Bourgault et al., 2019). With the refined detection methods and in-depth analysis, more and more minor wax components will be revealed from plants.

1.4.2 The synthesis of specialty components.

The ubiquitous wax component modification pathways are well-established in the past decades, mainly based on mutant analysis in model plants *Arabidopsis* and maize, however, the synthesis of specialty wax components is still far from clear. Most of specialty wax components contain hydrocarbon backbones similar to ubiquitous wax compounds but possessing secondary functional groups, indicating that their biosynthesis requires the basic wax synthesis modules, but shunt from the pathway forming ubiquitous wax compounds at least at one point (Figure 1-1B) (Busta and Jetter, 2018). In addition to the enzyme modules on ubiquitous wax biosynthesis pathways, there are various enzymes forming additional wax synthesis machinery that are required to fulfill the modification of specialty wax components in plants. They could install the additional functional groups before, during or after the synthesis of the core molecules. Here I introduce several types of non-canonical wax-forming enzymes, including Oxidosqualene

cyclases (OSCs), desaturases, thioesterases, polyketide synthases (PKSs), and cytochrome P450s (CYPs), that have been reported making up the machineries that participate in the synthesis of specialty wax components.

1.4.2.1 Oxidosqualene cyclases (OSCs)

Triterpenoids derived from α -amyrin, β -amyrin, and lupeol are widely accumulated as wax composition in different plants species in various organs, and developmental stages. Instead of a VLC aliphatic backbone, these wax components are derived from isoprenoids. The production of triterpenoids is determined by oxidosqualene cyclases (OSCs). All OSCs in eukaryotes accept the linear isoprenoid 2,3-oxidosqualene as substrate to produce different pentacyclic scaffolds. Different from other enzymes, OSCs are able to produce a set of products from a single substrate, mainly because of the high activity of their reactive carbocationic intermediates generated during reaction and their ability to handle these intermediates. Multiple OSCs presenting, the catalytic versatility/multifunctionality of each OSC, and sometimes the presence of downstream modification enzymes (e.g., cytochrome P450s, acyltransferases and cytochrome P450 reductases), leads to miscellaneous triterpenoid alcohol, ketone and acid profiles in plant cuticular waxes.

Triterpenoids are highly accumulated in the cuticular waxes of tomato (*Solanum lycopersicum*) fruits. In tomato cultivar MicroTom, triterpenoids made up ca. 25% of total fruit wax and the proportion decreased amid fruit development (Vogg et al., 2004; Leide et al., 2007). Two OSCs, SITTS1 and SITTS2, obtained from the epidermis of tomato fruits, produced single product β -amyrin and seven terpenoids with δ -amyrin as the dominating product, respectively in yeast heterologous expression. Overexpression of SITTS1 and SITTS2 in tomato led to increased triterpenoid coverage of the same products that formed in yeast expression (Wang et al., 2011).

These results confirmed SITTS1 as a monofunctional OSC generating β -amyrin while SITTS2 as a multifunctional OSC forming mainly δ -amyrin in tomato cuticular waxes.

Oleanane and ursane type triterpenoids are also important wax compositions for many medicinal plants. In *Artemisia annua* transcriptome analysis, an OSC gene *OSC2* overrepresented in filamentous trichomes was identified. The expression of *OSC2* in yeast and tobacco resulted in the accumulation of α -, β - and δ -amyrin, the precursors of cuticular triterpenoid ketones in *A. annua*. Further silencing of *OSC2* in *A. annua* confirmed its involvement in the cuticular triterpenoid synthesis (Moses et al., 2015).

The OSC mining from *Kalanchoe daigremontiana*, a species that produces a number of triterpenoids in the leaf waxes, characterized several multifunctional OSCs generating lupeol, taraxerol, and glutinol as the major product, respectively. Particularly, a multifunctional friedelin synthase was first identified, which was able to handle highly reactive carbocationic intermediates and catalyze ten steps of pentacyclic carbon backbone rearrangement in a single enzymatic reaction (Wang et al., 2010).

A recent study in sorghum (*Sorghum bicolor*) leaf cuticular wax found the uncommon hopane type plant triterpenoids were highly accumulated on leaf surfaces of adult plants but not those of juvenile plants. Genome-wide OSC analysis and yeast expression revealed two multifunctional OSCs: one produced β - and α -amyrin in an almost 1:1 ratio; the other one generated three hopane triterpenoids with the domination of isoarborinol. The products of the amylin synthase and the isoarborinol synthase, together with potential downstream modification, could explain the triterpenoid profile of sorghum leaf surface wax (Busta et al., 2020).

1.4.2.2 Desaturases

Linear monounsaturated components can form specialty wax components. Besides traditional synthesis reactions, these components require an additional desaturation step. Different acyl-ACP and acyl-CoA desaturases were reported to produce monounsaturated carbon skeletons en route to wax biosynthesis. These desaturases introduce the double bond to a specific position of the carbon skeleton, thus generating a series of unsaturated wax homologs/isomers.

The minor wax components n-6 monounsaturated primary alcohol homologs were recently characterized from *Arabidopsis* inflorescence stem waxes. A loss-of-function mutation in *CER17*, which was found to encode acyl-CoA desaturase 4 (ADS4), led to the depletion of these monounsaturated fatty alcohols. Further *in planta* and yeast investigation found that ADS4 conducted n-6 (ω -6) desaturation likely on very-long-chain acyl-CoAs, which produced n-6 monounsaturated substrates en route to alcohol-forming pathway and subsequent reduction by CER4 (Yang et al., 2017).

Cuticular monounsaturated alkenes have been reported from a wide range of plant species, however, only few of their structures have been clarified. In these limited studies, alkene homologs with different double bond positions have been identified and double bonds locate mostly between C-9 and C-10. These 9-alkenes were found in wax on spikes of *Agropyron intermedium* (Tulloch and Hoffman, 1976) and *Hordeum vulgare* (von Wettstein-Knowles, 2007), flower surfaces of *Ophrys sphegodes* (Schlüter et al., 2011) and leaves of *Populus trichocarpa* (Gonzales-Vigil et al., 2017). Alkenes with other double bond positions are relative rare reported. 7-alkenes and 5-alkenes were found from *O. exaltata* labellae and *Rosa damascena* flower, respectively (Sedeek et al., 2016); while 4-, 6- and 10-alkenes in *Z. mays* leaf waxes (Bourgault et al., 2019) and 12-alkenes on *O. sphegodes* flowers (Schlüter et al., 2011). The

synthesis of 9-alkene and 12-alkene in *O. sphegodes* requires the plastidial Δ -9 (= ω -9) 18:1 and Δ -4 16:1 acyls, which were desaturated by a flower-specific stearyl-acyl carrier protein desaturase SAD2 that performed Δ -9 desaturation on C₁₈ precursor and Δ -4 desaturation on C₁₆ precursor, respectively (Schlüter et al., 2011). 7-Alkenes in *O. exaltata*, stem from elongation of Δ -9 (= ω -7) 16:1 fatty acyl precursor, which catalyzed by SAD5 (Sedeek et al., 2016). In chapter 4, I will describe my work on a desaturase generating monounsaturated alkenes in Arabidopsis.

1.4.2.3 Thioesterases

Thioesterases are generally involved in wax biosynthesis. Besides FATB and FATA that releases principally C_{16:0} and C_{18:1} fatty acyl-ACP, respectively, there are more thioesterases that release fatty acyl precursors with different acyl chain lengths and functional groups.

Wheat wax β -diketone metabolic gene cluster contains a key thioesterase/hydrolase encoded by *Diketone Metabolism Hydrolase (DMH)*. The heterologous expression of *DMH* in *E. coli* led to the production of C₁₅ 2-ketone, which was likely decarboxylated from C₁₆ 3-ketoacid (Hen-Avivi et al., 2016). DMH was considered releasing lipid precursors specifically participate in wax biosynthesis. The biochemical function of DMH in barley will be tested and discussed in chapter 3.

1.4.2.4 Polyketide synthases (PKSs)

Polyketides and their derivatives are common or even dominant wax components especially in Poaceae species. β -diketones, hydroxy- β -diketones, 2-alkanol esters, alkylresorcinols and methyl alkylresorcinols are common polyketides presenting in leaf and spike surfaces of wheat, rye, sorghum and barley (Ji and Jetter, 2008; Adamski et al., 2013; Racovita et al., 2016; Schneider et al., 2016; Busta et al., 2020). The polyketide carbon backbones mostly require the assembly of

by polyketide synthases (PKSs). Plant PKSs generally take an acyl-CoA substrate as the starter, use malonyl-CoA as extender, and perform one to eight rounds of decarboxylative condensation between starter and extender, sometimes followed by a final cyclization (Abe and Morita, 2010).

A study in rye (*Secale cereale*) characterized a type III PKS, ScARS that is involved in the formation of cuticular alkylresorcinols. ScARS was highly expressed in flag leaf blades where the alkylresorcinols and methyl alkylresorcinols actively accumulated. Yeast expression of ScARS led to the accumulation of alkylresorcinols with substitutional carbon chains ranging from C₇ to C₂₅. This indicates that ScARS could incorporate LC- and VLC- fatty acyl-CoAs as starters, conduct three rounds of malonyl-CoA condensation with a final stilbene type cyclization, producing cuticular alkylresorcinols in a single enzymatic reaction (Sun et al., 2020).

PKSs are also considered the core enzymes controlling cuticular β -diketone formation. Type III PKSs found in β -diketone metabolic genetic clusters both in wheat and barley are thought to work downstream of DMH. The mutation within the PKS genetic fragment led to the depletion of both surface β -diketones and their derivative hydroxy- β -diketones in barley mutants (Hen-Avivi et al., 2016; Schneider et al., 2016). In wheat, the silencing of PKSs within the β -diketone metabolic genetic cluster resulted in reduced β -diketones and hydroxy- β -diketones levels in waxes of spikes and flag leaf sheaths (Hen-Avivi et al., 2016). However, the bona fide biochemical functions of these enzymes are still unknown. This will be further discussed in chapter 3.

1.4.2.5 Cytochrome P450s (CYPs)

Cytochrome P450s (CYPs), representing one of the largest protein superfamilies in plants, catalyze monooxygenations of various metabolites. They commonly participate in metabolism of

lipophilic compounds, including the oxidation of terpenoids, phenolics, alkaloids and LC/VLC aliphatics.

Numerous CYP monooxygenases have been reported to participate in cutin modification. For example, CYP86A4 is a fatty acid ω -hydroxylase and CYP77A6 subsequently hydroxylates its products to produce 10,16-dihydroxypalmitate, a major cutin monomer in *Arabidopsis* (Li-Beisson et al., 2009).

CYPs that specifically participate in wax biosynthesis have also been reported. In *Arabidopsis*, *CYP96A15* encodes a midchain alkane hydroxylase (MAH1) that initiates the oxidation on the mid-carbon of C₂₉ alkane, which is generated on the alkane-forming pathway, to produce C₂₉ secondary alcohol and continues with a second oxidation on the same carbon to produce C₂₉ ketone, one of the major wax components on *Arabidopsis* inflorescence stems (Greer et al., 2007). A CYP from *A. annua*, CYP716A14v2, catalyzes the C-3 oxidation on α - and β -amyrin to produce corresponding triterpenoid ketones that are present in cuticular waxes (Moses et al., 2015). In rice, *wax crystal-sparse leaf 5* (*WSL5*)/*CYP96B5* encodes a terminal alkane hydroxylase that catalyzes the hydroxylation of alkanes to odd-numbered primary alcohols in cuticular waxes (Zhang et al., 2020).

1.5 The diversity of cuticular waxes in land plants

Cuticular waxes are the fingerprints of plants that are characteristic of each species. The basic set of ubiquitous wax components, together with the specialty wax components, makes up the basis of cuticular waxes diversity in land plants. Variations in coverage, compound class, homolog as well as isomer distributions of both ubiquitous wax components and specialty wax components contribute to cuticular wax diversity. For example, in moss (*Funaria hygrometrica*), fatty acid

alkyl esters and β -hydroxy fatty acid alkyl esters are the major wax components of leafy gametophyte (Busta et al., 2016); while in gymnosperm *Ginkgo biloba* leaves, fatty acids, primary alcohols and secondary alcohol (nonacosanol-10-ol) are dominant (Gülz et al., 1992). These variations also present in the same species, in different organs and developmental stages. For instance, alkanes ranging from C₂₇ to C₃₅ make up ca. 70% of total cuticular waxes in *Arabidopsis* leaves, whereas relatively short chain components, mainly C₂₉ alkane and ketone accumulate on *Arabidopsis* inflorescence stems. In bread wheat (*Triticum aestivum*), the primary alcohols are the major components of leaves in seedling stage, while alkanes and the specialty wax component β -diketones are dominant wax components in leaves formed during the reproductive stage (Li et al., 2019). The cuticular waxes are unique even in different plant cell types. A recent study identified a series of exceptional VLC alkane and alkene homologs (\geq C₃₂) in *Arabidopsis* young leaves. The following analysis on trichome deficient and trichome abundant mutants revealed that these characteristic VLC alkanes and alkenes were enriched in trichome abundant mutants compared to trichome deficient mutants (Hegebarth et al., 2016). Further analysis on the trichome cells confirmed that characteristic VLC alkanes and alkenes are highly accumulated on trichome but not on pavement cell surfaces (Hegebarth et al., 2016). Corresponding to the high accumulation of these VLC wax components on trichome cells, the KCS elongating the C₃₄ fatty acyls are also highly expressed in trichome cells (Hegebarth et al., 2017).

1.6 Objectives of the current study

Cuticular waxes are vital in plant adaptation to terrestrial conditions. During the long evolution and adaptation to different environments, plants selectively kept the ubiquitous wax components and generated specialty wax components. The ubiquitous wax components and canonical

enzymes involved in wax synthesis have been reported from a wide spectrum of plant species. However, our understanding of plant specialty wax components is still restricted. My PhD studies focused on the wax biosynthesis in both model plant *Arabidopsis* and non-model plants especially in crop species. I aimed to explore the ubiquitous wax-forming machineries in crop species, and to further identify non-canonical enzymes involved in forming specialty compounds in both *Arabidopsis* and crop species.

In chapter 2, I investigate the ubiquitous wax components in wheat. My specific goals are to explore the i) cuticular alkane accumulation profile in wheat, ii) alkane-forming enzymes in wheat and iii) the regulation of alkane formation in wheat. I first use the model wax biosynthesis pathway from *Arabidopsis* as a guide to investigate the alkane biosynthesis in bread wheat. In this chapter, firstly the CER1 homologs that associated with alkane formation in wheat are selected by the correlation analysis between alkane coverage and transcriptome data from different tissues. Then wheat nullisomic-tetrasomic substitution lines as well as *Arabidopsis* and rice heterologous expression systems are used to clarify that *TaCER1-1A* is a core gene involved in wheat alkane biosynthesis. Finally, the transcriptional regulation of *TaCER1-1A* in wheat are investigated.

In chapter 3, I investigate the specialty wax component synthesis in barley, my goals are to i) identify the β -diketone derived wax components in barley, ii) characterize the biochemical functions of the core enzymes involved in this process and iii) link the enzyme preferences with the β -diketone profile in barley. In this study, β -diketone-related wax components are profiled. With the C13 isotope analysis of barley wax components and barley elongase mutant wax

analysis, we revisited the β -diketone forming pathway. The biochemical functions of core enzymes, a thioesterase and a PKS, are clarified by *in vivo* and *in vitro* assays.

In chapter 4, I explore the minor wax components in Arabidopsis. My specific goals are to i) document the homolog as well as isomer profile of characteristic monounsaturated alkenes in Arabidopsis, ii) identify the desaturase(s) that install the secondary functional group in Arabidopsis and iii) explore the alkene biosynthesis pathway in Arabidopsis. In this chapter, I first analyze the structure of Arabidopsis characteristic alkenes in young leaves. The following chemical screening of loss-of-function mutants, complementation assays along with yeast heterologous expressions are used to identify the desaturase associated with alkene accumulation. Finally, the characteristic alkene synthesis pathway in Arabidopsis is investigated by the wax mutant analysis.

Chapter 2: Identification of the core enzyme involved in alkane biosynthesis in bread wheat

2.1 Introduction

Bread wheat is a major staple crop worldwide that provides 20% of energy and protein intake by humans (Lobell and Gourdj, 2012; WHO, 2017). Abiotic stresses substantially impede plant development and, thus, cause significant damage to global crop production (Lesk et al., 2016). Wheat is sensitive to drought and heat stress especially during flowering and grain-filling stages (Zampieri et al., 2017). These climate extremes drastically reduce wheat yield and grain quality (Kulkarni et al., 2017). As a crucial element in stress responses, cuticular wax plays a fundamental role in limiting transpirational water loss in wheat. Previous studies have found that cuticular wax traits have influences on wheat stress responses, water use efficiency (WUE) and even yield. A study on glaucousness isogenic durum wheat lines found that the glaucous wheat lines had longer leaf retaining time, lower temperature of photosynthetic tissues and higher WUE under drought condition comparing to their non-glaucous isogenic counterparts (Richards et al., 1986). Research on two groups of sixteen durum wheat lines with contrasting glaucousness over two years found the glaucous lines had higher grain yield in Mediterranean climate (Merah et al., 2000). In a later study using a set of 167 bread wheat lines originated from a cross between two high-yield wheat cultivars differing in leaf angle, leaf rolling and surface glaucousness found that higher grain weight and yield were associated with glaucousness even under irrigated conditions (Monneveux et al., 2004).

Wheat waxes have been investigated in much chemical detail, revealing substantial variation between different cultivars, organs, and growth stages (Racovita et al., 2016; Racovita and Jetter,

2016a, b). Further research suggested that wax alkanes accumulated mostly in the heading and later stages of wheat development, in particular on flag leaf blades, peduncles, and spikes (Wang et al., 2015c). Based on these wax compositional data, wheat likely possesses three independent (branch) pathways leading to primary alcohols, β -diketones, and alkanes.

The acyl reduction pathway in wheat is relatively well understood. *TAA1a* was the first gene verified to function in the synthesis of fatty alcohols, encoding a FAR specifically expressed in wheat anthers (Wang et al., 2002). More recently, eight other FARs encoded by *TaFAR* genes were found involved in biosynthesis of wax alcohols in various wheat organs (Wang et al., 2015d; Wang et al., 2015e; Wang et al., 2016; Chai et al., 2018). Simultaneously, several genes crucial for β -diketone biosynthesis in wheat (and barley) have been identified (Hen-Avivi et al., 2016; Schneider et al., 2016), including a hydrolase that likely generates crucial ketoacyl precursors for β -diketone formation (Hen-Avivi et al., 2016).

Further research is needed to understand how the three different wax biosynthesis pathways differentially affect cuticle composition, structure, and performance in different growth stages and organs. With the limited detailed wax studies on cereal crops, the wheat pathway leading to wax alkanes has not been investigated so far, and the present study hence aimed to isolate and characterize a first enzyme defining it.

In the model plant *Arabidopsis*, CER1 and CER3 are the core enzymes in the biosynthesis of the ubiquitous wax VLC alkanes (Bernard et al., 2012). They form an enzymatic complex catalyzing the conversion of VLC acyl-CoAs to VLC alkanes. Accordingly, *cer1* mutants exhibit glossy phenotype due to dramatic reduction of n-alkanes, secondary alcohols and ketones. A recent study found CER1-like1 also interacts with CER3 and can form alkanes with chain lengths ranging from C₂₅ to C₃₅, but contributing relatively little to the synthesis of alkanes longer than

C₂₉ (Pascal et al., 2019). It is generally assumed that the ubiquitous wax components are formed along similar pathways in other plant species as well. Similar alkane synthesis machinery has been identified in numerous species. For example, based on the sequence similarity to *Arabidopsis CER1*, the *OsGLI-6* antisense-RNA transgenic rice plants showed remarkable reduction of alkanes and aldehydes of the wax composition and severe drought sensitivity compared with wild-type plants, which suggests its function in alkane production (Zhou et al., 2013). In cucumber, the overexpression and RNAi lines of *CsCER1* were generated and their phenotype also confirmed the gene is involved in the alkane production pathway (Wang et al., 2015b). However, this has not been verified in many other species, most importantly in crops. In addition, the accumulation of alkanes is (negatively) correlated with cuticle permeability in *Arabidopsis* and thus increases the drought tolerance of the plants (Bourdenx et al., 2011). Thus, it is crucial to study wheat cuticular alkane formation in order to enable breeding of drought-resistant wheat lines.

Because the *CER1* gene has been particularly well characterized in *Arabidopsis*, we focused on its homologs in wheat. We first queried the wheat genome to identify *CER1* gene candidates and then analyzed the transcriptomes and wax compositions of several wheat organs to select a *CER1* gene likely involved in wax alkane formation. Finally, we tested the biochemical and physiological functions of the encoded protein using gain-of-function and loss-of-function plants, as well as investigating the role of the alkane products in drought resistance.

2.2 MATERIALS AND METHODS

2.2.1 Plant materials and growth conditions

The wheat cv. W87 was used to study the composition of wheat cuticular waxes, to clone candidate genes and characterize them using quantitative real-time PCR (qRT-PCR). Wheat cv. Chinese Spring (CS) nullisomic-tetrasomic lines were used to test the effect of lack-of-function mutations on cuticular wax formation. All plant materials were grown at the experimental farm of Northwest A&F University in Yangling, Shaanxi, during the 2014–2015 and 2015–2016 wheat-growing seasons.

To analyze the expression pattern of *TaCER1-1A* under drought stress, wheat cvs. W87, CS, and W51 were field-grown for 150 days and then transferred to soil in pots in a greenhouse with a photoperiod of 14-hour light:10-hour dark and temperatures between 18°C and 30°C. Once spikes had emerged, plants were deprived of water for 10 days and then harvested for wax analysis or RNA extraction. Meanwhile, control plants were well-watered every 3 days throughout. For other abiotic stress induction assays, wheat cv. W87 was grown in soil in a growth chamber at 24/18°C in 14/10-hour day/night cycles. Four weeks after germination, seedlings were transferred to solutions containing 100 µM abscisic acid (ABA) or 20% polyethylene glycol (PEG), or they were kept in soil at 4°C (day and night) for 24 hours. Leaves were harvested at different time points (0, 1, 2, 4, 6, 12, and 24 hour) after start of each treatment for immediate RNA extraction.

Arabidopsis wild-type (Col-0) and *cer1* mutant (SALK_008544C, obtained from TAIR) seeds were cold-treated at 4°C for 2 days in the dark, then surface sterilized with 75% ethanol for 1 min, washed twice with sterile water, air-dried, then plated on half-strength Murashige and Skoog (MS) agar medium, and germinated in a growth chamber at 22/19°C with photo-periods of 16/8 hour in day/night cycles. After 2 weeks, the seedlings were transferred to soil (Sunshine

Mix 4, Sungro, Canada) and grown under the same conditions as before, with watering every 4 days.

Table 2-1: Primers used in Chapter 2

Category	Primer Name	Primer Sequence (5'-3')
Gene cloning	TaCER1-1A-F1	ATGGCCACAAACCCCGGCCTCTTCA
	TaCER1-1A-R1	TCAAGCCTCAGCAACGGGGCGAAAC
Cloning the promoter of rice OsGL1-1	OsP25850-F	CGTCGTCAGGCAATGCCGCAATG
	OsP25850-R	GATCGCAAGCCCCTCGAGCTTGAT
Subcellular localization of TaCER1-1A	TaCER1-1A-F2	GAGAACACGGGGGACTCTAGAGATGCCGAGCGTGCGGAGGTTCC
	TaCER1-1A-R2	CCCCGCTCGAGATCCTCTAGAGTAGCTTTGGTGAGAGGGACGAA G
Chromosomal localization of TaCER1-1A	TaCER1-1A-F3	CATTTTCAGTACAAAAATCTATTTC
	TaCER1-1A-R3	GTAATCTGCACTGTTGCTTCTAGG
qRT-PCR	TaCER1-1A-F4	GCCCCAAAATACCAGAAGATGC
	TaCER1-1A-R4	CATCTGCGCCTTCTCCGAT
Reference gene	TaActin-F	TGTTGTTCTCAGTGGAGGTTCT
	TaActin-R	CTGTATTTTCCTTTCAGGTGGTG

2.2.2 Isolation of *TaCER1-1A* gene from wheat

Total RNA was isolated from wheat cv. W87 spikes using Trizol reagent (TaKaRa) and treated with DNase I (Promega) to remove genomic DNA contamination. cDNA synthesis was carried out using PrimeScript® reverse transcriptase (TaKaRa) with anchored oligo (dT) 18 primers. A pair of gene specific primers TaCER1-1A-F1 and TaCER1-1A-R1 (Table 2-1) was used to amplify the full-length cDNA sequence of *TaCER1-1A* with KOD DNA polymerase (TOYOBO) as follows: denaturation for 2 min at 94°C, followed by 35 cycles of 10 s at 98°C, 30 s at 58°C,

and 2 min at 68°C, with a final extension for 7 min at 68°C. The PCR product was cloned into pMD™ 18-T vector (TaKaRa) and sequenced to confirm the presence of *TaCER1-1A* cDNA.

2.2.3 Sequence alignment and phylogenetic analysis

The sequences of CER1 proteins previously reported in other plants were retrieved from the National Center for Biotechnology Information (<http://www.ncbi.nlm.nih.gov>) and the Arabidopsis Information Resource (<http://www.arabidopsis.org>). ClustalW was used to perform a multiple sequence alignment, and a phylogenetic tree was constructed with the neighbour-joining method in MEGA7 (Thompson et al., 2003; Tamura et al., 2011).

2.2.4 Cuticular wax extraction and chemical analysis

Seedling and flag leaf blades, flag leaf sheaths, and spikes were harvested and imaged, the surface areas were measured by ImageJ software (<http://rsb.info.nih.gov/ij/>) based on digital images. Plant organs were immersed twice in CHCl₃ (20 ml) for 1 min, then 20 µg of n-tetracosane (C₂₄ alkane) was added as an internal standard, and the wax mixtures were concentrated under a stream of nitrogen and then transferred to GC vials. The extracted waxes were treated with 50 µl pyridine (Alfa Aesar) and 50 µl *bis*-N,O-trimethylsilyltrifluoroacetamide (BSTFA, Fluka) at 70°C for 60 min, and then excessive reagents were evaporated under a nitrogen stream (Leide et al., 2011; Zhang et al., 2013; Wang et al., 2015e). Finally, the samples were dissolved in 500 µl CHCl₃ for analysis by gas chromatography-mass spectrometry (GC-MS) using a GCMS-QP2010 system (Shimadzu) with Rxi-5ms column (length 30 m, id 0.25 mm, film thickness 0.25 µm) as follows: 2 min at 50°C, increased by 20°C min⁻¹ to 200°C and held for 2 min, further increased by 5°C min⁻¹ to 280°C and held for 8 min, with final injector and detector temperatures set to 200°C. The wax compounds were identified by comparing their mass spectra with those of authentic standards or with reference spectra and quantitated by

comparing peak areas with that of the internal standard. The total amount of cuticular wax was expressed per unit of extracted surface area.

2.2.5 Scanning electron microscopy analysis

To observe epicuticular wax crystals of wheat, cv. W87 leaves were collected at the seedling and heading stages, cut into segments, and dried at 37°C for 4 days. Leaf pieces of approximately 5 × 5 mm were mounted on specimen stubs and coated with superfine gold particles using 90-s bursts from a sputter coater (Hitachi E-1045, Japan). Images were collected on a Hitachi S-4800 microscope at an accelerating voltage of 10 kV.

2.2.6 Overexpression of *TaCER1-1A* in rice (*Oryza sativa* L. ssp. japonica cv. Zhonghua11)

For heterologous expression in rice, the full-length cDNA of wheat cv. W87 *TaCER1-1A* was inserted into the *XcmI* site of a pCXS vector, resulting in the construct *pCXS-TaCER1-1A*. A 1,946-bp genomic fragment of the *OsGLI-1* promoter was isolated from rice cv. Zhonghua11 by using primer pair OsP25850-F and OsP25850-R (Table 2-1) and inserted upstream of the *TaCER1-1A*. The rice *OsGLI-1* gene is a *CER3* homolog highly expressed in leaf epidermal cells (Qin et al., 2011). The construct was introduced into *Agrobacterium tumefaciens* strain EHA105, which was used to transform rice calli generated from mature seeds of rice cv. Zhonghua11. The transgenic plants were screened with 50 mg L⁻¹ hygromycin and confirmed by PCR. T₁ plants were used to analyze the wax composition. Plants carrying the empty pCXS vector were analyzed as a negative control. All transgenic rice plants were grown in a greenhouse under ambient conditions as mentioned before.

2.2.7 Overexpression of *TaCER1-1A* in Arabidopsis

The full-length cDNA of wheat cv. W87 *TaCER1-1A* was inserted into the *XcmI* site of a pCXS vector under the control of Cauliflower mosaic virus 35S promoter. The expression plasmid pCXS-*TaCER1-1A* or empty vector pCXS was introduced into *A. tumefaciens* strain GV3101, which was used to transform Arabidopsis (wild type Col-0 or *cer1*) plants by floral dipping (Clough and Bent, 1998). Transgenic plants were selected on hygromycin half MS medium and confirmed by PCR, and T₂ plants were grown in a growth chamber as described previously and used for wax composition analysis.

2.2.8 Subcellular localization of *TaCER1-1A* in Arabidopsis mesophyll protoplasts

To generate *pro35S:TaCER1-1A-GFP*, the full-length coding region of *TaCER1-1A* without stop codon was amplified by PCR with a pair of specific primers TaCER1-1A-F2 and TaCER1-1A-R2 (Table 2-1), and the product was cloned into the PA7-GFP vector. The fusion construct and ER marker mCherry-HDEL (ER retrieval tetrapeptide) were co-transformed into Arabidopsis protoplasts by PEG-mediated transfection as described before (Yoo et al., 2007). Fluorescence signal was imaged with a Leica TCS-SP4 confocal microscope. The TaCER1-1A-GFP images were obtained with excitation at 488 nm and emission collected at 525 nm. And mCherry-HDEL images were obtained with the excitation at 561 nm and emission collected at 595–625 nm.

2.2.9 Analysis of transcript levels by qRT-PCR

qRT-PCR was used to investigate *TaCER1-1A* transcript levels in seedling leaf blades, flag leaf blades, flag leaf sheaths, peduncles, glumes, awns, pistils, and roots of wheat cv. W87. All organs were sampled from plants at heading stage, except for seedling leaf blades collected from

40-day-old seedlings. Total RNA was extracted and treated following the method described in section 2.2. qRT-PCR was carried out in a volume of 25 µl with SYBR Premix Ex Taq™ Kit (TaKaRa), and gene specific primer pairs TaCER1-1A-F4, TaCER1-1A-R4, and TaActin-F, TaActin-R on a CFX96 RT-PCR detection system (BioRad) with thermal cycles as follows: one cycle of 60 s at 95°C, followed by 40 cycles of 15 s at 95°C, 15 s at 58°C, and 45 s at 72°C, and completed with a melting curve analysis programme. Amplification efficiency was tested for all primer pairs and confirmed to be between 90 and 110%. Three biological replicates were analyzed for each organ. The relative expression levels were calculated by the $2^{-\Delta\Delta C_t}$ method (Livak and Schmittgen, 2001), normalized against the wheat *Actin* gene (AB181991).

2.2.10 Epidermal permeability analysis

Leaf surface permeability was determined by chlorophyll leaching and water loss assays. Transgenic and wild-type rice plants were grown in the greenhouse for 12 weeks. For chlorophyll leaching tests, the method described by Lolle et al (1998) was followed. Plants were kept in the dark and immersed in ultrapure water for 1 hr. Then leaves were collected and immersed in 80% ethanol in the dark, and the amount of chlorophyll extracted was quantified using a U-60 spectrophotometer at 647 and 664 nm every 60 min for 12 hours. The amounts of chlorophyll leached were expressed as percentages of the chlorophyll extracted at 12 hours. The water loss rate tests were performed as described by Kosma et al (2009) with minor modification. The leaves were initially soaked in water in the dark for 1 hour to ensure the closure of stomata, and then leaf weights were measured every 60 min for 12 hours.

2.3 Results

In the present study, we first compared transcriptome and wax profiling data to identify a wheat gene potentially encoding an alkane-forming CER1 enzyme. To characterize this gene, we then tested its spatial expression patterns, biochemical function, and role in stress resistance.

2.3.1 Identification of a wheat *CER1* candidate gene

2.3.1.1 Wheat wax composition and morphology

To identify genes likely involved in wax alkane biosynthesis, the compositions of wax mixtures on various wheat organs were compared with corresponding transcriptome profiles of candidate genes. For compositional analysis, wax mixtures were extracted from intact surfaces of various organs of the wheat cultivar W87 and analyzed using GC-MS. Seedling leaf blades had a relatively low total wax load ($5.61 \mu\text{g cm}^{-2}$), compared with flag leaf blades ($12.13 \mu\text{g cm}^{-2}$) and flag leaf sheaths ($12.59 \mu\text{g cm}^{-2}$; Table 2-2). Based on specific leaf areas reported for various wheat cultivars ($500\text{- to }600\text{- cm}^2 \text{ g}^{-1}$ dry weight; (Equiza et al., 2001)), the latter leaf wax coverages correspond to relative wax quantities of $6000\text{- to }7000\text{- } \mu\text{g g}^{-1}$ dry weight. In comparison, the wheat cultivar W87 spikes accumulated relatively low wax amounts of $392 \mu\text{g g}^{-1}$ dry weight. The wax coverage of the spikes could not be determined on a per-surface-area basis, due to the complex and irregular geometry of this organ.

The wax mixture on seedling leaf blades consisted mainly of primary alcohols, whereas the wax on flag leaf sheaths was dominated by β -diketones. Flag leaf blade wax had an intermediate composition, with equally high concentrations of primary alcohols and β -diketones, and spike wax was characterized by high amounts of alkanes and β -diketones. Fatty acids, aldehydes, and alkyl esters were found on all organs sampled.

Further analysis of the chain length distributions within compound classes showed that the alkane fractions of all wheat wax mixtures comprised odd-numbered homologs ranging from C₂₅ to C₃₃ (Figure 2-1). The alkane chain length profiles varied strongly between organs, with fairly even distributions peaking at C₂₉ on flag leaf blades and sheaths, predominantly C₂₉ and C₃₁ on spikes, and a bimodal distribution around C₂₇ and C₃₃ on seedling leaf blades.

Table 2-2: Cuticular wax compositions and amounts in different organs of wheat cv. W87

Wax load on leaf blade, flag leaf blade and flag leaf sheath were expressed as $\mu\text{g cm}^{-2}$ of surface area, and the wax amount of spike was expressed as μg of wax per g of spike (dry weight). Values represent means of three replicates. Error bars = SD. ND, compound class was not detected. Trace, compound class was detected but could not be quantified accurately.

Compound class	Measurement	Seedling leaf blade	Flag leaf blade	Flag leaf sheath	Spike
Fatty acids	Percentage	1.21±0.09	1.95±0.03	0.97±0.04	2.62±0.43
	Amount	0.07±0.00	0.24±0.00	0.12±0.01	10.18±0.93
Primary alcohols	Percentage	79.20±7.24	30.36±1.47	4.12±1.78	7.30±0.56
	Amount	4.66±0.45	3.68±0.19	0.53±0.26	28.51±0.68
Alkyl esters	Percentage	0.04±0.00	0.50±0.02	0.38±0.02	0.99±0.17
	Amount	0.04±0.00	0.06±0.00	0.05±0.01	3.93±0.94
Aldehydes	Percentage	5.55±0.89	8.58±0.22	2.51±0.95	2.75±0.16
	Amount	0.32±0.03	1.04±0.03	0.32±0.14	10.76±0.38
Alkanes	Percentage	3.39±0.30	11.94±0.68	5.05±0.34	29.28±1.01
	Amount	0.20±0.01	1.45±0.08	0.63±0.06	114.59±5.83
β -Diketones	Percentage	ND	37.45±1.49	74.42±3.99	34.09±1.43
	Amount	ND	4.55±0.17	9.34±0.52	133.89±15.85
Hydroxy- β -diketones	Percentage	ND	Trace	4.88±0.39	14.62±2.31
	Amount	ND	Trace	0.61±0.07	57.76±13.33
Unidentified	Percentage	5.33±0.74	9.23±0.49	7.68±1.32	8.34±1.37

	Amount	0.31±0.03	1.12±0.06	0.97±0.24	32.40±2.64
Total	Amount	5.61±0.50	12.13±0.04	12.59±1.03	392.01±32.15

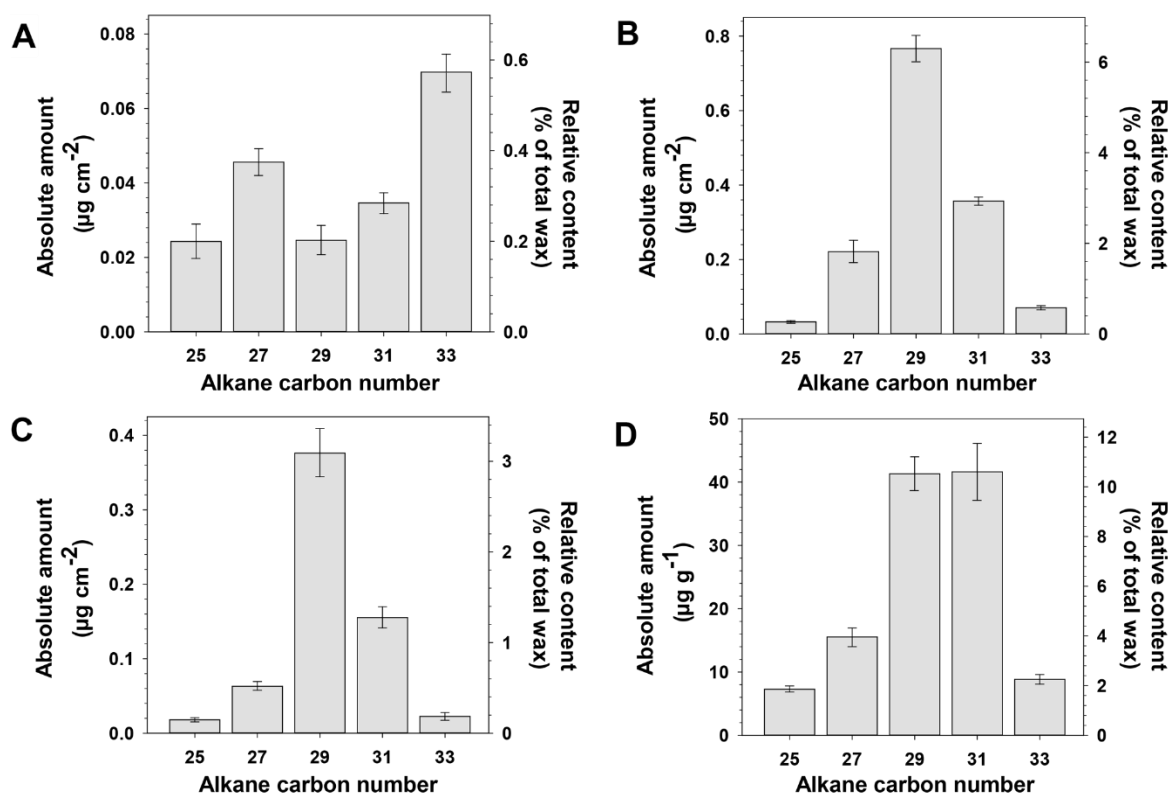


Figure 2-1: Composition of wax alkanes on different organs of wheat cv. W87

A) Seedling leaf blades. B) flag leaf blades. C) Flag leaf sheathes. D) Spikes. Values represent means of three replicates. Error bars = SD.

To further characterize the different organ surfaces of wheat cv. W87, epicuticular wax crystals on them were visualized using scanning electron microscopy. Both the adaxial and the abaxial sides of seedling leaf blades displayed a similar microrelief, with a dense network of wax crystals in the form of platelets (Figure 2-2 A–D). In contrast, the abaxial side of flag leaves was covered with wax tubules (Figure 2-2 G–H), whereas the corresponding adaxial surface had

platelet-shaped wax crystals (Figure 2-2 E-F). The spike and flag leaf sheath surfaces were also covered with wax tubules (Figure 2-2 I-L).

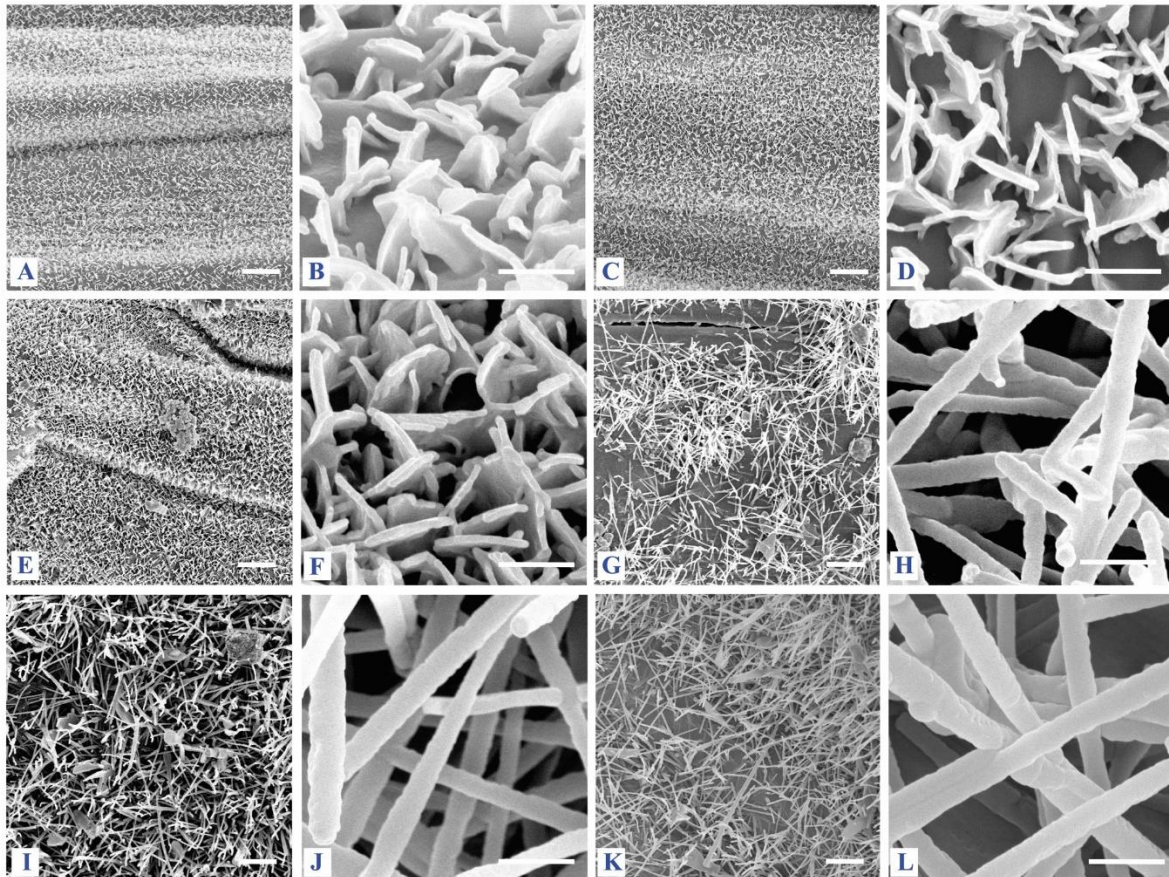


Figure 2-2: Ultrastructure of epicuticular wax crystals on different organs of wheat cv. W87

Representative scanning electron micrographs of: (A-B) the adaxial side of fourth-leaf blades, (C-D) the abaxial side of fourth-leaf blades, (A-D) were from seedling leaf blades, (E-F) the adaxial side of flag leaf blades, (G-H) the abaxial side of flag leaf blades, (I-J) the abaxial side of flag leaf sheaths, (K-L) the abaxial side of spike glumes. Images A, C, E, G, I and K were taken at $\times 2,000$ magnification (scale bars = $2\ \mu\text{m}$), and images B, D, F, H, J and L at $\times 30,000$ magnification (scale bars $0.4\ \mu\text{m}$).

2.3.1.2 Transcriptome analysis of wheat *CER1* homologs

To identify wheat genes involved in wax alkane formation, we first queried the wheat genome (<https://urgi.versailles.inra.fr/blast/blast.php>) with the Arabidopsis CER1 amino acid sequence (AT1G02205). Nine potential CER1 homologs were found, which were located on the wheat chromosomes 1, 4, and 6 in each of the three wheat genomes (A, B, and D). They were hence designated *CER1-1A/B/D*, *CER1-4A/B/D*, and *CER1-6A/B/D*. Inspection of our previous transcriptome data showed that *CER1-1A* was highly expressed overall and particularly in flag leaf blades and spikes (Figure 2-3A; (Wang et al., 2016)). Thus, *CER1-1A* was the CER1 homolog most highly expressed in those organs accumulating the highest levels of wax alkanes, and it was therefore selected as the best candidate for our further investigations into alkane biosynthesis in wheat.

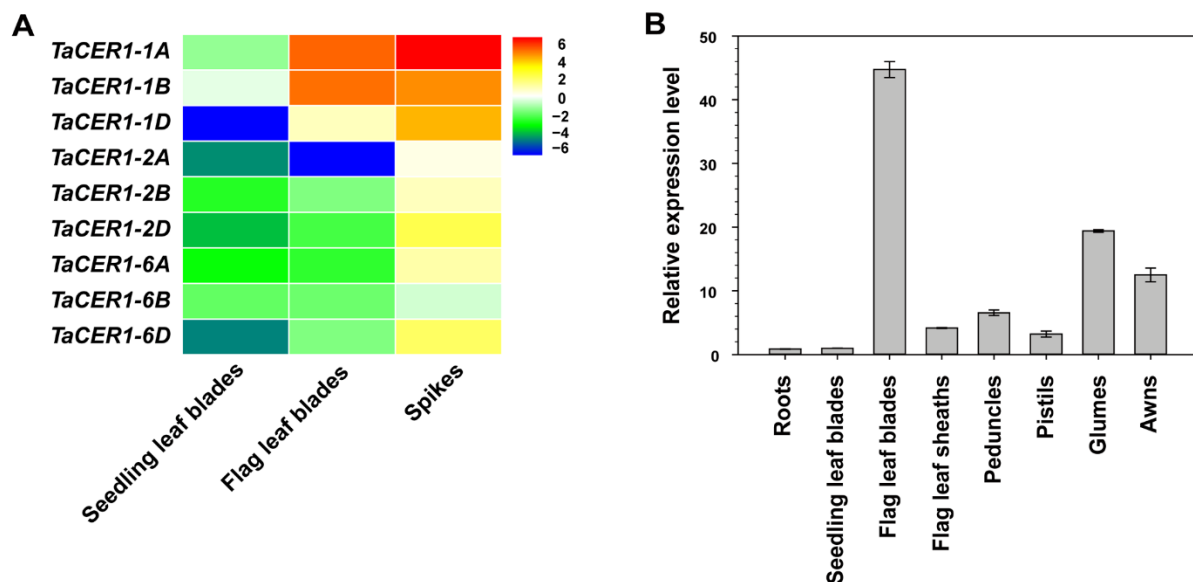


Figure 2-3: *CER1* expression profile from different organs of wheat cv. W87.

A) Heat map for expression levels of nine wheat *CER1* candidate genes in different organs of wheat cv. W87. The relative expression levels were determined based on previously published

transcriptome data calculated as $\text{Log}_2^{\text{(FPKM}+0.01\text{)}}$. B) qRT-PCR analysis of *TaCER1-1A* in various organs of wheat cv. W87. *TaCER1-1A* expression levels were normalized against *TaActin* and plotted relative to seedling leaf blades. Spikes were separated into glumes and awns. Values represent means of three replicates. Error bars = SD.

2.3.1.3 Sequence analysis of the *TaCER1-1A* gene

Based on the reference genome of wheat cv. CS, *TaCER1-1A* is predicted to span 10379 bp of genomic DNA. To clone *TaCER1-1A* from wheat cv. W87, gene was amplified from spikes samples by PCR using primers matching the terminal regions of the corresponding open reading frame (ORF) in the reference genome of wheat cv. CS. The *TaCER1-1A* cDNA (NCBI accession number: MK214738) shared 99.83% sequence identity with the corresponding ORF on chromosome 1A of the wheat cv. CS reference genome. In contrast, the *TaCER1-1A* cDNA had only 95.54% and 96.20% identity with the homologous genome sequences from wheat chromosomes 1B and 1D, respectively, overall confirming that *TaCER1-1A* is located on chromosome 1A. The full-length cDNA of *TaCER1-1A* was found to be 1946 bp, with 68, 1818, and 60 bp spanning the 5'-UTR, ORF, and 3'-UTR, respectively. It contained eight exons (Figure 2-4A), together encoding 605 amino acids. The *TaCER1-1A* sequence comprises an N-terminal fatty acid hydroxylase domain, including three His-rich motifs (HX3H, HX2HH, and HX2HH), and a C-terminal WAX2 domain thought to be required for alkane biosynthesis (Figure 2-4B; (Bernard et al., 2012)).

To further assess whether the wheat cv. W87 *TaCER1-1A* sequence is suitable for further investigations into wax alkane biosynthesis, a phylogenetic analysis comparing it with homologous genes from other species was conducted. It revealed two clades, one comprising exclusively CER1 sequences and the other one only CER3s, each of them consisting of two

subgroups defined by monocot or dicot species (Figure 2-4C). Thus, *TaCER1-1A* grouped in the monocot subclade together with *OsGL1-5* and in the larger *CER1* clade together with *AtCER1*. Overall, our analysis of the *TaCER1-1A* sequence predicted that this gene may indeed function in alkane biosynthesis.

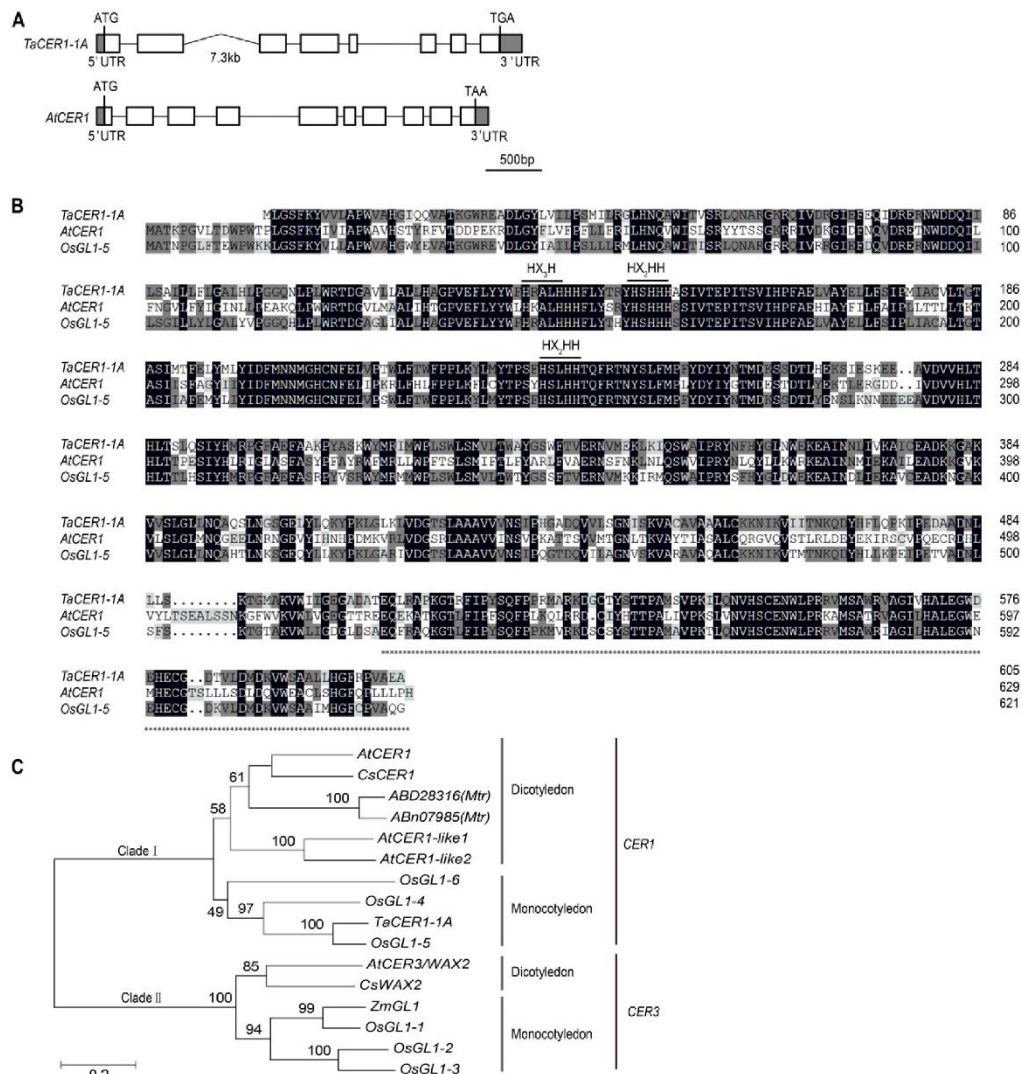


Figure 2-4: Sequence and phylogenetic position of *TaCER1-1A*

A) Structure analysis of the *TaCER1-1A* and *AtCER1* genes. White boxes, grey boxes and black lines represent exons, UTRs and introns, respectively. B) Amino acid sequence alignment of

TaCER1-1A with AtCER1 and OsWDA1. Three conservative histidine-rich motifs are highlighted by text above the sequences, and the conserved C-terminal WAX2 domain by a row of asterisks below the sequences. C) Phylogenetic analysis of TaCER1-1A and its homologs in various species. Accession numbers are: *Arabidopsis thaliana CER1*; AT1G02205; *Cucumis sativus CER1*, Csa024936; *Medicago truncatula CER1* ABD28316 and ABN07985; *A. thaliana CER1-like1*, At1g02190; *A. thaliana CER1-like2*, At2g37700; *Oryza sativa GLI-6*, LOC_Os02g56920; *O. sativa GLI-5*, LOC_Os10g33250; *O. sativa GLI-4*, LOC_Os02g40784; *A. thaliana CER3*, AT5G57800; *C. sativus WAX2*, Csa020530; *O. sativa GLI-3*, LOC_Os06g44300; *O. sativa GLI-2*, LOC_Os02g08230; *O. sativa GLI-1*, LOC_Os09g25850; *Zea mays GLI*, ACG35856.

2.3.2 Spatial expression pattern of *TaCER1-1A*

To assess the spatial distribution of *TaCER1-1A*, its organ-specific expression and subcellular localization were investigated. First, qRT-PCR analyses showed *TaCER1-1A* transcript levels widely varying among wheat cv. W87 organs (Figure 2-3b), with highest expression in flag leaf blades and substantial transcript levels also in glumes and awns (the leaf-like structure that below a spikelet in the inflorescence). In contrast, only modest expression was found in flag leaf sheaths, peduncles, and pistils and very little expression in seedling leaf blades as well as roots. Overall, the qRT-PCR results thus confirm our original findings on the organ-specific transcriptome data.

To determine the subcellular localization of the TaCER1-1A protein, its C-terminus was tagged with Green fluorescent protein (GFP), and the fusion protein transiently expressed in *Arabidopsis* protoplasts along with the ER marker mCherry-HDEL. The resulting cells showed complete colocalization between TaCER1-1A-GFP and the marker (Figure 2-5), demonstrating that the TaCER1-1A protein resides in the ER.

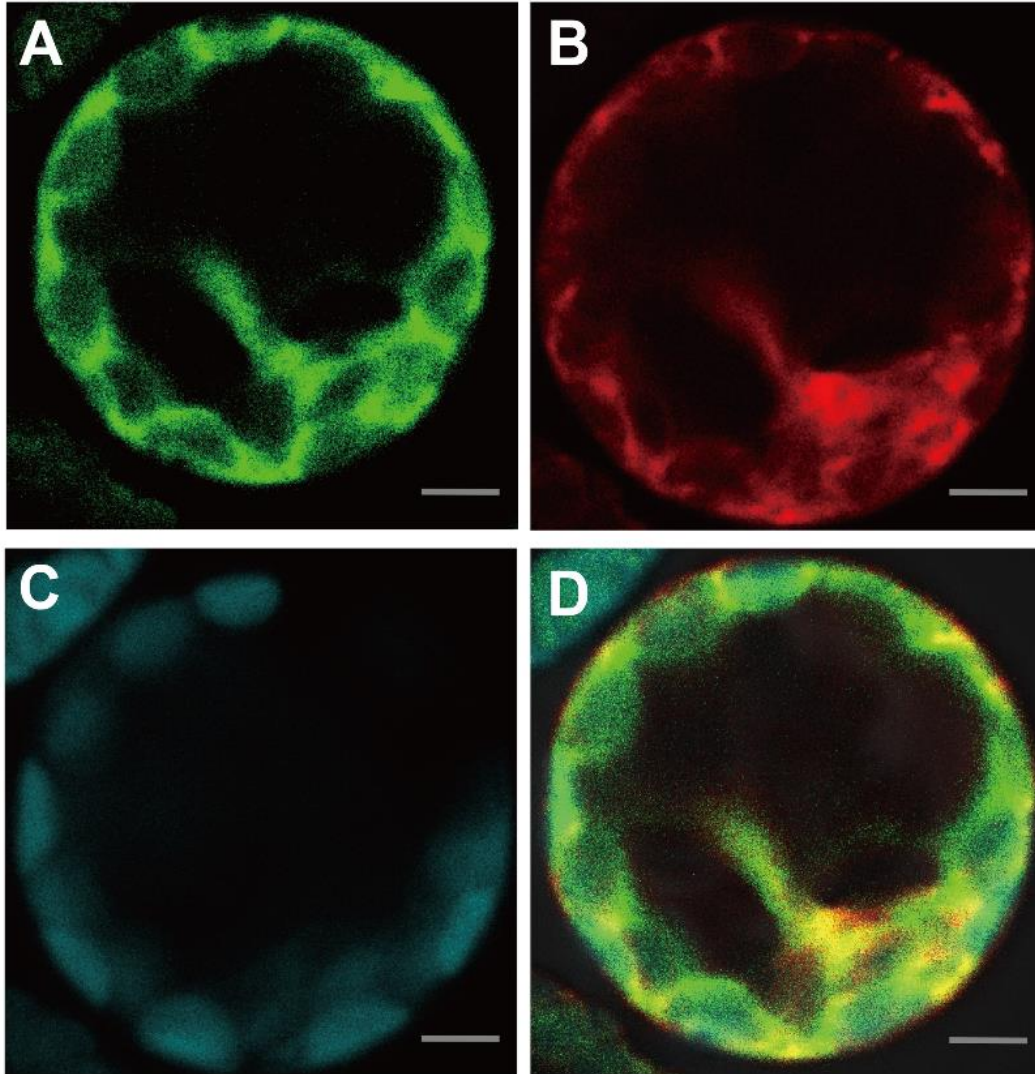


Figure 2-5: TaCER1-1A localized to ER

Subcellular localization of TaCER1-1A in Arabidopsis protoplasts expressing *35S:TaCER1-1A-GFP*. A) GFP fluorescence, B) ER marker mCherry-HDEL, C) chlorophyll autofluorescence signal, and D) merged image of A, B and C. Scale bars = 5 μm .

2.3.3 Functional characterization of *TaCER1-1A*

To test the involvement of *TaCER1-1A* in alkane formation, both loss-of-function and gain-of-function approaches were taken. In particular, the wax mixtures of a wheat chromosome

substitution line lacking *TaCER1-1A* as well as rice and Arabidopsis lines expressing the gene were analyzed.

2.3.3.1 Wax analysis of nullisomic-tetrasomic substitution lines

Nullisomic-tetrasomic substitution lines of CS were used to assess the effect of a loss of *TaCER1-1A*. To this end, first, a pair of gene-specific primers (Table 1-1) was used to test the presence of the *TaCER1-1A* gene in a set of 11 wheat substitution lines each lacking another chromosome. As expected, all the lines having chromosome 1A possessed *TaCER1-1A*, whereas the line (N1AT1B) without chromosome 1A lacked the gene (Figure 2-6A). Therefore, we used this line to determine effects of the *TaCER1-1A* deletion on wax composition, focusing on flag leaf blade wax because it is especially rich in wax alkanes.

Wax of line N1AT1B contained $1.16\text{-}\mu\text{g cm}^{-2}$ alkanes, representing an approximately 30% reduction from the wild-type alkane load of $1.68\text{ }\mu\text{g cm}^{-2}$ (Figure 2-6B). The substitution line and the wild type contained the same five alkane homologs in similar relative distributions, but the substitution line had significantly reduced amounts of the C₃₃ alkane relative to the wild type (Figure 2-6C). Overall, the chain length distribution within the alkane fraction was thus shifted slightly towards shorter chains in the substitution line lacking *TaCER1-1A*. All other compound classes present in flag leaf blade wax had quantities not differing from wild type (Figure 2-6B). These results confirm that the wheat TaCER1-1A enzyme is involved in wheat wax alkane biosynthesis.

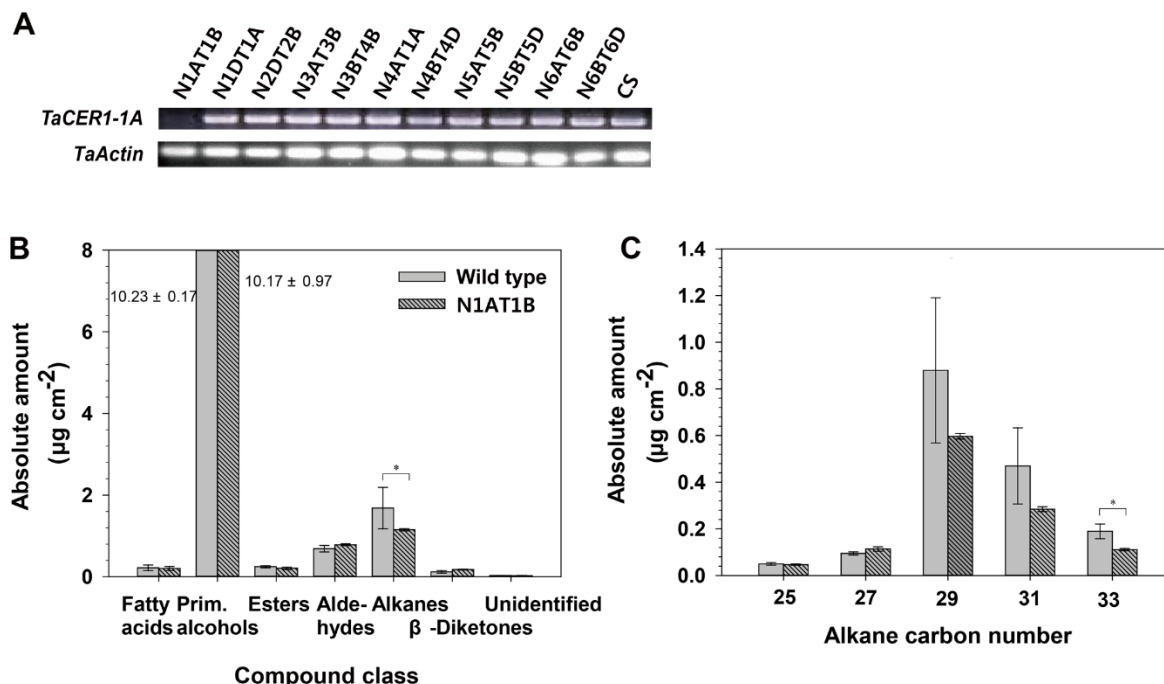


Figure 2-6: *TaCER1-1A* expression profiles and composition of wax alkanes in wheat cv. CS wild type and various nullisomic-tetrasomic lines

A) RT-PCR amplification of *TaCER1-1A* transcript in the flag leaf blades of wheat cv. CS and nullisomic-tetrasomic lines each lacking one chromosome. The lines are designated “NxxTyy” to first indicate the missing chromosome (xx = 1A, 1D, 2D, etc) and then the doubled chromosome replacing it (yy = 1B, 1A, 2B, etc). N1AT1B is a *TaCER1-1A* knock-out line based on (A). B) Compound class loads within the wax mixtures on the flag leaf blades of cv. CS and the nullisomic-tetrasomic line N1AT1B lacking chromosome 1A. C) Composition of wax alkanes on the flag leaf blades of cv. CS and the nullisomic-tetrasomic line N1AT1B lacking chromosome 1A (at jointing stage). Values represent means of three replicates. Error bars = SD, Significant differences are marked with asterisks (t-test: *P<0.05; **P<0.01).

2.3.3.2 Heterologous expression of *TaCER1-1A* in Arabidopsis and rice

To further test the biochemical activity of *TaCER1-1A*, gain-of-function mutants of Arabidopsis overexpressing the wheat gene were generated. A resulting *TaCER1-1A* overexpression line had a leaf wax load of 1.63 μg cm⁻², increased by more than two-fold relative to the empty-vector control (Figure 2-7A). The amount of alkanes was increased from 0.34 ± 0.04 μg cm⁻² in the

control to $1.19 \pm 0.10 \mu\text{g cm}^{-2}$ in the overexpressing line. In both the overexpression line and empty-vector control, the alkane fraction was strongly dominated by homologs with odd-numbered chain lengths, with only traces of even-numbered homologs present. Amounts of all homologs were significantly increased upon expression of *TaCER1-1A*, in the series of n-alkanes and iso-branched alkanes alike (Figure 2-7B). Interestingly, also the alkenes accumulated to higher concentrations in the overexpressor ($0.034 \pm 0.0038 \mu\text{g cm}^{-2}$) than in the control ($0.005 \pm 0.0003 \mu\text{g cm}^{-2}$), with similar ratios of C₃₅ and C₃₇ homologs in both wax mixtures. All other leaf wax compound classes, including fatty acids, n-primary alcohols, aldehydes, and sterols, were found at concentrations significantly decreased relative to control plants (Figure 2-7A).

The biochemical function of *TaCER1-1A* was further assessed by complementing the *Arabidopsis cer1* mutant (SALK_008544C) with *TaCER1-1A* under the control of Cauliflower mosaic virus 35S promoter. One line in the T2 generation of the *TaCER1-1A* transgenics was used for detailed wax analyses, in comparison with wild type and the *cer1* mutant harboring the empty vector. The *TaCER1-1A* expressor had a leaf wax load of $0.38 \pm 0.03 \mu\text{g cm}^{-2}$, intermediate between those of the empty-vector control and wild type (0.30 ± 0.02 and $0.73 \pm 0.01 \mu\text{g cm}^{-2}$, respectively). All the alkanes detected, with odd-numbered chain lengths between C₂₅ and C₃₅, had amounts in *TaCER1-1A* transgenic plants significantly increased over those of the empty-vector control (Figure 2-8A). Expression of the wheat gene thus complemented the *Arabidopsis* mutant phenotype across the entire range of alkane chain lengths. However, *TaCER1-1A* expression only partially restored the wild-type alkane levels, with the three major alkane homologs C₂₉, C₃₁, and C₃₃ accumulating to only less than half of the wild-type

amounts. In contrast, C27 alkane was found at higher concentration in the overexpressor wax than in the wild type. The *TaCER1-1A* overexpressing line also had the macroscopic appearance of inflorescence stems partially restored from the glossy appearance of the *cer1* mutant to the glaucous phenotype of the wild type (Figure 2-8B). Furthermore, the *cer1* conditional male-sterile phenotype was partially rescued in *TaCER1-1A* transgenic plants, as indicated by slightly increased silique length compared with *cer1* (data not shown).

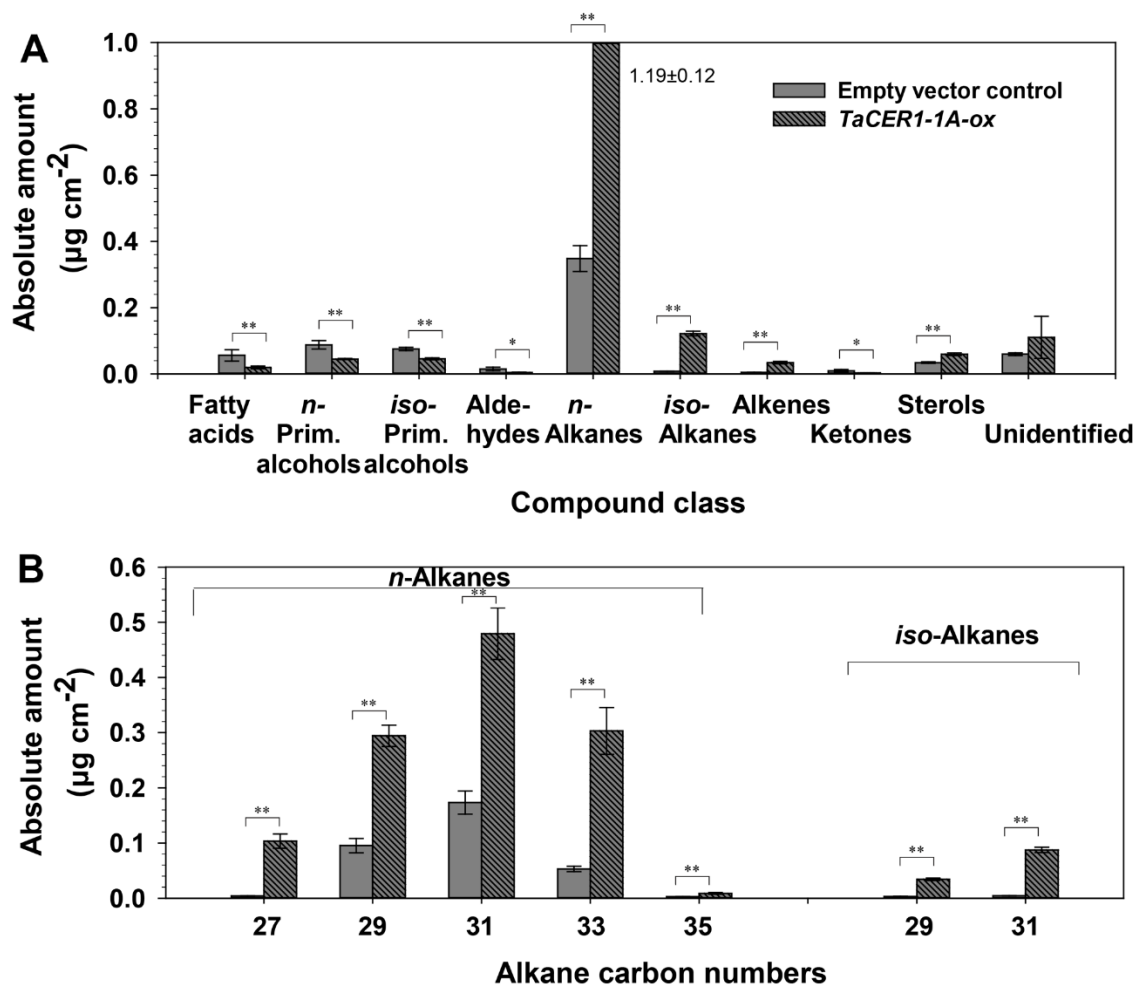


Figure 2-7: Composition of cuticular waxes on Arabidopsis leaves expressing *TaCER1-1A*

A) Compound class loads within the wax mixtures on leaves of transgenic lines expressing *TaCER1-1A* or harboring empty vector. B) Composition of wax alkanes on leaves of transgenic

lines expressing *TaCER1-1A* or harboring empty vector. Values represent means of three replicates. Error bars = SD. Significant differences are marked with asterisks (t-test: * $P < 0.05$; ** $P < 0.01$).

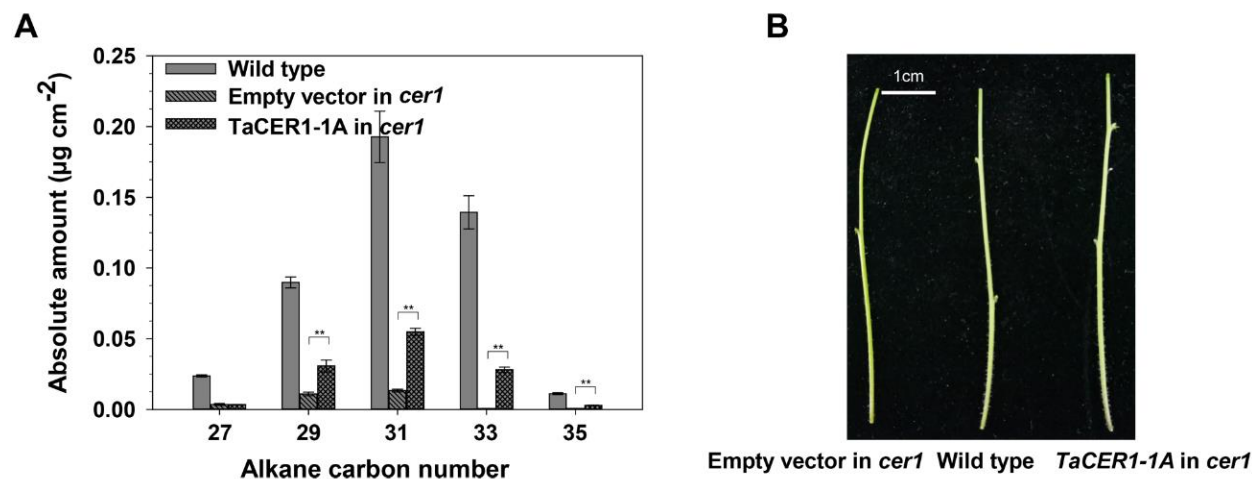


Figure 2-8: *TaCER1-1A* complementation assay in the *Arabidopsis cer1* mutant

A) Composition of wax alkanes on leaves of *cer1* plants expressing *35S:TaCER1-1A* or empty vector, B) Macroscopic appearance of *cer1* inflorescence stems expressing *35S:TaCER1-1A* or empty vector, compared with *Arabidopsis* wild type. Values represent means of three replicates. Error bars = SD. Significant differences are marked with asterisks (t-test: * $P < 0.05$; ** $P < 0.01$).

Finally, the biochemical function of *TaCER1-1A* in alkane biosynthesis was tested by overexpressing the gene in rice, under the transcriptional control of rice *OsGLI-1* promoter (Qin et al., 2011). No significant morphological variations were observed between lines carrying *TaCER1-1A* or empty vector. Three lines (*TaCER1-1A*-ox5, *TaCER1-1A*-ox12, and *TaCER1-1A*-ox21) were randomly selected from 20 independent transgenic events for detailed leaf wax analyses using GC-MS. The transgenic lines harboring *TaCER1-1A* had wax compositions very similar to those of empty-vector controls, with primary alcohols and aldehydes as major components, accompanied by alkanes, fatty acids, and esters. Among these compound classes,

only the alkanes had concentrations differing significantly between *TaCER1-1A* overexpressors and control (Figure 2-9A). In all three overexpressing lines, all the alkane homologs with odd-numbered chain lengths between C₂₅ and C₃₃ accumulated to levels at least two-fold those of the control (Figure 2-9B).

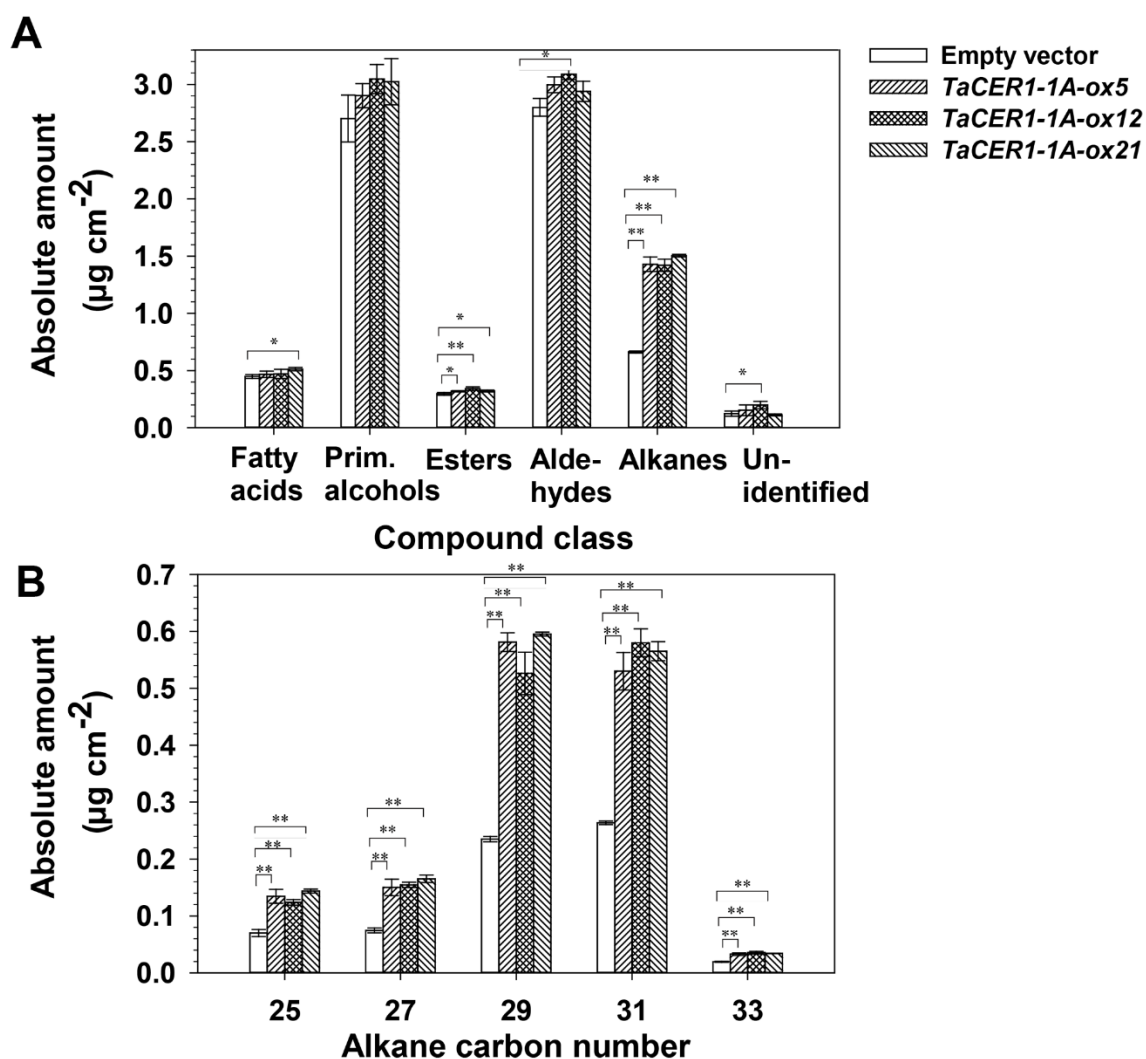


Figure 2-9: Composition of cuticular waxes on rice leaves expressing *TaCER1-1A*

A) Compound class loads within the wax mixtures on fourth-leaf blades of transgenic lines expressing *TaCER1-1A* or harboring empty vector. B) Composition of wax alkanes on fourth-

leaf blades. Values represent means of three replicates. Error bars = SD. Significant differences are marked with asterisks (t-test: * $P < 0.05$; ** $P < 0.01$).

2.3.4 Testing the role of *TaCER1-1A* in stress resistance

The main function of cuticular wax is to restrict nonstomatal water loss and, thus, contribute to drought tolerance. We therefore sought to test the role of *TaCER1-1A* in the overall resistance of plants against drought stress and the underlying barrier properties of the organ surface.

2.3.4.1 Effect of *TaCER1-1A* on surface barriers of Arabidopsis and rice leaves

To test whether increases in *TaCER1-1A* expression and wax alkane production can impact surface barrier properties, rice and Arabidopsis lines overexpressing the wheat gene (see above) were further characterized with respect to their leaf surface permeability. Leaves of the rice line *TaCER1-1A-ox5* were selected for this experiment and found to display lower water loss rates than corresponding wild type leaves, with loss of approximately 60% of the total water from the transgenic compared to approximately 70% loss from control leaves after 12 hr (Figure 2-10A). Further assays showed that the *TaCER1-1A-ox5* overexpressor leached chlorophyll less rapidly from intact leaves than the empty-vector control, up to 56% for the overexpressor instead of 83% for the control after 10 hr (Figure 2-10B). Overall, these results show that expression of *TaCER1-1A*, and the resultant increase of cuticular wax alkanes (see above), enhanced the leaf surface barrier properties of rice. Similar results were also observed for Arabidopsis transgenics (data not shown), leading to higher drought resistance of the line over-expressing *TaCER1-1A* compared with empty-vector control (Figure 2-11).

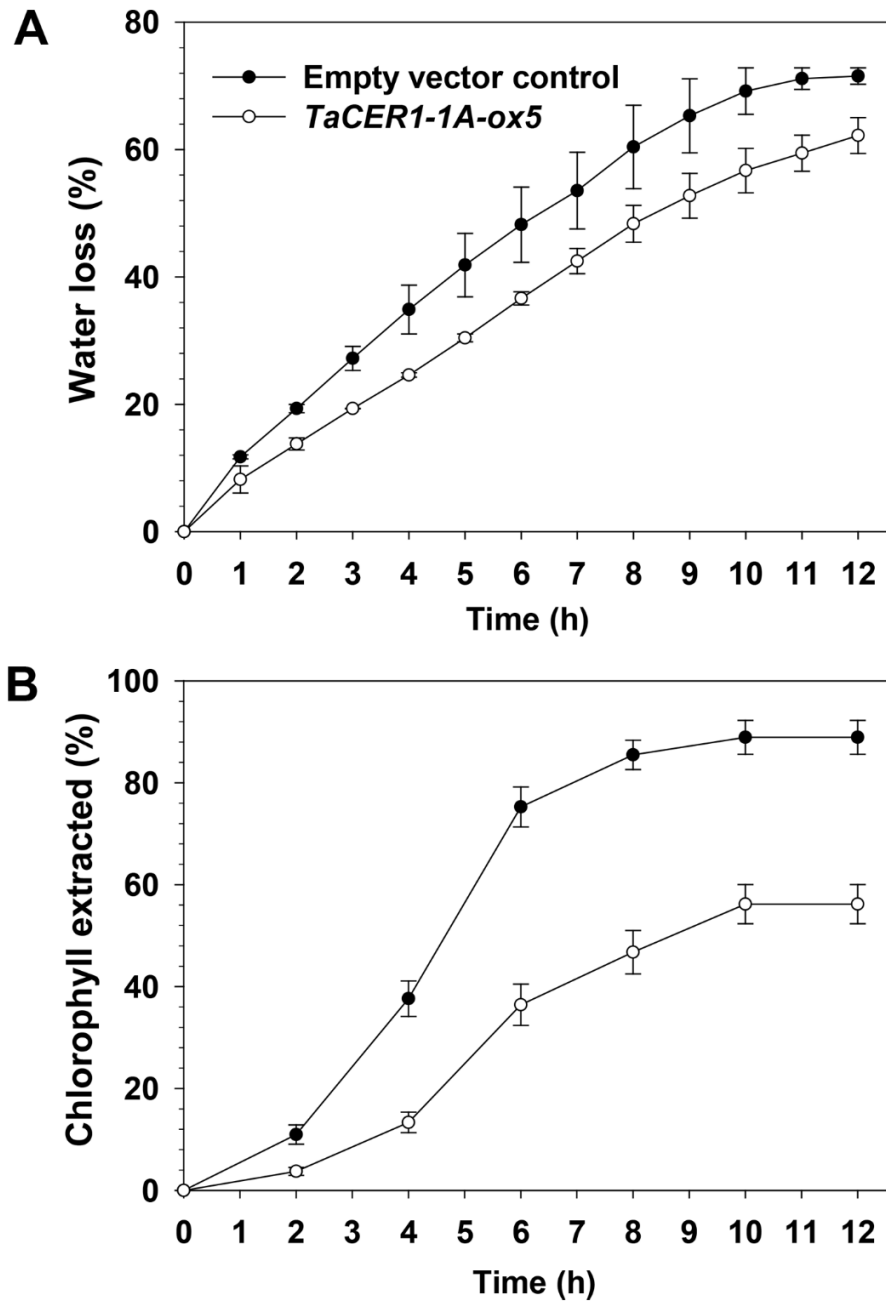


Figure 2-10: Surface permeability of rice leaves expressing *TaCER1-1A*

A) Water loss rates and B) chlorophyll extraction yields were assessed using intact leaves of 12-week-old rice plants overexpressing *TaCER1-1A* or harboring empty vector. Values represent means of three replicates. Error bars = SD.

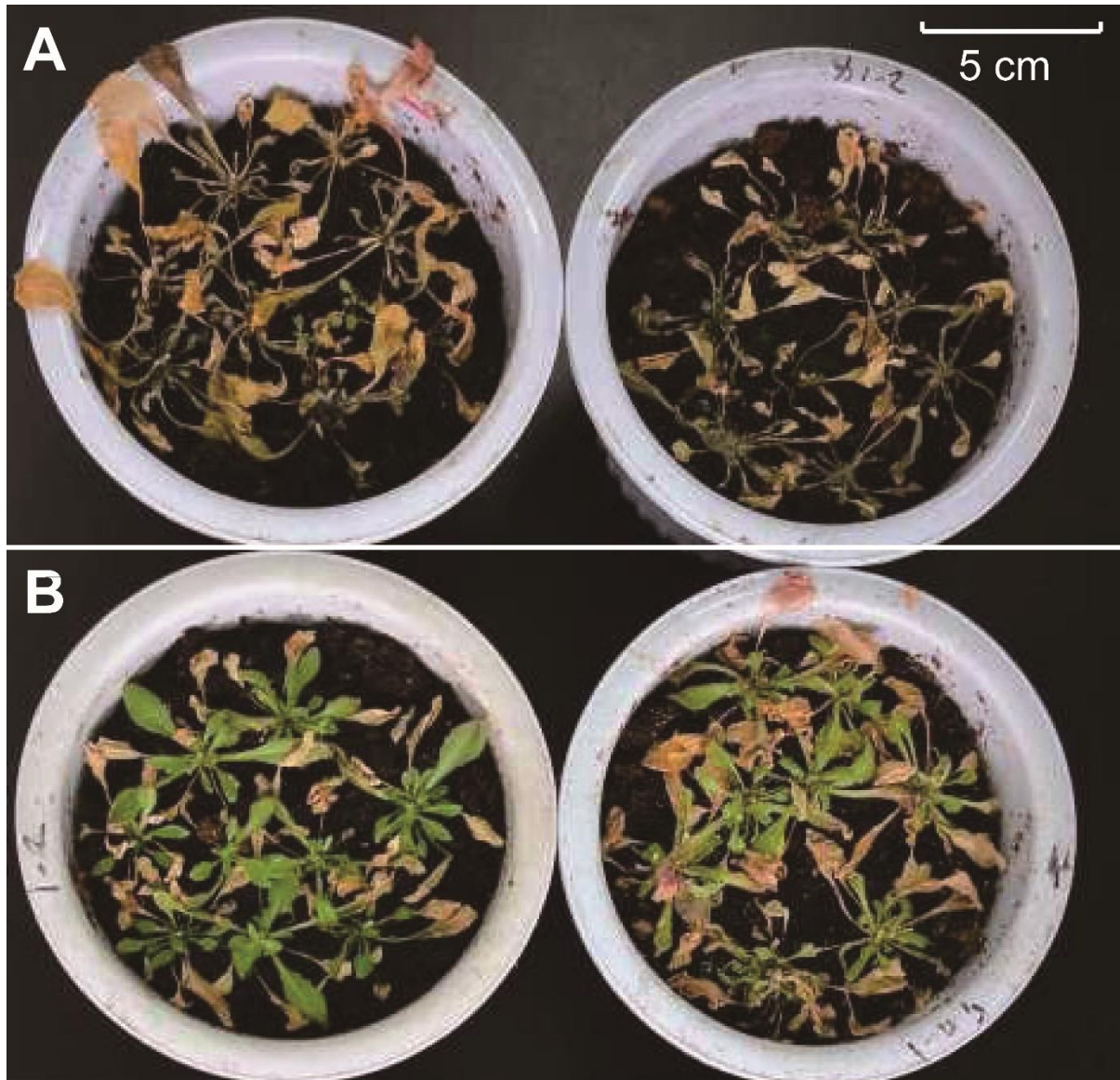


Figure 2-11: Soil water deprivation experiment of Arabidopsis overexpression lines

5-week-old Arabidopsis plants expressing A) empty vector or B) *TaCER1-1A* were exposed to 20 d of water deprivation, followed by three days of watering.

2.3.4.2 Effect of abiotic stress on wheat *TaCER1-1A* expression and wax composition

The promoter region of *TaCER1-1A* contains several elements predicted to be responsive to the phytohormone ABA (Table 2-3), suggesting that this gene may be involved not only in

formation of the wheat surface waxes but also in their dynamic adjustments in response to abiotic stress. To test this hypothesis, we first investigated the *TaCER1-1A* response under various abiotic stresses, exposing wheat seedlings to relatively drastic conditions involving ABA (100 μ M), the osmotic agent PEG6000 (20%), or low temperature (4°C). *TaCER1-1A* expression increased after 4 hr of ABA treatment, peaking at 6 hr and then decreasing to normal levels (Figure 2-12). All other stress treatments also resulted in increased expression of *TaCER1-1A*, albeit peaking at lower levels already at 4 hr and for shorter periods.

Table 2-3: Analysis of cis-acting regulatory elements in the *TaCER1-1A* promoter sequence (2 Kb)

Site Name	Position	Strand	Sequence	Function
ABRE	601	+	CACGTG	cis-acting element involved in the abscisic acid responsiveness
	623	+	CACGTG	cis-acting element involved in the abscisic acid responsiveness
	767	+	CCGCGTAGGC	cis-acting element involved in the abscisic acid responsiveness
	829	-	TACGTG	cis-acting element involved in the abscisic acid responsiveness
	897	-	TACGTG	cis-acting element involved in the abscisic acid responsiveness
	928	+	GCAACGTGTC	cis-acting element involved in the abscisic acid responsiveness
	930	+	TACGTG	cis-acting element involved in the abscisic acid responsiveness
5UTR Py-rich stretch	566	-	TTTCTTCTCT	cis-acting element conferring high transcription levels
	1100	-	TTTCTTCTCT	cis-acting element conferring high transcription levels
	1439	-	TTTCTTCTCT	cis-acting element conferring high transcription levels
	1471	-	TTTCTTCTCT	cis-acting element conferring high transcription levels
A-box	65	+	CCGTCC	cis-acting regulatory element
ACE	1070	-	ACGTGGA	cis-acting element involved in light responsiveness
AE-box	513	+	AGAAACAA	part of a module for light response
Box 4	1392	-	ATTAAT	part of a conserved DNA module involved in light responsiveness
Box III	492	+	CATTTACACT	protein binding site
Box-W1	541	-	TTGACC	fungal elicitor responsive element
CAAT-box	191	+	CAAT	common cis-acting element in promoter and enhancer regions

	268	+	TGCAAATCT	common cis-acting element in promoter and enhancer regions
	270	+	CAAAT	common cis-acting element in promoter and enhancer regions
	288	+	CAAAT	common cis-acting element in promoter and enhancer regions
	317	+	CAAAT	common cis-acting element in promoter and enhancer regions
	349	+	CAAAT	common cis-acting element in promoter and enhancer regions
	375	+	CAAAT	common cis-acting element in promoter and enhancer regions
	382	-	CAAAT	common cis-acting element in promoter and enhancer regions
	443	-	CCAAT	common cis-acting element in promoter and enhancer regions
	467	+	CAAT	common cis-acting element in promoter and enhancer regions
	472	+	CAAT	common cis-acting element in promoter and enhancer regions
	544	+	CAAT	common cis-acting element in promoter and enhancer regions
	581	+	CAATT	common cis-acting element in promoter and enhancer regions
	721	-	CAAT	common cis-acting element in promoter and enhancer regions
	732	-	CAAAT	common cis-acting element in promoter and enhancer regions
	738	-	CAAAT	common cis-acting element in promoter and enhancer regions
	867	-	CCAAT	common cis-acting element in promoter and enhancer regions
	912	+	CAAT	common cis-acting element in promoter and enhancer regions
	941	-	CAAAT	common cis-acting element in promoter and enhancer regions
	985	-	CAAT	common cis-acting element in promoter and enhancer regions
	1119	+	CAAAT	common cis-acting element in promoter and enhancer regions
	1152	-	CAAAT	common cis-acting element in promoter and enhancer regions
	1164	+	CAAAT	common cis-acting element in promoter and enhancer regions
	1259	+	CAAT	common cis-acting element in promoter and enhancer regions
	1280	+	CAAT	common cis-acting element in promoter and enhancer regions
	1284	+	CAAT	common cis-acting element in promoter and enhancer regions
	1395	-	CAATT	common cis-acting element in promoter and enhancer regions
	1396	-	CAAT	common cis-acting element in promoter and enhancer regions
CCGTCC-box	65	+	CCGTCC	cis-acting regulatory element related to meristem specific activation
G-Box	601	+	CACGTG	cis-acting regulatory element involved in light responsiveness
	930	-	CACGTA	cis-acting regulatory element involved in light responsiveness
	829	+	CACGTA	cis-acting regulatory element involved in light responsiveness
	1232	+	CACACATGGAA	cis-acting regulatory element involved in light responsiveness
	623	+	CACGTG	cis-acting regulatory element involved in light responsiveness

	897	+	CACGTA	cis-acting regulatory element involved in light responsiveness
	424	+	CACGTC	cis-acting regulatory element involved in light responsiveness
	897	-	TACGTG	cis-acting regulatory element involved in light responsiveness
	829	-	TACGTG	cis-acting regulatory element involved in light responsiveness
	1234	+	CACATGG	cis-acting regulatory element involved in light responsiveness
	623	+	CACGTG	cis-acting regulatory element involved in light responsiveness
	930	+	TACGTG	cis-acting regulatory element involved in light responsiveness
	894	+	TAACACGTAG	cis-acting regulatory element involved in light responsiveness
	928	-	GACACGTAGT	cis-acting regulatory element involved in light responsiveness
	601	+	CACGTG	cis-acting regulatory element involved in light responsiveness
	1072	+	CACGTC	cis-acting regulatory element involved in light responsiveness
	827	+	GACACGTAGT	cis-acting regulatory element involved in light responsiveness
GA-motif	1466	+	AAGGAAGA	part of a light responsive element
GAG-motif	686	+	AGAGAGT	part of a light responsive element
GARE-motif	509	+	AAACAGA	gibberellin-responsive element
	794	+	AAACAGA	gibberellin-responsive eleme
GCN4_motif	1131	-	CAAGCCA	cis-regulatory element involved in endosperm expression
I-box	152	-	GTATAAGGCC	part of a light responsive element
	1222	+	ATGATATGA	part of a light responsive element
MBS	1228	-	CGGTCA	MYB Binding Site
Skn-1_motif	788	-	GTCAT	cis-acting regulatory element required for endosperm expression
	1227	-	GTCAT	cis-acting regulatory element required for endosperm expression
	1167	-	GTCAT	cis-acting regulatory element required for endosperm expression
TATA-box	89	+	TTTTA	core promoter element around -30 of transcription start
	185	-	TTTTA	core promoter element around -30 of transcription start
	197	-	TTTTA	core promoter element around -30 of transcription start
	212	-	TATAAA	core promoter element around -30 of transcription start
	213	-	TATAA	core promoter element around -30 of transcription start
	214	+	TATAAAT	core promoter element around -30 of transcription start
	225	-	TTTTA	core promoter element around -30 of transcription start
	245	-	TTTTA	core promoter element around -30 of transcription start
	297	+	TTTTA	core promoter element around -30 of transcription start
	397	-	TTTTA	core promoter element around -30 of transcription start

	477	-	TTTAAAAA	core promoter element around -30 of transcription start
	478	+	TTTTA	core promoter element around -30 of transcription start
	481	-	TTTTA	core promoter element around -30 of transcription start
	1010	-	TTTTA	core promoter element around -30 of transcription start
	1033	+	TAATA	core promoter element around -30 of transcription start
	1317	+	TCTATATATT	core promoter element around -30 of transcription start
	1319	-	TATA	core promoter element around -30 of transcription start
	1320	-	ATATAT	core promoter element around -30 of transcription start
	1321	-	TATA	core promoter element around -30 of transcription start
	1414	-	TTTTA	core promoter element around -30 of transcription start
TC-rich repeats	1180	+	GTTTTCTTAC	cis-acting element involved in defense and stress responsiveness

We further investigated *TaCER1-1A* response under drought stress. The transcript levels of *TaCER1-1A* in wheat spikes were analyzed, because *TaCER1-1A* is highly expressed in this reproductive organ contributing directly to wheat yield. We found that drought treatment increased *TaCER1-1A* transcript levels slightly in wheat cv. CS and substantially in cvs. W87 and W51, compared with respective controls (Figure 2-13A).

To assess whether the drought-induced increases in *TaCER1-1A* expression were strong enough to affect surface accumulation of alkanes, the wax composition was analyzed after drought stress. The wax coverage increased by approximately 13%, 46%, and 24% in wheat cvs. W87, CS, and W51, respectively, after drought treatment (Figure 2-13 B-D). Of special interest in the context of the present work, the wax alkane amounts increased significantly in all three cultivars: from 91.73 ± 9.17 to $114.72 \pm 5.29 \mu\text{g g}^{-1}$ in cv. W87, from 59.49 ± 2.65 to $91.63 \pm 12.26 \mu\text{g g}^{-1}$ in cv. CS, and from 54.16 ± 1.88 to $66.95 \pm 3.74 \mu\text{g g}^{-1}$ in cv. W51. The drought stress also led to changes in the concentrations of alkyl esters, aldehydes, and β -diketones but had no apparent effect on plant morphology.

Overall, our results thus show that the transcription of *TaCER1-1A* can be induced by abiotic stress, resulting in increased alkane synthesis and accumulation on the wheat epidermal surface.

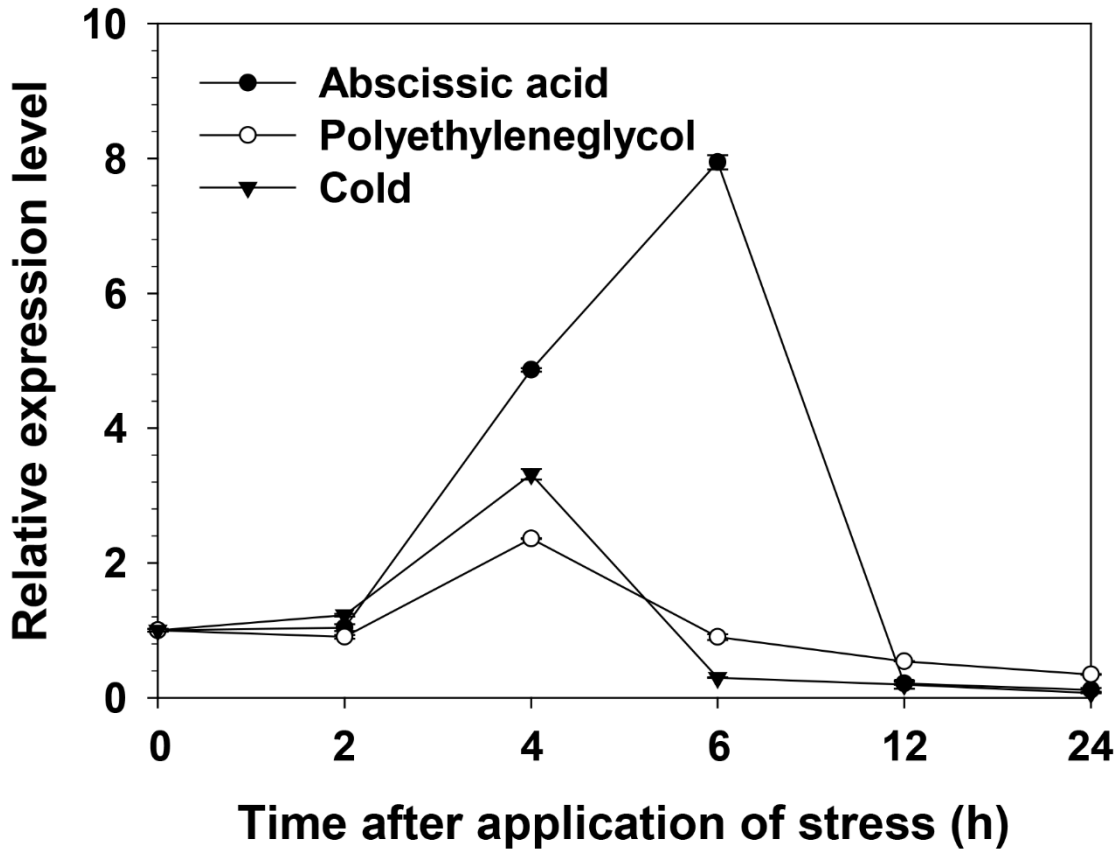


Figure 2-12: *TaCER1-1A* expression patterns under various abiotic stress conditions

The seedlings of wheat cv. W87 were exposed to ABA (100 μ M), PEG (20% PEG6000), or cold (4°C for 3 d). *TaCER1-1A* expression levels were measured by qRT-PCR and normalized against *TaActin* and plotted relative to untreated plants (t = 0 h).

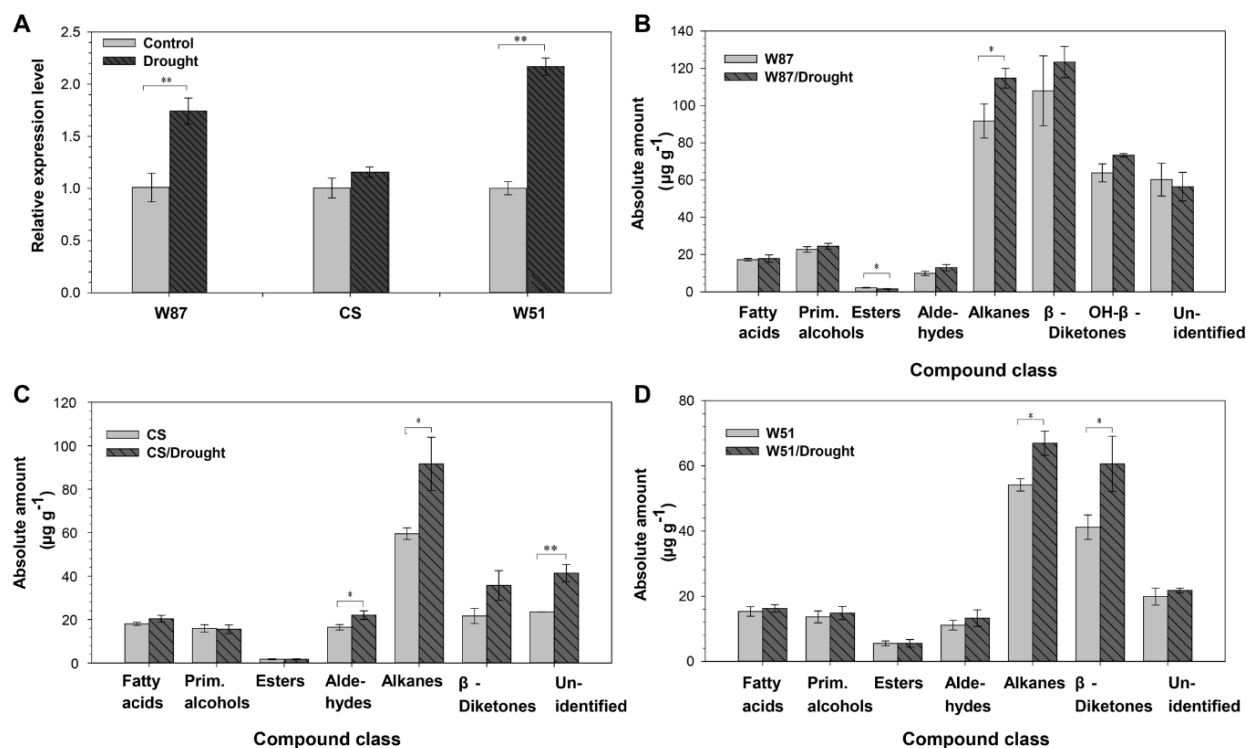


Figure 2-13: *TaCER1-1A* expression levels and compositions of waxes on wheat spikes under drought stress

A) qRT-PCR analysis of *TaCER1-1A* expression in spikes of wheat cvs. W87, CS and W51 after drought treatment. *TaCER1-1A* expression levels were normalized against *TaActin* and plotted relative to untreated plants. The corresponding cuticular wax compositions on drought-stressed spikes from B) wheat cv. W87, C) cv. CS and D) cv. W51. Wax coverage is expressed as $\mu\text{g g}^{-1}$ of spikes dry weight. Values represent means of three replicates. Error bars = SD. Significant differences are marked with asterisks (t-test: * $P < 0.05$; ** $P < 0.01$).

2.4 DISCUSSION

In this study, we identified *TaCER1-1A* as a primary candidate gene to be involved in wax alkane formation in bread wheat. Our major findings on the biochemical activity of the encoded enzyme, on its effect on whole-organ stress resistance, and on the redundancy of homologous genes in hexaploid wheat will be discussed below.

2.4.1 *TaCER1-1A* is involved in wheat wax alkane biosynthesis

First, indirect information on the biochemical function of TaCER1-1A came from the finding that the protein is localized to the ER. Previous studies in *Arabidopsis* had shown that all wax biosynthesis enzymes, catalyzing the entire pathway from initial C₁₆ acyl-CoA substrate to final products (VLC alkanes, ketones, primary alcohols, and esters), all share the same subcellular localization in the ER (Rowland et al., 2006; Greer et al., 2007; Li et al., 2008; Bourdenx et al., 2011). It therefore appeared plausible that *TaCER1-1A* was also involved in wax formation.

Next, the biochemical function of TaCER1-1A was tested *in planta* using various mutants and transgenic systems. We found that the wheat enzyme can partially complement the *Arabidopsis cer1* mutant phenotype, showing that TaCER1-1A is a functional enzyme with biochemical characteristics similar to those of its *Arabidopsis* homolog. This finding strongly suggests that TaCER1-1A functions in the final step of alkane formation, likely by formal decarbonylation of aldehyde substrates. This conjecture is supported by our further findings that overexpression of *TaCER1-1A* in both *Arabidopsis* and rice led to increases in the amounts of their leaf wax alkanes. These results are similar to experiments where the *Arabidopsis CER1* was overexpressed in the *Arabidopsis* wild type, also prompting drastic increases in alkanes (Bourdenx et al., 2011). Conversely, a wheat loss-of-function mutant, the nullisomic-tetrasomic substitution line, showed reduced alkane amounts, again similar to the *cer1* mutant phenotypes of other species (Aarts et al., 1995; Wang et al., 2015b).

Interestingly, detailed analyses of the wax alkanes in our loss-of-function and gain-of-function lines showed that, in all cases, alkanes with various chain lengths were affected roughly equally. It therefore appears that TaCER1-1A has little or no substrate/product chain length preference, at least in the range of the alkane homologs tested here, between C₂₅ and C₃₅. This finding matches

previous results on the Arabidopsis CER1 enzyme (Bourdenx et al., 2011). Of note, *TaCER1-1A* overexpression in Arabidopsis also showed that the wheat enzyme can accept branched and unsaturated substrates, to form iso-alkanes and alkenes, respectively.

Overall, our results demonstrate that the *TaCER1-1A* gene encodes an active enzyme directly involved in alkane formation in wheat. Our findings further imply that wheat likely has an alkane-forming pathway similar to Arabidopsis, where elongated acyl-CoA intermediates are first reduced to aldehydes, before these are then decarbonylated to the alkane products. The two steps involved are catalyzed by CER3 and CER1 enzymes in Arabidopsis, and based on our current findings, we propose that wheat may utilize two homologous enzymes to catalyze the same biochemical reactions. This hypothesis is backed by the result that the TaCER1-1A enzyme worked compatibly with CER3s from other species (rice and Arabidopsis) to form alkanes. Future research is required to characterize the CER3 enzyme(s) from wheat interacting with TaCER1-1A.

2.4.2 Accumulation of cuticular alkanes affects cuticle properties and leads to enhanced drought tolerance

It is well established that cuticular waxes are the major structural element establishing the surface barrier of primary plant parts (Schönherr, 1976) and that the sealing properties of plant surfaces thus largely depend on wax composition (Riederer and Schreiber, 2001). Our experiments on *TaCER1-1A* back this view, showing that Arabidopsis and rice leaves overaccumulating alkanes on their surfaces both exhibited decreased chlorophyll leaching and water loss. These findings parallel previous reports where overexpression of the homologous Arabidopsis *CER1* gene resulted in increased relative water content after water deprivation, higher biomass accumulation, and, thus, enhanced drought resistance. Similar effects were also

observed for rice and cucumber *CER1* homologs (Zhou et al., 2013; Wang et al., 2015b).

Overall, our results confirmed that *TaCER1-1A*, like *CER1s* in other species, plays an important role in reducing plant surface permeability and, hence, contributes to drought tolerance.

Plant surface wax compositions vary in relative chain length distribution, compound class amounts, and total wax coverage and, through each of these three characteristics, may affect surface barrier properties of plant tissues. It has been speculated that alkanes in particular may contribute substantially to the transport barrier, due to their highly hydrophobic nature (Bourdenx et al., 2011). Our present results can be interpreted as confirmation to this notion, because an increase in alkane amounts led to improved barrier properties in all transgenics tested, whereas decreased alkane amounts had the opposite effect. However, it should be noted that all changes of alkane amounts were accompanied by corresponding changes in total wax amounts and, in some cases, also by slight shifts in chain length distributions. Because both relative compositions and absolute amounts thus varied concomitantly, it is impossible to infer effects of a single compositional feature, and the relative contribution of alkanes to the surface barrier cannot be assessed based on our results.

In the present study, we further found that various adverse conditions or stresses, including low temperature and drought, induced *TaCER1-1A* expression within hours and led to increased accumulation of alkanes in wheat wax. This finding is similar to previous reports on other plant species, where diverse wax biosynthesis genes were found induced by stress conditions as well as plant hormones involved in stress responses: Drought, osmotic stress, or ABA treatment strongly induced expression, for example, of the Arabidopsis *CER6* and *CER1* genes (Hooker et al., 2002; Kosma et al., 2009; Bourdenx et al., 2011) and of diverse wax biosynthesis genes in

bread wheat and *Brachypodium* (Wang et al., 2015d; Wang et al., 2015e; Wang et al., 2016; Chai et al., 2018).

Overall, our results suggest that expression of the *TaCER1-1A* gene is induced by drought stress and that the encoded enzyme contributes to formation of wax alkanes and thus of the cuticular transpiration barrier in this important staple crop. This gene may, therefore, serve as a genetic marker in future wheat drought resistance breeding.

It will also be interesting to study the regulation of *TaCER1-1A* in follow-up experiments. One target for such studies may be the wheat transcription factor TaSHN1, a member of the APETALA2/ethylene response factor (AP2/ERF) family whose overexpression leads to altered wax composition, including elevated alkane amounts (Bi et al., 2018). TaSHN1 might activate the expression of *TaCER1-1A* in wheat, either by direct interaction with the promoter region of *TaCER1-1A* or by indirectly through other transcription factors. Further experiments including the expression level of *TaCER1-1A* in wheat TaSHN1 overexpression lines and TaSHN1 chromosome binding assays will be of great interest.

2.4.3 Polyploidy of wheat and wax biosynthesis

The evolution and domestication of bread wheat is tightly associated with its polyploid genome, and it is therefore an ideal system to investigate the effects of multiple genomes on plant adaptation (Yang et al., 2014; Soltis et al., 2015). Bread wheat possesses an allohexaploid genome composed of three closely related subgenomes, causing substantial redundancy. The bread wheat genome was sequenced fairly recently, using a chromosome-based approach, and high-quality sequence information and annotations are available only now (Eversole and Director, 2008; Appels et al., 2018). The resulting data have begun to reveal how

interchromosomal and intrachromosomal gene duplication has been driving wheat adaptation (Choulet et al., 2014). In the process, multiple loci, resulting from duplication and working synergistically, may contribute to important agronomic traits. Conversely, asymmetric expression may establish local and temporal patterns, with dominance of a subgenome or chromosomal region in certain cell types or developmental stages (Pfeifer et al., 2014).

The complex interplay of the three subgenomes greatly affects stress adaptation and acclimatization traits of bread wheat, including the cuticular waxes sealing its organ surfaces against excessive water loss. The wheat waxes comprise various classes of VLC aliphatics including β -diketones, alkanes, and primary alcohols, similar to many other monocots and dicots. Recent reports revealed that β -diketone formation largely depends on genes clustered in the W1, W2, and W3 loci residing on different chromosomes in separate subgenomes (Tsunewaki and Ebana, 1999; Adamski et al., 2013; Zhang et al., 2015). Other studies showed that at least eight functional FAR enzymes are involved in formation of VLC primary alcohols, all with different expression profiles (Wang et al., 2015d; Wang et al., 2015e; Wang et al., 2016; Chai et al., 2018). The present work further underscores the high redundancy among wax biosynthesis genes in wheat, demonstrating that its genome contains nine *CER1* homologs with characteristic expression patterns. Although TaCER1-1A was shown to be an active enzyme with important function in wax alkane formation, the nullisomic line lacking this enzyme had substantial amounts of residual alkanes, suggesting that other CER1s have overlapping functions that may be the focus of future investigations.

Chapter 3: Unravelling the biosynthesis of the very-long-chain β -diketones sealing barley (*Hordeum vulgare*) surfaces: a type III polyketide synthase produces cuticular β -diketones through head-to-head condensation.

3.1 Introduction

The three stages of wax biosynthesis are highly conserved in terrestrial plants (Chapter 1): i) the *de novo* fatty acid formation from FAS complexes that build up the LC fatty acyl precursors in plastids; ii) the elongation of fatty acyl precursors to VLC acyl-CoAs by FAE complexes in ER and iii) further modification of VLC acyl-CoAs through alcohol-forming or alkane-forming pathways to generate the final wax composition.

In the course of evolution, different plant species developed unique shunts alongside the traditional pathways to synthesize specialized cuticular waxes. Many Poaceae species, including durum wheat (*Triticum durum*), bread wheat (*Triticum aestivum*), barley (*Hordeum vulgare*), rye (*Secale cereale*) and oat (*Avena sativa*), and some dicots, including *Eucalyptus* and *Acacia* species, produce characteristic VLC β -diketones and their derivatives (Horn and Lamberton, 1962; von Wettstein-Knowles, 2017), which are not found in model plants such as Arabidopsis, rice, and maize (Hen-Avivi et al., 2016; von Wettstein-Knowles, 2017).

The structure of β -diketones was clarified during early rye wax analysis by mass spectra analyses of wax compounds, identifying C₃₁ 14,16-diketone, hydroxy-C₃₁ 14,16-diketone alongside the model substances C₂₂ 7,9-diketone and its enolo-acetate (Trka and Streibl, 1974). In the following studies, β -diketones with varying carbon chain length and β -diketo group positions have been identified in different plant species. In barley, C₂₉ 12,14- and 14,16-diketones, C₃₁ 14,16-diketone and C₃₃ 16,18-diketone have been reported (Mikkelsen, 1979). Predominantly

C₃₁ 14,16-diketone has been found in *Triticum* species (Tulloch et al., 1980). C₂₉ 12,14-Diketone and C₃₁ 14,16-diketone were found in *Eucalyptus risdoni*, while *Acacia podalyriaefolia* and *Festuca glauca* produced C₃₃ 16,18-diketone and C₃₃ 12,14-diketone, respectively (Horn and Lamberton, 1962). *Helianthus annuus* possessed extremely complicated β -diketone profiles with chain length ranging from C₁₉ to C₃₃ and β -diketo group in position -4,6, -6,8 and -10,12 (Schulz et al., 2000). In *Vanilla fragrans*, β -diketones ranging from C₂₅ to C₃₃ with exclusively 2,4-diketo group position were found (Ramaroson-Raonizafinimanana et al., 2000). And varying chain length of 2-alkanols accumulated as side products in the form of esters in different β -diketone-producing species, for instance C₁₁-C₁₇ 2-alkanols in barley (von Wettstein-Knowles and Netting, 1976), C₇-C₁₇ 2-alkanols in *T. aestivum* (Racovita et al., 2016) and C₉-C₁₅ 2-alkanols in *E. risdoni* (Horn and Lamberton, 1964).

β -Diketone biosynthesis is well organized in Poaceae species, so that they are barely produced in seedling stage but abundant in later vegetative and reproductive stages including the flag leaf blades, sheaths and spikes in wheat, and the leaf sheaths and spikes in barley (Wang et al., 2015c; von Wettstein-Knowles, 2017). They are also one of the most dynamically regulated wax components during drought stress in wheat (Bi et al., 2017). suggesting their importance for both reproductive development and stress tolerance. Indeed, as the predominant components in cuticular waxes of many cereal crops, they form characteristic crystals on the plant surfaces, endowing crops with various levels of glaucous morphological phenotypes; on the other hand, β -diketones are associated with plant water use efficiency, reducing crop canopy temperature, and thus stabilize grain yield especially during drought or heat stress likely by enabling the routine photosynthesis (Richards et al., 1986; Clarke et al., 1993; Monneveux et al., 2004; Huang et al., 2017). Thus, the glaucousness becomes a favorable agronomy trait that highly selected in

modern durum and bread wheat cultivars (Zhang et al., 2013). Therefore, it is very important to understand the biochemical mechanisms leading to β -diketone formation and the underlying genetic elements.

Early on, biochemical experiments were used to deduce a model of β -diketone synthesis pathway. In particular, a series of radio-labeled wax precursors, including acetate, different carbon-chain length fatty acids/ fatty acyl-CoAs, 3-ketoacids, 3-hydroxyacids, 2-ketones and 2-alkanols were fed to barley tissue slices, and the radioactive labels were detected in various products, where possible after chemical fragmentation (von Wettstein-Knowles and Netting, 1976; Mikkelsen and von Wettstein-Knowles, 1978; Mikkelsen, 1979, 1984). The authors concluded that synthesis of the major product, C₃₁ 14,16-diketone, proceeds via C₁₈ 3-ketoacid as a key intermediate. It is thought to be generated by elongation adding C₂ units diverging from fatty acid *de novo* biosynthesis, and elongated with further C₂ units to a C₃₂ diketoid intermediate similar to the processes leading to other wax components. Thus, the model implies that both hydrocarbon tails of the β -diketone are synthesized consecutively, first growing the longer acyl moiety and then extending it in the same direction. However, final proof for this pathway model was lacking since the enzymes involved could not be isolated or cloned.

Progress on the genetic underpinning of β -diketone synthesis was hindered for decades due to the lack of genomic information for Poaceae crop species. In early β -diketone research, many studies were carried out to map the loci associated with β -diketone formation. Two β -diketone forming loci *WAX1* (*W1*) and *W2* were mapped to the short arm of 2B and 2D chromosome in bread wheat, respectively, using near-isogenic lines (Tsunewaki and Ebana, 1999; Lu et al., 2015). Independently, two inhibitor loci, *Inhibitor of wax 1* (*Iw1*) and *Iw2*, were also mapped to chromosomes 2BS and 2DS, respectively (Tsunewaki and Ebana, 1999; Adamski et al., 2013).

Expression of genes at either *W1* or *W2* could lead to the glaucous phenotype of wheat, while the presence of either inhibitors will hinder it (Tsunewaki and Ebana, 1999). Accordingly, early work on barley mapped the β -diketone synthesis-related loci *Cer-c*, *Cer-q*, *Cer-u* in the telomeric region on the short arm of chromosome 2H (Schondelmaier G, 1992), a syntenic region to *W1* locus in bread wheat (Tsunewaki and Ebana, 1999), and suggested these three loci residing within roughly 0.0012 map units formed either a gene cluster or a multifunctional gene (von Wettstein-Knowles and Sogaard, 1980).

Only very recently, with the advance in high throughput sequencing and available high-quality genome data, the key genes within these gene loci involved in β -diketone synthesis were unraveled in barley and wheat. Fine mapping with near-isogenic lines and characterization of *cer-c*, *q*, *u* loss-of-function mutants showed that the *Cer-q* gene encodes a hydrolase/carboxylesterase, the *Cer-c* gene encodes a type-III polyketide synthase, and the *Cer-u* gene encodes a cytochrome P450 involved in β -diketone (and derivatives) formation in barley (Schneider et al., 2016). A second study compared the transcriptome data of a β -diketone-lacking 2BS chromosome-arm substitution hexaploid wheat line with its corresponding β -diketone-rich line, combined with fine-mapping and gene expression correlation analysis, and identified the *Diketone Metabolism Hydrolase* (*DMH*, orthologous to *Cer-q*), *Diketone Metabolism PKS* (*DMP*, orthologous to *Cer-c*) and *Diketone Metabolism CYP450* (*DMC*, orthologous to *Cer-u*) within the *W1* region associated with the production of β -diketones and related wax components (Hen-Avivi et al., 2016). These studies together revealed that, instead of a multifunctional gene, a metabolic gene cluster is involved in β -diketone formation in barley and wheat. (Hen-Avivi et al., 2016; Schneider et al., 2016).

The genetic basis of β -diketone formation pathway could be combined with our previous understanding of the biochemistry of pathway reactions. A refined model for β -diketone biosynthesis (Figure 3-1A, Figure 3-5) predicted that DMH works in plastids or ER to intercept the fatty acyl intermediates, releasing 3-ketoacid intermediates likely in acid form (Hen-Avivi et al. 2016; von Wettstein-Knowles, 2017). 3-Ketoacyl intermediates may subsequently be activated to 3-ketoacyl-CoAs, which are taken as starters by DMP and elongated with malonyl-CoA extenders to respective 3,5-diketoacyl-CoAs (von Wettstein-Knowles, 2017). FAE-type elongase(s) may then extend the 3,5-diketoacyl-CoAs to VLC β -diketoacyl-CoAs, which are finally decarboxylated to form VLC β -diketones. In summary, this pathway model relies on sequential elongation of the β -diketone backbone.

The new, refined model for β -diketone formation has not been tested experimentally yet. However, the expression of the barley DMH in *E. coli* led to production of C16 3-keto fatty acid (represented by C15 2-ketone), which was likely the precursor of β -diketones (Hen-Avivi et al., 2016). This finding supported the first key reaction steps proposed in the biosynthesis model, but did not allow conclusions on the further pathway and the biochemical activity of the DMP enzyme in particular. The elongation model revolves around DMP catalyzing a condensation 3-ketoacyl-CoA starters and malonyl-CoA extenders, and further FAE-type elongation. The predicted activity of DMP thus resembles the reactions carried out by most PKSs, which take CoA substrates as the starter and malonyl-CoA as the extender, and catalyze one or more decarboxylative condensations (Austin and Noel, 2003). However, the proposed FAE-type elongase(s)/complex(es) involved in 3,5-diketoacyl-CoA elongation remained elusive because, despite the isolation of numerous barley β -diketone-deficient mutants, no elongase mutants have been identified.

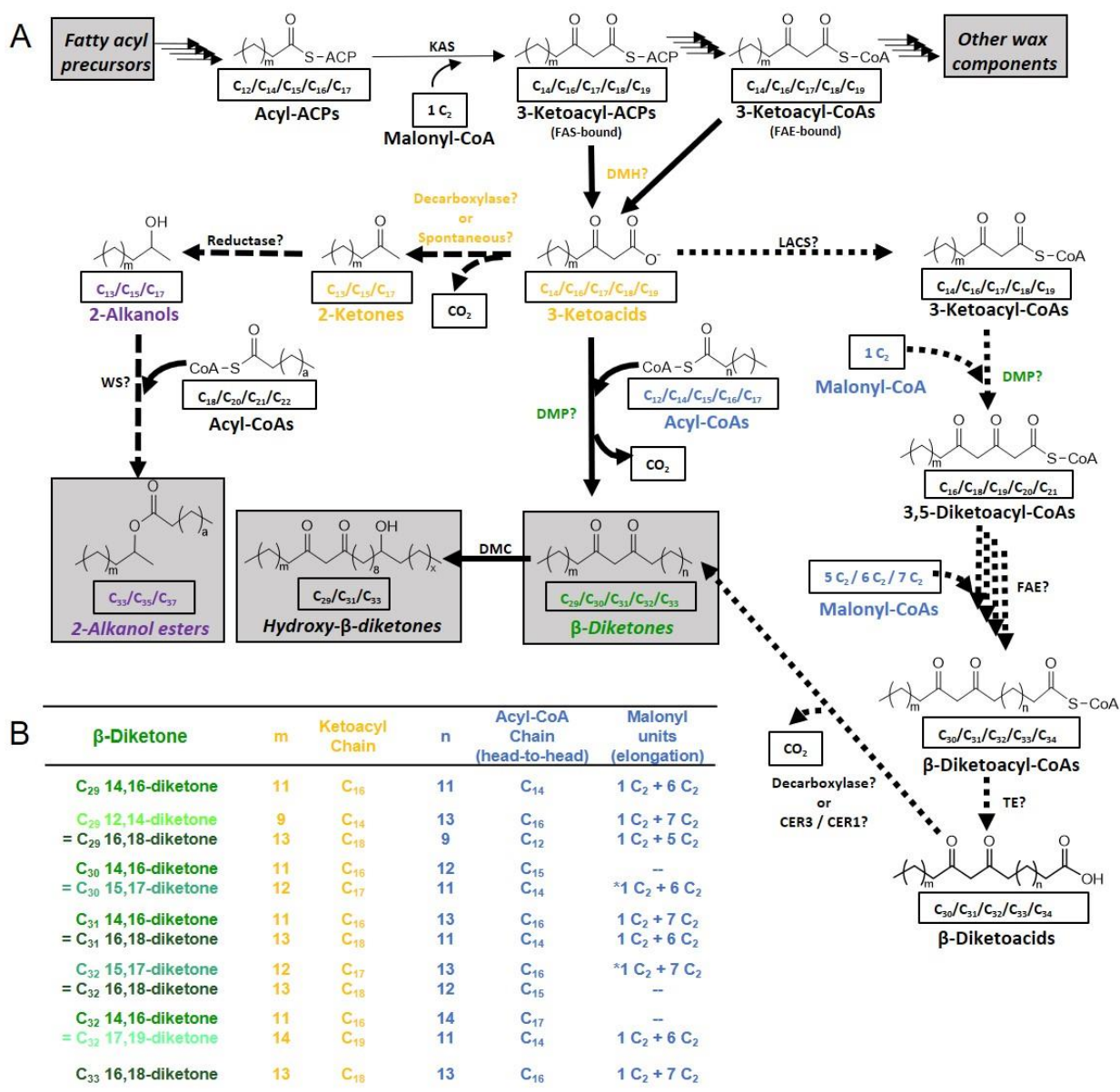


Figure 3-1: Proposed β-diketone-forming pathways in barley

A) Pathways leading from acyl precursors (top left grey box) to various wax components (other grey boxes). The formation of common wax components involves elongation of acyl-ACPs and acyl-CoAs (top row). The branch pathways leading to β-diketones and associated 2-alkanol esters (bottom half of the reaction scheme) are thought to proceed via central 3-ketoacid intermediates. For this, the enzyme Diketone Metabolism Hydrolase (DMH) is thought to intercept either 3-ketoacyl-ACP intermediates of plastidial Fatty Acid Synthase (FAS) complexes or 3-ketoacyl-CoA intermediates of ER-bound Fatty Acid Elongase (FAE) complexes. Its 3-ketoacid products are then be converted either into 2-alkanol esters (left side; long-dashed lines) or into β-diketones (right side). Two reaction paths from 3-ketoacids to β-diketones are feasible: (i) Previous studies suggested a pathway (elongation hypothesis; short-dashed arrows) involving activation by a Long-

Chain Acyl-CoA Synthetase (LACS), condensation with a C₂ unit (from malonyl-CoA) by the Diketone Metabolism Polyketide synthase (DMP) enzyme, further elongation rounds catalyzed by FAE complex(es), and head group removal by a thioesterase (TE) and a decarboxylase or CER3/CER1-like enzymes. (ii) Alternatively, DMP could catalyze a non-canonical PKS condensation (head-to-head condensation hypothesis; solid arrows), involving decarboxylative condensation of fatty acyl-CoA starters and 3-ketoacid extenders. A Diketone Metabolism Cytochrome-P450 (DMC) enzyme then likely hydroxylates β -diketones at a specific position to produce hydroxy- β -diketones. B) List of the β -diketones found in barley waxes, with names of isomers color-coded according to the position of the diketo-group. Numbers m and n define the length of the hydrocarbon tails on either side of the functionality, and for isomers with $n \neq m$ two alternative names based on counting from either terminus are given. The chain length of the ketoacyl intermediate generating each β -diketone is given in yellow. The chain length of the acyl-CoA required to generate each β -diketone via head-to-head condensation is given in blue, along with the numbers of malonyl extender units required for the alternative elongation pathway. Dashes indicate that a particular β -diketone isomer cannot be synthesized by elongation. KAS, β -ketoacyl-ACP synthase; WS: wax ester synthase; CER3, ECERIFERUM 3; CER1, ECERIFERUM 1.

An alternative mechanism for β -diketone formation not relying on elongation to the final product must be considered at this point, even though it had been discarded early on (Netting and von Wettstein-Knowles, 1976). In particular, DMP could use the 3-ketoacid intermediates as extenders, not as starters, and condense them with common fatty acyl-CoAs as starters (Figure 3-1A, Figure 3-5). The results of the radiotracer assays with different wax precursors equally support the direct condensation model (Mikkelsen, 1984). In summary, this model thus invokes the head-to-head condensation of two preformed acyl chains rather than sequential addition of C₂ units.

While two alternative pathway models surrounding the activity of DMP must be considered, the other reactions associated with the β -diketone synthesis pathway are unambiguous. It seems very plausible that DMC works downstream of β -diketone formation to produce hydroxy- β -diketones. On the side path, 3-ketoacids are decarboxylated to produce 2-ketones, which are further reduced

to 2-alkanols and esterified with fatty acyl CoAs to form 2-alkanol esters (Figure 3-1A, Figure 3-5).

Here, we tested the two alternative models of wax β -diketone synthesis. To this end, the β -diketones and related wax components from barley cuticular waxes were first analyzed, with special emphasis on the wild-type β -diketone homolog and isomer profiles and the accompanying 2-alkanol esters, the wax profile of a barley wax elongase mutant, and the ^{13}C isotope abundance of β -diketones. Based on these chemical results, we then aimed to characterize the core pathway enzymes DMH and DMP, with both *in vivo* and *in vitro* assays testing their substrate requirements. And unlike other type III PKSs, DMP showed no activity on malonyl-CoA. The fatty acyl-ACP pool, alongside the specificity of DMH and DMP, could explain the unique β -diketone profile in barley. In particular, our study characterized a non-canonical type III PKS that clarified the β -diketone formation mechanism and revised the model of β -diketone synthesis pathway in barley.

3.2 Materials and methods

3.2.1 Plant materials and growth conditions

Seeds of the wild-type *Hordeum vulgare* cv. Morex (NGB23015) were obtained from the Nordic Genetic Resource Center (Alnarp, Sweden), those of wild-type cv. Ingrid and *emr1* mutant were kindly provided by Dr. Ulrich Schaffrath (Rheinisch-Westfälische Technische Hochschule Aachen, Germany). Seeds were germinated on moist filter paper in Petri dishes at room temperature, then transferred to soil (Sunshine Mix 5, Sun Gro) in 10-l pots. Plants were grown in a growth chamber under 16-h light/21°C, 8-h dark/19°C cycles.

For barley protoplast preparation, barley cv. Morex seeds were germinated on moist filter papers in petri-dishes and transferred to soil in small pots and covered with plastic domes in growth chamber for 10 days using the growth conditions described above.

Tobacco plants were grown under same conditions for 1 month and used for leaf transient expression.

3.2.2 RNA isolation, reverse transcription, plasmid construction and transformation

Flag leaf sheaths and spikes of *H. vulgare* cv. Morex were excised and immediately frozen in liquid nitrogen for RNA isolation. Total RNA was extracted using PureLink RNA mini kit (Invitrogen), and genomic DNA was removed by on-column DNA digestion with PureLink DNase (Invitrogen) following the manufacturer's protocol. 1 µg of resulting total RNA and Oligo(dT)₂₀ primer (Invitrogen) were used to synthesize first-strand complementary DNA (cDNA) with SuperScript III Reverse Transcriptase (Invitrogen). The resulting cDNA was used as template in gene cloning.

E. coli expression vectors pET28-DMH, pET28-DMP and pET28-TEVH were kindly provided by Dr. Asaph Aharoni (Weizmann Institute of Science, Rehovot, Israel). The expression cassette contains an N-terminal 6xHis-tag followed by a TEV cleavage site and the open reading frame (ORF) of the target gene. The plasmids were transformed into *E. coli* BL21 (DE3) competent cells (Invitrogen) according to the manufacturer's protocol, and presence of the gene insert verified by colony PCR and Sanger sequencing. Three to four independent transformants of each *E. coli* line were selected for further *in vivo* assay or protein purification.

To construct plant expression vectors, the coding region of DMH and DMP were amplified from *H. vulgare* cv. Morex flag leaf sheath cDNA with Phusion polymerase (NEB) using primers DMH-

F, DMH-R and DMP-F, DMP-R, respectively (Table 3-1). PCR products were ligated to Gateway entry vector pCR8/GW/TOPO (Invitrogen) according to the manufacture's protocol, and presence of the target sequences was verified by colony PCR and Sanger sequencing. LR reactions were performed with LR Clonase II enzyme mix (Invitrogen) to transfer target genes from the entry vector to the destination vector pGWB5 for in-frame C-terminal fusion with GFP. Positive transformants were identified again by colony PCR and Sanger sequencing. The resulting constructs were then transformed into *A. tumefaciens* GV3101 competent cells by electroporation, screened on LB plates containing proper antibiotics, and verified by colony PCR. Three verified *A. tumefaciens* transformants were cultured for tobacco transient expression.

Table 3-1. Primers used in Chapter 3

Construct	Primer name	Primer sequence
pGWB5-35Spro::DMH-GFP	DMH-F	5'-ATGCCTGCAAACAAGACTTAC-3'
	DMH-R	5'-GAAACAGTTGTTTCATCATGGATC-3'
pGWB6-35Spro::GFP-DMP	DMP-F	5'-ATGGCAGGCAGCTCACC-3'
	DMP-R	5'-TTTTTCTTGAGAGCGCCGG-3'
pESC-Trp-GAL1::LACS1-MYC	LACS1-BamHI-F	5'-AGAGGATCCATGAAGTCTTTTGCGGCTAAG-3'
	LACS1-SalI-R	5'-AGAGTCGACTGAGATTTTCTTTGAGGCCAAT-3'
pESC-Trp-GAL1::LACS1-MYC-GAL10:: DMP-FLAG	DMP-EcoRI-F	5'-TCTGAATTCATGGCAGGCAGCTCACC-3'
	DMP-SpeI-R	5'-GGACTAGTAGCCATTTTTTCTTGAGAGCGC-3'

To construct yeast expression vectors, the coding sequence of LACS1 was amplified from Arabidopsis stem cDNA using primers LACS1-BamHI-F and LACS1-SalI-R and inserted into the pESC-Trp yeast expression vector in frame with C-terminal MYC epitope tag, for expression under control of galactose-inducible promoter GAL1, resulting in construct pESC-Trp-GAL1::LACS1-MYC. DMP was subcloned from pGWB6-35Spro::GFP-DMP using primers DMP-EcoRI-F and DMP-SpeI-R and spliced into pESC-Trp-GAL1::LACS1-MYC vector, C-terminally in frame with FLAG epitope tag, resulting in construct pESC-Trp-GAL1::LACS1-

MYC-GAL10::DMP-FLAG. Yeast transformed with either constructs were screened on LB plates containing 100 µg/ml ampicillin, and verified by colony PCR, restriction digestions and Sanger sequencing. The resulting expression vectors were transformed into yeast strain INVSc1 (*MATa his3D1 leu2 trp1-289 ura3-52*) as described by Gietz and Woods (2002) and the resulting transformants screened on yeast minimal medium plates lacking the appropriate amino acids. The transformed yeast colonies were verified by colony PCR. Three or four verified yeast transformants were selected for further *in vivo* assay.

3.2.3 Chemical synthesis of standards and substrates

3.2.3.1 Chemical synthesis of C₃₁ 14,16-diketone

1 g hexadecanol (Sigma-Aldrich) was stirred at room temperature with 2.5 g of Dess-Martin reagent periodinane (1.5 eq) (Sigma-Aldrich) in 30 ml CH₂Cl₂. Upon completion of the oxidation (monitored by TLC), the reagent was quenched by adding 5 ml saturated aqueous Na₂S₂O₃. The mixture was extracted three times with CH₂Cl₂, and the combined organic fractions were washed with saturated aqueous NaHCO₃, dried with Na₂SO₄ and concentrated under vacuum. The product, hexadecanal, was purified by CHCl₃ and verified by GC-MS analysis.

0.7 g pentadecan-2-one was stirred at 0°C with 0.1 M lithium diisopropylamide in 11.5 ml tetrahydrofuran (Sigma-Aldrich) for 10 min, then 0.8 g hexadecanal in 2 ml tetrahydrofuran was added, and after 1 h the reaction was quenched by adding 5 ml 20% H₂SO₄. The mixture was extracted three times with CH₂Cl₂, and the combined organic solutions were washed with saturated aqueous NaHCO₃, dried with Na₂SO₄ and concentrated under vacuum. The product, 16-hydroxyhentriacontan-14-one, was purified by column chromatography (1:1 hexane:CHCl₃) and verified by GC-MS analysis.

0.5 ml 1 M oxalyl chloride (1 eq) (Sigma-Aldrich) in CH_2Cl_2 was added to 150 μl dimethylsulfoxide (5 eq) in 2 ml CH_2Cl_2 under stirring at -78°C . After gas evolution had ceased, 0.2 g 16-hydroxyhentriacontan-14-one in 3 ml CH_2Cl_2 were added drop-wise, the reaction mixture was allowed to warm to room temperature, and then 0.3 ml Et_3N (5 eq) was added. 5 ml water. The resulting solid was re-dissolved by adding 5 ml water, and organic products were extracted three times with CH_2Cl_2 . The combined organic phases were washed with diluted HCl followed by water, dried with Na_2SO_4 , and concentrated under vacuum. The resulting product, C_{31} 14,16-diketone, was purified by column chromatography (3:1 hexane: CHCl_3) and verified by MS analysis.

Other diketone homologs were synthesized following the same protocols from starting materials with respective chain lengths.

3.2.3.2 Chemical synthesis of C_{21} 2-alkanol

91 mg (1.5 eq.) of LiAlH_4 95% powder (Aldrich) were added to a solution of 500 mg heneicosan-2-one (Roth) in 10 ml CH_2Cl_2 at room temperature. The reaction was quenched after 1 h by adding 2 ml of 1 N HCl, and products were recovered by extraction with CHCl_3 . Organic fractions were combined, washed with saturated aqueous NaH_2CO_3 , dried with Na_2SO_4 , and concentrated under vacuum. The final product was purified by CHCl_3 .

3.2.3.3 Chemical synthesis of C_{14} – C_{18} 3-ketoacids

C_{16} 3-ketoacid methyl ester was synthesized as described by Brinkerhoff et al. (2014), with small modifications: 2 g myristic acid (Sigma-Aldrich) (1 eq.) were dissolved in 10 ml CH_2Cl_2 containing 2 g N,N'-dicyclohexylcarbodiimide (1 eq.) (Sigma-Aldrich). Separately, 1.9 g 4-dimethylaminopyridine (Sigma-Aldrich) (1 eq.) were added to 20 ml pyridine containing 1.6 g

Meldrum's acid (TCI) (1 eq.). Both mixtures were stirred at room temperature for 15 min before combining them. After stirring at room temperature for 16 h, the solvent was evaporated under vacuum and the solid redissolved in 20 ml methanol supplemented with two drops of concentrated H_2SO_4 , and the mixture was refluxed for 16 h. The mixture was extracted three times with diethyl ether, the combined organic fractions were washed consecutively with aqueous NaHCO_3 solution, distilled water and saturated NaCl , the organic phase was removed and dried with Na_2SO_4 , and the solvent was evaporated under vacuum. The resulting solid was purified by CHCl_3 and product purity verified by GC-MS analysis.

0.5 g C_{16} 3-ketoacid methyl ester was dissolved in 20 ml glacial acetic acid supplemented with five drops of concentrated HCl , and the mixture kept at 10°C for one week. The product was extracted with diethyl ether, the organic phase removed and washed with deionized water, and the solvent evaporated under vacuum. GC-MS analysis showed that the crude product contained non-hydrolyzed C_{16} 3-ketoacid methyl ester and C_{16} 3-ketoacid as main products, accompanied by small amounts of the decarboxylation product, C_{15} 2-ketone. This mixture was separated by flash CHCl_3 , to yield pure C_{16} 3-ketoacid for use in biochemical assays (while C_{16} 3-ketoacid methyl ester was recovered for further hydrolysis).

The same protocols were used to synthesize C_{14} , C_{17} and C_{18} 3-keto fatty acids.

3.2.4 *In vivo* assays

3.2.4.1 *E. coli in vivo* assay

Three independent *E. coli* BL21 (DE3) colonies each carrying pET28-TEVH or pET28-DMH were inoculated into 1 ml LB liquid medium with kanamycin and precultured at 37°C overnight. Then, each broth was diluted 1:100 in 100 ml LB liquid medium supplemented with kanamycin,

cultivated at 37°C to OD₆₀₀ ~ 0.6, supplemented with 0.5 mM IPTG to induce the expression of recombinant protein, and incubated at 22°C overnight. The OD₆₀₀ of resulting *E. coli* were measured and *E. coli* cells were collected by centrifugation for lipid analysis.

3.2.4.2 Yeast *in vivo* assay

Three independent yeast colonies expressing pESC-Trp-GAL1::LACS1-MYC (used as negative control) or pESC-Trp-GAL1::LACS1-MYC-GAL10:: DMP-FLAG were inoculated into 2 ml appropriate liquid minimal medium supplemented with 2% glucose and incubated at 28°C overnight. The precultures were then expanded to 30 ml and cultivated for another 18 h. Yeast cells were then harvested by centrifuge, transferred into liquid minimal medium supplemented with 2% galactose to induce the expression of target genes and cultivating at 28°C for 16 h. Then, yeast cells were transferred to 30 ml liquid minimal medium based on phosphate buffer (20 mM Na₂HPO₄/ NaH₂PO₄, 300 mM NaCl, pH 7.4) and containing 2% galactose. All the substrates are dissolved in ethanol and the final concentration for fatty acids are 0.22 mM and 0.22 mM for 3-ketoacids and the yeast cells were cultivated for another 24 h at 22°C. Finally, the OD₆₀₀ of resulting yeast cells were measured and cells were harvested by centrifugation and used for further product analysis. To test the preferred fatty acyl substrate(s) of DMP, C₁₂, C₁₃, C₁₄ and C₁₅ fatty acids were supplemented to yeast media to a final concentration of 1.2 mM, 0.66 mM, 0.33mM and 0.33 mM, respectively. Fatty acids used in yeast assay are obtained from Sigma-Aldrich.

3.2.5 Protein purification and *in vitro* assay

E. coli BL21 (DE3) colonies carrying pET28-DMP were inoculated into 5 ml LB liquid medium with kanamycin and precultured at 37°C overnight. *E. coli* precultures were diluted 1:100 in LB liquid medium supplemented with kanamycin and cultivated at 37°C to OD₆₀₀ ~ 0.6, and 0.5 mM

IPTG was added to induce expression of recombinant protein. After incubating at 16°C overnight. *E. coli* cells were collected by centrifugation (10,000 g, 4°C). All following steps of protein purification were performed using phosphate-based buffers (20 mM Na₂HPO₄/ NaH₂PO₄, 300 mM NaCl with imidazole, pH 7.4) supplemented with 1% Triton X-100, and equilibration buffer was supplemented with 100 µM PMSF protease inhibitor. *E. coli* pellets were resuspended in buffer and lysed by sonication at 4°C. The 6×His-PKS recombinant protein was obtained by Ni-NTA affinity purification with HisPur Ni-NTA resin (Invitrogen) following the manufacturer's protocol. The recombinant protein was eluted in phosphate buffer and dialyzed three times in dialysis buffer (0.1 M Na₂HPO₄/NaH₂PO₄, 2.5 mM DTT, 10 mM MgCl₂, 0.025% Triton X-100) at 4°C. The purity of recombinant protein His-DMP was verified by SDS-PAGE, and the protein concentration was determined by protein assay using the Bradford method with Protein Assay Dye Reagent Concentrate (Bio-Rad). The obtained protein was used immediately in enzyme assays.

For *in vitro* assay, 50 µg of purified recombinant DMP protein was incubated in 3 ml 50 mM phosphate buffer (pH 7.4) containing 2.5 mM DTT, 10 mM MgCl₂ and 0.025% Triton X-100. C₁₄, C₁₆ and C₁₈ 3-ketoacids alongside malonyl-CoA lithium salt, myristoyl-CoA lithium salt, palmitoyl-CoA lithium salt and stearoyl-CoA lithium salt were used as substrates for the different assays. A final concentration of 0.15 mM of 3-ketoacids, 0.15 mM CoA lithium salts and 0.45 mM of malonyl-CoA were supplemented in DMP enzyme function assays. Incubation was performed at room temperature for 14 h with gentle shaking. The reaction was quenched by adding 200 µl 10% H₂SO₄, and the reaction products were extracted immediately for lipid analysis. Malonyl-coenzyme A lithium salt, myristoyl-coenzyme A lithium salt, palmitoyl-coenzyme A lithium salt, stearoyl-CoA lithium salt and malonic acid were obtained from Sigma-Aldrich.

3.2.6 Lipid analysis

3.2.6.1 Wax analysis

Flag leaf sheaths and spikes were excised from *H. vulgare* cv. Morex plants grown 85 d after germination. Surface waxes were extracted by submerging tissues twice for 30 s in CHCl₃, extracts were combined, and the solvent was evaporated under gentle N₂ flow. Samples were transferred into GC vials and derivatized with 10 µl *bis*-N,O-trimethylsilyltrifluoroacetamide (BSTFA) (Sigma-Aldrich) in 10 µl pyridine (Sigma-Aldrich) at 72°C for 45 min. The reagents were evaporated under gentle N₂ flow, and the product was dissolved in 200 µl CHCl₃. The derivatized wax mixtures were then analyzed on a Gas Chromatography system (6890N, Agilent) equipped with HP-1 capillary column (30 m × 0.32 mm i.d., 1 µm film thickness, Agilent) coupled with Mass Selective Detector (5793N, Agilent) using cool-on-column injection and the following oven program: 50°C held for 2 min, raised by 40°C min⁻¹ to 200°C and held for 2 min, raised by 3°C min⁻¹ to 320°C and held for 30 min.

3.2.6.2 *E. coli* lipid analysis

E. coli pellets were washed with distilled water, collected by centrifugation and allowed to air-dry. Known quantities of C₂₁ 2-ketone, C₂₁ 2-alkanol and C₂₀ 2-hydroxyacid methyl ester were added to each sample for quantification of respective compound classes, *E. coli* cells were resuspended in 1 ml methanol containing 0.5 M sulfuric acid and 2% (v/v) 2,2-dimethoxypropane, and incubated at 80°C for 3 h. Then 2.5% NaCl solution (w/v) was added and the mixture extracted three times with hexane, and the combined organic phases were concentrated under N₂ flow and derivatized as described above. The final products were dissolved in CHCl₃ and analyzed by GC-MS as above, but with the following oven program: 50°C held for 2 min, raised by 40°C min⁻¹ to 100°C and held for 2 min, raised by 3°C min⁻¹ to 320°C and held for 5 min. The correction factor

between 3-hydroxyacids and 2-hydroxyacids was experimentally determined by authentic standards C₁₆ 3-hydroxyacid and C₂₀ 2-hydroxyacid.

3.2.6.3 Yeast lipid analysis

30 ml-yeast cultures were split into 25 ml for β -diketone analysis and 5 ml for fatty acid profiling, and cells were collected by centrifugation, washed with distilled water and allowed to air-dry. For product analysis, C₃₅ diketone was supplemented to yeast pellets as internal standard. Yeast cells were resuspended in 3 ml distilled water and lysed with 0.5 mm glass beads (BioSpec) by vortexing. 2 ml saturated NaCl solution was added, and total lipids were extracted three times with CHCl₃, the combined organic phases were dried with Na₂SO₄ and filtered, and the solvent was evaporated under vacuum. The resulting lipids were transferred into GC vials, derivatized and analyzed by GC-MS as described for wax analysis. All diketones were quantified using m/z 100 selected-ion traces. For fatty acid profiling, yeast cells were resuspended in 1 ml methanol containing 0.5 M sulfuric acid and 2% (v/v) 2,2-dimethoxypropane. The transmethylation reaction was performed as described above, and products were extracted with hexane, derivatized as previously described and analyzed by GC-MS as described for *E. coli* lipid analysis.

3.2.6.4 *In vitro* product analysis

The reaction mixture was extracted twice for 30 s with CHCl₃, and the combined organic phases were concentrated under vacuum, derivatized and analyzed by GC-MS as described for wax analysis.

3.2.7 Carbon isotope analysis

Wax was extracted from *H. vulgare* cv. Morex flag leaf sheaths as described above and fractionated by TLC (CHCl₃: hexane (1:1); 0.25 mm layer thickness; Analtech). TLC bands were

by staining with primuline (1% in acetone) under UV light, target fractions were scratched from the plate and extracted with CHCl_3 , and fraction purities were verified by GC-MS analysis. For the two fractions containing esters/alkanes and β -diketones, compound-specific carbon isotope compositions were determined using GC-IRMS as described before (Zhang et al., 2021). In brief, a trace GC system equipped with Rxi-5ms column (30 m x 0.25 mm, film thickness 0.25 μm) and a programmable temperature vaporizing injector operated in solvent split mode was connected via a GC Isolink to a combustion furnace at 1000°C and via a Conflo IV interface further to a DeltaVPlus isotope ratio mass spectrometer (Thermo Scientific). The CO_2 reference gas was analyzed daily with a standard deviation of < 0.06‰ for instrument stability and linearity. Six reference peaks of CO_2 bracketed analyte peaks during the course of a GC-IRMS run; two were used for standardization, the rest were used to monitor stability. Samples were interspersed with standard compound mixtures of known isotopic composition. Data were normalized to the VPDB carbon isotopic scale by comparing with an external standard (A6mix) obtained from Dr. A. Schimmelmann, Indiana University, Bloomington, containing 15 alkane compounds (C_{16} to C_{30}), with $\delta^{13}\text{C}$ values ranging from -33.34 to -26.15‰.

3.2.8 Barley protoplast, tobacco leaf transient expression and microscopy

pGWB5-35Spro::DMH-GFP, pGWB5-35Spro:: GFP-DMP and ER specific marker p35S:HDEL-RFP (a kind gift from Dr. Mathias Schuetz and Lacey Samuels (UBC, Vancouver)) were used for protoplast transient expression. Ten-day-old barley cv. Morex seedlings were used for protoplast preparation and transformation following the method described previously (Yoo et al., 2007). Transformed protoplasts were incubated for 16–18 h and imaged by an Olympus FV1000 multiphoton confocal laser scanning microscope equipped with 405, 473, and 559 nm

lasers. Excitation of GFP, RFP and chlorophyll fluorescence were achieved using argon laser 473 and 559 nm.

Transient expression of pGWB5-35Spro:: GFP-DMP alongside p35S:HDEL-RFP in *N. benthamiana* was performed as described previously (Sun et al., 2020). Similar microscopy setting was used in imaging. ImageJ 1.51r software were used for image processing.

3.3 Results

The present study aimed to test the hypothesized pathways leading to β -diketones by detailed chemical analysis of barley wax and biochemical characterizations of the enzymes involved. To these ends, we analyzed the (i) β -diketone products, (ii) 2-alkanol ester by-products, and (iii) ^{13}C isotope profiles of various wax constituents, and then investigated the (iv) specificity of the DMH catalyzing the first reaction of the pathway, (v) the biochemical activity of the DMP catalyzing the second reaction and (vi) its specificity, and (vii) the subcellular localization of both enzymes.

3.3.1 Homolog and isomer distributions of β -diketones

To distinguish potential wax polyketide pathways, we first aimed to identify all β -diketone homolog and isomer structures accumulating in barley cv. Morex wax. To this end, we extracted wax from spikes (without awns), separated it by TLC, and isolated the most prominent fraction (with polarity expected for β -diketones, R_f 0.56) for GC-MS analysis. All compounds in this fraction shared similar mass spectra (Figure 3-2), with base peaks m/z 100 likely due to double-McLafferty rearrangement and, thus, indicating a β -constellation of two carbonyl groups. Molecular ions $[\text{M}]^+$, together with $[\text{M}-18]^+$ ions formed by loss of water, enabled the assignment of overall chain lengths for each compound and their identification as C_{29} - C_{33} β -diketones. Other prominent fragments were due to α -cleavage near either of the carbonyl groups, or single-

McLafferty rearrangement along with loss of water ($\Delta m/z$ -18) or loss of water and acetone ($\Delta m/z$ -76) (Trka and Streibl, 1974). Together, these ions enabled the assignment of positional isomers within each homolog, leading to the identification of C₂₉ 12,14- and 14,16-diketone, C₃₁ 14,16-diketone and C₃₃ 16,18-diketone structures, as reported before. The two even-numbered homologs, comprising three isomers, were unprecedented structures, identified as C₃₀ 14,16-diketone and a mixture of C₃₂ 14,16- and C₃₂ 15,17-diketones. Similar β -diketone homologs and isomers were observed in the corresponding TLC fraction of barley flag leaf sheath wax (data not shown).

The relative amounts of all identified barley wax β -diketones were determined by GC-MS using the common signature ion m/z 100 for homolog quantification and characteristic α -fragments for isomer quantification. Integration of both datasets showed that C₃₁ 14,16-diketone comprised 96.4% of the compound class, along with 0.4% C₂₉ 12,14-diketone, 0.3% C₂₉ 14,16-diketone, and 2.6% C₃₃ 16,18-diketone (Figure 3-3A). The C₃₀ 14,16-diketone, C₃₂ 14,16-diketone and C₃₂ 15,17-diketone made up 0.1%, 0.2% and 0.1% of the fraction, respectively.

While all the previously known β -diketone structures comprised exclusively even-numbered acyl moieties, the newly identified C₃₀ and C₃₂ homologs included one odd-numbered acyl moiety that may provide important new information on β -diketone biosynthesis. Odd-numbered acyls can be formed either at the onset of elongation by incorporating odd-numbered starters to yield unbranched or subterminally branched products, or late in elongation by incorporating methylmalonate extenders to yield mid-chain-branched products. To distinguish between these scenarios, we aimed to determine whether the novel β -diketone homologs had branched or unbranched carbon backbones, and for this assessed their GC retention behavior as a proxy for boiling point differences. Under all conditions used here, the C₃₀ and C₃₂ β -diketones eluted at or shortly after the half-way points between neighboring odd-numbered homologs, diverging less

than 2% from the average retention time differences between C_n and C_{n+1} homologs (Figure 3-4). In contrast, previous reports on various very-long-chain wax compounds had shown that, under GC conditions very similar to ours, skeletal isomers with subterminal methyl branches (*iso*-compounds) are separated from corresponding unbranched compounds by more than 25% of the homolog retention time difference (Busta and Jetter, 2017). Therefore, all the evidence taken together identified the novel barley wax β -diketones as unbranched C_{30} and C_{32} compounds, implying that their odd-numbered acyl moiety is formed at the onset of *de novo* fatty acid synthesis. Based on the elongation hypothesis, the proposed major precursor C_{18} 3-ketoacid would require five, six and seven rounds of FAE-type elongation to form C_{29} 12,14-, C_{31} 14,16- and C_{33} 16,18-diketone, respectively. These three products made up 0.3%, 96.4% and 2.6% of total diketones, indicating that the majority of the precursor underwent six rounds of FAE elongation, while only minor amounts were elongated five or seven times by FAE. Accordingly, the elongation hypothesis further predicted that the minor precursors C_{16} and C_{19} 3-ketoacid are elongated six times to form C_{29} 14,16-diketone and C_{32} 14,16-diketone, which indeed accounted for 0.4% and 0.2% of the total diketones, respectively (Figure 3-1B; Figure 3-5). However, the C_{30} 14,16-diketone and C_{32} 15,17-diketone, predicted to be formed from another minor precursor, C_{17} 3-ketoacid, by six and seven rounds of FAE elongation, respectively, were present in approximately equal amounts (0.1% of total diketones, Figure 3-1B, indicated by “*”; Figure 3-5). It is difficult to explain why C_{17} 3-ketoacid, in contrast to all other 3-ketoacid substrates with slightly longer or shorter chain lengths, had equal possibility to undergo six or seven rounds of FAE-type elongation. The newly evidence from our β -diketone profiling in barley waxes thus leads to contradictory conclusions from the elongation-decarboxylation hypothesis, overall casting doubt on this model for β -ketone formation.

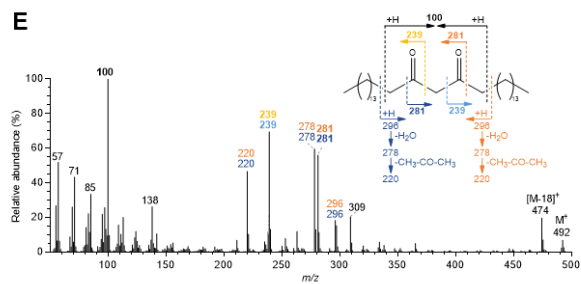
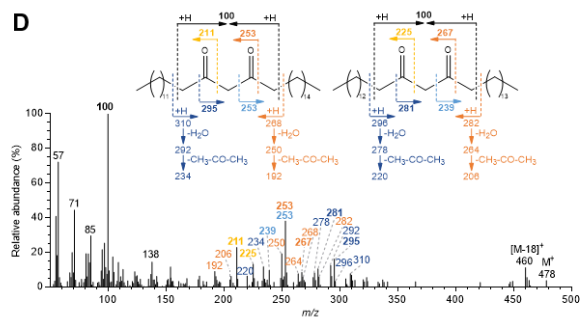
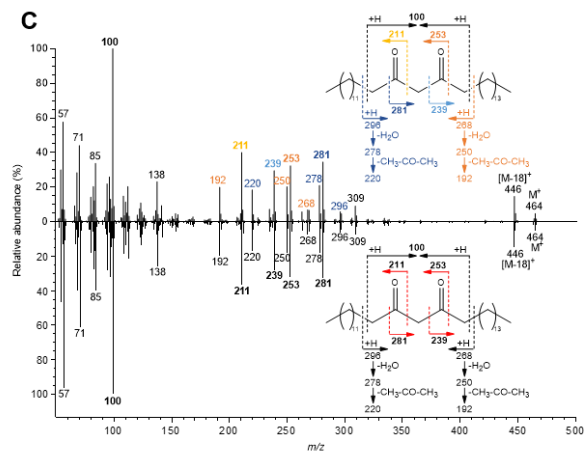
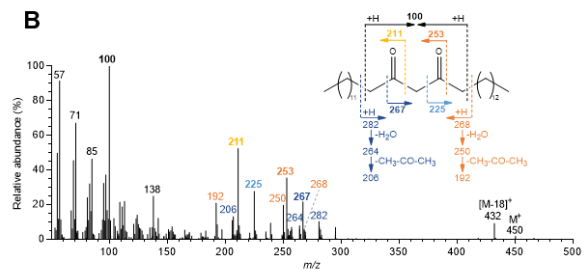
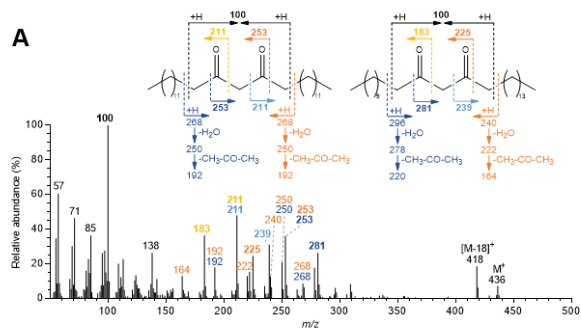


Figure 3-2: Mass spectra of β -diketone homologs/isomers identified in barley cv. Morex spike and flag leaf sheath waxes

A) Mass spectrum of the mixture of C_{29} β -diketones and fragmentation patterns of C_{29} 14,16-diketone (left) and C_{29} 12,14-diketone (right). B) Mass spectrum and fragmentation pattern of C_{30} 14,16-diketone. C) Mass spectrum and fragmentation pattern of 14,16-diketone. D) Mass spectrum of the mixture of C_{32} β -diketones and fragmentation patterns of C_{32} 14,16-diketone (left) and C_{32} 15,17-diketone (right). E) Mass spectrum and fragmentation pattern of C_{33} 16,18-diketone.

3.3.2 Homolog and isomer distributions of 2-alkanol ester side products of the β -diketone pathway

To further assess the mechanisms forming β -diketones, we aimed to shed light on the chain length distributions of key intermediates and for this analyzed the 2-alkanols known to be pathway side products. In the TLC fraction of barley spike wax (R_f 0.73) dominated by 1-alkanol esters, a series of 2-alkanol esters with total carbon numbers ranging from C_{33} to C_{37} were identified based on MS comparisons with previously published information (Racovita et al., 2016). GC-MS analyses using the characteristic acylium ion fragments (Racovita et al., 2016) revealed that the C_{33} , C_{35} , C_{36} and C_{37} homologs accounted for 8.3%, 58.5%, 2.9% and 30.3% of the compound class, respectively (Figure 3-3B). Similar 2-alkanol ester homolog distributions were observed in barley flag leaf sheath wax (data not shown).

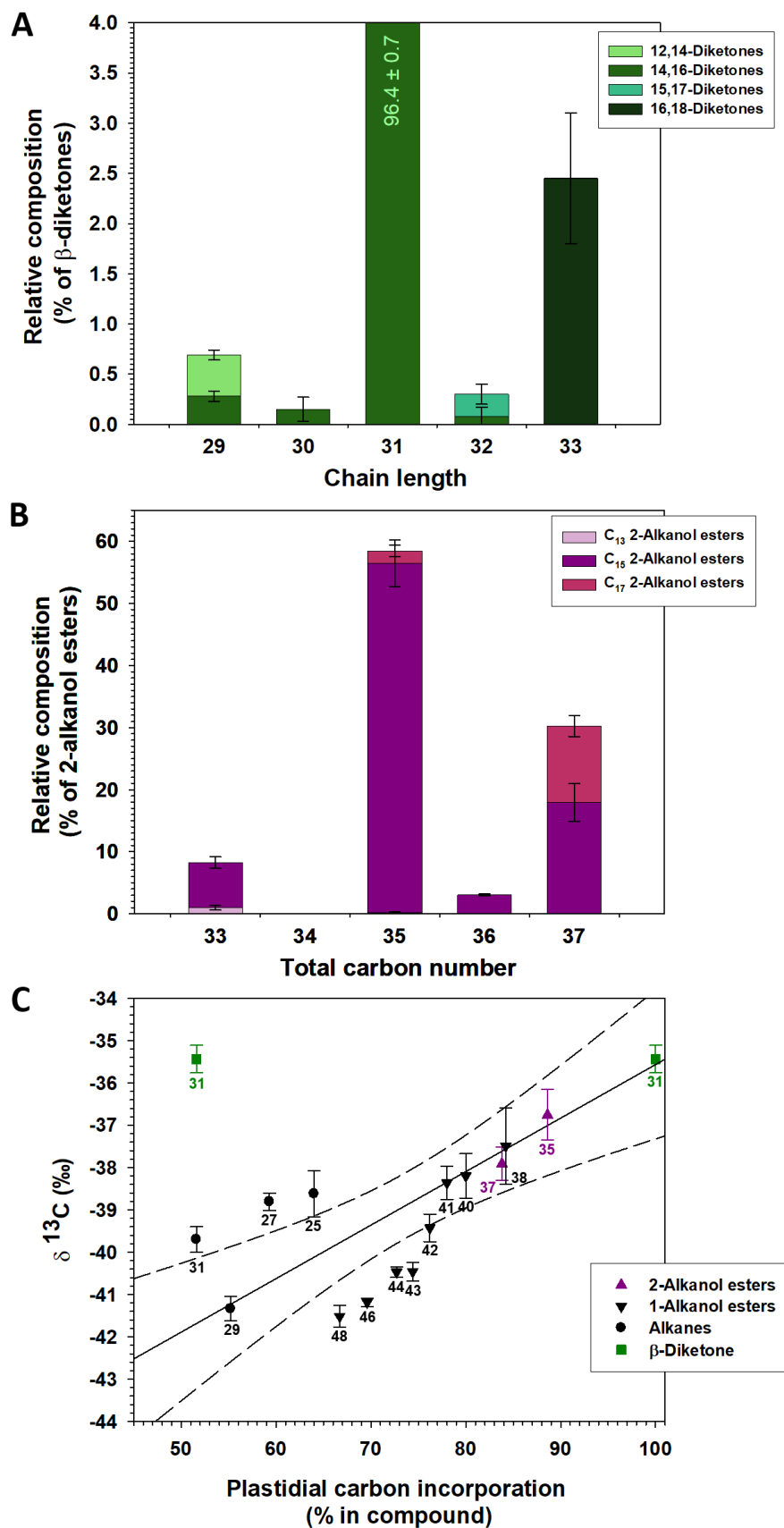


Figure 3-3: Chemical characterization of the β -diketones and associated 2-alkanol esters in the wax mixture covering barley cv. Morex spikes

A) Relative amounts of β -diketones with chain lengths $C_{29} - C_{33}$, and isomer distribution for each homolog (stacked bars). B) Relative amounts of 2-alkanol esters with total carbon numbers $C_{33} - C_{37}$, and isomer distribution for each homolog (stacked bars). C) Correlation analysis between ^{13}C isotope enrichment values of barley spike wax compounds (carbon numbers given next to each data point) and their incorporation of plastidial carbon. Alkanes are known to be formed by initial assembly of C_{16} chains in plastids and addition of further carbons up to the final chain length in the ER. The C_{25} , C_{27} , C_{29} and C_{31} alkanes in barley wax can thus be expected to contain 64%, 59.3%, 55.2% and 51.6% plastidial carbon. Similarly, the 1-alkanol and 2-alkanol esters consist of alkyl and acyl moieties each incorporating C_{16} precursors assembled in the plastid (i.e., 32 plastid-derived carbons overall), and % of plastidial carbon could be accordingly calculated against their total carbon numbers. The result of linear regression analysis is shown as solid line ($r^2 = 0.60$), with 95% confidence intervals as dashed lines. Finally, the plastidial carbon amounts of C_{31} β -diketone was predicted based on the pathway hypotheses illustrated in Figure 3-1: The elongation pathway relies on plastidial elongation to C_{16} and addition of 15 more carbons in the ER (hence, 51.6% plastidial carbon); in contrast, the head-to-head condensation hypothesis predicts incorporation of two C_{16} moieties both generated in the plastid (hence, 100% plastidial carbon). Error bars in each panel represent standard deviations of three biological replicates for A) and B) and three technical replicates in C).

Additional GC-MS analysis revealed that all four homologs had mainly C_{15} 2-alkanol esterified with various acids, amounting to 88%, 96%, 59% and 100% of the C_{33} , C_{35} , C_{36} and C_{37} esters, respectively (Figure 3-3B). Overall, the pool of esterified alcohols (across all ester homologs) comprised 84% C_{15} 2-alkanol, along with only 1% of the C_{13} and 14% of the C_{17} 2-alkanols. Based on the general understanding that 2-alkanols are biosynthesized from 3-ketoacids one carbon longer, the high concentration of C_{15} 2-alkanol esters suggests a precursor pool dominated by C_{16} 3-ketoacid. However, this result conflicts with the long-held tenet that C_{18} 3-ketoacid is the major substrate for elongation towards the β -diketone products, thus further questioning the previously assumed mechanism for β -diketone formation.

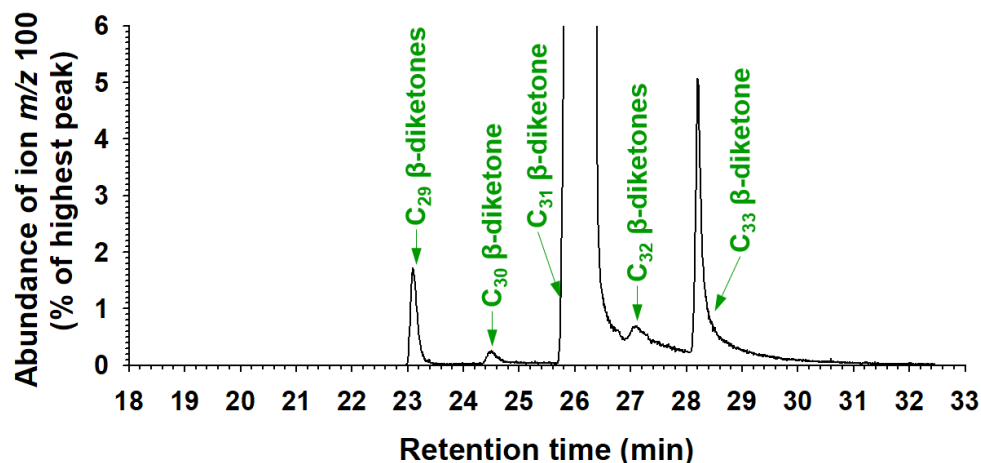


Figure 3-4: GC-MS analysis of the TLC fraction containing β -diketones from barley cv. Morex spike wax.

GC trace of the extracted ion m/z 100 characteristic of β -diketones.

3.3.3 The core wax elongation enzyme is not required for β -diketone formation

To further test whether β -diketone formation involved acyl elongation steps, we investigated the impact of defects in *KCS6/CER6*, the core enzyme of the FAE complexes elongating wax precursors, on β -diketone products. To this end, we analyzed the wax of flag leaf sheaths of the barley *emr1* mutant deficient in *KCS6/CER6*. Overall, the mutant wax mixture showed a distinct elongation phenotype, with chain length distributions shifted to shorter homologs in comparison with the corresponding wild type (*H. vulgare* cv. Ingrid). Significant shifts were observed in all wax compound classes comprising chain lengths longer than C_{24} , including alkanes, 1-alkanols (primary alcohols), 1-alkanol esters and alkylguaiacols (Figure 3-6, Basas-Jaumandreu et al., 2014), matching previous reports on the wax composition of lower leaves of these lines (Weidenbach et al., 2014). In contrast, those compound classes comprising only homologs shorter than C_{24} , including the esters combining C_{15} 2-alkanol and $C_{<20}$ acid, showed no mutant effect. Finally, the C_{31} β -diketones and hydroxy- β -diketones dominating the flag leaf sheath wax were

also found in similar concentrations in the mutant and wild type. Formation of their carbon backbones thus does not involve KCS6/CER6, the major wax elongation enzyme.

3.3.4 Natural carbon isotope abundance in β -diketones and other wax compounds

Plant lipids have characteristic depletion patterns of the natural isotope ^{13}C known to encode information on growth conditions as well as biosynthetic mechanisms (Collister et al., 1994). In particular, previous studies revealed ^{13}C concentration differences between wax compound classes and chain lengths, suggesting differential isotope incorporation at various stages of wax biosynthesis from the onset of fatty acyl elongation to final product elaboration (Bi et al., 2005; Rommerskirchen et al., 2006; Chikaraishi and Naraoka, 2007). Therefore, we aimed to test in how far the biosynthetic pathways leading to β -diketones and other wax components overlapped in early or late stages, by comparing ^{13}C amounts across wax compound classes. To span all stages of biosynthesis, our comparative analysis had to include a range of wax compounds with known biosynthesis pathways but different degrees of acyl chain elongations occurring in plastids and the ER. We hypothesized that β -diketone synthesis mechanisms involving ketoacid elongation should rely on the same (ER-located) malonyl-CoA extender pool as the FAE elongation reactions leading to other VLC compounds, and β -diketones should therefore have isotope compositions similar to those of other wax constituents with the same hydrocarbon chain lengths (e.g., C_{31} β -diketone vs. C_{31} alkane). In contrast, the alternative pathway revolving around head-to-head condensation of a 3-ketoacid and an acyl-CoA (compare Figure 3-1 and Figure 3-5) assumes incorporation of two fatty acyl units produced in the plastids instead of ER-derived malonate, suggesting that β -diketones should have isotope concentrations similar to those of shorter-chain compounds (e.g., C_{31} β -diketone vs. C_{31} ester consisting of C_{16} acid + C_{15} 2-alkanol).

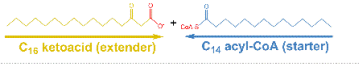
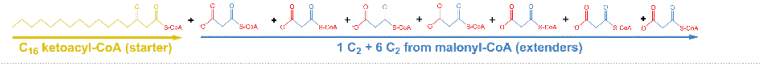
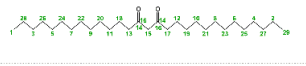
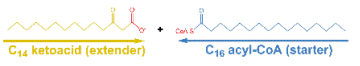
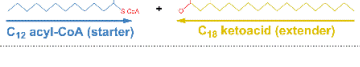
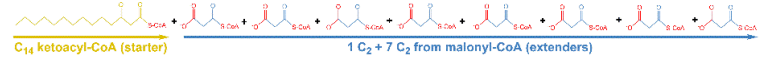
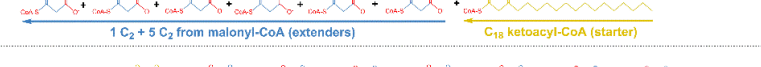

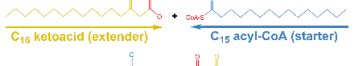
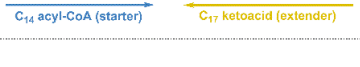
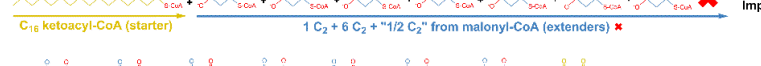

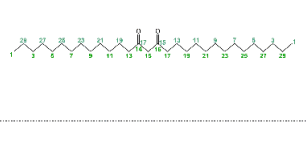
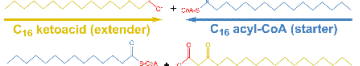
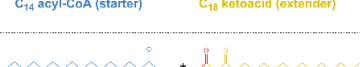
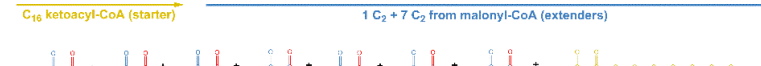
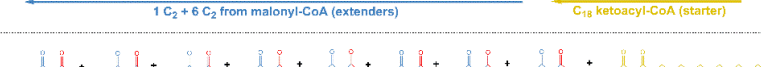
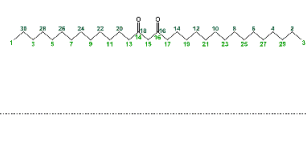
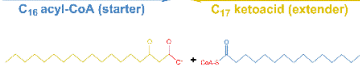

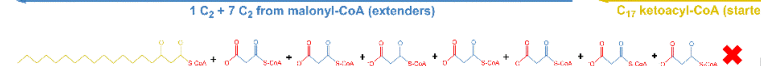
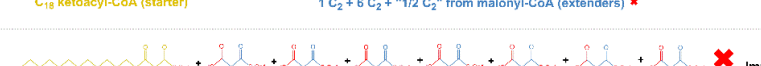
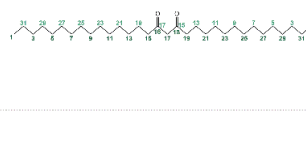
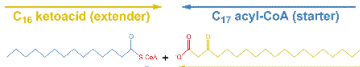

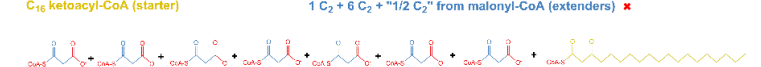

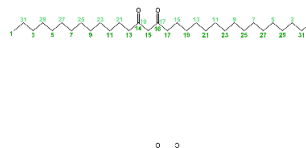



Head-to-head condensation of substrates	Elongation of substrates	β -Diketone products	%
 <p>C₁₅ ketoacid (extender) + C₁₄ acyl-CoA (starter)</p>	 <p>C₁₆ ketoacyl-CoA (starter) + 1 C₂ + 6 C₂ from malonyl-CoA (extenders)</p>	 <p>C₂₉ 14,16-diketone</p>	0.3%
 <p>C₁₄ ketoacid (extender) + C₁₆ acyl-CoA (starter)</p>  <p>C₁₂ acyl-CoA (starter) + C₁₈ ketoacid (extender)</p>	 <p>C₁₄ ketoacyl-CoA (starter) + 1 C₂ + 7 C₂ from malonyl-CoA (extenders)</p>  <p>C₁₈ ketoacyl-CoA (starter) + 1 C₂ + 5 C₂ from malonyl-CoA (extenders)</p>	 <p>C₂₉ 12,14-diketone alias C₂₉ 16,18-diketone</p>	0.4%
 <p>C₁₉ ketoacid (extender) + C₁₅ acyl-CoA (starter)</p>  <p>C₁₄ acyl-CoA (starter) + C₁₇ ketoacid (extender)</p>	 <p>C₁₆ ketoacyl-CoA (starter) + 1 C₂ + 6 C₂ + "1/2 C₂" from malonyl-CoA (extenders) ✗ Impossible</p>  <p>C₁₇ ketoacyl-CoA (starter) + 1 C₂ + 6 C₂ from malonyl-CoA (extenders)</p>	 <p>C₃₀ 14,16-diketone alias C₃₀ 15,17-diketone</p>	0.1%
 <p>C₁₆ ketoacid (extender) + C₁₆ acyl-CoA (starter)</p>  <p>C₁₄ acyl-CoA (starter) + C₁₈ ketoacid (extender)</p>	 <p>C₁₆ ketoacyl-CoA (starter) + 1 C₂ + 7 C₂ from malonyl-CoA (extenders)</p>  <p>C₁₈ ketoacyl-CoA (starter) + 1 C₂ + 6 C₂ from malonyl-CoA (extenders)</p>	 <p>C₃₁ 14,16-diketone alias C₃₁ 16,18-diketone</p>	96.4%
 <p>C₁₆ acyl-CoA (starter) + C₁₇ ketoacid (extender)</p>  <p>C₁₈ ketoacid (extender) + C₁₅ acyl-CoA (starter)</p>	 <p>C₁₇ ketoacyl-CoA (starter) + 1 C₂ + 7 C₂ from malonyl-CoA (extenders)</p>  <p>C₁₈ ketoacyl-CoA (starter) + 1 C₂ + 6 C₂ + "1/2 C₂" from malonyl-CoA (extenders) ✗ Impossible</p>	 <p>C₃₂ 15,17-diketone alias C₃₂ 16,18-diketone</p>	0.1%
 <p>C₁₆ ketoacid (extender) + C₁₇ acyl-CoA (starter)</p>  <p>C₁₄ acyl-CoA (starter) + C₁₉ ketoacid (extender)</p>	 <p>C₁₆ ketoacyl-CoA (starter) + 1 C₂ + 6 C₂ + "1/2 C₂" from malonyl-CoA (extenders) ✗ Impossible</p>  <p>C₁₉ ketoacyl-CoA (starter) + 1 C₂ + 6 C₂ from malonyl-CoA (extenders)</p>	 <p>C₃₂ 14,16-diketone alias C₃₂ 17,19-diketone</p>	0.2%
 <p>C₁₈ ketoacid (extender) + C₁₈ acyl-CoA (starter)</p>	 <p>C₁₈ ketoacyl-CoA (starter) + 1 C₂ + 7 C₂ from malonyl-CoA (extenders)</p>	 <p>C₃₃ 16,18-diketone</p>	2.6%

Figure 3-5: Predicted building blocks for head-to-head condensation or elongation towards individual β -diketone homologs and isomers

Structures, names and relative amounts (%) of β -diketone products are shown on the right. The building blocks required to form each product by head-to-head condensation are shown on the left, and building blocks required to form the products instead by elongation are shown in the center (compare Figure 3-1). 3-Ketoacid intermediates are given in yellow, and the fatty acyl-CoA or malonyl-CoA for the two alternative synthesis mechanisms are given in blue. The groups labeled in red are lost during decarboxylative reactions. Arrows below acyl chains indicate in which direction they have been extended, and arrows below malonyl units show the direction of sequential C_2 unit additions. The latter are counted as “1 C_2 + X C_2 ”, to designate that the first C_2 unit is incorporated by DMP and “X” further C_2 units are incorporated by FAE complex(es). Where biosynthesis of a particular β -diketone product can occur in two directions, both alternatives are shown. Red symbols “×” indicate that formation of a particular β -diketone product by elongation in that direction is impossible.

To distinguish between both hypotheses, we extracted wax from barley spikes, fractionated the mixture by TLC, and analyzed the fraction containing $C_{25} - C_{31}$ alkanes, $C_{38} - C_{48}$ 1-alkanol esters and $C_{35} - C_{37}$ 2-alkanol esters by gas chromatography coupled with isotope-ratio mass spectrometry (GC-IRMS). The resulting ^{13}C enrichment values of individual compounds were plotted as a function of their plastidial carbon percentages, assuming elongation in the plastids up to C_{16} and further elongation in the ER to the final chain lengths. Overall, the alkanes and esters together had ^{13}C concentrations positively correlated with plastidial carbon amounts ($r^2 = 0.60$), with slightly larger linear increases within each compound class (Figure 3-3C). A second TLC fraction containing only β -diketones (>95% C_{31} 14,16-diketone) had a ^{13}C enrichment of $-35.3 \pm 0.3\text{‰}$, relatively close to those of 1- and 2-alkanol esters. This value fits the trend established for all other compound classes only if assuming 100% plastidial carbon content in the β -diketone and, thus, favors the head-to-head condensation hypothesis (Figure 3-3C, indicated by “*”). In contrast, the β -diketone isotope enrichment value varies significantly from that predicted by the ketoacid elongation hypothesis, implying a plastidial carbon content of 51.6% for C_{31} β -diketone (Figure 3-

3C). Therefore, the isotope abundance determined here cast further doubt on the elongation pathway to β -diketones and favors the head-to-head condensation mechanism.

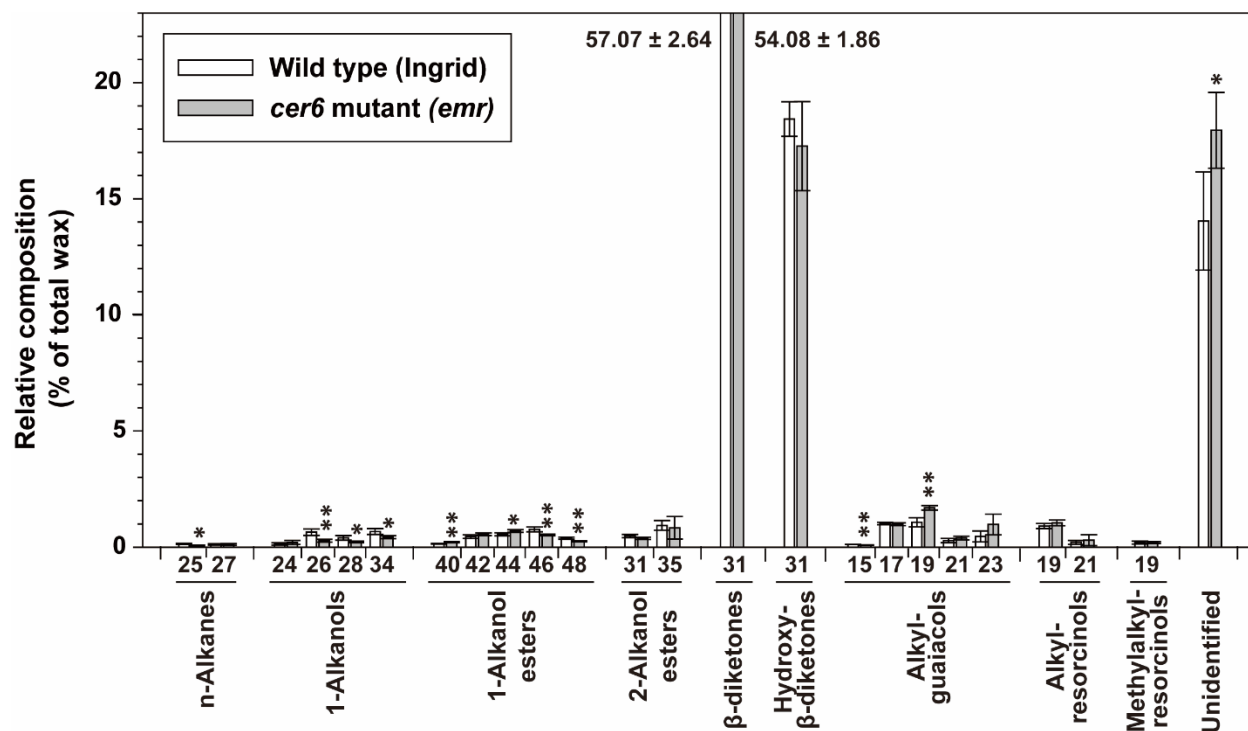
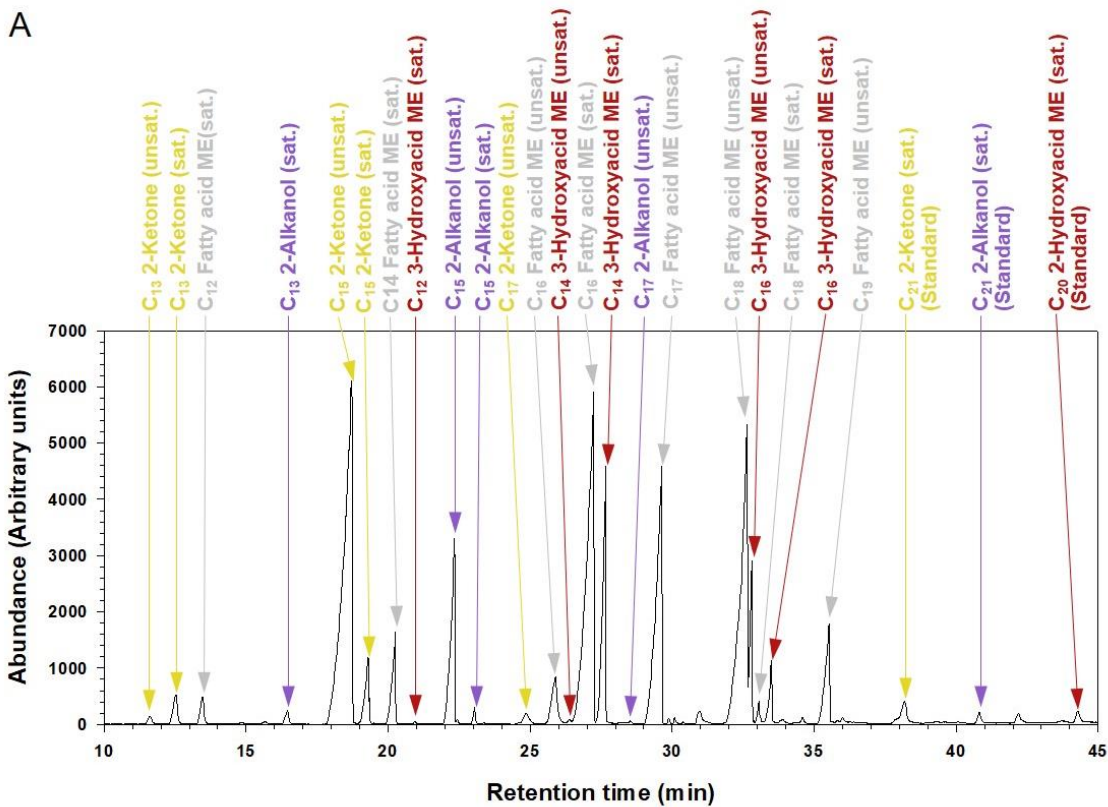


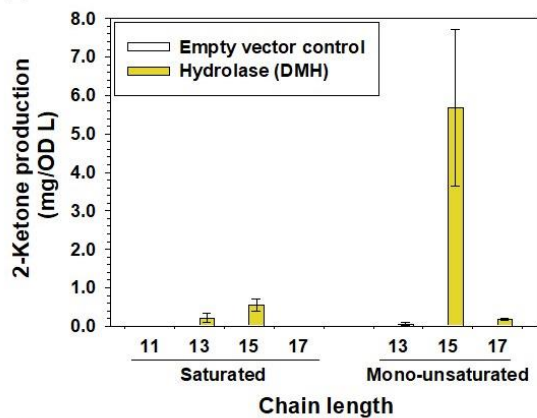
Figure 3-6: Wax analysis of a barley mutant deficient in elongation to very-long-chain compounds

Wax was extracted from flag leaf sheaths (at heading stage) of barley wild type (cv. Ingrid) and the *cer6* (*emr*) mutant known to have a defect in elongation of wax precursors beyond chain lengths C₂₄. GC-FID analysis confirmed the mutant phenotype, with amounts of C_{>24} alkanes, 1-alkanols (primary alcohols) and esters which contain these alkanols significantly reduced relative to wild type. In contrast, the amounts of β -diketones were not affected in the *cer6* (*emr*) mutant. C₃₀ 1-alkanol and C₃₃ 2-alkanol ester could not be separated from C₂₁ alkylresorcinol under the present conditions and were, therefore, not quantified. Similarly, C₃₂ 1-alkanol could not be separated from C₃₁ β -diketone and was not quantified. Error bars represent standard deviations of four biological replicates. Asterisks indicate discovery of statistically significant differences between wild type and mutant based on Student's *t* test (**P* < 0.05, ***P* < 0.01).

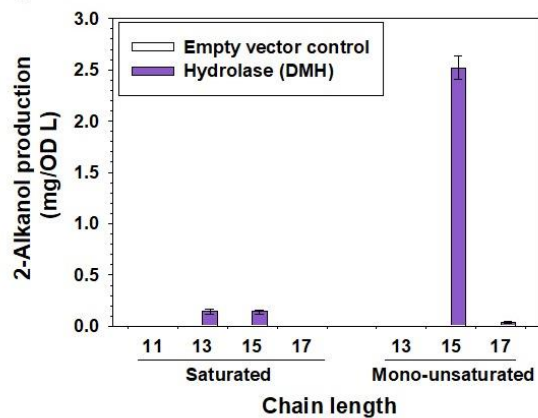
A



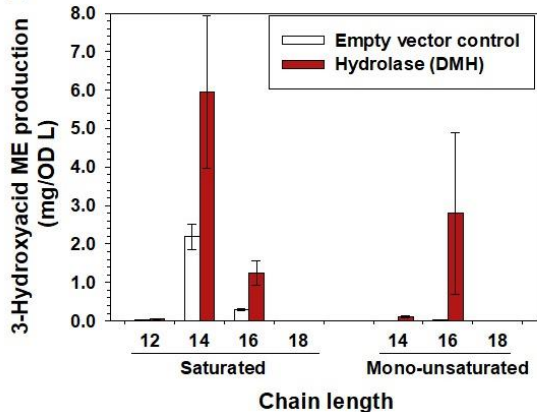
B



C



D



E

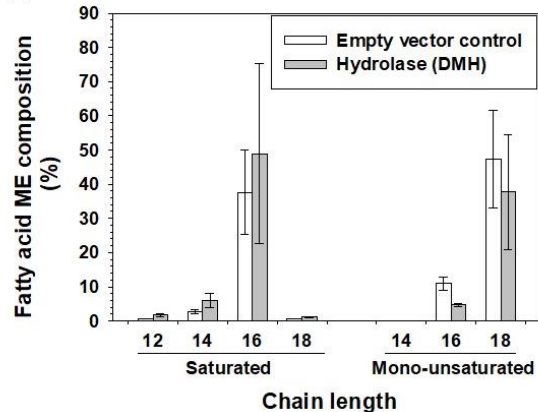


Figure 3-7: Characterization of the barley Diketone Metabolism Hydrolase (DMH) producing the key intermediates on the β -diketone synthesis pathway

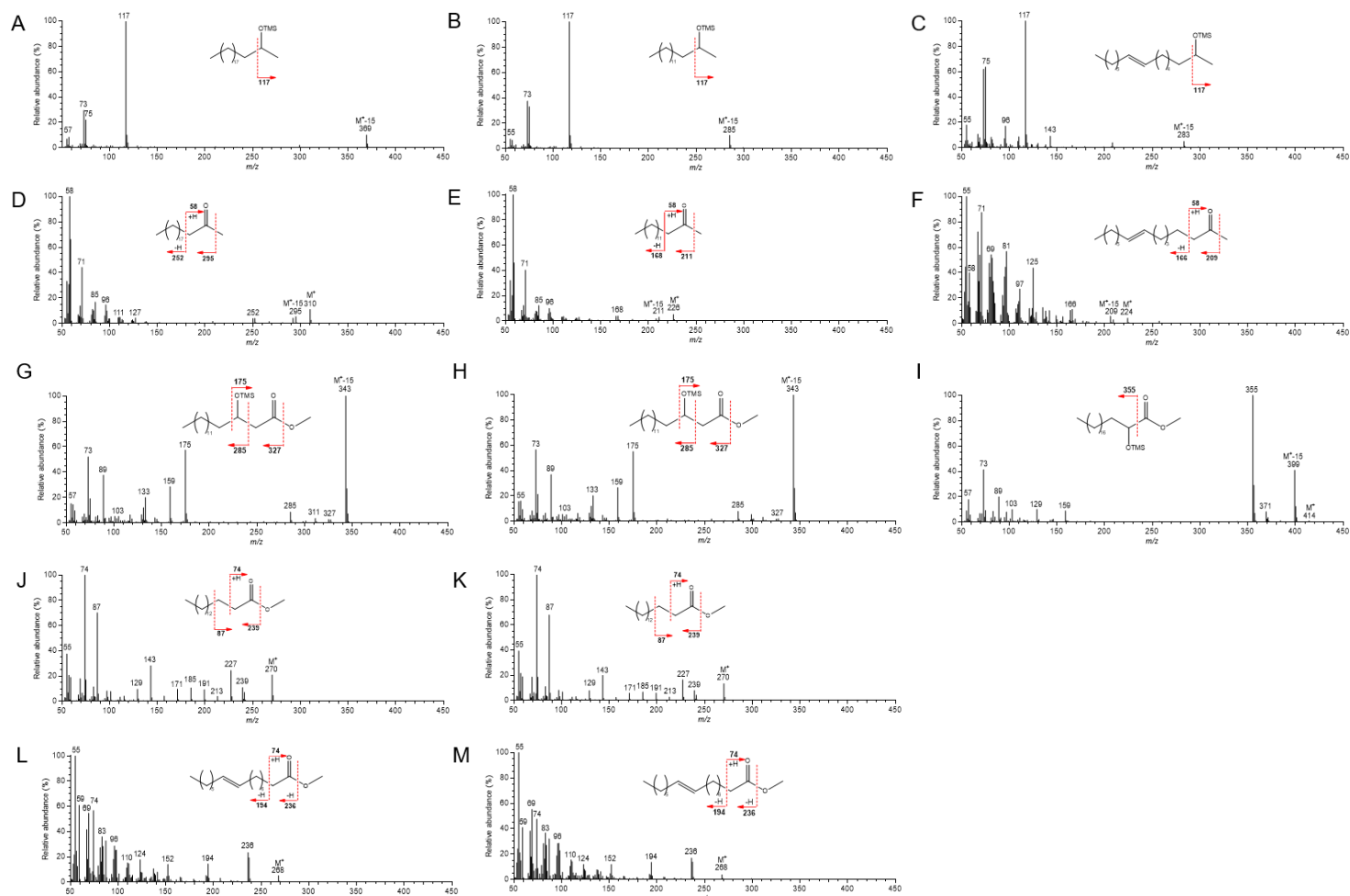
A) Total ion chromatogram of lipids from *E. coli* expressing DMH. Neutral lipids were extracted, acyls were released by transesterification into methyl esters (MEs), and hydroxyl groups were converted into trimethyl-silyl (TMS) derivatives. Homolog series of saturated and monounsaturated 2-ketones (yellow), 2-alkanols (purple), 3-hydroxyacid MEs (red) and fatty acid MEs (grey) were detected. B) Amounts of 2-ketones in *E. coli* expressing DMH (quantified against internal standard C₂₁ 2-ketone). C) Amounts of 2-alkanols in *E. coli* expressing DMH (quantified against internal standard C₂₁ 2-alkanol). D) Amounts of 3-hydroxyacid MEs in *E. coli* expressing DMH (quantified against internal standard C₂₀ 2-hydroxyacid ME and normalized to C₁₆ 3-hydroxyacid ME). E) Amounts of fatty acid MEs in *E. coli* expressing empty vector or DMH. Error bars represent standard deviations of three biological replicates.

3.3.5 Barley DMH producing a narrow range of intermediates on the β -diketone synthesis pathway

To further establish the chain length distribution of the intermediates in the β -diketone pathway, we aimed to analyze the specificity of the barley DMH enzyme proposed to generate respective 3-ketoacids in the first reaction of the pathway. Detailed GC-MS analyses of *E. coli* expressing DMH identified saturated and mono-unsaturated C₁₃ - C₁₇ 2-ketones and 2-alkanols, together with C₁₂ - C₁₆ 3-hydroxy fatty acids (Figure 3-7A; Figure 3-8). Further quantitative analyses revealed that the 2-alkanol and 2-ketone series were each dominated by respective unsaturated C₁₅ compounds, accompanied by much lesser, approximately equal amounts of the saturated C₁₃ and C₁₅ homologs (Figure 3-7B, C; Figure 3-9). None of these compounds could be detected in corresponding empty-vector controls. The series of 3-hydroxyacids comprised predominantly saturated C₁₄ and C₁₆ as well as unsaturated C₁₆ compounds (Figure 3-7D). The concentrations of all these 3-hydroxyacids were increased approximately two-fold over those of empty-vector controls. In separate analyses, the *E. coli* extracts were subjected to transesterification and the resulting fatty acid methyl esters (FAMES) were analyzed by GC-FID to assess the available

fatty acyl pools in *E. coli* for lipid synthesis. The DMH expressors and empty-vector control lines had similar profiles, with saturated C₁₂ - C₁₈ fatty acyls peaking in C₁₆ and corresponding unsaturated acyls peaking in C₁₈ (Figure 3-7E).

It seems plausible that the 2-ketones and 2-alkanols were formed by decarboxylation of corresponding 3-ketoacids and 3-hydroxyacids, respectively, either spontaneously during sample preparation and analysis, or enzymatically by endogenous *E. coli* proteins. To assess β -diketone intermediate chain length distributions, the homolog distribution of the keto/hydroxyacids can therefore be taken together with that of the 2-ketones and 2-alkanols each one carbon shorter. Thus, our results showed that DMH generated predominantly (saturated and unsaturated) C₁₆ 3-ketoacid and 3-hydroxyacid in *E. coli*. Due to the differences in unsaturated fatty acyl pools of *E. coli* and plants (Sayanova et al., 2007), details of our heterologous expression experiment cannot be directly extrapolated to the *in planta* activity of DMH. However, the chain length preferences found match our initial results that the wax β -diketones and 2-alkanol esters mostly comprised C₁₆ ketoacyl moieties (or their derivatives), thus underscoring that the central ketoacid intermediate of the β -diketone/2-alkanol pathway is 16 carbons long.



A) Mass spectrum and fragmentation pattern of (saturated) C₂₁ 2-alkanol standard. B) Mass spectrum and fragmentation pattern of (saturated) C₁₅ 2-alkanol produced by *E. coli* expressing DMH. C) Mass spectrum and fragmentation pattern of monounsaturated C₁₅ 2-alkanol produced by *E. coli* expressing DMH. D) Mass spectrum and fragmentation pattern of (saturated) C₂₁ 2-ketone standard. E) Mass spectrum and fragmentation pattern of (saturated) C₁₅ 2-ketone produced by *E. coli* expressing DMH. F) Mass spectrum and fragmentation pattern of monounsaturated C₁₅ 2-ketone produced by *E. coli* expressing DMH. G) Mass spectrum and fragmentation pattern of (saturated) C₁₆ 3-hydroxyacid methyl ester (ME) standard. H) Mass spectrum and fragmentation pattern of (saturated) C₁₆ 3-hydroxyacid ME produced by *E. coli* expressing DMH. I) Mass spectrum and fragmentation pattern of (saturated) C₂₀ 2-hydroxyacid ME standard. J) Mass spectrum and fragmentation pattern of (saturated) C₁₆ fatty acid ME standard. K) Mass spectrum of (saturated) C₁₆ fatty acid ME produced by *E. coli* expressing DMH. L) Mass spectrum and fragmentation pattern of monounsaturated C₁₆ fatty acid ME standard. M) Mass spectrum and fragmentation pattern of (monounsaturated) C₁₆ fatty acid ME produced by *E. coli* expressing DMH.

3.3.6 Biochemical function of the barley DMP enzyme

Based on all the evidence implying C₁₆ 3-ketoacid as the central intermediate of the β -diketone pathway, our next goal was to test its role as a direct substrate of the ensuing step and, thus, to establish the biochemical activity of DMP. In a first set of experiments, we aimed to characterize DMP by heterologous expression in yeast (*Saccharomyces cerevisiae*). However, yeast lines expressing DMH did not produce detectable amounts of 2-ketones, 2-alkanols or 3-hydroxyacids, implying very low or no hydrolase activity in yeast (in contrast with our *E. coli* experiments above). Accordingly, yeast lines expressing both DMH and DMP also did not reveal either enzyme activity and contained only lipids also found in empty-vector controls (data not shown). Therefore, yeast expressing DMP was supplemented with exogenous C₁₆ 3-ketoacid substrate, and after incubation was found to contain three compounds not present in corresponding negative controls (either expressing empty vector or not fed the substrate). Based on their GC-MS characteristics, the major new product was identified as C₃₁ 14,16-diketone, and the minor compounds as C₂₉ 14,16-diketone

and a monounsaturated C₃₁ 14,16-diketone (Figure 3-10A, B). This result showed that DMP is active in yeast, and that it accepts long-chain 3-ketoacid (or a derivative thereof) as a substrate. It seems plausible that C₁₆ 3-ketoacid is directly condensed with C₁₆ fatty acyl-CoA to form C₃₁ 14,16-diketone, however interference by endogenous yeast metabolism could not be ruled out and, therefore, neither the exact role of the 3-ketoacid nor the co-substrate(s) for the reaction(s) can be concluded from this experiment.

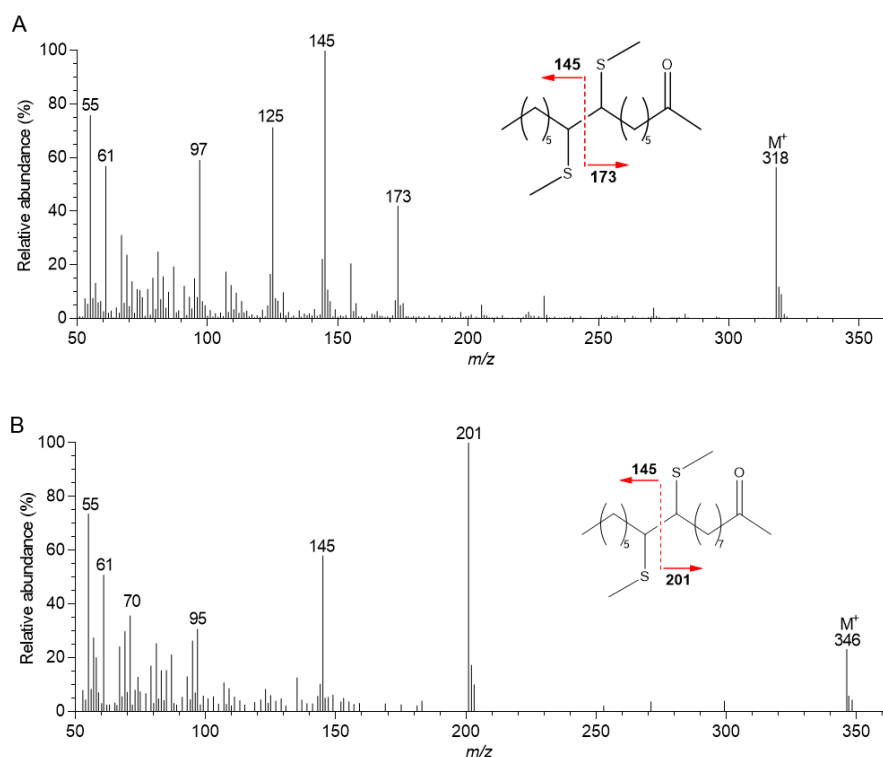


Figure 3- 9: MS analysis of double bond positions in monounsaturated 2-ketones produced in *E. coli* expressing barley *Diketone Metabolism Hydrolase* (DMH)

A) Mass spectrum of the DMDS adduct of monounsaturated C₁₅ 2-ketone produced by *E. coli* expressing DMH. B) Mass spectrum of the DMDS adduct of monounsaturated C₁₇ 2-ketone produced by *E. coli* expressing DMH. The structure inserts show major fragmentation reactions. Both compounds show characteristic α-fragments *m/z* 145, revealing that the double bonds in the original 2-ketones were located seven carbons away from the methyl terminus. The 2-ketones are thus identified as ω-7 isomers.

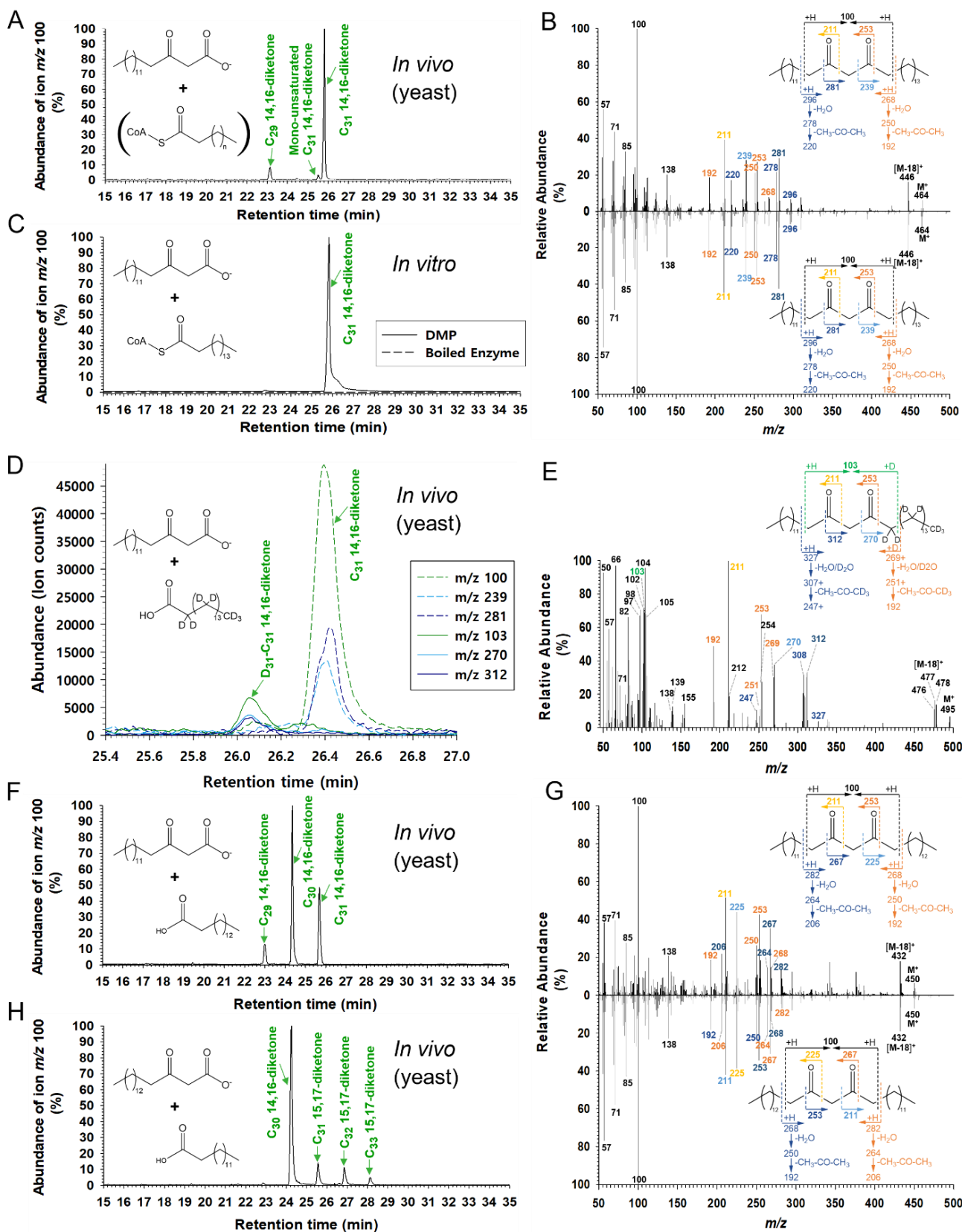


Figure 3-10: Characterization of the barley Diketone Metabolism Polyketide synthase (DMP) catalyzing the condensation between 3-ketoacids and acyl-CoAs to β -diketones

GC-MS analysis of various *in vivo* and *in vitro* assays feeding acyl-CoA and/or ketoacid substrates to DMP. Chromatograms of fragments m/z 100 selectively reporting β -diketones are shown on the left, and mass spectra of key β -diketone products on the right. A) Selected-ion chromatogram of lipids obtained from yeast expressing DMP and supplemented with C_{16} 3-ketoacid ($n = 11, 13$). Yeast expressing empty vector with C_{16} 3-ketoacid feeding and yeast expressing DMP without C_{16} 3-ketoacid feeding served as negative controls in this *in vivo* assay (data not shown). B) Mass spectra of C_{31} 14,16-diketone peaks in A) (upper panel) and C) (lower panel). C) Selected-ion chromatogram of lipids obtained from DMP *in vitro* assay incubated with C_{16} 3-ketoacid and C_{16} acyl-CoA. The boiled recombinant enzyme incubated with C_{16} 3-ketoacid and C_{16} acyl-CoA served as control in this *in vitro* assay. D) Selected-ion chromatograms of six characteristic fragments (selectively reporting undeuterated and deuterated β -diketones) of lipids obtained from yeast expressing DMP and supplemented with C_{16} 3-ketoacid and per-deuterated fatty acid $C_{15}D_{31}COOH$. E) Mass spectrum of the D_{31} -labelled C_{31} 14,16-diketone in D), showing two α -fragments (m/z 211 and 253) together with corresponding ions resulting from McLafferty rearrangement (ion cluster m/z 269+) and water/acetone loss (m/z 251+ and 192), all diagnostic for the C_{14} acyl moiety of the C_{31} 14,16-diketone structure. Analogous fragments comprising the other hydrocarbon tail of the compound were all shifted by 31 amu relative to the unlabeled C_{31} 14,16-diketone (α -fragments m/z 270 and 312; ions due to McLafferty rearrangement m/z 327 and loss of water/acetone m/z 307+ and 247+). The compound also showed a molecular ion 31 amu higher than the unlabeled diketone, along with a corresponding water loss ion $[M-18]^+$. Finally, the spectrum showed a cluster of ions centered around m/z 103, consistent with double-McLafferty rearrangement on both sides of the β -diketo group and involving a double-deuterated α -methylene and γ -deuterium transfer on one side. The other fragments in this cluster suggested further H/D transfer mechanisms involved in the rearrangements, however the exact structure of those fragments could not be assigned. Together, the GC and MS characteristics (Figure 3-11) unambiguously identified this compound as C_{31} 14,16-diketone with one normal and one per-deuterated hydrocarbon tail ($C_{13}H_{27}$ and $C_{15}D_{31}$, respectively). F) Selected-ion chromatogram of lipids obtained from yeast expressing DMP and supplemented with odd-numbered 3-ketoacid (C_{15}) and odd-numbered fatty acid (C_{15}). G) Mass spectra of C_{30} 14,16-diketone in F) (upper panel) and H) (lower panel). H) Selected-ion chromatogram of lipids obtained from yeast expressing DMP and supplemented with even-numbered 3-ketoacid (C_{16}) and even-numbered fatty acid (C_{14}). Arabidopsis *LACSI* was expressed in all the yeast used in *in vivo* assays to enhance exogenous substrate uptake (Pulsifer et al., 2012) (Pulsifer, Kluge and Rowland, 2012).

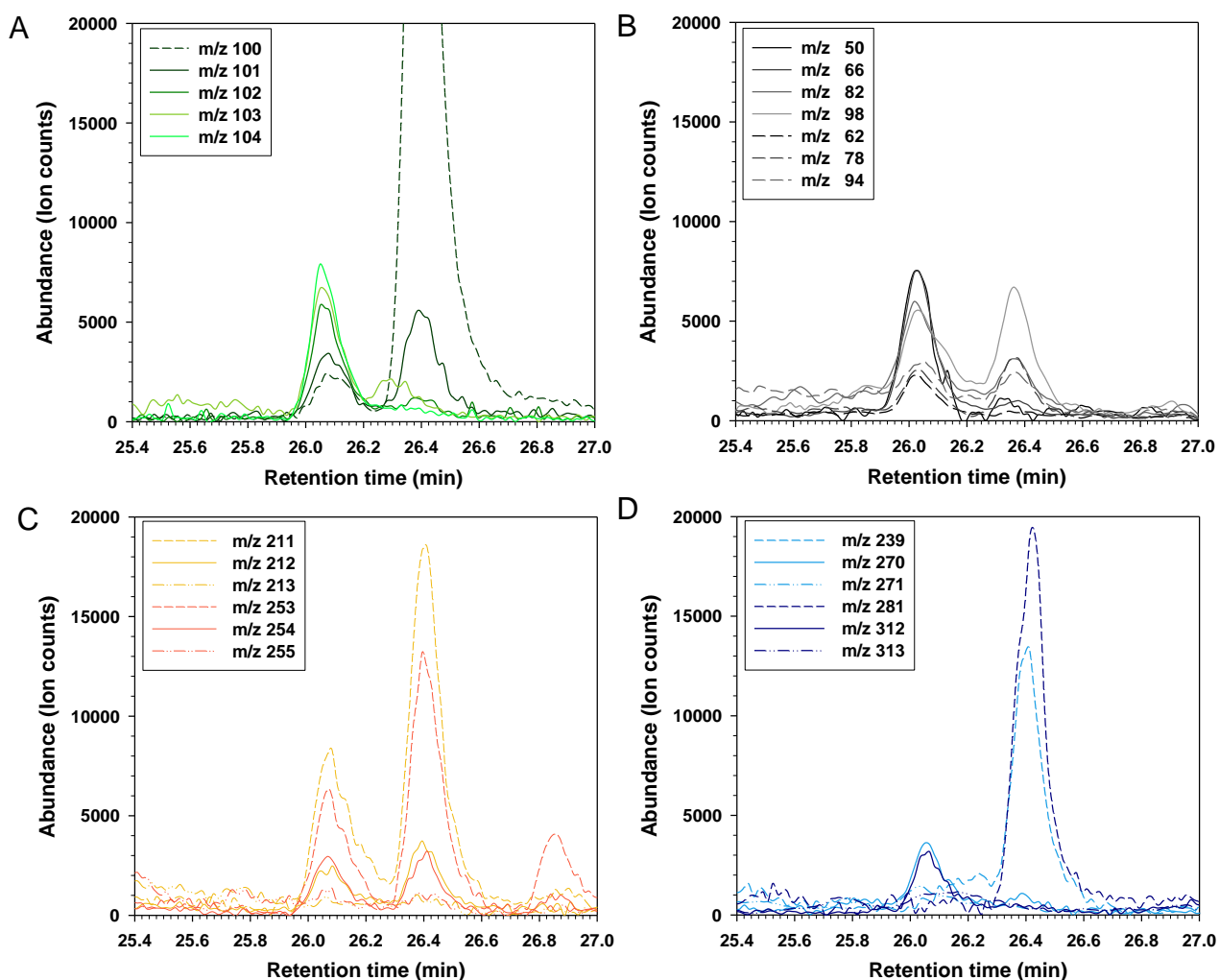


Figure 3-11: GC-MS analysis of deuterium-labeled β -diketone products from yeast *in vivo* assay

Selected-ion chromatograms of characteristic fragments from D_{31} -labelled C_{31} 14,16-diketone produced in yeast expressing DMP and supplemented with C_{16} 3-ketoacid and per-deuterated fatty acid $C_{15}D_{31}COOH$. A) Traces of ion m/z 100 characteristic of the undeuterated β -diketo group and of ions m/z 101-104 characteristic of the deuterated β -diketo group. B) Traces of small-mass ions further characterizing the deuterated β -diketone product. It is plausible that the fragments m/z 50, 66, 82 and 98 have structures $[CD_3-(CD_2)_n]^+$ with $n = 2-5$, indicating alkyl decay of the perdeuterated chain terminus. The fragments m/z 62, 78 and 94 may be tentatively interpreted as $[CD_3-(CD_2)_n-CO]^+$ with $n = 2-4$. C) Traces of two α -fragments (m/z 211 and 253) characteristic of one undeuterated hydrocarbon tail of the β -diketone and of corresponding deuterated fragments (m/z 212/213 and 254/255). D) Traces of two α -fragments (m/z 239 and 281) characteristic of the other undeuterated hydrocarbon tail of the β -diketone and of corresponding perdeuterated fragments (m/z 270/271 and 312/313).

To test the incorporation of the fatty acyl chain by DMP, we first fed per-deuterated C₁₆ fatty acid together with C₁₆ ketoacid to yeast expressing DMP and analyzed the resulting lipids by GC-MS. The yeast extracts contained unlabeled C₃₁ 14,16-diketone as in our previous assays, along with a novel compound with shorter GC retention time (Fig 4D) and similar mass spectrum (Figure 3-10E), both suggesting a deuterated derivative of C₃₁ 14,16-diketone. The compound also showed a molecular ion 31 amu higher than the unlabeled diketone, along with a corresponding water loss ion [M-18]⁺. Finally, the spectrum showed a cluster of ions centered around *m/z* 103, consistent with double-McLafferty rearrangement on both sides of the β-diketo group and involving a double-deuterated α-methylene and γ-deuterium transfer on one side. The other fragments in this cluster suggested further H/D transfer mechanisms involved in the rearrangements, however the exact structure of those fragments could not be assigned. Together, the GC and MS characteristics (Figure 3-11) unambiguously identified this compound as C₃₁ 14,16-diketone with one normal hydrocarbon tail (C₁₃H₂₇, from 3-ketoacid) and one per-deuterated hydrocarbon tail originating from the exogenous labeled fatty acid (C₁₅D₃₁). The formation and exact structure of this product indicated the direct incorporation of the entire acyl moiety into the β-diketone product.

In further metabolic labeling experiments, we used exogenous substrates with odd-numbered acyl chains to test whether DMP condensed entire ketoacid and fatty acyl-CoA units. In one assay, yeast expressing DMP were fed equimolar amounts of C₁₅ fatty acid and C₁₆ ketoacid, and their lipid mixture was found to contain three compounds absent from empty-vector controls. The major product was identified as C₃₀ 14,16-diketone, along with C₂₉ 14,16-diketone and C₃₁ 14,16-diketone (Figure 3-10F, G). In a similar assay, C₁₇ ketoacid and C₁₄ fatty acid were fed to yeast expressing DMP, and the resulting lipid extracts were found to contain C₃₀ 14,16-diketone as a major product together with C₃₁ 15,17-diketone, C₃₂ 16,18-diketone and C₃₃ 15,17-diketone

(Figure 3-10H, I, Figure 3-5). The predominance of the respective β -diketone product homologs, together with the common acyl structure in one part of the products of each assay, further confirmed that DMP catalyzed the direct condensation of fatty acyl-CoA and ketoacid substrates. Finally, to further assess the biochemical activity of DMP, and exclude the elongation system and metabolites from yeast, the recombinant enzyme was assayed *in vitro* with select combinations of possible substrates. Upon incubation of the enzyme with C₁₆ ketoacid and C₁₆ fatty acyl-CoA, a single new product was detected and, based on its GC-MS characteristics, identified as C₃₁ 14,16-diketone, which was not detected in the control (Figure 3-10 B, C). In contrast, corresponding assays of DMP with varying molar ratios of C₁₆ 3-ketoacid and malonyl-CoA yielded no detectable β -diketone or triketide/tetraketide products (data not shown). Incubation of the enzyme with C₁₆ fatty acyl-CoA and malonyl-CoA in diverse concentrations also did not lead to formation of detectable products. Together, our findings thus suggest that DMP does not, like other PKSs, accept malonyl-CoA as extenders for the condensation reaction, but instead links a 3-ketoacid with a fatty acyl-CoA to directly form β -diketone.

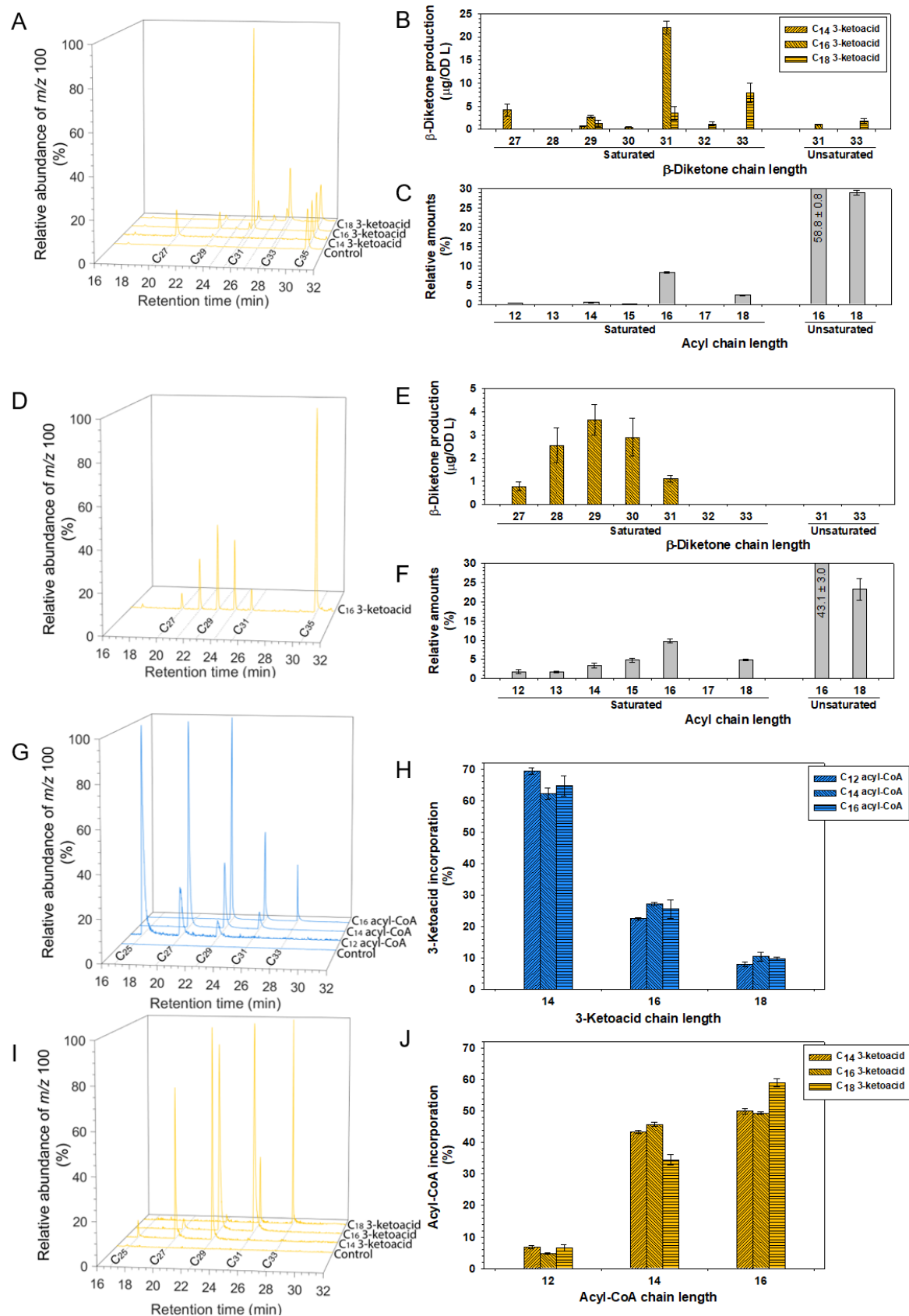


Figure 3-12: Assessment of DMP substrate preferences

GC-MS analysis of various *in vivo* and *in vitro* assays feeding different acyl-CoA and/or ketoacid substrates to DMP. Chromatograms of fragments m/z 100 selectively reporting β -diketones are shown on the left, and the corresponding β -diketone product profile(s) on the right. A) Selected-ion chromatograms of lipids obtained from yeast expressing DMP and supplemented with C₁₄, C₁₆, or C₁₈ 3-ketoacid or only buffer. B) β -diketone profiles produced in A) (quantified against internal standard C₃₅ 14,16-diketone). C) Relative composition of fatty acyl pools in yeast expressing DMP (quantified after transmethylation of total lipid extracts of yeast not supplemented with ketoacid). D) Selected ion chromatogram of lipids obtained from yeast expressing DMP and supplemented with C₁₆ 3-ketoacid alongside C₁₂-C₁₅ fatty acids (to adjust the fatty acyl profile). E) β -diketone profiles produced in D) (quantified against internal standard C₃₅ 14,16-diketone). F) Relative composition of fatty acyl pools in yeast expressing DMP (quantified after transmethylation of total lipid extracts of yeast supplemented with C₁₂ to C₁₅ fatty acids). G) Selected-ion chromatograms of lipids obtained from DMP *in vitro* assays combining equal molar concentration of C₁₆-C₁₈ 3-ketoacids - alongside C₁₂, C₁₄ or C₁₆ fatty acyl-CoA. The boiled recombinant enzyme incubated with equimolar concentrations of C₁₆-C₁₈ 3-ketoacids - alongside C₁₆ fatty acyl-CoA served as control. H) Proportions of 3-ketoacids incorporated with each fatty acyl-CoA co-substrate into the β -diketones shown in G). I) Selected-ion chromatograms of lipids obtained from DMP *in vitro* assays combining equal molar concentration C₁₂-C₁₆ fatty acyl-CoAs with C₁₄, C₁₆ or C₁₈ 3-ketoacid. The boiled recombinant enzyme incubated with equimolar concentrations C₁₂-C₁₆ fatty acyl-CoAs and C₁₆ 3-ketoacid served as control. J) Proportions of fatty acyl CoAs incorporated with each 3-ketoacid co-substrate into the β -diketones shown in I). Arabidopsis *LACS1* was expressed in all the yeast used in *in vivo* assays to enhance exogenous substrate uptake (Pulsifer et al., 2012) (Pulsifer, Kluge and Rowland, 2012). Error bars in (B-C), (E-F) and (H-G) represent standard deviations of three biological replicates.

3.3.7 Chain-length specificity of DMP for fatty acyl-CoA and 3-ketoacid substrates

Based on our findings thus far, we hypothesized that the very narrow range of β -diketone homologs accumulating in barley surface wax reflects the chain length distribution of substrates available *in planta* as well as substrate specificities of the DMP enzyme. To test the latter, we performed four sets of experiments with varying chain lengths of acyl-CoA and/or ketoacid substrates.

In a first set of assays, we supplemented yeast expressing *PKS* with equal molar amounts of C₁₄, C₁₆ or C₁₈ keto acids and quantified the resulting β -diketone products. Upon feeding C₁₄ keto acid,

a mixture of 86% C₂₇ 12,14-diketone and 14% C₂₉ 12,14-diketone (alias 16,18-diketone) was formed (Figure 3-12A, B). In contrast, feeding of C₁₆ 3-ketoacid led to production of mainly C₃₁ 14,16-diketone (84%) and C₂₉ 14,16-diketone (10%), along with small amounts of C₃₀ 14,16-diketone (2%) and mono-unsaturated C₃₁ 14,16-diketone (4%). Finally, assays with exogenous C₁₈ 3-ketoacid yielded a mixture dominated by C₃₃ 16,18-diketone (51%) and C₃₁ 14,16-diketone (22%), accompanied by C₂₉ 12,14-diketone (8%), C₃₂ 15,17-diketone (7%), and mono-unsaturated C₃₃ 16,18-diketone (12%). The overall β -diketone product amounts varied between 4.9, 26.3 and 15.7 $\mu\text{g}/\text{OD}\cdot\text{l}$ for C₁₄, C₁₆ and C₁₈ 3-ketoacid substrates, respectively. Together, the three assays showed that DMP accepts a range of 3-ketoacid substrates, and that it condenses each of them with different preferences for the acyl-CoA co-substrates. Interestingly, the major products came from reactions of C₁₄ 3-ketoacid with C₁₄ acyl, C₁₆ 3-ketoacid with C₁₆ acyl, and C₁₈ 3-ketoacid with C₁₄ and C₁₆ acyls.

To gauge the effect of available fatty acyl chain lengths on the *in vivo* assays, we quantified the fatty acyl homologs in the total lipid mixture of the yeast lines (after transformation into methyl esters). The acyl pools of control yeast (without substrate feeding) comprised mainly mono-unsaturated C₁₆ and C₁₈ chains (together accounting for 88% of the total acyls), and a series of saturated C₁₂ - C₁₈ acyls dominated by C₁₆ (8%) and C₁₈ (3%) (Figure 3-12C). Based on this acyl profile, our DMP assay results implied that the enzyme greatly preferred saturated over unsaturated acyl substrates, and to some degree also C₁₄ acyls over the more abundant C₁₆ and C₁₈ homologs (Figure 3-13A).

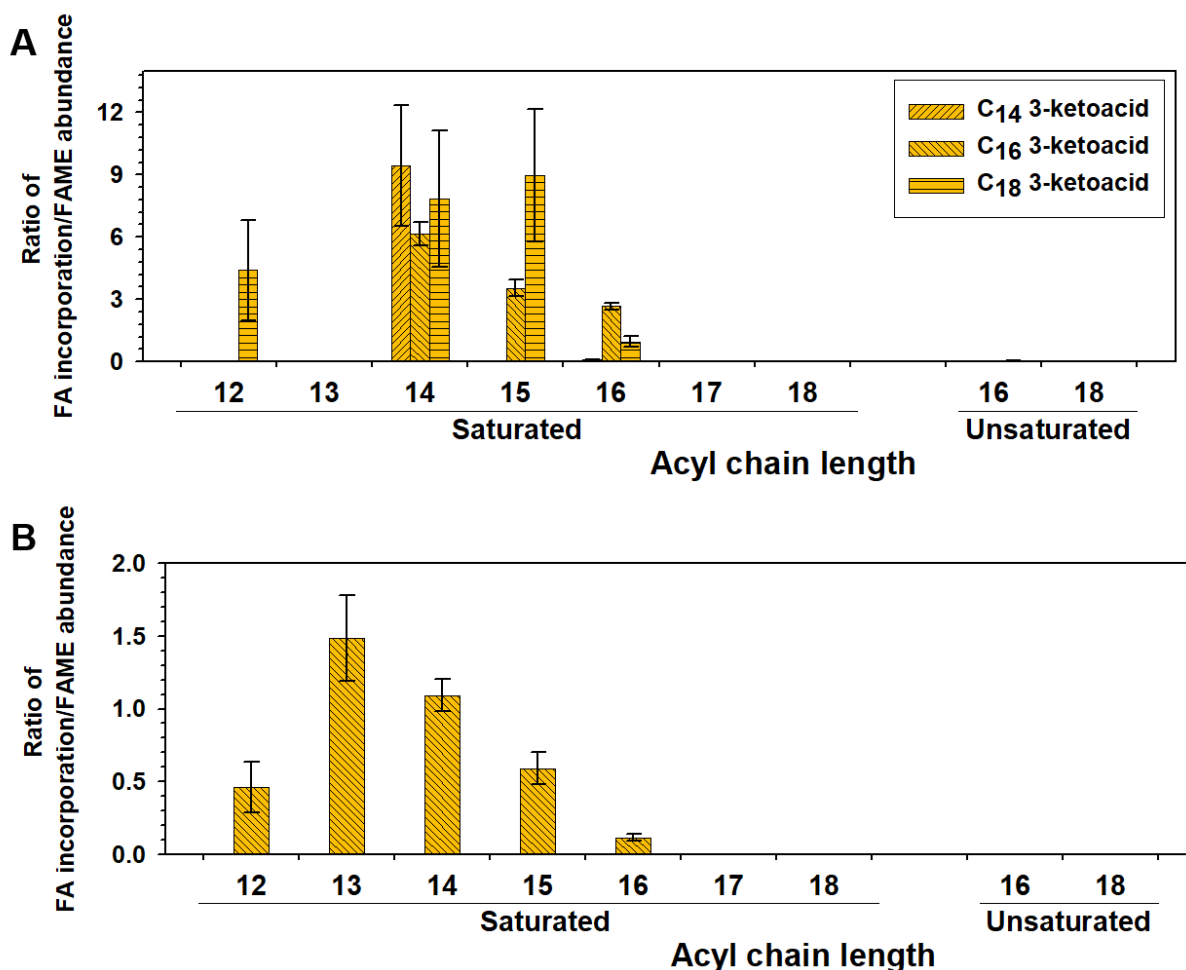


Figure 3- 13: Determination of DMP substrate preferences by *in vivo* assays

A) Ratios of fatty acyl substrate amount incorporated into particular β -diketones (together with a given ketoacid co-substrate) to the amount of the corresponding fatty acyl available in yeast under the assay conditions (calculated from data in Figure 3-12 A-C). B) Ratios of fatty acyl substrate amount incorporated into particular β -diketones (together with C₁₆ ketoacid co-substrate) to the amount of the corresponding fatty acyl available in yeast complemented with C₁₂-C₁₅ fatty acids (to adjust the fatty acyl profile) (calculated from data in Figure 3-12 D-F). Arabidopsis *LACS1* was expressed in all the yeast used in *in vivo* assays to enhance exogenous substrate uptake (Pulsifer et al., 2012) (Pulsifer, Kluge and Rowland, 2012). Error bars represent standard deviations of three biological replicates.

The preference of DMP for certain acyl-CoA chain lengths was assessed in a second *in vivo* experiment where we supplemented yeast expressing the enzyme with various exogenous fatty acids to augment minor homologs. Preliminary tests showed that co-feeding of C₁₆ 3-ketoacid with

either C₁₁ or C₁₇ fatty acids yielded the same β -diketones as controls lacking exogenous acids (data not shown), suggesting that DMP did not accept these two acyl chain lengths. However, co-feeding of C₁₆ 3-ketoacid with a mixture of C₁₂-C₁₅ fatty acids led to production of C₂₇-C₃₁ β -diketones (Figure 3-12D). The product mixture had a near-symmetric chain length distribution centered around the C₂₉ homolog, including substantial amounts of two even-numbered β -diketone homologs, C₂₈ and C₃₀ (Fig 5E). In contrast to the controls lacking exogenous fatty acids, unsaturated β -diketones could not be detected in this assay. Fatty acid profiling of the total yeast lipids showed that fatty acid feeding resulted in substantially increased amounts of available C₁₂-C₁₅ acyls (Figure 3-12F), albeit with C₁₆ acyls still dominating. In summary, the DMP enzyme was able to condense C₁₆ 3-ketoacid with C₁₂-C₁₆ acyls, with a preference for C₁₃/C₁₄ acyl co-substrate (Figure 3-13B).

Finally, the interdependence between the chain length preferences of DMP for both 3-ketoacid and acyl substrates was explored using *in vitro* assays with defined, limiting substrate concentrations. In a first set of experiments, the 3-ketoacid preference of DMP in the presence of different fatty acyl co-substrates was tested by competition assays with limited amounts of each fatty acyl-CoA. Recombinant DMP was incubated with a ketoacid pool containing one molar equivalent each of C₁₄, C₁₆ and C₁₈ ketoacids and supplemented with 1.5 equivalents of either C₁₂, C₁₄ or C₁₆ fatty acyl-CoA, respectively. In all three assays, over 60% of the β -diketone products were formed by incorporation of C₁₄ 3-ketoacid substrate, accompanied by 20% of C₁₆ 3-ketoacid condensation products and circa 10% of C₁₈ ketoacid products (Figure 3-12G, H). The DMP enzyme, thus, had strong C₁₄ chain length preference for its 3-ketoacid substrate, irrespective of acyl-CoA co-substrate chain length.

In a second set of experiments, the acyl-CoA preference of was tested in competition assays with limited amounts of 3-ketoacid co-substrates. The enzyme was incubated with a fatty acyl-CoA pool of C₁₂, C₁₄ and C₁₆ homologs (1:1:1 molar ratio) and supplemented with either C₁₄, C₁₆ or C₁₈ 3-ketoacid (1.5 molar equivalents), respectively. In all three assays, the majority of β -diketone products incorporated C₁₄ and C₁₆ fatty acyl-CoAs, and <7% of the β -diketones originated from C₁₂ acyl-CoA substrate (Figure 3-12I, J). The C₁₆ fatty acyl-CoA substrate was preferred over C₁₄ fatty acyl-CoA in the presence of all 3-ketoacids tested, and most pronouncedly for condensation with C₁₈ ketoacid. Overall, the *in vitro* characteristics of DMP thus suggested that the enzyme preferentially condensed C₁₆ fatty acyl-CoA with C₁₄ 3-ketoacid to form C₂₉ 14,16-diketone.

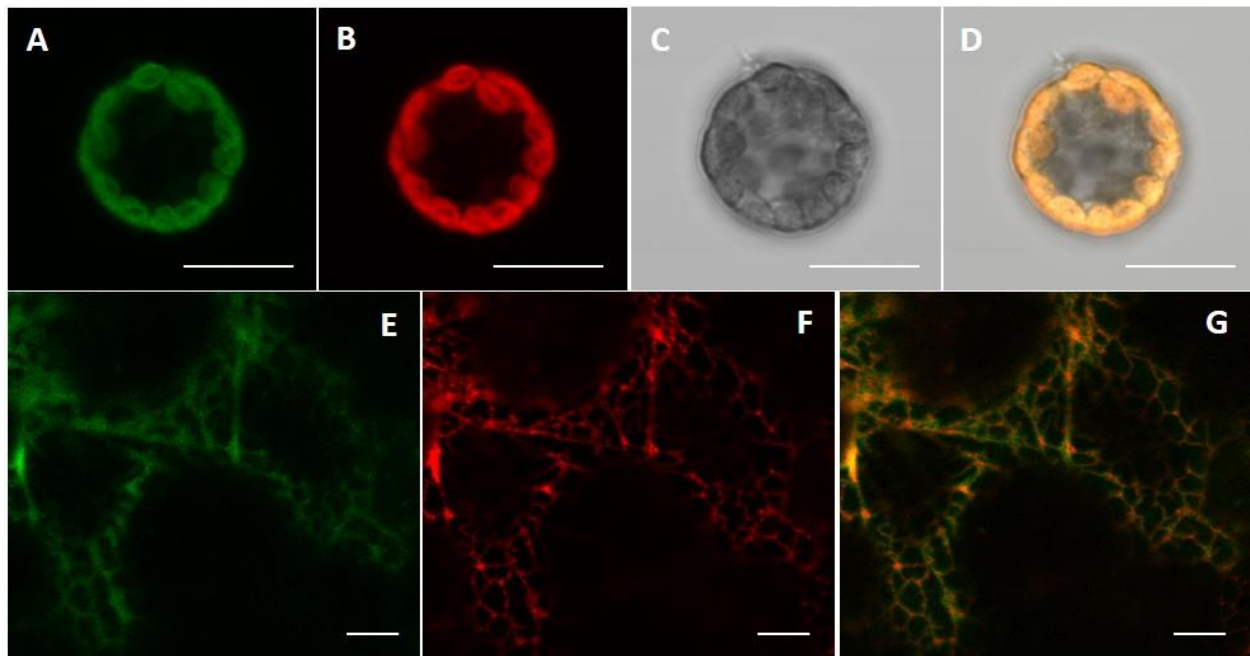


Figure 3-14: Subcellular localization of DMH and DMP

Confocal microscope images of barley protoplasts transiently expressing Pro35S:DMH-GFP, showing A) Pro35S:DMH-GFP, B) chloroplast autofluorescence, C) bright field, and D) the merged image of (A-C). Confocal microscope images of *N. benthamiana* leaves coexpressing E) Pro35S:GFP-DMP, F) the ER marker Pro:35S:HDEL-RFP and G) the merged image of (E-F). Bars = 10 μ m.

3.3.8 Subcellular compartmentation of the β -diketone-forming enzymes

Based on our biochemical results showing that only two enzymes, DMH and DMP, were required for β -diketone formation, we aimed to locate the biosynthetic pathway across the cellular compartments. For this, we first determined the subcellular localization by confocal microscopy of barley protoplasts transiently expressing GFP fusion constructs of DMH under control of the 35S promoter. The fluorescence signal obtained from DMH with C-terminally fused GFP matched the chlorophyll autofluorescence patterns within the cells (Figure 3-14A-D), indicating that this enzyme resided in the chloroplast. The hydrolase is, thus, able to access the FAS complexes involved in *de novo* fatty acid synthesis, and can intercept ketoacyl-ACP intermediates from them to release free 3-ketoacid product still in the plastid.

Since coexpression of ER-maker and GFP fused DMP in barley protoplasts failed, we assessed the subcellular localization of GFP-DMP by transient expression in tobacco leaves. In this assay, fluorescence signals of N-terminal fusions of DMP showed a reticulate pattern and colocalized with ER-specific marker HDEL-RFP (Figure 3-14E-G), suggesting that this protein resides in the ER. The second enzyme of the β -diketone pathway therefore has direct access to its acyl-CoA substrates, while its 3-ketoacid co-substrates must be exported from the plastids to the ER for the condensation reaction. Assembly of the β -diketone products by DMP in the ER then coincides with formation of all other known wax compounds in the same cellular compartment.

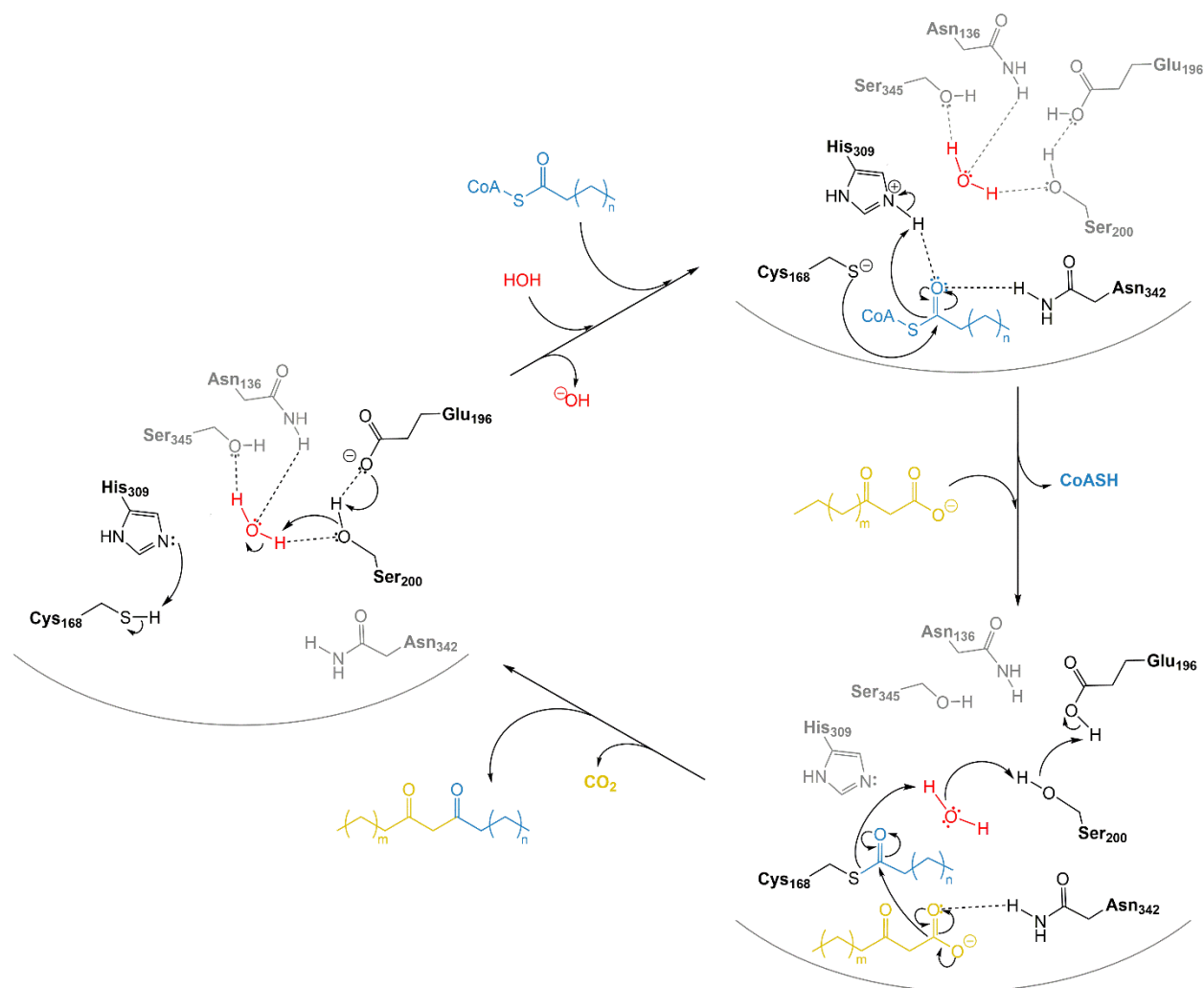


Figure 3- 15: Schematic representation of the proposed DMP reaction mechanism

On the left, the empty enzyme active site is shown with core amino acids predicted to participate in the mechanism. In the first step of the reaction cycle, a fatty acyl-CoA starter molecule is loaded into the catalytic center and covalently bound to Cys₁₆₈. Hydrogen bonds between the fatty acyl-CoA head group and His₃₀₉ and Asn₃₄₂ facilitate the bond formation. In the second step of the catalytic cycle, a 3-ketoacid extender molecule enters the active site and, assisted by Asn₃₄₂, undergoes decarboxylation into the corresponding enolate. Finally, nucleophilic attack of the enolate on the carbonyl carbon of the starter and proton transfer via an adjacent water molecule (facilitated by Ser₃₄₅, Asn₁₃₆, Ser₂₀₀ and Glu₁₉₆) yield the β-diketone product and re-set the active site.

3.4 Discussion

Previous studies on wheat and barley found a metabolic gene cluster, comprising at least three genes, involved in the formation of β-diketones, hydroxy- β-diketones and 2-alkanol esters (Hen-

Avivi et al., 2016; Schneider et al., 2016). However, the multiple enzyme system, varying chain length of the aliphatic intermediates, and the almost symmetric chemical structure of the final products, made it difficult to unravel each step of β -diketone biosynthesis. In current study, we started from the barley wax analysis and re-assessed the wax products from this pathway, continued with the biochemical function analysis of the core enzymes by *in vivo* and *in vitro* assays. Our study found an un-canonical PKS and clarified the key steps of β -diketone formation, which revise the model of β -diketone synthesis pathway.

3.4.1 β -Diketones are unlikely synthesized through the elongation-decarboxylation pathway

The sequential elongation β -diketone synthesis model was deduced based on the early radioactive-labeled wax precursor incorporation assays. The C_2 unit donor acetate, and short elongation precursors C_{12} - C_{16} fatty acids, were readily incorporated into β -diketones when fed to barley *cer-u* (corresponding to DMC) spikes tissue slices, while longer elongation precursor C_{18} fatty acid was hardly incorporated into β -diketones (Mikkelsen and von Wettstein-Knowles, 1978; Mikkelsen, 1979; von Wettstein-Knowles, 2017). In another labeled wax precursor feeding study, the C_{14} fatty acid, C_{14} fatty acyl-CoA and C_{16} fatty acyl-CoA, were again found to be efficient precursors for β -diketones and 2-alkanol esters; Additionally, the elongation intermediate C_{16} 3-ketoacyl-CoA was found incorporated into both β -diketones and 2-alkanol esters with a high efficiency, while another elongation intermediates C_{16} 3-hydroxyacid-CoA and 3-hydroxyacids ranging from C_{14} - C_{18} were incorporated into β -diketone-related products with a low efficiency (Mikkelsen, 1984). Thus C_{18} 3-ketoacyl primer were deduced as the major β -diketone intermediate, which could be formed through elongation of both short fatty acyl (C_{12} - C_{16}) and 3-ketoacyl (C_{16}) precursors but not the long fatty acyl precursors (C_{18}) (Mikkelsen, 1984; von Wettstein-Knowles, 2017). In the following steps of the proposed model, the proposed

major precursor C₁₈ 3-ketoacyl intermediate could undergo sequential C₂ unit addition to form β -diketoacids, which could be further decarboxylated to release β -diketones (Figure 3-1A).

However, this model failed to explain why in the precursor feeding assay, another type of short elongation intermediates 3-hydroxyacyl primers (C₁₂-C₁₆) could not be efficient precursors for β -diketones.

The early β -diketone synthesis inhibitor assays shed light on the β -diketone synthesis pathway.

The radioactive-labeled acetate was readily incorporated into both β -diketones and hydrocarbons in barley spikes tissue feeding assay. However, when the barley spikes were preincubated with different elongation enzyme inhibitors, the incorporation rate of labeled acetate into β -diketones changed differently from that into hydrocarbons, indicating different enzymatic machineries are involved in the synthesis of these two wax products (Mikkelsen and von Wettstein-Knowles, 1978).

In our study, four pieces of data did not support the elongation-decarboxylation β -diketone synthesis model. Firstly, we identified two novel even-numbered β -diketone homologs comprising three isomers which were not reported in previous studies. The C₃₀ 14,16-diketone and C₃₂ 15,17-diketone, which were both synthesized from C₁₇ 3-ketoacyl intermediate, underwent six- and seven-round of FAE elongation, respectively, had 1:1 concentration ratio based on elongation-decarboxylation model (Figure 3-1B, indicated by “*”; Figure 3-5; Figure 3-3A). However, this ratio conflicted with that of the β -diketones synthesized from C₁₈ 3-ketoacyl intermediate: the five-round elongation product (C₂₉ 12,14-diketone) made up 0.3% of total β -diketones, the six-round elongation product (C₃₁ 16,18-diketone) made up 96.4% of total β -diketones, and the seven-round elongation product (C₃₃ 16,18-diketone) accounted for 2.6% of total β -diketones, indicating the majority of 3-ketoacyl intermediate undergoes six-round of FAE

elongation. This observation could also be found in β -diketones synthesized from C_{16} and C_{19} 3-ketoacyl intermediates (Figure 3-1B; Figure 3-5; Figure 3-3A). Thus, the similar abundance of the novel even-numbered β -diketone homologs is unlike synthesized from elongation. Secondly, the 2-alkanol ester homolog/isomer distribution provided information of the β -diketone precursors. Among all 2-alkanol ester homologs, C_{13} , C_{15} and C_{17} 2-alkanol incorporated isomers made up 1%, 84% and 14% of the total pool, respectively (Figure 3-3B). Since 2-alkanols were decarboxylative derivatives of 3-ketoacids, this result indicates that C_{16} , instead of C_{18} 3-ketoacyl intermediate (Mikkelsen, 1984) should be the most abundant 3-ketoacyl precursor in barley. Thirdly, the uninterrupted β -diketone-related wax products formation in flag leaf sheaths of barley *cer6* mutant (Figure 3-6) suggested at least the major wax elongase CER6-associated FAE complex did not participate in β -diketone formation. Lastly, the ^{13}C isotope profiling of various wax components found that β -diketones possessed different ^{13}C enrichment than the FAE-elongated wax components. ^{13}C isotope heterogeneity was observed in the metabolites derived from different pathways particularly in cuticular waxes. Previous studies found the ^{13}C isotope abundance of alkanes was negatively correlated with their carbon chain length (Collister et al., 1994; Bi et al., 2005; Chikaraishi and Naraoka, 2007), in another words, was positively correlated with the proportion of carbon that originated from plastids. This correlation was also observed in our study. The ^{13}C isotope abundance of each VLC wax component, including homologs in 1-alkanol esters, 2-alkanol esters and n-alkanes, was positively correlated with its percentage of carbon that originated from plastids (Figure 3-3C). Esters contains high percentage of plastidial-originated carbon compared to alkanes that synthesized through FAE elongation. The close ^{13}C isotope abundance between C_{31} β -diketone and the esters (not alkanes) suggested β -diketones were also consist of high proportion of plastidial-originated carbon. Thus β -

diketones were unlikely synthesized through ER hydrocarbon elongation pathway. These results together made the β -diketone elongation-decarboxylation formation model suspicious.

3.4.2 The biochemical function and substrate specificity of DMH

DMH is the first enzyme on β -diketone synthesis pathway which serves as the master switch that controls the formation of the β -diketone-related wax components. We conducted a full spectra analysis of its products in *in vivo* system to assess its biochemical function. With the accumulation of 2-ketones and 2-alkanols ranging from C14 to C18 in *E. coli* expressing DMH which were lacking in control, and increased concentration of 3-hydroxyacids after expressing DMH, we confirmed its biochemical function as an acyl-ACP thioesterase that intercepts the intermediates from FAS complex(s). 2-Ketones and 2-alkanols are likely the decarboxylative products of the corresponding 3-ketoacids and 3-hydroxyacids, respectively, which were processed spontaneously or by an unspecific decarboxylase present in *E. coli* (Hen-Avivi et al., 2016). In this scenario, 3-ketoacyl and 3-hydroxyacyl intermediates are the direct products of DMH. Alternatively, 2-alkanols and 3-hydroxyacids could be the reduced products that derived from 2-ketones and 3-ketoacyl intermediates, respectively, which required an unspecific reductase to catalyze these reactions. If this is true, 3-ketoacyl intermediates are the only direct products of DMH. The similar homolog profiles of these three products made it difficult to distinguish these two scenarios. Because decarboxylase and reductase activities cannot be distinguished in *in vivo* systems, we still lack the direct evidence showing 3-ketoacyl intermediates are the products. Moreover, similar decarboxylase and reductase are likely present *in planta* as well. In barley wax precursor feeding experiments, the 3-ketoacid, 2-ketone and 2-alkanol substrates all could be incorporated into esters (Mikkelsen, 1984), indicating the decarboxylase and reductase activity *in planta*.

We compared the 2-ketone/2-alkanol homolog distribution generated in *in vivo* assays and the barley 2-alkanol profile obtained from 2-alkanol ester analysis (Figure 3-3B; Figure 3-7B, C). In both systems, DMH exhibited narrow product chain length range. Products ranging from C₁₄ to C₁₈ were detected and C₁₆ homologs (detected as 2-ketones) were dominant in both systems, indicating DMH could accept 3-ketoacyl substrates ranging from C₁₄ to C₁₈. However, the monounsaturated C₁₆ products were extremely concentrated in DMH *E. coli* expression system, which could not be detected in plants. This discrepancy might be due to the differences between the acyl-ACP pools of these two organisms. The mono-unsaturated lipids are present both in *E. coli* and plants. Plant leaf tissue contains negligible mono-unsaturated C₁₆ fatty acyl precursors with the predominance of saturated C₁₆ fatty acyl (Sayanova et al., 2007) while *E. coli* lipids contained roughly 10% mono-unsaturated C₁₆ fatty acyl in our tested conditions (Figure 3-7E). Additionally, we found the double-bonds of mono-unsaturated 2-ketones were in the ω -7 position (Figure 3-9), which matched that of the mono-unsaturated fatty acyls in *E. coli* (Feng and Cronan, 2009), indicating that the mono-unsaturated 2-ketones were derived from the preformed, mono-unsaturated lipids in *E. coli* and not desaturated by other desaturase(s) or DMH. These results indicate that both the enzyme substrate specificity and the available fatty acyl-pool influence the products of DMH. Thus, the barley fatty acyl pool, together with the DMH substrate specificity led to the 2-alkanol/3-ketoacyl intermediate profile *in planta*.

The DMH-GFP fusion protein localized to plastids in barley protoplasts clarified the plastidial compartmentalization of DMH (Figure 3-14A-D). Thus, DMH is unlikely to intercept 3-ketoacyl-CoA intermediates from FAE complex to generate 3-ketoacid precursor directly in ER. We then conclude that DMH is a ketoacyl-ACP thioesterase generate 3-ketoacyl intermediates with very restricted substrate chain-length specificity.

Moreover, DMH failed to produce any 3-ketoacyl intermediates or their derivatives in yeast expression. This result suggests DMH may be not compatible with yeast type I FAS system, which contains cytosol-located multifunctional proteins to catalyze the iterative elongation of fatty acyl (Harwood and Murphy, 2005), and that the thioesterase function of DMH likely requires the type II FAS machineries which present both in *E. coli* and plants.

The identified plant thioesterases involved in lipid metabolism generally belong to the hotdog family. Hotdog thioesterases could be further divided into fatty acyl thioesterase (FAT)-type thioesterases that contain two hotdog domains (e.g. FATA and FATB from Arabidopsis) and acyl-lipid thioesterase (ALT)-type thioesterases that contain one hotdog domain (e.g. ShMKS2 from tomato) (Yu et al., 2010; Pulsifer et al., 2014; Kalinge et al., 2020). Unlike its plant counterparts, DMH possesses a α/β hydrolase domain and belongs to the more functionally diverse α/β hydrolase superfamily (Holmquist, 2000). It possesses a canonical Ser₁₈₄, His₃₅₉ and Asp₃₀₁ as its nucleophile-His-acid catalytic triad to interact with acyl molecules (Devedjiev et al., 2000; Holmquist, 2000; Huhtinen et al., 2002). However, since there is substrate and function diversity of α/β hydrolase members, how DMH interacts with its substrates cannot be extrapolated at this point.

The narrow substrate chain length specificity of DMH is of particular interest. The FAS-dependency of DMH may shed light on its specificity. DMH specifically intercepts C₁₄-C₁₈ 3-ketoacyl intermediates. It may interact with KAS I and KAS II that decide the chain length of the acyl substrates in FAS complexes to fetch 3-ketoacyls with specific lengths. Alternatively, the length of substrate channel in DMH may also play a role in limiting the length of acyl chain. DMH may interact with ACP, together with the limited channel length to decide the substrate specificity. This mechanism has been found in FAT-type thioesterases. Recent research on

Cuphea viscosissima thioesterases (CvFATB1, CvFATB2) with domain-swapping and site-directed mutagenesis found positively charged subregions on the enzyme surface that could facilitate the binding of thioesterase with the negatively charged ACP moiety, and another group of amino acids residue in N-terminal hotdog fold delimited the depth of substrate pocket that interact with acyl chain. These two factors together determine the substrate/product chain length specificity of these thioesterases (Jing et al., 2018). Similar acyl pocket and positively charged surface subregions may also be present in α/β hydrolase thioesterases, which thus ensure the interactions with the substrate and define their product specificity.

3.4.3 The non-canonical PKS and the revised model of β -diketone biosynthesis pathway

In current study, three sets of experiments were performed to test the substrates of DMP and determine its biochemical function. The production of β -diketones in DMP yeast *in vivo* assay after the supplement of C₁₆ 3-ketoacid made it possible to further clarify the incorporation of different precursors during β -diketone formation. Firstly, we used deuterium-labeled fatty acids to test the incorporation of the fatty acyl precursor by DMP. After feeding per-deuterated C₁₆ fatty acid (C₁₅D₃₁COOH) together with C₁₆ ketoacid to yeast expressing DMP, a new product eluted 0.4 min before unlabeled C₃₁ 14,16-diketone. Particularly, in addition to a molecular ion 31 amu higher than the unlabeled diketone, along with a corresponding water loss ion [M-18]⁺, the deuterium-labeled C₃₁ 14,16-diketone showed two α -fragments (m/z 211 and 253) together with corresponding ions resulting from McLafferty rearrangement (ion cluster m/z 269+) and water/acetone loss (m/z 251+ and 192), all diagnostic for a C₁₄ acyl moiety of the C₃₁ 14,16-diketone structure. Analogous fragments comprising the other hydrocarbon tail of the compound were all shifted by 31 amu relative to the unlabeled C₃₁ 14,16-diketone, including α -fragments (m/z 270 and 312) and ions due to McLafferty rearrangement (m/z 327) and loss of water/acetone

(m/z 307+ and 247+), confirmed its per-deuterated identity (Figure 3-10E, Figure 3-11). The production of deuterium-labeled C₃₁ 14,16-diketone, with one unlabeled hydrocarbon tail (C₁₃H₂₇, from 3-ketoacid) and one per-deuterated hydrocarbon tail (C₁₅D₃₁), suggested incorporation of the entire hydrocarbon tail from the fatty acid substrate (Figure 3-10D, E). Secondly, the rare *in vivo* substrates with odd-numbered acyl chains were used to test the incorporation of entire units of both ketoacid and fatty acyl-CoA during β -diketone formation. The production of C₃₀ 14,16-diketone after feeding C₁₅ fatty acid and C₁₆ 3-ketoacid in the yeast assay suggested that DMP condensed the entire odd-numbered fatty acyl tail during its reaction. And the major product C₃₀ 14,16-diketone after the supplement of C₁₇ 3-ketoacid and C₁₄ fatty acid in yeast assay, suggested the incorporation of the entire hydrocarbon tail from the 3-ketoacid during β -diketone formation. Lastly, the *in vitro* DMP assay corroborated the head-to-head condensation model of β -diketone formation. The production of C₃₁ 14,16-diketone after incubation of the recombinant DMP with C₁₆ 3-ketoacid and C₁₆ fatty acyl-CoA, for the first time, suggested that the fatty acyl-CoA and the 3-ketoacid are the bona fide substrates of DMP. Moreover, it indicated that DMP alone was able to produce β -diketones and FAE or other type of elongase was not required in β -diketone formation. Additional substrate combination in DMP *in vitro* assays indicate that unlike other PKS, DMP has no activity on malonyl-CoA extender. These results together clarified the biochemical function of DMP: DMP takes the LC fatty acyl-CoA as the starter unit, accepts the 3-ketoacid as the extender molecule and catalyzes a decarboxylative Claisen condensation between fatty acyl-CoA and 3-ketoacid to form the corresponding β -diketone.

DMP, a type III PKS, from our analysis, is different from other PKSs in the following aspects: firstly, DMP accepts a fatty acyl-CoA with specific carbon chain length as the starter molecule

instead of an aromatic or short chain substrates. Secondly, DMP is not able to condense a malonyl-CoA, or a fatty acyl-CoA, with the starter substrate. Instead, it uses a 3-keto acid as the extender molecule to catalyze a decarboxylative Claisen condensation between fatty acyl-CoA and 3-ketoacid. Lastly, DMP does not further hydrolyze or cyclize the condensation product since it does not introduce an additional high energy molecule during the extension.

Additionally, DMP localized to ER, indicating its accessibility of LC fatty acyl-CoA, however, made it difficult to access plastidial-produced 3-ketoacids. Thus, 3-ketoacids must be transported from plastids to ER in either acid or CoA-ester form at one point.

Based on these findings, we revised the model of β -diketone synthesis pathway. DMH works as a thioesterase that intercepts 3-ketoacyl-ACPs from type II FAS complex to produce 3-ketoacids in plastids. After being redirected to the ER, DMP takes fatty acyl-CoAs and 3-ketoacids to catalyze a decarboxylative condensation forming β -diketones. And DMC likely further hydroxylates β -diketones at specific positions of their hydrocarbon chain to produce hydroxy- β -diketones. On the other side, 3-ketoacids are decarboxylated either spontaneously or by a decarboxylase producing 2-ketones, which are further reduced to 2-alkanols and esterified with fatty acyl-CoAs forming 2-alkanol esters (Figure 3-1A). And we cannot rule out the possibility that 3-ketoacids are first reduced to 3-hydroxyacids and further decarboxylated to 2-alkanols, although it is less likely than the previous scenario.

Two functionally characterized PKSs, curcumin synthase (CURS) in *Curcuma longa* and curcuminoid synthase (CUS) in *Oryza sativa*, catalyze reactions similar to DMP leading to β -diketide scaffolds from different substrates. In *C. longa*, the diketide-CoA synthase (DCS) first generates feruloyl-diketide-CoA which released as feruloyl-diketide acid by condensing feruloyl-CoA with malonyl-CoA, and CURS condenses the starter feruloyl-CoA with the extender

feruloyl-diketide acid to produce curcumin (Katsuyama et al., 2009). Another PKS CUS is able to catalyze two steps of condensation, one between 4-coumaroyl-CoA and malonyl-CoA to form diketide intermediate, the other one between a second 4-coumaroyl-CoA with the diketide to produce bisdemethoxycurcumin, although its *in planta* function is still unclear in rice (Morita et al., 2010). In the homology-based modeling, DMP was predicted to form homodimer and has a single active site and substrate cavity within each lobe, which is similar to other type III PKS (Austin and Noel, 2003; Abe and Morita, 2010). It contains the canonical Cys-His-Asn catalytic triad and shares 55% similarity with CUS, 42% similarity with CURS and 44% similarity with *Medicago sativa* CHS. Comparing the conserved amino acid residues in type III PKS, we propose its reaction mechanism: firstly, a fatty acyl-CoA starter molecule is loaded into the catalytic center and covalently bound to Cys₁₆₈ by release of the CoA. Hydrogen bonds between the fatty acyl-CoA head group and His₃₀₉ and Asn₃₄₂ facilitate the bond formation. Secondly, a 3-ketoacid extender molecule (in deprotonated form) enters the catalytic center and, assisted by Asn₃₄₂, undergoes decarboxylation into the corresponding enolate. Finally, nucleophilic attack of the enolate on the carbonyl carbon of the starter and proton transfer via an adjacent water molecule (facilitated by Ser₃₄₅, Asn₁₃₆, Ser₂₀₀ and Glu₁₉₆) yield the β -diketone product and re-set the active site (Figure 3-15).

Similar to DMH, DMP also showed high substrate specificity. Because of the product specificity of the first enzyme DMH, the extender substrate of DMP is restricted to C₁₄-C₁₈ 3-ketoacids *in planta*. It also takes limited fatty acyl-CoAs as the starter substrate ranging from C₁₂ to C₁₆ in our tested conditions (Figure 3-12; Figure 3-13). This is indicated by the substrate incorporation both *in vivo* and *in vitro*. Our *in vitro* test directly showed the specificity of DMP: C₁₆ and C₁₄ fatty acyl-CoAs were favored starter molecules compared to the C₁₂ homolog, and C₁₄ 3-keto acid was

preferentially incorporated as the extender molecule (Figure 3-12G-J). The yeast assay also suggested C₁₄ acyl-CoA was highly incorporated by DMP but C₁₆ homolog was not (Figure 3-12A-F; Figure 3-13). This is probably because of the C₁₆ fatty acyl-CoA were overrepresented by C₁₆ fatty acyl from phospholipids, as shown by acyl profiling in the assayed yeast.

Surprisingly, the *in planta* major product C₃₁-14,16-diketone, which is condensed between C₁₆ fatty acyl-CoA and C₁₆ 3-ketoacid, is not the most preferred substrate combination of DMP. This is likely due to the limited C₁₄ 3-ketoacid produced by DMH *in planta*, thus making DMP take more C₁₆ 3-ketoacid as the extender. The acyl-ACP pool, the substrate preference of DMH and DMP together could explain the unique β -diketone profile *in planta*.

How DMP determines its substrate specificity is still unclear at this point. Comparing the crystal structure of DMP with that of other PKSs will be helpful to understand the substrate selection mechanism. The β -diketide backbone containing compounds, such curcumin, 6-gingerol, 1-dehydro-10-gingerdione have shown strong anti-inflammatory and anti-oxidative function, and thus are widely used in Chinese and Indian medicine (Jolad et al., 2004; Tanaka et al., 2015). Understanding the substrate selection mechanism of DMP has huge potential to facilitate drug production to modify and produce designed functional molecules. Additionally, the β -diketide group could change the chemical properties of the molecule. Introducing this group to molecules of industry raw materials by genetic engineering may improve the quality and production of desired industrial compounds (Oyarce et al., 2019).

The β -diketone synthesis in plants has puzzled scientists for decades. Here for the first time, we demonstrated the key steps of the pathway in Poaceae and demonstrated that the 3-ketoacids are the central precursors and that a decarboxylative condensation without further elongation catalyzed by a non-canonical PKS is required to form the β -diketone backbone. As one of the most

dynamically regulated wax components in Poaceae family during drought stress (Bi et al., 2017), the understanding of the biosynthesis of β -diketones and related wax components will facilitate the breeding and improvement of plant drought tolerance through cuticle engineering.

Chapter 4: The acyl-CoA desaturase ADS4.2 is required in formation of characteristic wax alkenes in young *Arabidopsis* leaves

4.1 Introduction

Arabidopsis, an important model plant in biological research, is a major system to identify the wax biosynthesis machineries. Cuticular wax compositions of *Arabidopsis* from different organs are well characterized. Besides ubiquitous wax components, recent studies have identified several specialty wax components from *Arabidopsis* including iso-alkanes, iso-primary alcohols, n-6 monounsaturated alcohols and alkenes (Hegebarth et al., 2016; Busta et al., 2017; Busta and Jetter, 2017; Yang et al., 2017). VLC alkenes are of particular interest, since the double bond in their hydrocarbon chain results in special molecular and biological properties (Small, 1984; Gibbs and Pomonis, 1995; Gibbs, 2002). Accordingly, wax alkenes enhance cuticle functions, on leaves increasing water use efficiency (Gonzales-Vigil et al., 2017) and on petals modulating pollinator behaviour (Schiestl and Cozzolino, 2008; Schlüter et al., 2011).

Alkenes have been detected in cuticular waxes from diverse monocots and dicots, including species in the Asphodelaceae, Poaceae, Salicaceae, Ranunculaceae, Ericaceae, Primulaceae, Polygonaceae, Rosaceae and Asteraceae (Herbin and Robins, 1968; Lütz and Gülz, 1985; Jung et al., 2006), but mostly without detailed structure elucidation. Comprehensive analyses were reported from relatively few species, revealing that in most cases alkenes had predominantly odd-numbered hydrocarbon chains ranging from C₂₁ to C₃₃ with double bonds located mostly between C-9 and C-10. These 9-alkenes were found, for example, in wax on spikes of *Agropyron intermedium* (Tulloch and Hoffman, 1976) and *Hordeum vulgare* (Tulloch and Hoffman, 1976; von Wettstein-Knowles, 2007), on leaves of *Populus trichocarpa* (Gonzales-Vigil et al., 2017)

and on flower surfaces of *Ophrys sphegodes* (Schlüter et al., 2011; Gonzales-Vigil et al., 2017). In contrast, 7-alkenes were found only in the waxes from *O. exaltata* labellae (Sedeek et al., 2016) and *Zea mays* stigmas (Dennison et al., 2019), 5-alkenes in *Rosa damascena* flower and *R. canina* fruit waxes (Wollrab, 1968), 4-, 6- and 10-alkenes in *Z. mays* leaf waxes (Bourgault et al., 2019) and 12-alkenes on *O. sphegodes* flowers (Schlüter et al., 2011). Arabidopsis alkenes are unique compared to other reported plant surface alkenes. They possess characteristic carbon chain lengths and had been discovered in the cuticular wax mixtures extracted from young leaf surfaces, likely associated with trichomes (Hegebarth et al., 2016). However, the chemical structure of these alkenes remained unknown.

The overall chain length distributions of the alkenes, in comparison with those of other compounds found in the same wax mixtures, suggested that the wax alkenes are biosynthesized on pathways similar or even partially identical with the three-stage processes generating the ubiquitous wax components. However, alkene formation must also include at least one additional step introducing the double bond into the hydrocarbon chain, and relatively little is known about the interplay between enzymes responsible for such desaturation and the rest of the pathways.

Two fundamentally different hypotheses for VLC alkene biosynthesis had been put forward (von Wettstein-Knowles, 2007; Perera et al., 2010), where desaturation occurs either before elongation and carboxyl head group removal (desaturation-elongation-modification pathways) or between elongation and head group removal (elongation-desaturation-modification pathways). These two scenarios imply distinct chain length specificities of the desaturases involved, in the first case for C₁₆/C₁₈ substrates and in the second for VLC acyls (Figure 4-1).

Wax alkene biosynthesis has been studied to some extent only in two genera so far, and in both was found to occur via a desaturation-elongation-modification pathway (Figure 4-1). Accordingly, 9-alkene and 12-alkene biosynthesis in *O. sphegodes* proceeds through elongation of pre-formed plastidial Δ -9 (= ω -9) 18:1 and Δ -4 16:1 acyls, respectively, while 7-alkenes in *O. exaltata*, stem from elongation of Δ -9 (= ω -7) 16:1 fatty acyl precursor (Schlüter et al., 2011; Sedeek et al., 2016). In accordance with this, alkene biosynthesis in poplar had been found to depend on a special KCS, encoded by *PotriKCS1*, capable of elongating unsaturated substrates derived from plastidial Δ -9 18:1 precursor (Gonzales-Vigil et al., 2017) (Figure 4-1). These studies thus established alkene-forming pathways featuring specialized desaturases and KCSs in a desaturation-elongation-process. In contrast, the desaturase(s) and elongation components as well as the biosynthesis pathway of the characteristic alkenes from Arabidopsis are still unknown.

The desaturases involved in wax alkene formation in *Ophrys* belong to the acyl-acyl carrier protein desaturase (AAD) enzyme family. Other AADs have been reported, all with C₁₆/C₁₈ acyl-acyl carrier protein (ACP) substrate preferences, which collectively serve to form unsaturated acyl precursors that can be elongated for incorporation into various VLC lipid pools (Shanklin and Cahoon, 1998). Arabidopsis possesses seven AADs (Kachroo et al., 2007), including the enzyme SSI2/FAB2 that generates Δ -9 18:1 required to regulate membrane unsaturation and influencing defense signaling (Kachroo et al., 2001; Kachroo et al., 2003). Among the other Arabidopsis AADs, SAD6/AAD6 desaturates acyls under hypoxic conditions in crown galls (Klinkenberg et al., 2014), AAD1 forms Δ -9 16:1 and 18:1 in embryos, and AAD2 and AAD3 yield Δ -9 16:1 en route to ω -7 acyl products found in seed aleurone (Bryant et al., 2016). Therefore, AAD enzymes are strong candidates to be involved in alkene formation, if Arabidopsis cuticular alkenes originate from

unsaturated C₁₆/C₁₈ acyls via a desaturation-elongation pathway analogous to that in poplar and *Ophrys*.

Alternatively, the *Arabidopsis* wax alkenes could be formed via an elongation-desaturation pathway, revolving around desaturation of previously elongated, VLC acyl substrates. Members of a second desaturase family, the acyl-CoA desaturases (ADSs), desaturate VLC acyls in various eukaryotes, and several mammal ADS homologs have been well characterized due to their importance in lipid metabolism and potential for treatment of metabolic diseases (Bai et al., 2015; Wang et al., 2015a). The *Arabidopsis* genome encodes nine ADSs, of which seven are localized to compartments other than the plastids and may have access to VLC substrates. One of them, ADS2, was shown to produce ω -9 24:1 and 26:1 acyls destined for seed lipids, sphingolipids and membrane phospholipids (Smith et al., 2013) (Figure 4-1). A second one, ADS4, catalyzes the formation of monounsaturated ω -6 26:1, 28:1 and 30:1 acyl-CoA intermediates that are ultimately converted into monounsaturated primary alcohols accumulating in *Arabidopsis* stem cuticular wax (Yang et al., 2017). The remaining *Arabidopsis* ADSs have not been characterized in detail and assigned to biosynthetic pathways leading to particular lipid products, however yeast expression showed that ADS1 has ω -9 desaturase activity, ADS1.2 and ADS1.4 have Δ -9 desaturase activity, and ADS1.3 and ADS4.2 have ω -7 desaturase activity (Smith et al., 2013). Therefore, ADSs are further candidates to be involved in installing the double bonds en route to wax alkenes (Figure 4-1).

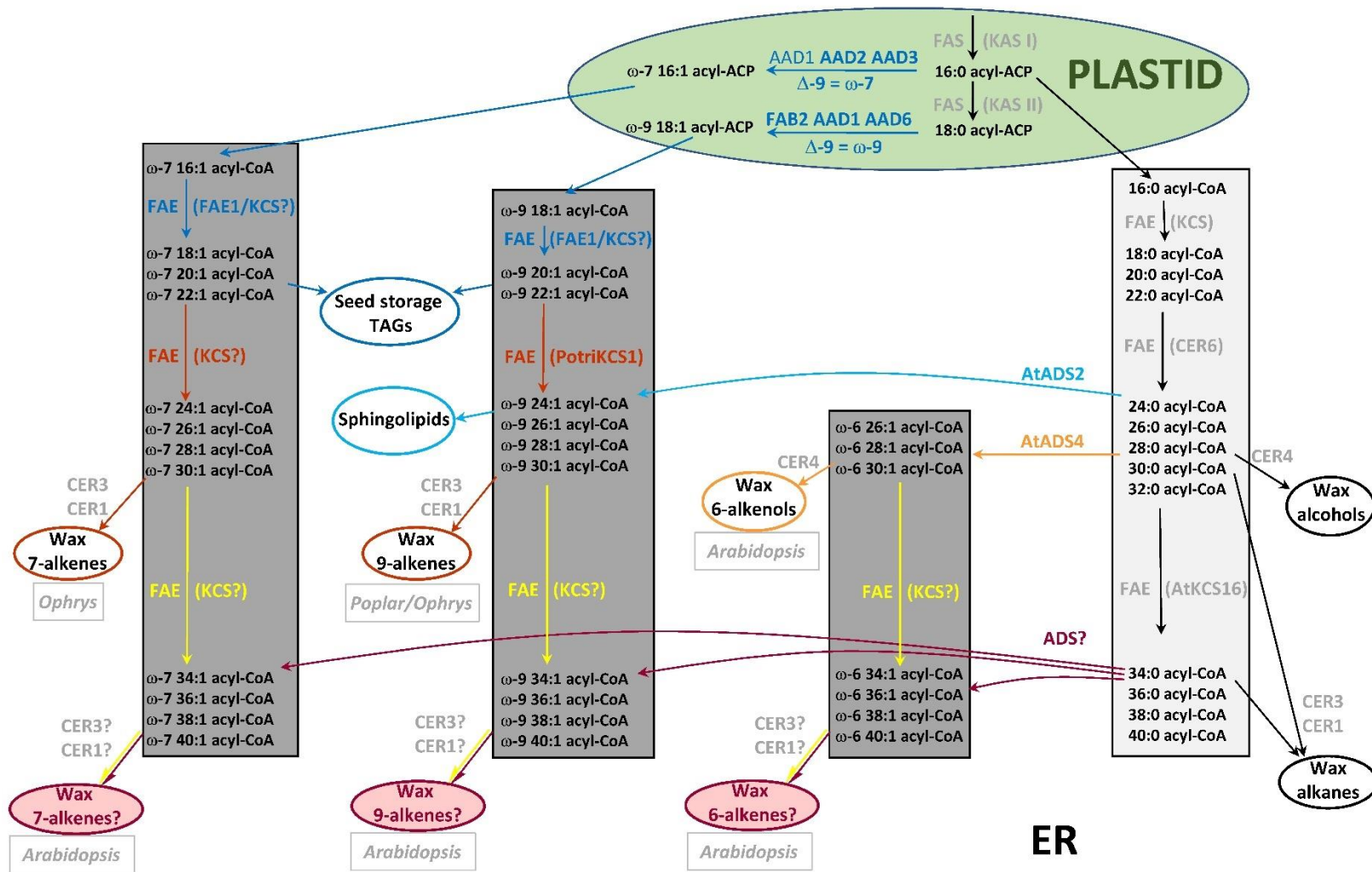


Figure 4-1: Biosynthesis pathways to VLC unsaturated lipids in plants

Plant VLC saturated lipids are biosynthesized from 16:0/18:0 acyl-ACPs via elongation in ER-bound FAE complexes (light-grey box) and further head group modification reactions (black arrows). Plant VLC unsaturated lipids have double bonds mainly in the ω -9, but sometimes also in ω -7 and ω -6 positions (dark-grey boxes), derived from 16:0/18:0 acyl-ACPs either via desaturation-elongation or via elongation-desaturation pathways. The unsaturated acyls of seed storage triacylglycerides (TAGs) are formed by desaturation involving plastidial AAD-type enzymes and elongation by ER-bound FAE complexes (dark-blue pathways). In contrast, the unsaturated acyl groups of sphingolipids are formed by elongation followed by desaturation involving ER-bound ADS-type enzymes (light-blue arrows). Only two classes of unsaturated wax compounds have been investigated to date, showing that they are formed by pathways paralleling those to TAGs and sphingolipids, respectively: the alkenes found in *Ophrys* and poplar waxes are synthesized by plastidial desaturation and subsequent elongation (dark-orange arrows), while Arabidopsis wax alkenols are formed by elongation and then desaturation (light-orange arrows). The various FAE complexes elongating fatty acyl chains with distinct carbon chain lengths and saturation/desaturation contain specific KCS enzymes indicated in brackets. Alkenes with particularly long hydrocarbon chains have recently been discovered in Arabidopsis leaf wax, but neither their double bond positions nor their biosynthesis have been investigated. Fundamentally different hypotheses (dark-red arrows) explain their formation either via elongation of 30:1 precursors (yellow arrows) or desaturation of 30:0 precursors (dark-red arrows).

In this study, we aimed to elucidate the biochemical mechanisms underlying Arabidopsis wax alkene formation. To this end, we first determined the double bond positions in the Arabidopsis wax alkenes and quantified their chain length and isomer distributions. We then screened AAD and ADS-deficient Arabidopsis lines for effects on wax alkenes, and to characterize the desaturase(s) involved in wax biosynthesis with respect to their expression patterns, biochemical substrate, product specificities and subcellular localization. Finally, we investigated in how far the pathway leading to wax alkenes shares key enzymes with the pathways forming saturated wax components, both upstream and/or downstream of the desaturation step. Our study elucidated a new alkene synthesis pathway following an elongation-desaturation pattern in Arabidopsis.

4.2 Materials and methods

4.2.1 Plant Material and Growth Conditions

Seeds of T-DNA insertion lines *ads1* (SALK_073508C), *ads1.3-2* (SAIL_697_D02/CS830693), *ads2* (SALK_079963C), *ads4.2-1* (SALK_039511C), *ads4.2-2* (SALK_093326), *aad2* (SALK_035796C), *aad3* (SALK_019167C), *cer1-1* (SALK_008544C), *cer3* (SALK_020265), *cer4* (SALK_038693C), *lacs1-3* (SALK_138782C), *cer6-2* (CS6242), *cer2-5* (SALK_84443) and *cer26* (SALK_087857) were obtained from the Arabidopsis Biological Resource Center. The *cer2 cer26* double mutant was kindly provided by Dr. Joubès (Bordeaux, France). Homozygous mutant lines were selected by PCR genotyping with primers listed in Table 4-1. All seeds were stratified for 3-4 days at 4°C, surface-sterilized with 75% ethanol, plated on agar plates containing half-strength Murashige and Skoog medium (Sigma-Aldrich) supplemented with antibiotics where necessary. Seedlings were transferred to soil (Sunshine Mix 5, SunGro) and grown in a growth chamber with light intensity 90-110 $\mu\text{mol m}^{-2} \text{s}^{-1}$ in 16-h light (21°C)/ 8-h dark (19°C) cycles. Tobacco plants were grown under same conditions.

4.2.2 Expression analysis

Total RNA was extracted using PureLink RNA Mini Kit (Invitrogen) with on-column DNA digestion. 1 μg of RNA was used to synthesize cDNA by Superscript III Reverse Transcriptase (Invitrogen). qRT-PCR was performed with iQ SYBR Green Supermix (BioRad) on a CFX Connect Real-Time System (Bio-Rad) with primers listed in Table 4-1. *ACTIN2* (AT3G18780) served as a constitutive-expression control. Amplification efficiency was tested for all primer pairs and confirmed to be between 90 and 110%. Relative expression levels of *ADS4.2* were calculated using the $2^{-\Delta\Delta\text{CT}}$ method (Livak and Schmittgen, 2001).

Table 4-1: Primers used in Chapter 4

	Name	Sequence	Purpose
Genotyping primers	SALK_008544C_LP	GGTCCTTTGTTTTCTTTTGC	Genotyping <i>cer1-1</i> T-DNA insertion lines
	SALK_008544C_RP	AGCGATCCAAATGCTATGTTT	
	SALK_020265_LP	TCTCTACGCTCCATTAGCTGC	Genotyping <i>cer3</i> T-DNA insertion lines
	SALK_020265_RP	CACAGCAAACACAAAACCTTGC	
	SALK_038693C_LP	GACTTCGACTTGGCTCATGAG	Genotyping <i>cer4</i> T-DNA insertion lines
	SALK_038693C_RP	GCCTTGAGGATTAGGTCTTC	
	SAIL_697_D02_LP	GGCACTTCAGGTAAATACTG	Genotyping <i>ads1.3-1</i> T-DNA insertion lines
	SAIL_697_D02_RP	CAATTACTCTCCAAAACCC	
	SALK_093326_LP	GAACCATGCTGCTCAAGTC	Genotyping <i>ads4.2-2</i> T-DNA insertion lines
	SALK_093326_RP	AAACGGATGGCATCAAATTC	
	SALK_84443_LP	TGGGAAAAACCAAACAACAC	Genotyping <i>cer2-5</i> T-DNA insertion lines and <i>cer2 cer 26</i> double mutant
	SALK_84443_RP	ACGTCGAAGAGTTCACAGTGG	
	SALK_087857_LP	AGGCCCAACCCTAATCCTCC	Genotyping <i>cer26</i> T-DNA insertion lines and <i>cer2 cer 26</i> double mutant
	SALK_087857_RP	TACTCAGCCGAGACAGCACG	
	SAIL_LB3	TCATAACCAATCTCGATACAC	LB primer of the SAIL T-DNA insertion lines
	LBb1.3	ATTTTGCCGATTCGGAAC	LB primer of the SALK T-DNA insertion lines
qRT-PCR primers	ACTIN2-F	CCAGAAGGATGCATATGTTGGTGA	qRT-PCR Internal control
	ACTIN2-R	GAGGAGCCTCGGTAAGAAGA	
	qrtADS4.2-F	CTCGTAACGTTTGGTGGCT	qRT-PCR ADS4.2
	qrtADS4.2-R	CAGTGGCTAACCCGAGAAC	
Cloning primers	ADS4.2-CDS-F	ATGTGTGATCCCATTAGAGAAGA	ADS4.2 CDS isolation
	ADS4.2-CDS-R	ACGAGTCAGAGCCAGTTTCT	
	ADS4.2P-F	ATACTGACTCGGTCTAATTCT	ADS4.2 promoter isolation
	ADS4.2P-R	CCGTTGAGGGGTTGTTTTTC	
Yeast expression primers	ADS4.2-CDS-EcoRI-F	TCCGAATTCATGTGTGATCCCATAGAG	ADS4.2 yeast expression
	ADS4.2-CDS-SpeI-R	TAACTAGTAGACGAGTCAGAGCCAGTTTC	
ADS4.2 Histidine cluster mutagenesis primers	ADS4.2-Muta-F	ATGTGTGATCCCATTAGAGAAGATGGC	ADS4.2 Histidine cluster mutagenesis overlapping extension
	ADS4.2-Muta-R	ACGAGTCAGAGCCAGTTTCTGTTTCT	
	ADS4.2-H77A-F	CATCACATTCTCATACGCTAGGAACCTGG	ADS4.2 first Histidine cluster mutagenesis (H77A)
	ADS4.2-H77A-R	CCAAGTTCTAGCGTATGAGAATGTGATG	
	ADS4.2-H114A-F	GAGCATAGCAAGGTTCCATCACCAGTT	ADS4.2 second Histidine cluster mutagenesis (H114A)
	ADS4.2-H114A-R	AACTGGTGATGGAACCTTGCTATGCTC	
	ADS4.2-H246A-F	CAATGGGAGAGAGTTGGGCGAATAATCAC	ADS4.2 third Histidine cluster mutagenesis (H246A)
	ADS4.2-H246A-R	GTGATTATTCGCCCAACTCTCTCCATTG	

4.2.3 Plasmid construction and plant transformation

The coding region of *ADS4.2* was amplified from cDNA synthesized from young Arabidopsis Col-0 rosette leaf samples using Phusion polymerase (NEB) with primers ADS4.2-CDS-F and ADS4.2-CDS-R and ligated into pCR8/GW/TOPO vector (Invitrogen), confirmed by Sanger sequencing, and transferred to the destination vectors pGWB5 or pGWB6 by Gateway LR Clonase II Enzyme Mix (Invitrogen). Resulting destination constructs were transformed into *Agrobacterium tumefaciens* (GV3101) for transformation of 4-week-old Arabidopsis *ads4.2-1*

plants by floral dipping (Clough and Bent, 1998). Transformed lines were selected by resistance to antibiotics hygromycin, and 15 T₂ transgenic lines were further confirmed by western blot with anti-GFP antibody (Invitrogen, #A-6455).

4.2.4 GUS histochemical staining

Arabidopsis Col-0 genomic DNA was isolated with CTAB method (Abdel-Latif and Osman, 2017). A 2360-bp fragment upstream of the *ADS4.2* coding region was amplified from the obtained genomic DNA with primers ADS4.2P-F and ADS4.2P-R (Table 4-1), and recombined into the pGWB3 vector as described above. The resulting destination vector was introduced into Col-0 plants as described above and fifteen T₂ transgenic plants were used for β -glucuronidase (GUS) staining. Plant samples were pretreated with 80% acetone for 30 min on ice, rinsed with water, and incubated in X-Glu solution [0.5 mM K₄FeCN₆, 0.5 mM K₃FeCN₆, 100 mM Na₂HPO₄, 100 mM NaH₂PO₄, 0.1% (w/v) Triton-X-100 and 0.1% 5-bromo-4-chloro-3-indolyl- β -D-glucuronide (Gold Biotechnology)] at 37°C for 2-3 h. Samples were fixed with ethanol: acetic acid solution (1:1) and cleaned with 70% ethanol twice. Samples were imaged under an Olympus SZX10 stereomicroscope.

4.2.5 Transient expression in tobacco and confocal microscopy

Transient expression in *Nicotiana benthamiana* was performed as described previously (Sun et al., 2020). The infiltrated leaves were analyzed and imaged by a PerkinElmer UltraView VoX Spinning Disk confocal equipped with a Leica DMI8 inverted microscope and a Hamamatsu 9100-02 charge-coupled device camera. Transformed leaves were mounted in water with abaxial surfaces facing the objective and observed with a 63 \times 1.3 NA glycerol objective. ADS4.2-GFP images were obtained using a 488-nm laser and 525/36-nm emission filter (excitation 488 nm,

emission 525 nm), and HDEL-RFP images were obtained with a 561-nm laser and a 595/50-nm emission filter (excitation 561 nm, emission 595–625 nm). The final images were processed using ImageJ (Abràmoff et al., 2004) software.

4.2.6 Wax analysis

Expanding rosette leaves of 2- to 3-week-old Col-0 were excised and photographed, and their surface areas quantified by ImageJ software (Abràmoff et al., 2004). Leaves were extracted twice with CHCl_3 for 30 s containing n-tetracosane (Sigma) as internal standard. The resulting mixtures were dried under nitrogen and subjected to trimethylsilyl (TMS) derivatization by incubation with *N,O*-bis(trimethylsilyl)-trifluoroacetamide (BSTFA, Sigma) in pyridine at 72°C for 45 min. The resulting mixtures were separated by capillary Gas Chromatography (GC, 6890N, Agilent, Avondale, PA, USA; column 30 m HP-1, 0.32 mm i.d., $d_f=0.1\ \mu\text{m}$) using on-column injection at 50°C and oven temperature held for 2 min at 50°C, raised by 40°C min⁻¹ to 200°C, held for 2 min at 200°C, raised by 3°C min⁻¹ to 320°C, and held for 30 min at 320°C. For compound identification, the GC was coupled to a mass spectrometric detector (5973N, Agilent) operating in total ion mode, and the inlet pressure was programmed for constant 1.4 ml min⁻¹ flow of He carrier gas. For quantification of wax compounds, the GC was coupled to a flame ionization detector (FID) and the inlet pressure programmed for constant flow of 2.0 ml min⁻¹ of H₂ carrier gas. The quantity (μg) of each wax component was established by comparison of GC-FID peak integrations with those of the internal standard. Extracted leaf surface areas (cm²) were measured with ImageJ software (Abràmoff et al., 2004) from digital photographs of the samples (and multiplied by 2 to account for adaxial and abaxial surfaces).

For alkene isomer analysis, total wax extracts from 2- to 3-week-old rosette leaves were fractionated by thin-layer chromatography (TLC) (Analtech, 0.25 mm) as described before (Busta

et al., 2017). The hydrocarbon fraction (R_f 1.00) was scratched out and extracted with CHCl_3 , and the resulting extracts dried under nitrogen. Dimethyl disulfide (DMDS) derivatization was performed as described (Shibahara et al., 2008), with a solution of 1.3% I_2 in DMDS (w/v) and incubation at 35°C for 30 min. DMDS adducts were dissolved in diethyl ether:hexane (1:9, v/v), loaded on a Silica Gel G mini-column (Macherey-Nagel, pretreated with $\text{Na}_2\text{S}_2\text{O}_3$ solution), eluted with diethyl ether:hexane, dried under nitrogen, dissolved in CHCl_3 and subjected to GC-MS analysis as described above. The ω -7 and ω -9 alkene isomers were quantified from GC profiles using selected ions m/z 145 and m/z 173, respectively.

Alternatively, the hydrocarbon fraction was oxidized with osmium tetroxide as previously described (Gonzales-Vigil et al., 2017). The products were TMS-derivatized, dissolved in CHCl_3 , and analyzed by GC-MS as described above.

4.2.7 Yeast assay and lipid analysis

The coding region of ADS4.2 was PCR-amplified from pCR8-ADS4.2 with primers ADS4.2-CDS-EcoRI-F and ADS4.2-CDS-SpeI-R (Table 4-1), purified, digested with EcoRI and SpeI, and ligated into the pESC-Trp and pESC-Ura vectors. Cells of wild-type yeast INVSc1 (*MATa his3-D1 leu2 trp1-289 ura3-52*), FAE-defective mutant *elo3* Δ (*MATa/a his3 Δ 1/his3 Δ 1 leu2 Δ 0/leu2 Δ 0 lys2 Δ 0/LYS2 MET15/met15 Δ 0 ura3 Δ 0/ura3 Δ 0 YLR372w::kanMX4/YLR372w::kanMX4*), and *INVSur4*# mutant yeast [generated by transformation of INVSc1 with p416 MET25-FLAG3:Sur4-F262A/K266L (Denic and Weissman, 2007; Bernard et al., 2012)] were transformed with pESC-Trp-ADS4.2, pESC-URA-ADS4.2, or corresponding empty vector using the LiAc/SS-DNA/PEG method (Gietz and Woods, 2002). Positive transformants were PCR-confirmed, cultivated in liquid minimal medium lacking appropriate amino acid at 28°C overnight, transferred to the same

medium supplemented with 2% (w/v) galactose, and harvested by centrifugation after 18 h incubation.

For fatty acid analysis, yeast cells were washed with 2.5% (w/v) NaCl solution, collected by centrifugation, resuspended in 0.5 M H₂SO₄ in methanol containing 2% (v/v) dimethoxypropane, and incubated at 85°C for 3 h for transmethylation. Resulting fatty acid methyl esters (FAMES) were extracted with hexane and analyzed by GC-MS as described above. FAMES were quantified based on GC profiles using selected ion m/z 74, with a correction factor of 4.08 for unsaturated acids (determined from spectra of *cis*-vaccenic acid (ω -7 18:1), oleic acid (ω -9 18:1) and stearic acid (18:0)) to account for the lower ionization yield of unsaturated FAMES.

For isomer analysis of unsaturated lipids, the yeast FAME mixtures (without TLC separation) were dried in GC vials, subjected to DMDS addition, and analyzed as described above. The ω -7 and ω -9 monounsaturated FAMES were quantified from GC profiles using selected ions m/z 145 and m/z 173, respectively.

4.2.8 Site-Directed Mutagenesis

pCR8-ADS4.2 was used as template for ADS4.2 site-directed mutagenesis following the method described previously (Ho et al., 1989). For ADS4.2 H77A mutagenesis, ADS4.2-Muta-F and ADS4.2-H77A-R (Table 4-1) were used to amplify the 5' fragment, while ADS4.2-H77A-F and ADS4.2-Muta-R (Table 4-1) were used to amplify the 3' fragment. For ADS4.2 H114A mutagenesis, ADS4.2-Muta-F and ADS4.2-H114A-R (Table 4-1) were used to amplify the 5' fragment, and ADS4.2-H114A-F and ADS4.2-Muta-R (Table 4-1) for the 3' fragment. For ADS4.2 H246A mutagenesis, ADS4.2-Muta-F and ADS4.2-H246A-R (Table 4-1) were used to amplify the 5' fragment, and ADS4.2-H246A-F and ADS4.2-Muta-R (Table 4-1) for the 3' fragment. All

resulting fragments were purified and mixed with the corresponding half-fragment. ADS4.2-CDS-EcoRI-F and ADS4.2-CDS-SpeI-R were used in all final overlap extension PCRs. The extension products were purified, digested by EcoRI and SpeI, and ligated into the pESC-Trp vector. The resulting vector constructs containing the mutated ADS4.2 were confirmed by Sanger sequencing and later used in yeast expression and lipid analysis.

4.2.9 Sequence alignment and protein structure modeling

Primary sequences of acyl-CoA desaturases retrieved from the NCBI database were aligned with ADS4.2 using the MUSCLE algorithm (Edgar, 2004). The tertiary structure of ADS4.2 was predicted using the protein homology/analogy recognition engine Phyre2 [<http://www.sbg.bio.ic.ac.uk/phyre2/html/page.cgi?id=index>; (Kelley et al., 2015)] based on the crystal structure of the mouse stearoyl-coenzyme A desaturase MsSCD1 (PDB: 4YMK) with 28% identity and 97% coverage.

4.2.10 Phylogenetic analysis

The amino acid sequence of ADS4.2 was used to blast against Phytozome database (v12.1.5) and fetched the ADS4.2-like protein sequences. The obtained sequences together with ADS family members were aligned using the MUSCLE algorithm (Edgar, 2004). Phylogenetic tree was generated by MEGA10.0 using the Maximum Likelihood method and JTT matrix-based model (Kumar et al., 2018).

4.2.11 Statistical analysis

GRAPHPAD PRISM v8.0 software was used for statistical analysis. Pair-wise comparisons were performed simultaneously on the entire dataset by using Student's *t*-tests (two-tailed), with a two-

stage linear step-up procedure of Benjamini, Krieger and Yekutieli for discovery, and adjustment of raw P-values using a false-discovery rate of 2%.

4.2.12 Sequence information

Sequence data of genes covered in this article can be found in the Arabidopsis Genome Initiative or GenBank/EMBL databases under the following accession numbers: *ADS1* (AT1G06080), *ADS1.3* (At1g06100), *ADS2* (AT2G31360), *ADS4.2* (AT1G06360), *AAD2* (AT3G02610), *AAD3* (AT5G16230), *CER1* (At1G02205), *CER3* (AT5G57800), *CER4* (AT4G33790), *LACS1* (AT2G47240), *CER6* (AT1G68530), *CER2* (At4g24510), *CER26* (At4g13840), *ScOLE1* (NP_011460), *MsSCD1* (NP_033153), *MsSCD3* (NP_077770) and *HsSCD1* (NP_005054).

4.3 Results

4.3.1 Arabidopsis wax alkenes have characteristic chain lengths and double bond positions

Our first goal was to provide chemical information essential for biochemical investigations, by performing detailed chemical analyses of the Arabidopsis wax VLC alkenes. For these, cuticular wax was extracted from expanding rosette leaves and analyzed by GC-MS. The wax mixture comprised large quantities of n-alkanes (ca. 41% of total wax), with predominantly odd-numbered chain lengths from C₂₇ to C₃₇ peaking at C₃₁. The GC traces showed three more peaks eluting 0.4 min before each of the three longest alkanes (Figure 4-2A, B), characterized by MS fragmentations lacking signature ions of oxygen functional group and thus suggesting hydrocarbon structures. The three compounds had molecular ions *m/z* 462, 490 and 518, respectively, two mass units lower than the alkanes eluting directly after them (Figure 4-2C). Based on these characteristics, and in accordance with the MS fragmentation patterns of shorter-chain standards, these three compounds were identified as C₃₃, C₃₅ and C₃₇ alkenes. A fourth compound with matching MS fragmentation

pattern and molecular ion m/z 536 was identified as C₃₉ alkene (also based on its GC retention time matching the prediction for higher homologs). Overall, the alkenes were dominated by the C₃₅ and C₃₇ homologs, with minor amounts of C₃₃ present and only traces of C₃₉ (that could not be reliably quantified within the complex wax mixtures). Thus, the chain length distribution of the unsaturated hydrocarbons differed from that of the alkanes, with alkene:alkane amount ratios > 1 for chain lengths C₃₅ and C₃₇ in particular (Figure 4-2D). Together, the alkene homologs constituted ca. 5% of the total wax mixture on young rosette leaves. Neither of the four VLC alkenes could be detected in the cuticular wax mixtures of mature or senescing leaves (data not shown).

To determine the double bond position in the four alkenes, the wax mixture extracted from young *Arabidopsis* leaves was separated by thin-layer chromatography (TLC). The resulting hydrocarbon fraction containing both alkanes and alkenes was collected, subjected to reaction with dimethyl disulfide (DMDS) and then analyzed with GC-MS. A homologous series of DMDS adducts was detected, all with MS ions $[M]^+$ and $[M-47]^+$ identifying them as derivatives of the C₃₃, C₃₅, C₃₇ and C₃₉ alkenes. Within each of these homologs, several regio-isomers of DMDS adducts were only partially separated by GC but could be fully distinguished based on their MS fragmentation patterns. The latter showed that each homolog contained one isomer characterized by an α -fragment m/z 145, paired with a second α -fragment (m/z 411, 439, 467 and 495) varying between homologs (Figure 4-2E). Together with respective molecular ions, these fragment combinations enabled the unambiguous localization of the functional groups in the DMDS derivatives, showing that the four alkenes all comprised isomers with double bonds seven carbons away from one end of the alkyl chain, thus representing a series of four homologous 7-alkenes. The C₃₇ DMDS adduct peak was found to contain a second compound with mass spectral α -fragments m/z 173 and 439 (Figure 4-2F), showing the presence of an alkene isomer with double bond nine carbons away

from the chain terminus. Corresponding combinations of α -fragments detected in the other DMDS adduct homologs indicated that the C₃₃, C₃₅ and C₃₉ alkenes also comprised small amounts of regio-isomers with this double bond position and, thus, a series of four homologous 9-alkenes paralleling that of the 7-alkenes.

The two series of alkene isomers had distinct chain length distributions. Specifically, the 7-alkenes were dominated by the C₃₅ homolog, accompanied by lesser amounts of C₃₃ and C₃₇ and only traces of C₃₉ (Figure 4-2G, H). In contrast, the series of 9-alkenes had a characteristic chain length distribution peaking at C₃₇. Within each alkene homolog, the 7-alkenes were the prevalent isomers.

Based on the presence of further α -fragments m/z 117, 131 and 159 (each paired with corresponding higher-mass α -fragments) in the mass spectra of the DMDS adducts, further series of 5-alkenes, 6-alkenes and 8-alkenes were identified in the wax extracted from young Arabidopsis leaves. Trace amounts of all three isomers were detected in the C₃₃, C₃₅ and C₃₇ alkenes (but not in C₃₉) (Figure 4-2G). More detailed GC-MS analyses of OsO₄ oxidation products of the same leaf wax fraction confirmed these minor isomer series and revealed the presence of further alkenes with double bonds in various positions between C-10 and C-15 (Figure 4-3). This second derivatization approach also enabled quantification of all isomers in alkene homologs ranging from C₃₁ to C₃₉, showing an overall link between isomer and homolog distributions. In particular, the 5-alkene series peaked at C₃₃, the 7-alkenes at C₃₅, the 9-alkenes at C₃₇, and the 11-/13-/15-alkenes at C₃₇ and C₃₉, thus marking a prevalence of compounds with the same length of the alkyl tail (C₂₇) on the far side of the double bond. These results matched the DMDS-based quantification of homolog and isomer distributions described above.

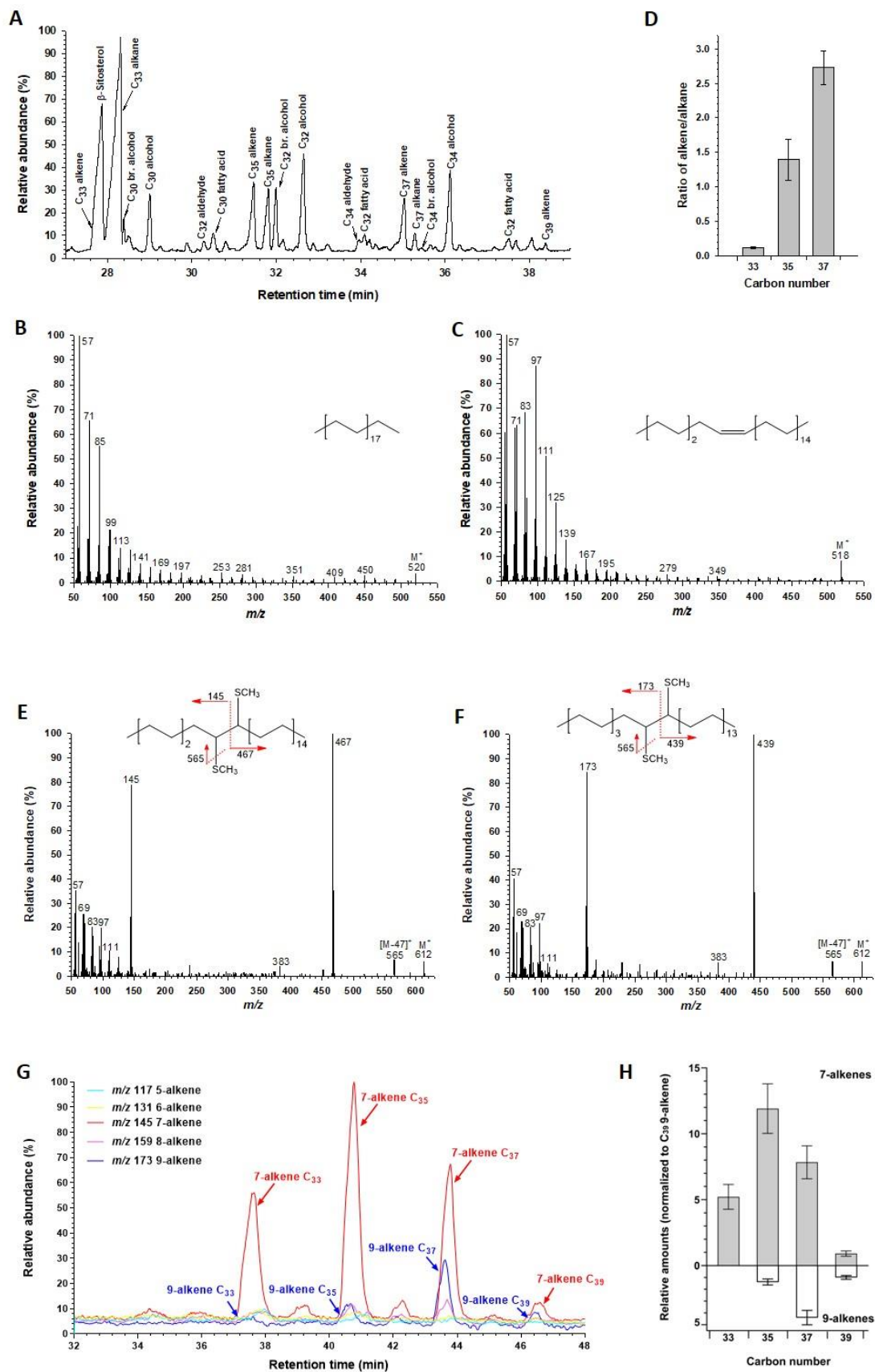


Figure 4-2: Identification of characteristic alkenes in young *Arabidopsis* leaves

A) Total ion gas chromatogram of the wax mixture extracted from young leaves of 2-week-old *Arabidopsis* plants. The characteristic alkenes elute just before the alkanes with corresponding chain lengths. B) Mass spectrum of C₃₇ alkane. C) Mass spectrum of C₃₇ alkene. D) Ratios of amounts of alkenes and alkanes with the same chain length. E) Mass spectrum of C₃₇ 7-alkene DMDS adduct. F) Mass spectrum of C₃₇ 9-alkene DMDS adduct. G) Single-ion gas chromatograms of characteristic fragments for DMDS adducts of various alkene isomers (relative amounts normalized to C₃₅ 7-alkene). H) Quantities of 7- and 9-alkene homologs (normalized to C₃₉ 9-alkene). Error bars represent the standard deviations of three biological replicates. The experiments were repeated twice, and similar results were obtained.

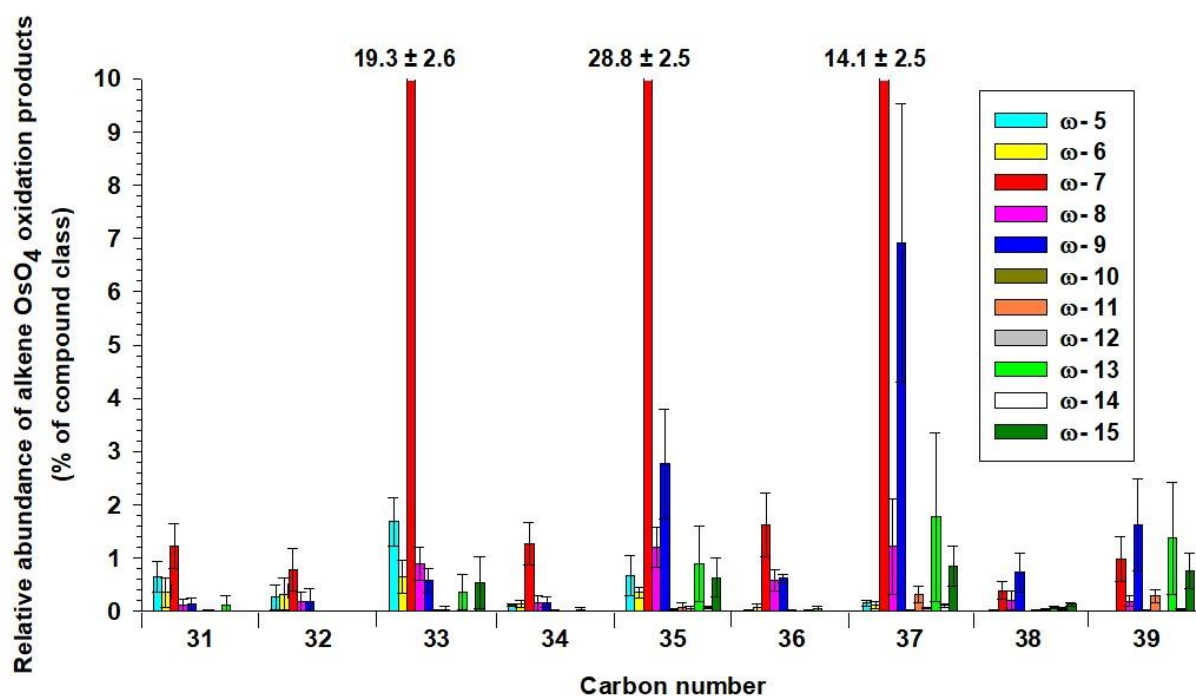


Figure 4-3: Relative abundances of wax alkene regio-isomers quantified by GC-MS analysis of OsO₄ oxidation products

Wax alkenes from young leaves of 2-week-old *Arabidopsis* wild type were extracted, purified by TLC and oxidized with OsO₄. The resulting diols (derivatized into TMS ethers) were separated by GC and quantified by MS. All data represent three biological replicates, and error bars show standard deviations. The experiment was independently carried out twice, with similar results.

4.3.2 The acyl-CoA desaturase ADS4.2 is involved in the synthesis of the Arabidopsis wax VLC alkenes

The characteristic structures of the predominant 7-alkenes and accompanying 9-alkenes in Arabidopsis leaf wax suggested that they were formed by one or more enzymes with high regio-specificity. We hypothesized that respective desaturases should install double bonds specifically in the ω -7 or ω -9 positions of acyl precursors, since Δ -8 or Δ -10 acyl desaturase activities that could lead to the same alkene products had not been described in any of the candidate enzyme families. Consequently, we aimed to test whether any of the desaturases with previously reported ω -7 or ω -9 specificity but unassigned biosynthetic function was involved in wax alkene formation. For this, we selected candidate desaturases with respective regio-selectivities from the AAD family known to introduce corresponding double bonds before elongation to VLC acyls (AAD2 and AAD3), along with those from the ADS family known to accept acyls after VLC elongation (ADS1, ADS1.3, ADS2 and ADS4.2) (Smith et al., 2013; Bryant et al., 2016).

To assess the involvement of the candidate enzymes, six mutant lines each with a confirmed T-DNA insertion in one of the candidate genes were grown alongside the corresponding wild type (Col-0), and cuticular waxes extracted from their expanding rosette leaves were analyzed using GC-MS and GC-FID. The wax mixtures of the *aad2*, *aad3*, *ads1* and *ads2* mutants were found identical to that of the wild type, comprising alkenes and all other compound classes (fatty acids, alcohols, aldehydes, alkanes and sterols) in the same quantities and with the same chain length distributions (Figure 4-4, Table 4-2). The *ads1.3* mutant leaf wax contained differed from that of wild type only in slightly elevated amounts of $C_{33} - C_{37}$ alkanes as well as C_{37} alkene. In contrast, preliminary tests showed that the *ads4.2-1* mutant had strongly reduced amounts of alkenes, and it was therefore selected for more detailed analysis.

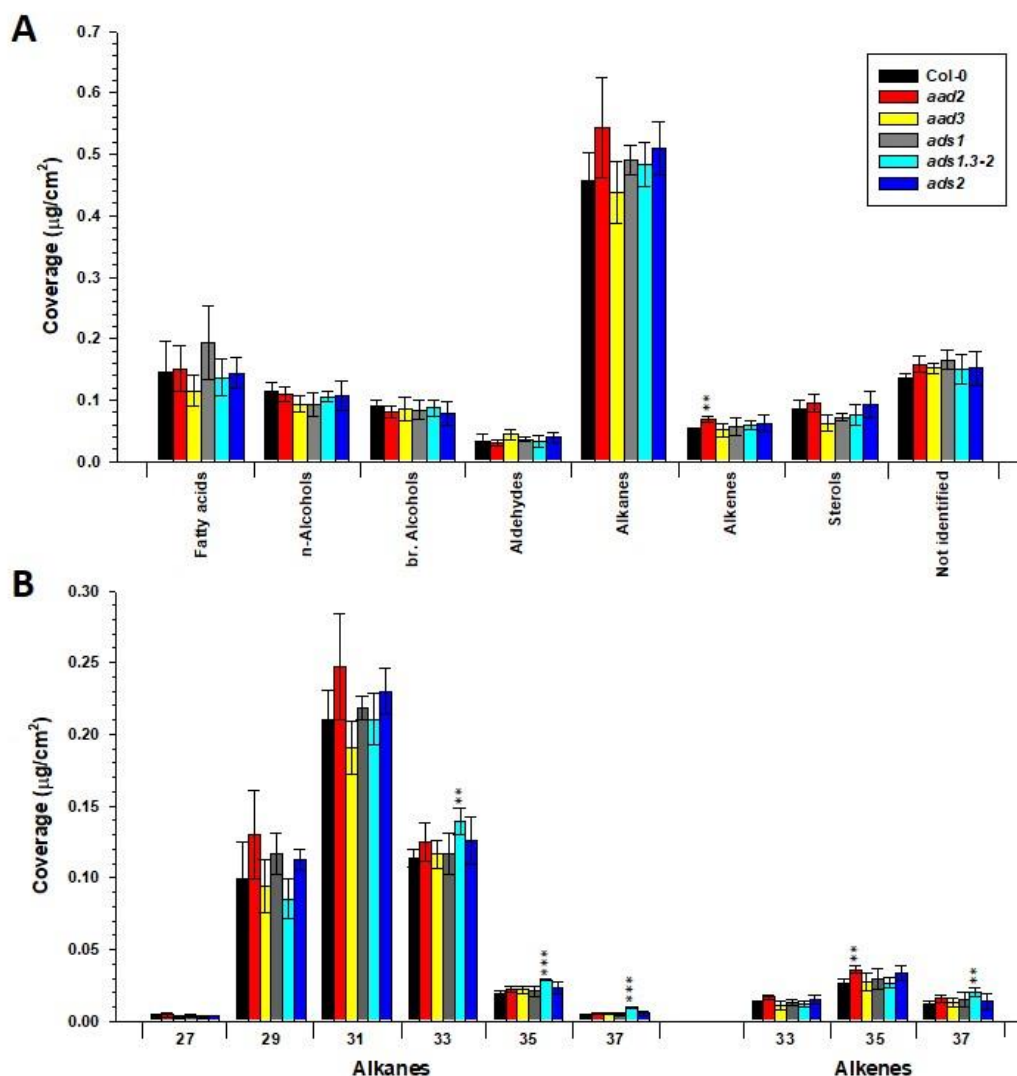


Figure 4-4: Screening of desaturase-deficient Arabidopsis mutants for wax alkene phenotypes

A) Compound class distribution in total wax mixtures on young leaves of Arabidopsis wild type (Col-0) and desaturase-deficient mutants. 2-week-old Arabidopsis plants were used for wax analysis. B) Chain length distribution of alkanes and alkenes in the wax mixtures of young Arabidopsis leaves. Numbers on the x-axis indicate homolog chain lengths. All data represent means of four or five independent biological samples, and error bars show standard deviations. Asterisks indicate discovery of statistically significant differences of coverage between wild type and each mutant based on Student's *t*-test (* $P < 0.05$, ** $P < 0.01$, *** $P < 0.001$).

Table 4-2: The wax analysis of Arabidopsis desaturase-deficient mutants

Unit	$\mu\text{g}/\text{cm}^2$																				
Compound classes	Chain length	Col-0	p-Value	aad2	p-Value	aad3	p-Value	ads1	p-Value	ads1.3-1	p-Value	ads1.3-2	p-Value	ads2	p-Value	ads4.2-1	p-Value				
Fatty acids	C20	0.0019 ± 0.0013	-	0.0023 ± 0.0015		0.0013 ± 0.0007		0.0018 ± 0.0020		0.0018 ± 0.0004		0.0011 ± 0.0006		0.0011 ± 0.0006		0.0024 ± 0.0010					
	C22	0.0011 ± 0.0004	-	0.0012 ± 0.0002		0.0012 ± 0.0003		0.0019 ± 0.0008		0.0011 ± 0.0004		0.0010 ± 0.0005		0.0012 ± 0.0003		0.0026 ± 0.0019					
	C24	0.0248 ± 0.0110	-	0.0325 ± 0.0040		0.0296 ± 0.0071		0.0361 ± 0.0088		0.0284 ± 0.0116		0.0185 ± 0.0034		0.0330 ± 0.0079		0.0267 ± 0.0126					
	C25	0.0008 ± 0.0003	-	0.0007 ± 0.0002		0.0008 ± 0.0005		0.0015 ± 0.0007		0.0014 ± 0.0006		0.0009 ± 0.0003		0.0008 ± 0.0002		0.0013 ± 0.0006					
	C26	0.0559 ± 0.0253	-	0.0614 ± 0.0257		0.0458 ± 0.0135		0.0847 ± 0.0313		0.0726 ± 0.0335		0.0465 ± 0.0102		0.0613 ± 0.0094		0.0637 ± 0.0291					
	C27	0.0015 ± 0.0005	-	0.0015 ± 0.0005		0.0016 ± 0.0005		0.0020 ± 0.0006		0.0016 ± 0.0001		0.0016 ± 0.0003		0.0019 ± 0.0009		0.0018 ± 0.0008					
	C28	0.0193 ± 0.0060	-	0.0177 ± 0.0068		0.0097 ± 0.0020		0.0221 ± 0.0098		0.0220 ± 0.0099		0.0231 ± 0.0046		0.0136 ± 0.0040		0.0177 ± 0.0080					
	C29	0.0218 ± 0.0033	-	0.0241 ± 0.0016		0.0175 ± 0.0040		0.0226 ± 0.0025		0.0173 ± 0.0107		0.0213 ± 0.0059		0.0227 ± 0.0036		0.0236 ± 0.0069					
	C30	0.0083 ± 0.0033	-	0.0042 ± 0.0014		0.0033 ± 0.0018		0.0108 ± 0.0045		0.0097 ± 0.0047		0.0129 ± 0.0041		0.0041 ± 0.0026		0.0075 ± 0.0021					
	C32	0.0064 ± 0.0027	-	0.0037 ± 0.0005		0.0030 ± 0.0008		0.0066 ± 0.0018		0.0078 ± 0.0010		0.0060 ± 0.0023		0.0028 ± 0.0006		0.0058 ± 0.0014					
n-Alcohols	C34	0.0032 ± 0.0017	-	0.0015 ± 0.0004		0.0016 ± 0.0004		0.0032 ± 0.0011		0.0050 ± 0.0026		0.0037 ± 0.0012		0.0018 ± 0.0008		0.0034 ± 0.0014					
	Total	0.1449 ± 0.0520	-	0.1510 ± 0.0370		0.1156 ± 0.0245		0.1933 ± 0.0597		0.1687 ± 0.0707		0.1366 ± 0.0294		0.1443 ± 0.0256		0.1564 ± 0.0603					
	22ol	0.0018 ± 0.0011	-	0.0023 ± 0.0013		0.0016 ± 0.0002		0.0019 ± 0.0007		0.0021 ± 0.0013		0.0015 ± 0.0005		0.0015 ± 0.0001		0.0022 ± 0.0012					
	24ol	0.0013 ± 0.0006	-	0.0013 ± 0.0005		0.0013 ± 0.0005		0.0013 ± 0.0004		0.0009 ± 0.0004		0.0016 ± 0.0009		0.0016 ± 0.0009		0.0016 ± 0.0010					
	26ol	0.0031 ± 0.0012	-	0.0024 ± 0.0010		0.0023 ± 0.0013		0.0016 ± 0.0004		0.0030 ± 0.0011		0.0021 ± 0.0005		0.0022 ± 0.0005		0.0028 ± 0.0017					
	28ol	0.0140 ± 0.0014	-	0.0147 ± 0.0010		0.0112 ± 0.0009		0.0101 ± 0.0014		0.0137 ± 0.0015		0.0120 ± 0.0014		0.0126 ± 0.0020		0.0140 ± 0.0037					
	29ol	0.0070 ± 0.0008	-	0.0108 ± 0.0016		0.0076 ± 0.0003		0.0076 ± 0.0013		0.0067 ± 0.0021		0.0059 ± 0.0015		0.0091 ± 0.0019		0.0074 ± 0.0011					
	30ol	0.0305 ± 0.0028	-	0.0311 ± 0.0056		0.0283 ± 0.0065		0.0267 ± 0.0063		0.0280 ± 0.0031		0.0301 ± 0.0023		0.0297 ± 0.0072		0.0278 ± 0.0016					
	31ol	0.0051 ± 0.0023	-	0.0053 ± 0.0013		0.0042 ± 0.0006		0.0052 ± 0.0008		0.0050 ± 0.0014		0.0058 ± 0.0003		0.0048 ± 0.0012		0.0058 ± 0.0019					
	32ol	0.0360 ± 0.0049	-	0.0287 ± 0.0037		0.0240 ± 0.0055		0.0247 ± 0.0076		0.0274 ± 0.0016		0.0317 ± 0.0036		0.0320 ± 0.0083		0.0329 ± 0.0044					
Aldehydes	34ol	0.0167 ± 0.0037	-	0.0128 ± 0.0022		0.0135 ± 0.0025		0.0131 ± 0.0027		0.0122 ± 0.0017		0.0156 ± 0.0009		0.0139 ± 0.0038		0.0153 ± 0.0019					
	Total	0.1098 ± 0.0132	-	0.1094 ± 0.0120		0.0942 ± 0.0131		0.0922 ± 0.0189		0.0991 ± 0.0043		0.1056 ± 0.0083		0.1072 ± 0.0230		0.1098 ± 0.0132					
	28ad	0.0069 ± 0.0036	-	0.0074 ± 0.0029		0.0124 ± 0.0044		0.0093 ± 0.0010		0.0076 ± 0.0013		0.0060 ± 0.0025		0.0090 ± 0.0041		0.0058 ± 0.0010					
	30ad	0.0102 ± 0.0035	-	0.0086 ± 0.0013		0.0105 ± 0.0025		0.0110 ± 0.0015		0.0117 ± 0.0012		0.0116 ± 0.0015		0.0116 ± 0.0028		0.0097 ± 0.0031					
	32ad	0.0094 ± 0.0029	-	0.0087 ± 0.0005		0.0110 ± 0.0002		0.0102 ± 0.0013		0.0098 ± 0.0023		0.0099 ± 0.0026		0.0115 ± 0.0017		0.0127 ± 0.0038					
	34ad	0.0060 ± 0.0029	-	0.0057 ± 0.0006		0.0070 ± 0.0017		0.0057 ± 0.0017		0.0030 ± 0.0016		0.0060 ± 0.0015		0.0078 ± 0.0006		0.0068 ± 0.0035					
	Total	0.0326 ± 0.0122	-	0.0304 ± 0.0044		0.0439 ± 0.0075		0.0362 ± 0.0039		0.0309 ± 0.0026		0.0335 ± 0.0094		0.0398 ± 0.0088		0.0350 ± 0.0107					
	30bl	0.0308 ± 0.0030	-	0.0245 ± 0.0036		0.0279 ± 0.0063		0.0249 ± 0.0047		0.0235 ± 0.0019		0.0284 ± 0.0041		0.0252 ± 0.0055		0.0257 ± 0.0017					
	31bl	0.0048 ± 0.0008	-	0.0044 ± 0.0008		0.0052 ± 0.0023		0.0048 ± 0.0019		0.0042 ± 0.0005		0.0046 ± 0.0013		0.0045 ± 0.0024		0.0042 ± 0.0012					
	32bl	0.0515 ± 0.0054	-	0.0500 ± 0.0069		0.0496 ± 0.0098		0.0520 ± 0.0075		0.0461 ± 0.0031		0.0515 ± 0.0079		0.0456 ± 0.0102		0.0484 ± 0.0019					
br. Alcohols	34bl	0.0029 ± 0.0011	-	0.0024 ± 0.0003		0.0026 ± 0.0005		0.0028 ± 0.0009		0.0027 ± 0.0006		0.0030 ± 0.0007		0.0029 ± 0.0012		0.0021 ± 0.0005					
	Total	0.0900 ± 0.0097	-	0.0814 ± 0.0104		0.0852 ± 0.0189		0.0845 ± 0.0146		0.0765 ± 0.0048		0.0875 ± 0.0133		0.0782 ± 0.0192		0.0803 ± 0.0044					
	27an	0.0034 ± 0.0012	-	0.0045 ± 0.0018		0.0031 ± 0.0011		0.0038 ± 0.0008		0.0048 ± 0.0017		0.0030 ± 0.0007		0.0038 ± 0.0004		0.0052 ± 0.0018					
	29an	0.0993 ± 0.0261	-	0.1298 ± 0.0307		0.0940 ± 0.0187		0.1169 ± 0.0144		0.1295 ± 0.0337		0.0854 ± 0.0138		0.1134 ± 0.0071		0.1515 ± 0.0334					
	30an	0.0070 ± 0.0011	-	0.0093 ± 0.0025		0.0067 ± 0.0011		0.0082 ± 0.0011		0.0090 ± 0.0023		0.0065 ± 0.0008		0.0078 ± 0.0005		0.0119 ± 0.0022					
	31an	0.2101 ± 0.0210	-	0.2469 ± 0.0369		0.1904 ± 0.0185		0.2188 ± 0.0083		0.2481 ± 0.0417		0.2107 ± 0.0175		0.2300 ± 0.0159		0.2875 ± 0.0476					
	33an	0.1136 ± 0.0064	-	0.1248 ± 0.0134		0.1164 ± 0.0096		0.1167 ± 0.0145		0.1384 ± 0.0053	3.50E-03	**	0.1395 ± 0.0090	5.67E-03	**	0.1261 ± 0.0165					
	35an	0.0193 ± 0.0022	-	0.0227 ± 0.0020		0.0220 ± 0.0024		0.0209 ± 0.0033		0.0279 ± 0.0016	3.03E-03	**	0.0289 ± 0.0007	2.63E-04	***	0.0234 ± 0.0036					
	37an	0.0046 ± 0.0008	-	0.0051 ± 0.0006		0.0050 ± 0.0005		0.0049 ± 0.0012		0.0093 ± 0.0010	1.10E-03	**	0.0096 ± 0.0006	6.50E-05	***	0.0055 ± 0.0013					
	Total	0.4574 ± 0.0446	-	0.5430 ± 0.0820		0.4377 ± 0.0498		0.4903 ± 0.0236		0.5671 ± 0.0812		0.4837 ± 0.0354		0.5091 ± 0.0435		0.6393 ± 0.1038					
Alkenes	33en	0.0131 ± 0.0012	-	0.0169 ± 0.0015		0.0112 ± 0.0030		0.0134 ± 0.0019		0.0164 ± 0.0007		0.0121 ± 0.0025		0.0154 ± 0.0030		0.0023 ± 0.0004	5.00E-06	***			
	35en	0.0263 ± 0.0030	-	0.0360 ± 0.0023	6.94E-03	**	0.0276 ± 0.0063		0.0295 ± 0.0075		0.0349 ± 0.0019	9.33E-03	**	0.0335 ± 0.0050		0.0098 ± 0.0040	8.73E-04	***			
	37en	0.0125 ± 0.0016	-	0.0158 ± 0.0029		0.0129 ± 0.0031		0.0148 ± 0.0052		0.0238 ± 0.0046	7.79E-03	**	0.0214 ± 0.0037	9.77E-03	**	0.0118 ± 0.0003	1.46E-05	***			
	Total	0.0519 ± 0.0033	-	0.0686 ± 0.0042	2.56E-03	**	0.0518 ± 0.0106		0.0578 ± 0.0143		0.0751 ± 0.0056	1.17E-03	**	0.0591 ± 0.0079		0.0627 ± 0.0128		0.0139 ± 0.0039	9.00E-06	***	
	Bras	0.0032 ± 0.0006	-	0.0046 ± 0.0012		0.0025 ± 0.0004		0.0025 ± 0.0007		0.0036 ± 0.0011		0.0036 ± 0.0011		0.0040 ± 0.0013		0.0026 ± 0.0002					
	campe	0.0226 ± 0.0015	-	0.0237 ± 0.0018		0.0175 ± 0.0025		0.0189 ± 0.0015		0.0228 ± 0.0013		0.0228 ± 0.0021		0.0237 ± 0.0047		0.0211 ± 0.0020					
	beta-sito	0.0603 ± 0.0152	-	0.0662 ± 0.0123		0.0424 ± 0.0104		0.0504 ± 0.0042		0.0640 ± 0.0047		0.0493 ± 0.0153		0.0656 ± 0.0150		0.0508 ± 0.0126					
	Total	0.0861 ± 0.0146	-	0.0903 ± 0.0039		0.0756 ± 0.0170		0.0718 ± 0.0062		0.0903 ± 0.0039		0.0756 ± 0.0170		0.0933 ± 0.0207		0.0745 ± 0.0138					
	br. Alkanes	C31	0.0038 ± 0.0009	-	0.0082 ± 0.0032		0.0067 ± 0.0005	6.40E-03	**	0.0049 ± 0.0023		0.0046 ± 0.0020		0.0041 ± 0.0014		0.0079 ± 0.0007	1.99E-03	**	0.0049 ± 0.0012		
	MAG	C18-1	0.0075 ± 0.0024	-	0.0063 ± 0.0013		0.0086 ± 0.0029		0.0066 ± 0.0016		0.0054 ± 0.0011		0.0065 ± 0.0026		0.0077 ± 0.0019		0.0045 ± 0.0012				
Not identified	-	0.1252 ± 0.0077	-	0.1423 ± 0.0145		0.1387 ± 0.0086		0.1533 ± 0.0139		0.1378 ± 0.0139		0.1427 ± 0.0230		0.1406 ± 0.0243		0.1356 ± 0.0234					
	Total wax	-	1.1255 ± 0.0983	-	1.2514 ± 0.1109		1.0579 ± 0.0598		1.2032 ± 0.0656		1.2683 ± 0.1401		1.1437 ± 0.0832		1.2025 ± 0.1525		1.2684 ± 0.1807				

MAG: Monoacylglycerol. All data represent means of four or five independent biological samples, and error bars show standard deviations. Asterisks indicate discovery of significant differences of coverage between wild type and each mutant based on Student's *t*-test (**P* < 0.05, ***P* < 0.01, ****P* < 0.01).

To further test the involvement of the ADS4.2 desaturase in wax alkene formation, two independent mutant alleles were obtained, with T-DNA insertions in the last exon and the promoter region designated as *ads4.2-1* (SALK_039511C) and *ads4.2-2* (SALK_093326), respectively (Figure 4-5A). qRT-PCR showed that both mutants had *ADS4.2* transcript levels less than 0.2% of the wild type (Figure 4-5B), confirming the almost complete loss of the ADS4.2 desaturase function in them. GC-MS analysis revealed that the waxes extracted from expanding leaves of *ads4.2-1* and *ads4.2-2* had total coverages of $1.28 \pm 0.13 \mu\text{g}/\text{cm}^2$ and $1.42 \pm 0.23 \mu\text{g}/\text{cm}^2$, respectively, close to that of wild type ($1.30 \pm 0.19 \mu\text{g}/\text{cm}^2$). Accordingly, the mutant wax mixtures comprised fatty acids, alcohols, aldehydes, alkanes and sterols in the same quantities as wild type wax (Figure 4-5C, Table 4-3). However, the leaf waxes of both mutant lines had alkene coverages, reduced to less than a fourth of the wild-type level. Detailed chain length analysis showed that the coverage of the C₃₅ and C₃₇ alkene homologs in particular were significantly reduced in both mutants (Figure 4-5D).

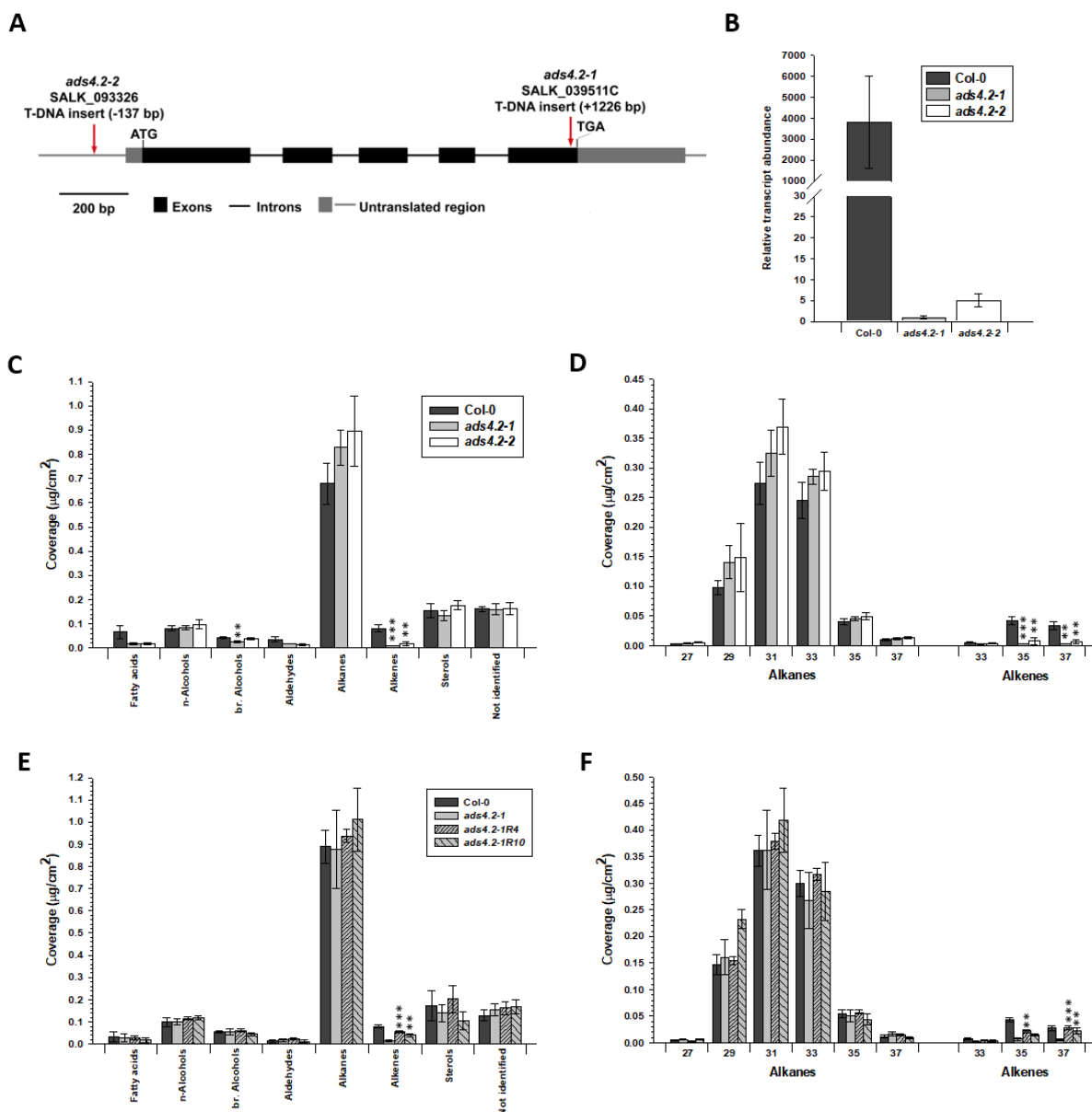


Figure 4-5: Analysis of wax mixtures from young leaves of Arabidopsis *ads4.2* mutant and rescue lines

A) Schematic representation of *ADS4.2* (At1g06360) gene structure and the positions of the T-DNA inserts in mutant alleles. Nucleotide positions are given relative to the translational start site (+1). Dark boxes indicate exons, black lines indicate introns, and light boxes indicate 5'- and 3'-untranslated regions. B) Relative expression levels of *ADS4.2* in young leaves of Arabidopsis wild type Col-0 and *ADS4.2* mutant alleles determined by qRT-PCR analysis. *ADS4.2* transcript abundance was normalized to *ACTIN2* and relative to *ads4.2-1*. The experiment was repeated twice, and similar results were obtained. C) Compound class distribution in total wax mixtures on young leaves of Arabidopsis wild-type (Col-0) and *ADS4.2* mutant alleles. D) Chain length distribution

of alkanes and alkenes on young leaves of Arabidopsis wild-type (Col-0) and *ADS4.2* mutant alleles. E) Compound class distribution in total wax mixtures on young leaves of Arabidopsis wild type (Col-0), *ads4.2-1* and corresponding *ADS4.2* rescue lines. F) Chain length distribution of alkanes and alkenes on young leaves of Arabidopsis wild type (Col-0), *ads4.2-1* and corresponding *ADS4.2* rescue lines. Young leaves of 2-week-old Arabidopsis plants were used in both qRT-PCR and wax analyses. All wax data represent the mean of three or four independent biological samples, and error bars show standard deviations. Asterisks in (C) and (D) indicate discovery of statistically significant differences of coverage between wild type and each mutant allele based on Student's *t*-test (**P* < 0.05, ***P* < 0.01, ****P* < 0.001). Asterisks in (E) and (F) indicate discovery of statistically significant differences of coverage between *ads4.2-1* mutant and each rescue line based on Student's *t*-test (**P* < 0.05, ***P* < 0.01, ****P* < 0.001).

To further establish the role of *ADS4.2* in wax alkene production, the *ads4.2-1* mutant was transformed with a vector carrying the coding region of *ADS4.2* fused with GFP, for expression under control of the cauliflower mosaic virus (*CaMV*) 35S promoter (35S::*ADS4.2*-GFP). Firstly, immunoblots confirmed the presence of the *ADS4.2* protein in young leaves of T₂ progenies of the transformed plants (Figure 4-6). Then, the waxes of expanding leaves of two independent transformants were analyzed by GC-MS and GC-FID to test whether the mutant wax alkene phenotype was rescued. Both lines, *ads4.2-1R4* and *ads4.2-1R10*, had alkene coverages ($0.055 \pm 0.005 \mu\text{g}/\text{cm}^2$ and $0.040 \pm 0.007 \mu\text{g}/\text{cm}^2$, respectively) substantially increased relative to the parent *ads4.2-1* ($0.001 \pm 0.006 \mu\text{g}/\text{cm}^2$), but lower than that of wild type controls ($0.078 \pm 0.007 \mu\text{g}/\text{cm}^2$) (Figure 4-5E, Table 4-4). Detailed chain length analysis showed that the transformants had C₃₅ alkene concentrations partially restored and C₃₇ alkene amounts fully restored to wild-type levels (Figure 4-5F). Taken together, our mutant wax analyses suggested that the desaturase *ADS4.2* was indeed involved in formation of the cuticular alkenes.

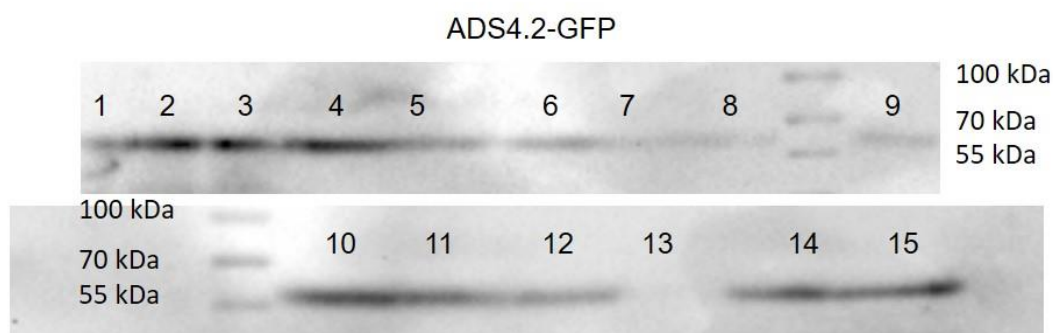


Figure 4-6: ADS4.2-GFP expression levels in *ads4.2-1* rescue T₂ plants

Western blot analysis was carried out using an anti-GFP antibody on the total protein extracts from leaves of 2-week-old T₂ progeny of plants transformed with *Pro35S:ADS4.2-GFP*. Numbers 1-15 designate the T₂ plant lines. The negative controls WT (Col-0) and untransformed *ads4.2-1* data were not shown.

Table 4-3: The wax analysis of *Arabidopsis ads4.2* deficient mutants

Unit		$\mu\text{g}/\text{cm}^2$					
Compound Classes	Chain length	Col-0	p-Value	<i>ads4.2-1</i>	p-Value	<i>ads4.2-2</i>	p-Value
Fatty acids	C20	0.0007 \pm 0.0002	-	0.0008 \pm 0.0002		0.0017 \pm 0.0004	
	C22	0.0012 \pm 0.0006	-	0.0005 \pm 0.0002		0.0005 \pm 0.0002	
	C24	0.0163 \pm 0.0051	-	0.0036 \pm 0.0016		0.0019 \pm 0.0006	8.44E-03 **
	C25	0.0009 \pm 0.0006	-	0.0002 \pm 0.0001		0.0004 \pm 0.0002	
	C26	0.0236 \pm 0.0101	-	0.0026 \pm 0.0015		0.0009 \pm 0.0005	
	C28	0.0096 \pm 0.0045	-	0.0038 \pm 0.0010		0.0041 \pm 0.0011	
	C30	0.0048 \pm 0.0037	-	0.0052 \pm 0.0005		0.0051 \pm 0.0006	
	C32	0.0057 \pm 0.0024	-	0.0012 \pm 0.0004		0.0020 \pm 0.0008	
	C34	0.0044 \pm 0.0026	-	0.0011 \pm 0.0002		0.0015 \pm 0.0009	
	Total	0.0671 \pm 0.0272	-	0.0189 \pm 0.0043		0.0182 \pm 0.0035	
n-Alcohols	C22	0.0012 \pm 0.0003	-	0.0015 \pm 0.0004		0.0032 \pm 0.0010	
	C24	0.0038 \pm 0.0067	-	0.0007 \pm 0.0002		0.0011 \pm 0.0007	
	C26	0.0020 \pm 0.0004	-	0.0089 \pm 0.0038		0.0054 \pm 0.0024	
	C28	0.0050 \pm 0.0006	-	0.0178 \pm 0.0062		0.0147 \pm 0.0083	
	C29	0.0029 \pm 0.0017	-	0.0048 \pm 0.0007		0.0052 \pm 0.0026	
	C30	0.0153 \pm 0.0017	-	0.0124 \pm 0.0007		0.0163 \pm 0.0016	
	C31	0.0000 \pm 0.0000	-	0.0000 \pm 0.0000		0.0000 \pm 0.0000	
	C32	0.0291 \pm 0.0045	-	0.0248 \pm 0.0033		0.0300 \pm 0.0046	
	C34	0.0223 \pm 0.0038	-	0.0135 \pm 0.0015		0.0216 \pm 0.0007	
	Total	0.0814 \pm 0.0095	-	0.0845 \pm 0.0089		0.0975 \pm 0.0185	
Aldehydes	C28	0.0054 \pm 0.0019	-	0.0030 \pm 0.0003		0.0026 \pm 0.0006	
	C30	0.0089 \pm 0.0026	-	0.0044 \pm 0.0003		0.0035 \pm 0.0009	
	C32	0.0116 \pm 0.0035	-	0.0065 \pm 0.0003		0.0051 \pm 0.0019	
	C34	0.0092 \pm 0.0026	-	0.0048 \pm 0.0007		0.0022 \pm 0.0005	
	Total	0.0352 \pm 0.0103	-	0.0187 \pm 0.0011		0.0134 \pm 0.0033	
br. Alcohols	C30	0.0167 \pm 0.0015	-	0.0095 \pm 0.0015	3.56E-03 **	0.0145 \pm 0.0018	
	C31	0.0028 \pm 0.0005	-	0.0042 \pm 0.0008		0.0037 \pm 0.0006	
	C32	0.0192 \pm 0.0019	-	0.0101 \pm 0.0017	3.45E-03 **	0.0184 \pm 0.0030	
	C34	0.0026 \pm 0.0008	-	0.0016 \pm 0.0004		0.0025 \pm 0.0008	
	Total	0.0413 \pm 0.0037	-	0.0253 \pm 0.0040	7.19E-03 **	0.0391 \pm 0.0045	
Alkanes	C27	0.0032 \pm 0.0003	-	0.0042 \pm 0.0011		0.0058 \pm 0.0016	
	C29	0.0979 \pm 0.0123	-	0.1406 \pm 0.0277		0.1484 \pm 0.0575	
	C30	0.0080 \pm 0.0012	-	0.0157 \pm 0.0026		0.0140 \pm 0.0016	6.23E-03 **
	C31	0.2741 \pm 0.0351	-	0.3241 \pm 0.0390		0.3689 \pm 0.0467	
	C33	0.2448 \pm 0.0303	-	0.2854 \pm 0.0128		0.2944 \pm 0.0322	
	C35	0.0404 \pm 0.0049	-	0.0458 \pm 0.0037		0.0495 \pm 0.0059	
	C37	0.0098 \pm 0.0015	-	0.0113 \pm 0.0015		0.0140 \pm 0.0019	
	Total	0.6782 \pm 0.0840	-	0.8271 \pm 0.0710		0.8951 \pm 0.1438	
Alkenes	C33	0.0056 \pm 0.0010	-	0.0029 \pm 0.0006		0.0040 \pm 0.0006	
	C35	0.0426 \pm 0.0072	-	0.0038 \pm 0.0004	4.89E-04 ***	0.0080 \pm 0.0061	3.01E-03 **
	C37	0.0333 \pm 0.0067	-	0.0034 \pm 0.0005	1.27E-03 **	0.0070 \pm 0.0033	3.45E-03 **
	Total	0.0816 \pm 0.0132	-	0.0100 \pm 0.0012	4.89E-04 ***	0.0191 \pm 0.0092	2.34E-03 **
Sterols	brass	0.0026 \pm 0.0002	-	0.0023 \pm 0.0003		0.0020 \pm 0.0001	
	campe	0.0293 \pm 0.0050	-	0.0243 \pm 0.0035		0.0361 \pm 0.0010	
	beta-sito	0.1240 \pm 0.0235	-	0.1073 \pm 0.0169		0.1385 \pm 0.0174	
	Total	0.1558 \pm 0.0284	-	0.1340 \pm 0.0205		0.1766 \pm 0.0180	
br. Alkanes	C31	0.0023 \pm 0.0010	-	0.0039 \pm 0.0009		0.0034 \pm 0.0011	
MAG	C18-1	0.0081 \pm 0.0048	-	0.0084 \pm 0.0026		0.0124 \pm 0.0044	
Not identified	-	0.1610 \pm 0.0097	-	0.1604 \pm 0.0225		0.1630 \pm 0.0258	
Total	-	1.3128 \pm 0.1046	-	1.2914 \pm 0.0975		1.4377 \pm 0.1625	

MAG: Monoacylglycerol. All wax data represent the mean of three or four independent biological samples, and error bars show standard deviations. Asterisks indicate discovery of significant differences of coverage between wild type and each mutant allele based on Student's *t*-test (* $P < 0.05$, ** $P < 0.01$).

Table 4-4: The wax coverages of Arabidopsis *ADS4.2* rescue plants

Unit	$\mu\text{g}/\text{cm}^2$													
Compound Classes	Chain length	Col-0	p-Value	<i>ads4.2-1</i>		p-Value	<i>ads4.2-1R4</i>		p-Value	<i>ads4.2-1R10</i>		p-Value		
Fatty acids	C24	0.0154 ± 0.0124	-	0.0119 ± 0.0077	-	0.0095 ± 0.0020	0.0048 ± 0.0027							
	C26	0.0125 ± 0.0093	-	0.0100 ± 0.0061	-	0.0104 ± 0.0045	0.0070 ± 0.0045							
	C28	0.0057 ± 0.0034	-	0.0061 ± 0.0034	-	0.0085 ± 0.0039	0.0052 ± 0.0027							
	Total	0.0336 ± 0.0213	-	0.0280 ± 0.0161	-	0.0285 ± 0.0084	0.0169 ± 0.0099							
n-Alcohols	C22	0.0021 ± 0.0012	-	0.0018 ± 0.0007	-	0.0012 ± 0.0003	0.0017 ± 0.0007							
	C24	0.0014 ± 0.0008	-	0.0013 ± 0.0004	-	0.0016 ± 0.0009	0.0015 ± 0.0003							
	C26	0.0046 ± 0.0046	-	0.0047 ± 0.0035	-	0.0027 ± 0.0018	0.0141 ± 0.0032							
	C28	0.0110 ± 0.0070	-	0.0134 ± 0.0046	-	0.0097 ± 0.0056	0.0268 ± 0.0039							
	C29	0.0020 ± 0.0007	-	0.0032 ± 0.0016	-	0.0029 ± 0.0005	0.0064 ± 0.0019							
	C30	0.0226 ± 0.0048	-	0.0220 ± 0.0014	-	0.0229 ± 0.0013	0.0190 ± 0.0029							
	C31	0.0000 ± 0.0000	-	0.0000 ± 0.0000	-	0.0000 ± 0.0000	0.0000 ± 0.0000							
	C32	0.0328 ± 0.0024	-	0.0396 ± 0.0084	-	0.0463 ± 0.0140	0.0307 ± 0.0039							
	C33	0.0000 ± 0.0000	-	0.0000 ± 0.0000	-	0.0000 ± 0.0000	0.0000 ± 0.0000							
	C34	0.0222 ± 0.0042	-	0.0147 ± 0.0053	-	0.0286 ± 0.0030	0.0167 ± 0.0038							
	Total	0.0985 ± 0.0220	-	0.1008 ± 0.0118	-	0.1160 ± 0.0055	0.1169 ± 0.0089							
Aldehydes	C28	0.0025 ± 0.0010	-	0.0017 ± 0.0007	-	0.0031 ± 0.0009	0.0020 ± 0.0011							
	C30	0.0040 ± 0.0013	-	0.0048 ± 0.0014	-	0.0070 ± 0.0013	0.0040 ± 0.0029							
	C32	0.0026 ± 0.0032	-	0.0063 ± 0.0032	-	0.0079 ± 0.0052	0.0020 ± 0.0010							
	C34	0.0035 ± 0.0012	-	0.0047 ± 0.0031	-	0.0072 ± 0.0020	0.0043 ± 0.0029							
	Total	0.0126 ± 0.0055	-	0.0175 ± 0.0079	-	0.0253 ± 0.0046	0.0123 ± 0.0053							
br. Alcohols	C30	0.0262 ± 0.0061	-	0.0261 ± 0.0072	-	0.0267 ± 0.0067	0.0191 ± 0.0053							
	C31	0.0027 ± 0.0009	-	0.0030 ± 0.0003	-	0.0030 ± 0.0003	0.0046 ± 0.0012							
	C32	0.0241 ± 0.0022	-	0.0262 ± 0.0066	-	0.0294 ± 0.0019	0.0178 ± 0.0035							
	C34	0.0020 ± 0.0007	-	0.0011 ± 0.0003	-	0.0022 ± 0.0006	0.0032 ± 0.0016							
	Total	0.0549 ± 0.0062	-	0.0563 ± 0.0135	-	0.0613 ± 0.0079	0.0447 ± 0.0075							
Alkanes	C27	0.0050 ± 0.0013	-	0.0058 ± 0.0013	-	0.0027 ± 0.0004	0.0070 ± 0.0012							
	C29	0.1478 ± 0.0187	-	0.1608 ± 0.0334	-	0.1542 ± 0.0070	0.2322 ± 0.0176							
	C30	0.0090 ± 0.0006	-	0.0126 ± 0.0031	-	0.0129 ± 0.0021	0.0155 ± 0.0032							
	C31	0.3612 ± 0.0300	-	0.3627 ± 0.0743	-	0.3793 ± 0.0145	0.4186 ± 0.0596							
	C33	0.3000 ± 0.0249	-	0.2679 ± 0.0523	-	0.3167 ± 0.0118	0.2849 ± 0.0544							
	C35	0.0553 ± 0.0073	-	0.0499 ± 0.0112	-	0.0574 ± 0.0038	0.0440 ± 0.0101							
	C37	0.0121 ± 0.0021	-	0.0160 ± 0.0037	-	0.0148 ± 0.0024	0.0096 ± 0.0022							
Alkenes	Total	0.8903 ± 0.0747	-	0.8758 ± 0.1757	-	0.9379 ± 0.0311	1.0119 ± 0.1415							
	C33	0.0072 ± 0.0025	-	0.0027 ± 0.0015	-	0.0045 ± 0.0009	0.0031 ± 0.0018							
	C35	0.0437 ± 0.0038	-	0.0066 ± 0.0026	-	0.0218 ± 0.0025	0.0143 ± 0.0022	1.65E-03 **						
	C37	0.0274 ± 0.0052	-	0.0048 ± 0.0020	-	0.0283 ± 0.0041	0.0228 ± 0.0054	6.49E-04 ***				5.59E-03 **		
Sterols	Total	0.0783 ± 0.0067	-	0.0141 ± 0.0060	-	0.0546 ± 0.0045	0.0403 ± 0.0070	4.89E-04 ***				8.11E-03 **		
	bras	0.0038 ± 0.0018	-	0.0049 ± 0.0008	-	0.0040 ± 0.0010	0.0044 ± 0.0020							
	campe	0.0279 ± 0.0155	-	0.0173 ± 0.0040	-	0.0202 ± 0.0080	0.0152 ± 0.0060							
	b-sito	0.1405 ± 0.0523	-	0.1174 ± 0.0377	-	0.1796 ± 0.0617	0.0842 ± 0.0323							
	Total	0.1723 ± 0.0670	-	0.1396 ± 0.0376	-	0.2039 ± 0.0611	0.1039 ± 0.0394							
br. Alkanes	C31	0.0047 ± 0.0024	-	0.0062 ± 0.0038	-	0.0042 ± 0.0023	0.0060 ± 0.0016							
MAG	C18-1	0.0107 ± 0.0030	-	0.0149 ± 0.0057	-	0.0182 ± 0.0072	0.0181 ± 0.0064							
Not Identified	-	0.1283 ± 0.0254	-	0.1555 ± 0.0277	-	0.1615 ± 0.0312	0.1691 ± 0.0327							
Total	-	1.4843 ± 0.0995	-	1.4086 ± 0.2717	-	1.6113 ± 0.0365	1.5401 ± 0.1824							

MAG: Monoacylglycerol. All wax data represent the mean of three or four independent biological samples, and error bars show standard deviations. Asterisks indicate discovery of significant differences of coverage between *ads4.2-1* mutant and each rescue line based on Student's *t*-test (* $P < 0.05$, ** $P < 0.01$).

4.3.3 ADS4.2 is highly expressed in young rosette leaves

To test whether *ADS4.2* expression patterns correlated with those of alkene product accumulation, we assessed its organ- and cell-type-specific expression in three experiments. Firstly, the publicly available transcriptome data were inspected (Winter et al., 2007; Marks et al., 2009; Pillitteri et al., 2011; Klepikova et al., 2016; Waese et al., 2017), showing that *ADS4.2* was most highly expressed in young leaves, especially in early stages of development and both in the lamina and the petiole (Figure 4-7). Secondly, the expression profile of *ADS4.2* was also investigated by qRT-PCR, confirming the high transcript levels in young rosette leaves along with moderate amounts in 2-week-old seedlings (Figure 4-8A). In contrast, little or no expression was detected in flowers, cauline leaves, old rosette leaves, apical and basal inflorescence stem portions, roots and young siliques. In a third experiment, the spatial expression pattern of the desaturase was tested by GUS reporter gene assays of the *ADS4.2* promoter (using a 2.3-kb fragment upstream of the translational start site). All T₂ plants analyzed showed similar staining patterns, indicating strongest GUS activity in the emerging and expanding rosette leaves of 14-day-old and 18-day-old seedlings (Figure 4-8 B-D). The inflorescence rachis, developing flower buds and mature stigmas showed moderate GUS activity (Figure 4-8E, F). In contrast, only weak GUS expression was detected in the distal region of inflorescence stems, stem branches and developing siliques, while no GUS activity was found in cotyledons, fully expanded rosette leaves, cauline leaves, stem bases and old siliques, or any part of the roots.

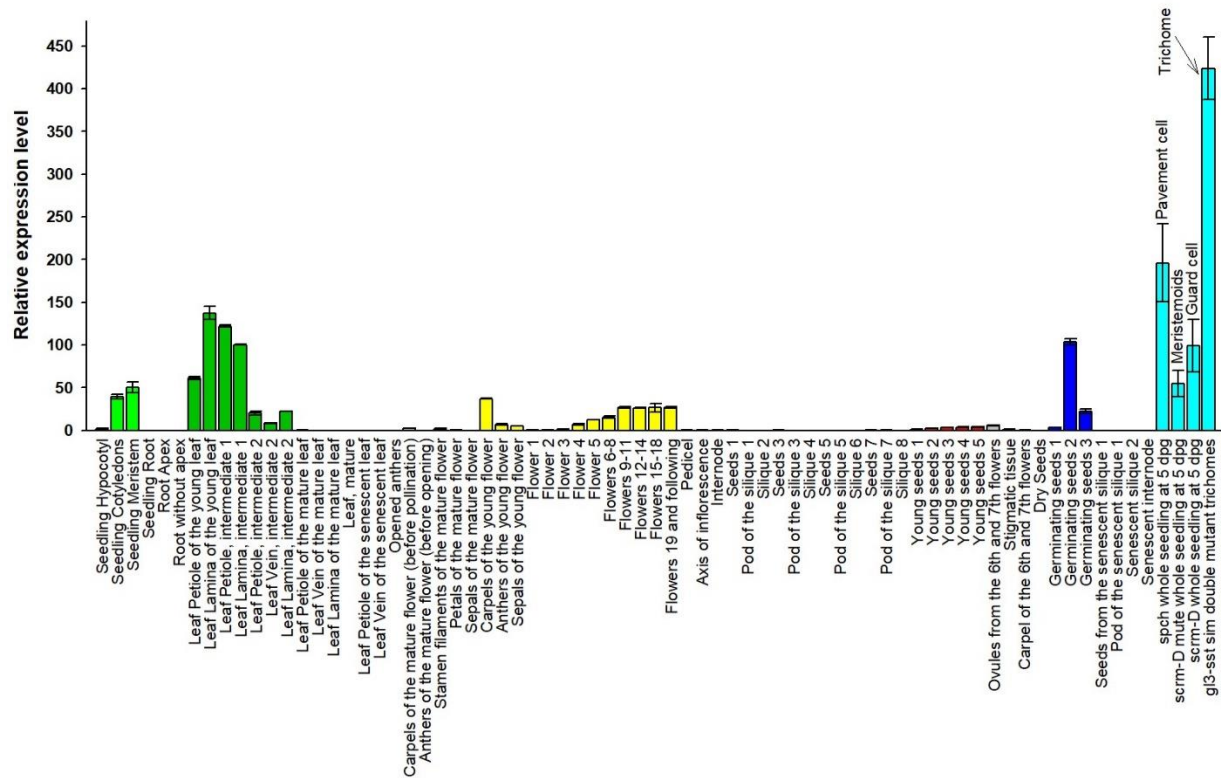


Figure 4-7: Transcriptome analysis of *ADS4.2* expression in different organs and cell types of Arabidopsis wild type Col-0 and mutants

Data were retrieved from eplant as originally posted by Winter et al. (2007); Marks et al. (2009); Pillitteri et al. (2011); Klepikova et al. (2016) and Waese et al. (2017). Error bars indicate standard deviations of two to three biological replicates.

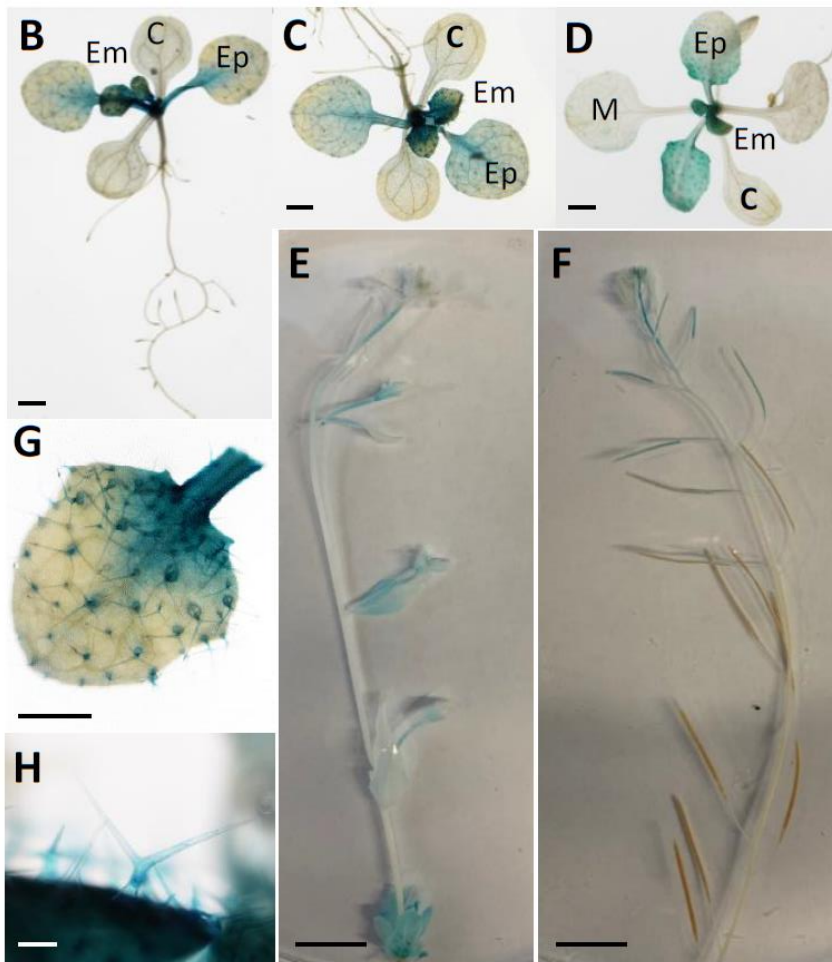
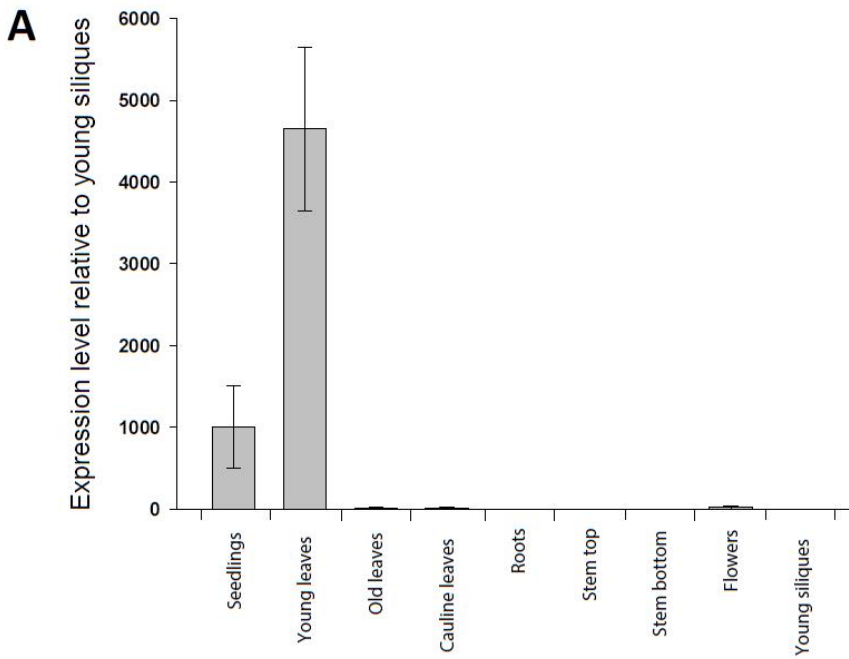


Figure 4- 8: Expression pattern of ADS4.2 in different Arabidopsis organs

A) *ADS4.2* expression in different organs of Arabidopsis wild type Col-0 determined by qRT-PCR. *ADS4.2* transcript abundances in different organs were normalized to corresponding *ACTIN2* expression levels and relative to the transcript of *ADS4.2* in young siliques. Bars represent means of three biological replicates, and error bars show standard deviations. Two independent experiments were performed, and similar trends were obtained. (B-H) Spatial expression pattern of *ADS4.2* in Arabidopsis wild type (Col-0) harboring *ADS4.2* promoter fused to the *GUS* gene. The activity of the *ADS4.2* promoter was visualized by histochemical staining on roots of 14-day-old seedlings (B), leaves of 14-day-old seedlings (C), 18-day-old seedlings (D), five-week-old inflorescence stems (E), six-week-old inflorescence stems and siliques (F), emerging leaves of 14-day-old seedlings (G) and trichomes on expanding leaves of 14-day-old seedlings (H). Two independent experiments were carried out, with similar results. C, cotyledon; Em, emerging leaf; Ep, expanding leaf; M, mature leaf. Bars = 1 mm in B to D; 0.5 mm in G; 0.1 mm in H and 1 cm in E and F.

To further assess the cell-type-specific expression of *ADS4.2*, we inspected the transcriptome data and GUS assay results in more detail. In silico transcriptome data mining revealed substantial *ADS4.2* transcript levels in trichomes of the *gl3-sst sim* double mutant (Figure 4-7), in which trichome development is arrested during early leaf expansion (Marks et al., 2009). GUS assays also showed particularly high *ADS4.2* promoter activity in trichomes on young rosette leaves (Figure 4-8G, H). Together, our findings on the cell-type-specific expression of *ADS4.2* suggest that the high transcript levels observed in young leaves are at least in part due to the high expression in trichomes, which develop early and comprise a great proportion of epidermal cells in early stages of leaf ontogeny (Larkin et al., 1996).

4.3.3 ADS4.2 prefers the longest available fatty acyls for ω -7 desaturation

To test the biochemical activity of *ADS4.2*, we expressed the enzyme in yeast (*S. cerevisiae*) and analyzed the resulting lipids using GC-MS. For this, we chose yeast lines mutated in the *SUR4/ELO3* gene encoding a fatty acid elongase involved in VLC fatty acyl formation, known to

have different VLC acyl pools available as substrates for desaturation. In particular, ADS4.2 activities were assessed in the loss-of-function mutant *elo3Δ* elongating acyls up to C₂₂ (Oh et al., 1997), wild type INVSc1 containing acyls up to C₂₆, and the line harboring the SUR4 F262A/K266L mutant (*INVSUR4#*) reported to contain acyls up to C₃₂ (Denic and Weissman, 2007; Bernard et al., 2012). We aimed i) to assess the distribution of unsaturated acyl homologs in these expression systems to infer substrate chain length preferences of ADS4.2 and ii) to quantify the major double-bond isomers within each homolog to infer its regio-specificity.

For the first purpose, mixtures of neutral lipids were extracted from control yeast lines transformed with empty vector and converted into fatty acid methyl esters (FAMES) to determine the VLC fatty acyl distributions present under our culture conditions. The *elo3Δ* mutant accumulated mainly C₂₂ acyl along with moderate amounts of C₂₀, whereas C₂₄ and C₂₆ acyls were not detectable (Figure 4-9A). In contrast, the wild type contained VLC acyls ranging from C₂₀ to C₂₆, with C₂₆ representing almost 70% of the total VLC lipids (Figure 4-9B). The yeast *INVSUR4#* mutant under our conditions elongated acyls up to C₃₄, with C₃₀ acyl as a major product accompanied by C₂₈, C₂₆ and C₃₂ acyls (Figure 4-9C). Further analysis of the three control yeast strains revealed the presence of monounsaturated VLC acyls (also detected as FAMES), with chain length ranges matching those of the saturated acyls in each line but with distinct quantitative distributions: the *elo3Δ* mutant contained 9% of monounsaturated fatty acyls, mainly 20:1 and accompanied by 22:1 (Table 4-5; Figure 4-9A); the wild type comprised 18% monounsaturated acyls, mainly 20:1 acyl together with 22:1 and 26:1 (Table 4-5; Figure 4-9B); the *INVSUR4#* mutant had 14% unsaturated acyls with 20:1 - 26:1 acyls similar to the wild type, but also an extended series of homologs up to 32:1 peaking at 30:1 (Table 4-5; Figure 4-9C).

Table 4-5: Amounts of unsaturated fatty acyls in yeast expressing *ADS4.2*

Relative quantities of monounsaturated fatty acyls are given as percent of total fatty acyls, and relative quantities of ω -7 isomers are given as percent of the monounsaturated fatty acyls in empty-vector controls and yeast expressing the desaturase *ADS4.2*. Data represent means of three independent yeast transformants, and error bars show SD. All experiments were independently repeated twice with similar results.

	Empty vector						<i>ADS4.2</i>					
	Monounsaturated fatty acyls			ω -7			Monounsaturated fatty acyls			ω -7		
	% of total acids			% of isomers			% of total acids			% of isomers		
<i>elo3Δ</i>	8.52	±	0.41	23.46	±	1.83	14.39	±	4.70	41.14	±	9.89
<i>INVSc1</i>	18.15	±	0.61	3.30	±	3.62	32.41	±	2.48	37.99	±	2.87
<i>INVSur4#*</i>	13.93	±	4.10	33.95	±	2.41	41.27	±	7.83	88.13	±	1.64

* Due to partial overlap of GC peaks with those of saturated VLC fatty acyls, quantities of unsaturated acyls given for *INVSur4#* include small amounts of 26:0 – 34:0.

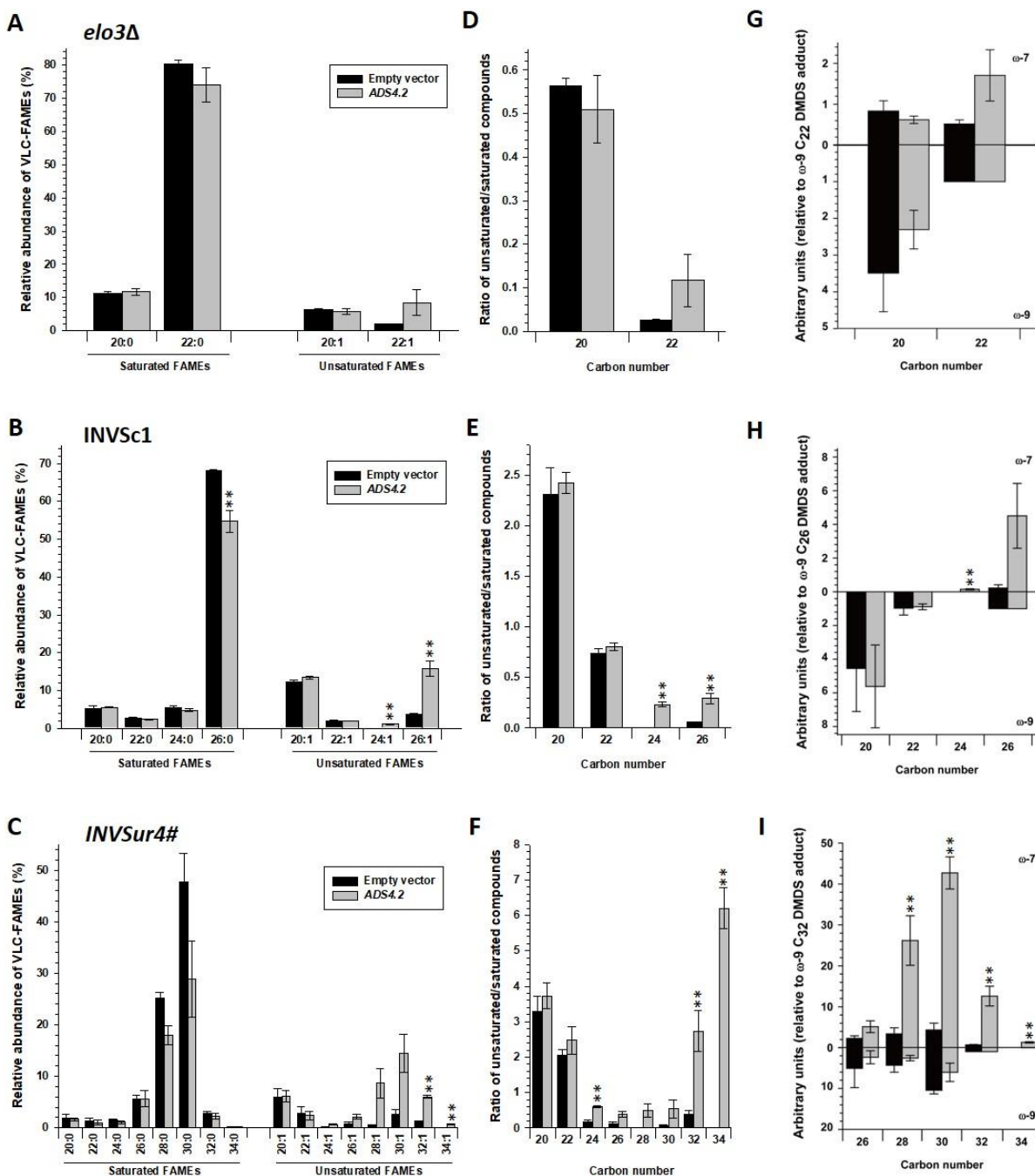


Figure 4-9: ADS4.2 activity on a broad range of VLC acyl-CoA substrates in yeast

A) VLC FAME profiles of yeast *elo3Δ* mutant expressing either empty vector or *ADS4.2*. B) VLC FAME profiles of yeast *INVSc1* wild type expressing either empty vector or *ADS4.2*. C) VLC FAME profiles of yeast *INVSUR4#* mutant expressing either empty vector or *ADS4.2*. D) Ratios of unsaturated FAME to the corresponding saturated FAME in yeast *elo3Δ* mutant expressing empty vector or *ADS4.2*. E) Ratios of unsaturated FAME to the corresponding saturated FAME in yeast *INVSc1* wild type expressing empty vector or *ADS4.2*. F) Ratios of unsaturated FAME to the

corresponding saturated FAME in yeast *INVSUR4#* mutant expressing empty vector or *ADS4.2*. G) Chain length distributions of ω -7 and ω -9 monounsaturated FAMES in yeast *elo3Δ* mutant expressing empty vector or *ADS4.2*. H) Chain length distributions of ω -7 and ω -9 monounsaturated FAMES in yeast *INVSc1* wild type expressing empty vector or *ADS4.2*. I) Chain length distributions of ω -7 and ω -9 monounsaturated FAMES in yeast *INVSUR4#* mutant expressing empty vector or *ADS4.2*. All data represent means of three independent yeast transformants, and error bars show standard deviations. All experiments were independently repeated twice with similar results. Asterisks indicate discovery of significant differences of coverage between yeast lines expressing empty vector and *ADS4.2* based on Student's *t*-test (**P* < 0.05, ***P* < 0.01, ****P* < 0.001).

Expression of *ADS4.2* in the three yeast lines decreased the overall percentage of saturated acyls without changing the chain length distributions (Figure 4-9 A-C). Instead, the amounts of unsaturated acyls increased (relative to empty-vector control), which represented 14%, 32% and 41% of total VLC acyls in the *elo3Δ*, wild type and the *INVSUR4#* mutant, respectively. In particular, *ADS4.2* expression led to a moderate increase of 22:1 acyl in the *elo3Δ* mutant, but did not change the level of 20:1. Wild-type yeast expressing *ADS4.2* had increased levels of 24:1 and 26:1 acyls, while 20:1 and 22:1 remained constant, making 26:1 the predominant unsaturated VLC acyl. Finally, expression of *ADS4.2* in the *INVSUR4#* mutant led to substantial increases in unsaturated acyls 24:1-34:1, with 28:1, 30:1 and 32:1 predominating.

To assess production of different unsaturated acyls regardless of the drastically varying levels of substrate homologs available in different yeast lines, we calculated ratios between the amounts of unsaturated and saturated acyls formed in each yeast line with different chain lengths. Expression of *ADS4.2* in the *elo3Δ* mutant did not affect the ratio of unsaturated:saturated C₂₀ acyls, but increased the corresponding ratio of C₂₂ acyl slightly (Figure 4-9D). Similarly, expression of the desaturase in yeast wild type did not change the unsaturated:saturated compound ratios for the lower chain length range (C₂₀ and C₂₂), but led to slightly higher ratios of C₂₄ and C₂₆ acyls (Figure

4-9E). Finally, the yeast *INVSUR4#* mutant expressing *ADS4.2* also had C₂₀ and C₂₂ ratios similar to the respective empty-vector control, but moderate increases in unsaturated:saturated ratios for acyls ranging from C₂₄ to C₃₀, and substantial increases in ratios for C₃₂ and C₃₄ (Figure 4-9F). These results suggest that *ADS4.2* accepts a broad spectrum of VLC substrates ranging from C₂₂ to C₃₄, with a preference for C₃₂₊ acyls.

To evaluate the regio-specificity of *ADS4.2*, we analyzed the double bond positions of monounsaturated fatty acyls from yeast lines expressing *ADS4.2* and corresponding empty-vector controls. Different isomers were quantified by GC-MS analysis of DMDS-derivatized FAME products. The *elo3Δ* mutant, wild type and *INVSUR4#* mutant controls were all found to contain two compounds identified as the DMDS adducts of ω-9 C₂₀ and C₂₂ acyls based on their characteristic MS α-fragment *m/z* 173 reported before (Francis, 1981; Biedermann et al., 2004). Both compounds were accompanied by ω-7 isomers, identified by α-fragments *m/z* 145 in accordance with previous reports (Sato et al., 2001) and characterized by slightly higher GC retention times than the ω-9 compounds (Figure 4-10). Further ω-9 and ω-7 acyl homologs were identified accordingly based on GC and MS characteristics (in the various yeast lines), including previously reported C₂₄ and C₂₆ and novel C₂₈ - C₃₄ compounds (Figure 4-11).

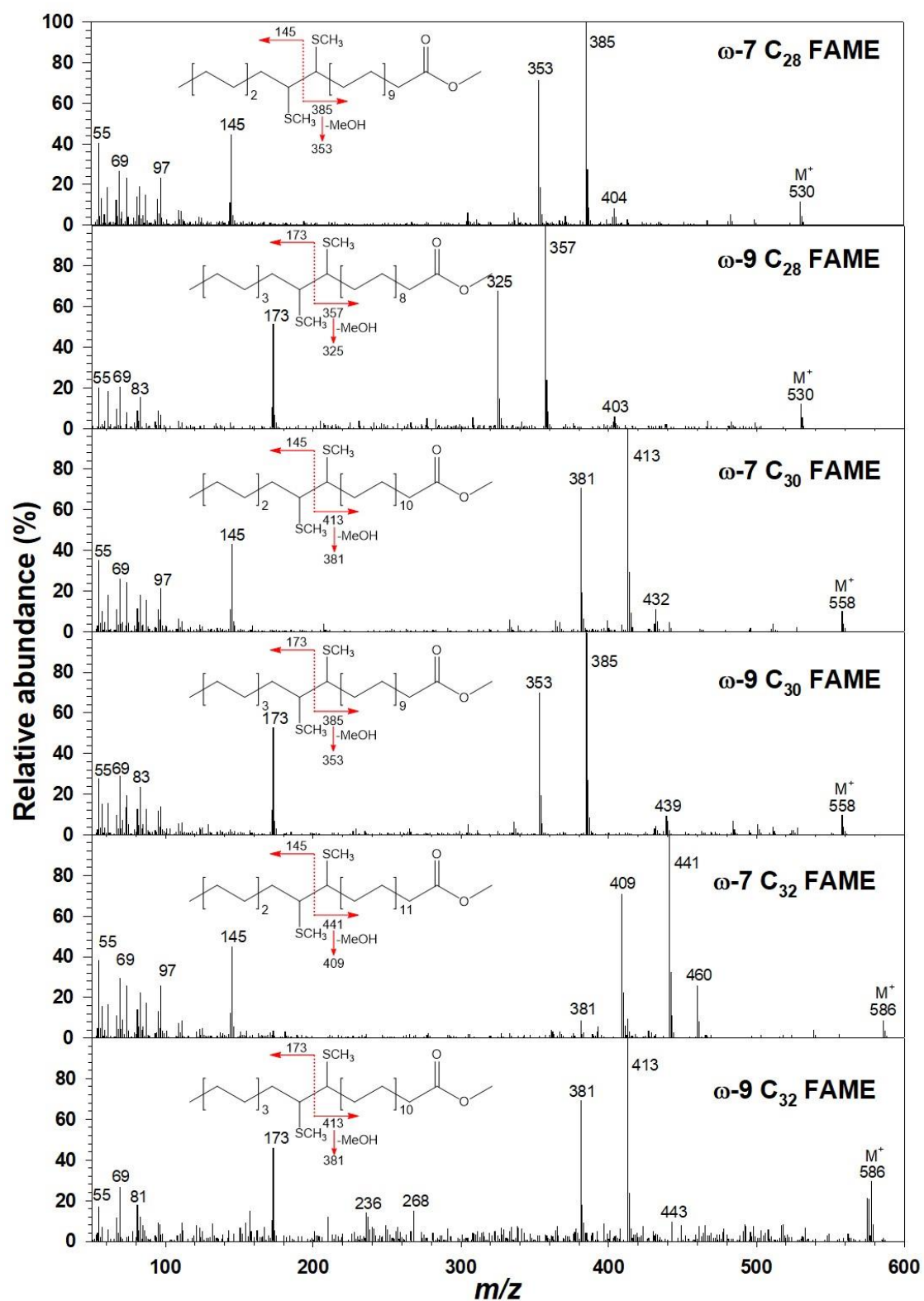


Figure 4-10: Mass spectra of DMDS adducts of ω -7 and ω -9 monounsaturated FAMES

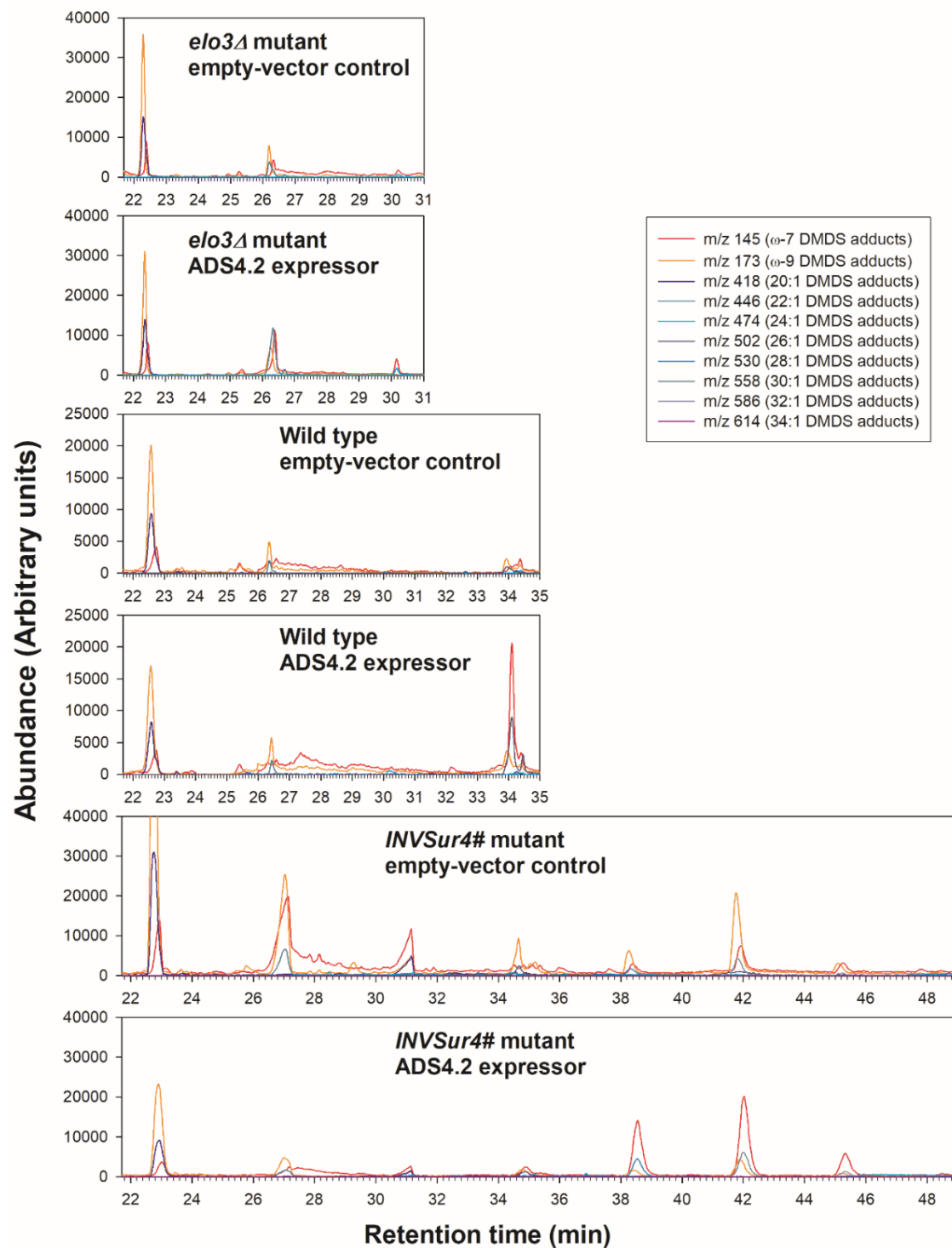


Figure 4-11: GC-MS analysis of DMS adducts of ω -7 and ω -9 monounsaturated FAMES in different yeast lines expressing ADS4.2

For each yeast line, single-ion chromatograms of α -fragments m/z 145 characteristic of ω -7 regio-isomers and α -fragments m/z 173 characteristic of ω -9 regio-isomers are shown, along with M^+ (m/z 418 – 614) corresponding to different chain lengths. Complete separation of homologs and partial separation of isomers was achieved. The single-ion chromatograms of the signature fragments m/z 145 and m/z 173 were integrated to quantify the ω -7 and ω -9 isomers, respectively, within each VLC acyl homolog. The *elo3* Δ mutant had 23% ω -7 and 77% ω -9 isomers overall, with similar isomer ratios for both the C₂₀ and C₂₂ homologs (Table 4-5; Figure 4-9G). In contrast, the *elo3* Δ mutant expressing *ADS4.2* had 41% ω -7 isomers, due to a substantial increase in ω -7 C₂₂ acyl, however the abundances of ω -7 C₂₀ acyl and all ω -9 isomers were undistinguishable from those of the control (Figure 4-9G). Of the monounsaturated acyl adducts in wild type control, 97% were ω -9 isomers (detected in the C₂₀, C₂₂, C₂₆ homologs) and only 3% were ω -7 isomer (detected only in the C₂₆ homolog; Table 4-5; Figure 4-9H). Expression of *ADS4.2* in wild-type yeast led to a significant increase of the ω -7 isomers (38% of total DMDS adducts), most pronouncedly in the C₂₄ and C₂₆ acyls (Table 4-5; Figure 4-9H), while the ω -9 adducts remained unchanged relative to the control. Finally, the *INVSur4#* mutant had 34% ω -7 isomers across all homologs, which increased to 88% of total unsaturated acyls upon expression of *ADS4.2*. In particular, the unsaturated ω -7 C₂₈ - C₃₄ acyls showed substantial increases in the *INVSur4#* mutant expressing *ADS4.2*, while the abundance of ω -9 isomers remained similar to those in the corresponding control (Table 4-5; Figure 4-9I).

4.3.4 The *ADS4.2* protein resides on the ER

To explore whether *ADS4.2* has access to acyl substrates accumulating in certain cell compartments, we determined the subcellular localization of the protein. To this end, two constructs encoding fusions of the green fluorescent protein (GFP) to either the N- or C-terminus

of ADS4.2 were transiently expressed in tobacco (*Nicotiana benthamiana*) leaves alongside the ER marker *HDEL-RFP*, under control of the *35S* promoter. Only weak GFP fluorescence was observed for the N-terminal fusion of ADS4.2, with no clear patterns (data not shown). In contrast, the C-terminal GFP-fusion of ADS4.2 co-localized with HDEL-RFP in a reticulate arrangement (Figure 4-12), showing that the protein is localized to the ER and, thus, has access to the VLC fatty acyl-CoAs known to accumulate in this cellular compartment.

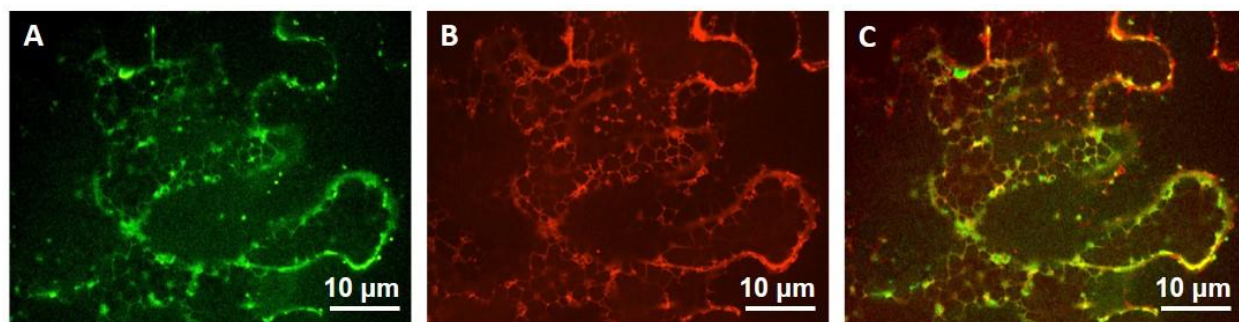


Figure 4-12: Subcellular localization of ADS4.2

Confocal microscope images of tobacco leaves transiently coexpressing *Pro35S:ADS4.2-GFP* (A) and ER marker *Pro:35S:HDEL-RFP* (B). C, Merged image of (A) and (B) showing that ADS4.2-GFP co-localized with ER marker. Bars, 10 μ m.

4.3.5 The biosynthesis pathway to cuticular alkenes shares enzymes with pathways forming other wax components

To place the desaturase function of ADS4.2 into context with the overall biosynthesis pathway leading to wax alkenes, we aimed to identify other enzymes acting either upstream or downstream of the desaturase. In particular, we tested in how far the alkene-forming pathway shared enzymes with the pathways leading to other wax components. To this end, Arabidopsis mutants each lacking

one of the known cuticular wax synthesis enzymes were grown, and the waxes covering their young rosette leaves were investigated by GC-MS in search of alkenes.

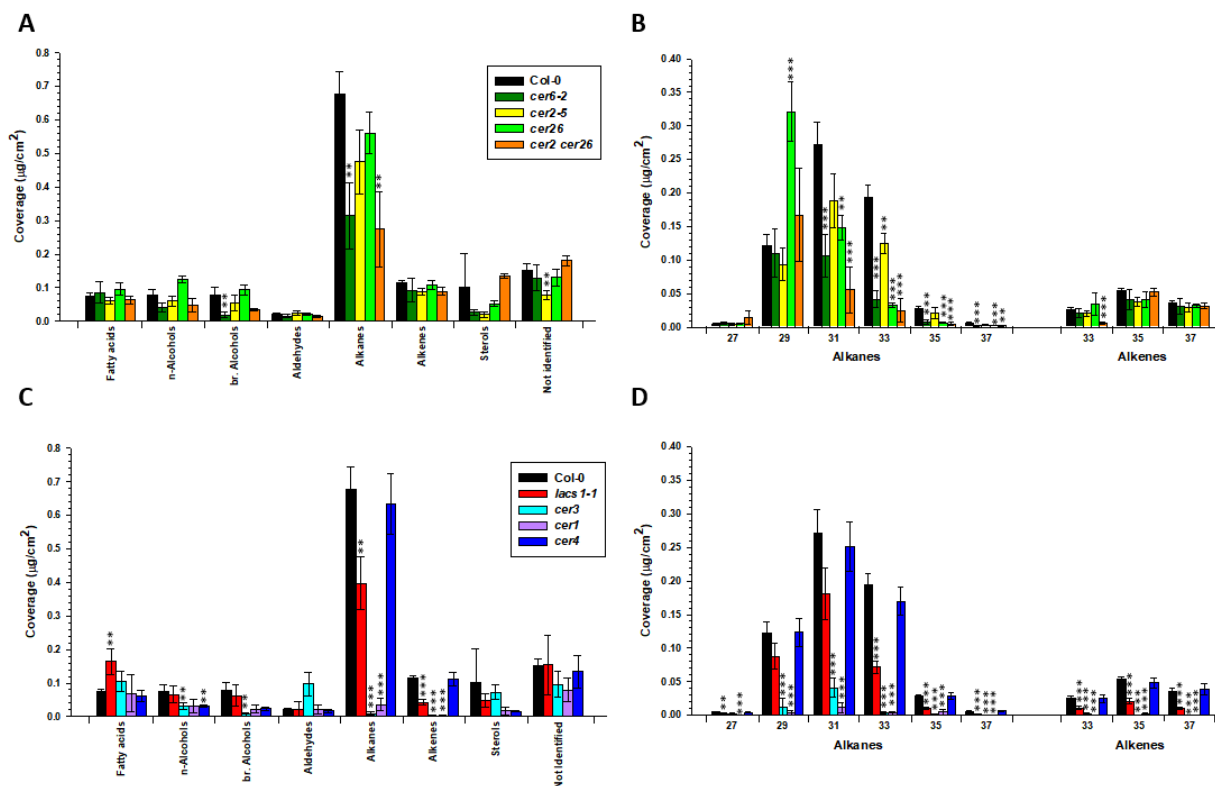


Figure 4-13: Coverages of characteristic alkenes in Arabidopsis mutants deficient in general wax synthesis genes

A) Compound class distribution in total wax mixtures on young leaves of Arabidopsis wild type (Col-0) and elongation-deficient mutants. B) Chain length distribution of alkanes and alkenes on young leaves of Arabidopsis wild type (Col-0) and elongation-deficient mutants. C) Compound class distribution in total wax mixtures on young leaves of Arabidopsis wild type (Col-0) and head group modification-deficient mutants. D) Chain length distribution of alkanes on young leaves of Arabidopsis wild type (Col-0) and head group modification-deficient mutants. Young leaves of 2-week-old plants were used for wax analysis. All data represent the mean of four or five independent biological samples, and error bars show standard deviations. Asterisks indicate discovery of statistically significant differences of coverage between wild type and each mutant based on Student's *t*-test (* $P < 0.05$, ** $P < 0.01$, *** $P < 0.001$).

To assess early steps on the wax biosynthesis pathway, we analyzed the waxes from mutants compromised in key enzymes for elongation of acyl precursors up to C₃₄, including *cer6*, *cer2*, *cer26* single mutants and a *cer2 cer26* double mutant. All four lines had reduced overall wax coverages, mainly due to decreases in alkane amounts relative to wild type (Figure 4-13A; Table 4-6). The mutants had characteristic chain length distributions across all compound classes, where for example the alkanes in all four mutants showed substantial decreases of all homologs with more than 30 carbons (Figure 4-13B). In contrast, all of the mutant waxes contained alkenes in amounts similar to the wild type, with very similar chain length distributions (except for a decline of C₃₃ alkene in the *cer2 cer26* double mutant).

To assess the role of enzymes catalyzing late steps on the wax biosynthesis pathway, we analyzed mutants deficient in enzymes modifying wax precursor head groups. The leaf wax of the *cer4* mutant known to lack the key reductase of the alcohol-forming branch-pathway showed a decrease in n-alcohols and branched alcohols relative to wild type, but no change in the other compound classes (Figure 4-13C). In contrast, the *lacs1*, *cer3* and *cer1* mutants affecting the decarbonylation branch pathway of wax biosynthesis had substantially reduced levels of alkanes and, most importantly, also significantly decreased alkene coverages. In the *lacs1* leaf wax, the amounts of all major alkene homologs (C₃₃, C₃₅ and C₃₇) were reduced to less than half of those in wild type, while in the leaf waxes of *cer3* and *cer1* all three homologs were decreased to trace levels (Figure 4-13D).

Table 4-6: The wax analysis of Arabidopsis wax synthesis deficient mutants

Unit	$\mu\text{g}/\text{cm}^2$																								
Compound Classes	Chain length	Col-0	p-Value	cer6-2	p-Value	cer2-5	p-Value	cer26	p-Value	cer2 cer26	p-Value	lacc3-3	p-Value	cer3	p-Value	cer1	p-Value	cer4	p-Value						
Fatty acids	C24	0.0146 ± 0.0071	-	0.0356 ± 0.0134	-	0.0123 ± 0.0042	-	0.0186 ± 0.0042	-	0.0157 ± 0.0022	-	0.0456 ± 0.0182	-	0.0307 ± 0.0060	-	0.0172 ± 0.0146	-	0.0128 ± 0.0027	-						
	C26	0.0425 ± 0.0118	-	0.0334 ± 0.0129	-	0.0395 ± 0.0089	-	0.0508 ± 0.0107	-	0.0259 ± 0.0067	-	0.0514 ± 0.0198	-	0.0526 ± 0.0180	-	0.0302 ± 0.0290	-	0.0357 ± 0.0129	-						
	C28	0.0065 ± 0.0015	-	0.0062 ± 0.0028	-	0.0034 ± 0.0014	-	0.0126 ± 0.0044	-	0.0092 ± 0.0027	-	0.0208 ± 0.0072	-	0.0160 ± 0.0145	-	0.0054 ± 0.0050	-	0.0048 ± 0.0024	-						
	C30	0.0023 ± 0.0005	-	0.0027 ± 0.0009	-	0.0014 ± 0.0007	-	0.0067 ± 0.0019	9.08E-03	**	0.0030 ± 0.0012	-	0.0213 ± 0.0092	-	0.0057 ± 0.0043	-	0.0104 ± 0.0074	-	0.0024 ± 0.0010	-					
	C32	0.0081 ± 0.0009	-	0.0058 ± 0.0027	-	0.0040 ± 0.0011	3.45E-03	**	0.0071 ± 0.0017	-	0.0012 ± 0.0006	7.20E-05	***	0.0248 ± 0.0146	-	0.0011 ± 0.0006	1.40E-05	***	0.0053 ± 0.0037	-					
	C34	0.0000 ± 0.0000	-	0.0000 ± 0.0000	-	0.0000 ± 0.0000	-	0.0000 ± 0.0000	-	0.0008 ± 0.0001	5.00E-06	***	0.0000 ± 0.0000	-	0.0000 ± 0.0000	-	0.0000 ± 0.0000	-	0.0000 ± 0.0000	-					
Total		0.0740 ± 0.0092	-	0.0858 ± 0.0316	-	0.0606 ± 0.0095	-	0.0958 ± 0.0179	-	0.0630 ± 0.0124	-	0.1640 ± 0.0373	5.69E-03	**	0.1061 ± 0.0297	-	0.0685 ± 0.0551	-	0.0611 ± 0.0166	-					
Aldehydes	C24	0.0004 ± 0.0001	-	0.0005 ± 0.0003	-	0.0000 ± 0.0000	3.45E-03	**	0.0003 ± 0.0004	-	0.0000 ± 0.0000	3.45E-03	**	0.0009 ± 0.0006	-	0.0003 ± 0.0003	-	0.0003 ± 0.0001	-						
	C26	0.0036 ± 0.0005	-	0.0041 ± 0.0017	-	0.0065 ± 0.0011	6.83E-03	**	0.0042 ± 0.0011	-	0.0000 ± 0.0000	4.60E-05	***	0.0049 ± 0.0044	-	0.0015 ± 0.0005	1.99E-03	**	0.0018 ± 0.0010	-					
	C28	0.0046 ± 0.0016	-	0.0052 ± 0.0024	-	0.0060 ± 0.0023	-	0.0036 ± 0.0006	-	0.0044 ± 0.0007	-	0.0033 ± 0.0015	-	0.0018 ± 0.0008	-	0.0035 ± 0.0015	-	0.0026 ± 0.0005	-						
	C30	0.0055 ± 0.0017	-	0.0033 ± 0.0013	-	0.0053 ± 0.0012	-	0.0084 ± 0.0014	-	0.0070 ± 0.0009	-	0.0018 ± 0.0023	-	0.0021 ± 0.0043	-	0.0061 ± 0.0038	-	0.0031 ± 0.0010	-						
	C32	0.0040 ± 0.0013	-	0.0013 ± 0.0006	-	0.0046 ± 0.0017	-	0.0019 ± 0.0006	-	0.0017 ± 0.0004	-	0.0051 ± 0.0055	-	0.0004 ± 0.0001	2.75E-03	**	0.0085 ± 0.0056	-	0.0027 ± 0.0010	-					
	C34	0.0020 ± 0.0008	-	0.0008 ± 0.0005	-	0.0022 ± 0.0010	-	0.0017 ± 0.0010	-	0.0014 ± 0.0007	-	0.0050 ± 0.0081	-	0.0000 ± 0.0000	4.24E-03	**	0.0026 ± 0.0020	-	0.0017 ± 0.0010	-					
Total		0.0202 ± 0.0052	-	0.0152 ± 0.0056	-	0.0246 ± 0.0058	-	0.0201 ± 0.0038	-	0.0145 ± 0.0026	-	0.0210 ± 0.0222	-	0.0065 ± 0.0051	-	0.0229 ± 0.0128	-	0.0165 ± 0.0037	-						
Alkanes	C25	0.0023 ± 0.0011	-	0.0026 ± 0.0018	-	0.0016 ± 0.0004	-	0.0016 ± 0.0004	-	0.0000 ± 0.0000	-	0.0021 ± 0.0006	-	0.0021 ± 0.0005	-	0.0022 ± 0.0007	-	0.0018 ± 0.0003	-						
	C26	0.0018 ± 0.0001	-	0.0025 ± 0.0004	-	0.0037 ± 0.0010	-	0.0027 ± 0.0009	-	0.0000 ± 0.0000	1.00E-06	***	0.0026 ± 0.0012	-	0.0016 ± 0.0004	-	0.0012 ± 0.0006	-	0.0023 ± 0.0006	-					
	C27	0.0050 ± 0.0005	-	0.0062 ± 0.0018	-	0.0042 ± 0.0011	-	0.0056 ± 0.0007	-	0.0145 ± 0.0097	-	0.0023 ± 0.0009	3.56E-03	**	0.0016 ± 0.0017	-	0.0006 ± 0.0003	1.00E-05	***	0.0043 ± 0.0009	-				
	C28	0.0020 ± 0.0004	-	0.0026 ± 0.0008	-	0.0015 ± 0.0004	-	0.0028 ± 0.0011	-	0.0000 ± 0.0000	3.78E-04	***	0.0015 ± 0.0004	-	0.0018 ± 0.0020	-	0.0009 ± 0.0002	3.93E-03	***	0.0020 ± 0.0006	-				
	C29	0.1218 ± 0.0168	-	0.1103 ± 0.0362	-	0.0937 ± 0.0242	-	0.3214 ± 0.0444	4.63E-04	***	0.1675 ± 0.0690	-	0.0880 ± 0.0192	-	0.0113 ± 0.0133	6.60E-05	***	0.0036 ± 0.0030	1.20E-05	***	0.1236 ± 0.0205	-			
	C30	0.0102 ± 0.0029	-	0.0073 ± 0.0026	-	0.0076 ± 0.0020	-	0.0086 ± 0.0010	-	0.0055 ± 0.0014	-	0.0078 ± 0.0012	-	0.0014 ± 0.0014	2.65E-03	**	0.0010 ± 0.0005	1.27E-03	***	0.0103 ± 0.0016	-				
Alkanes	C31	0.2719 ± 0.0342	-	0.1063 ± 0.0325	6.40E-04	***	0.1882 ± 0.0404	-	0.1484 ± 0.0186	3.07E-03	**	0.0555 ± 0.0350	4.64E-04	***	0.1809 ± 0.0391	-	0.0407 ± 0.0142	2.00E-05	***	0.0119 ± 0.0076	9.00E-06	***	0.2154 ± 0.0370	-	
	C32	0.0217 ± 0.0025	-	0.0117 ± 0.0035	5.86E-03	**	0.0139 ± 0.0023	-	0.0160 ± 0.0040	-	0.0000 ± 0.0000	1.50E-05	***	0.0172 ± 0.0083	-	0.0207 ± 0.0077	-	0.0027 ± 0.0028	6.00E-05	***	0.0146 ± 0.0020	7.12E-03	**		
	C33	0.1936 ± 0.0175	-	0.0415 ± 0.0128	1.10E-05	***	0.1247 ± 0.0148	3.45E-03	**	0.0329 ± 0.0029	1.40E-05	***	0.0248 ± 0.0179	5.00E-05	***	0.0715 ± 0.0092	2.00E-05	***	0.0337 ± 0.0014	1.00E-06	***	0.1698 ± 0.0214	-		
	C34	0.0113 ± 0.0021	-	0.0121 ± 0.0038	-	0.0064 ± 0.0025	-	0.0120 ± 0.0039	-	0.0000 ± 0.0000	2.67E-04	***	0.0089 ± 0.0024	-	0.0102 ± 0.0023	-	0.0011 ± 0.0006	1.24E-04	***	0.0119 ± 0.0030	-				
	C35	0.0280 ± 0.0031	-	0.0075 ± 0.0027	8.00E-05	***	0.0216 ± 0.0086	-	0.0065 ± 0.0007	7.00E-05	***	0.0048 ± 0.0021	8.60E-05	***	0.0103 ± 0.0018	8.40E-05	***	0.0011 ± 0.0007	5.00E-06	***	0.0049 ± 0.0039	1.20E-04	***	0.0287 ± 0.0051	-
	C36	0.0009 ± 0.0002	-	0.0028 ± 0.0021	-	0.0045 ± 0.0013	3.81E-03	**	0.0012 ± 0.0006	-	0.0000 ± 0.0000	4.63E-04	***	0.0019 ± 0.0016	-	0.0006 ± 0.0003	-	0.0021 ± 0.0016	-	0.0075 ± 0.0017	3.53E-04	***			
Alkanes	C37	0.0060 ± 0.0009	-	0.0018 ± 0.0008	6.98E-04	***	0.0034 ± 0.0015	-	0.0020 ± 0.0002	6.41E-04	***	0.0019 ± 0.0006	1.15E-03	**	0.0022 ± 0.0004	4.40E-04	***	0.0000 ± 0.0000	1.40E-05	***	0.0000 ± 0.0000	1.40E-05	***	0.0065 ± 0.0013	-
	Total	0.6765 ± 0.0695	-	0.3154 ± 0.0984	1.62E-03	**	0.4749 ± 0.0264	-	0.5614 ± 0.0611	-	0.2745 ± 0.1127	2.47E-03	**	0.3973 ± 0.0789	3.06E-03	**	0.0969 ± 0.0357	9.00E-06	***	0.0356 ± 0.0191	4.00E-06	***	0.6347 ± 0.0910	-	
	C33	0.0258 ± 0.0029	-	0.0209 ± 0.0073	-	0.0206 ± 0.0040	-	0.0348 ± 0.0163	-	0.0058 ± 0.0021	1.49E-04	***	0.0107 ± 0.0023	2.84E-04	***	0.0026 ± 0.0019	1.40E-05	***	0.0004 ± 0.0004	5.00E-06	***	0.0246 ± 0.0056	-		
	C35	0.0543 ± 0.0036	-	0.0407 ± 0.0154	-	0.0372 ± 0.0069	-	0.0408 ± 0.0115	-	0.0521 ± 0.0061	-	0.0211 ± 0.0044	3.00E-05	***	0.0000 ± 0.0000	1.00E-06	***	0.0012 ± 0.0027	1.00E-06	***	0.0480 ± 0.0083	-			
	C37	0.0354 ± 0.0045	-	0.0311 ± 0.0117	-	0.0301 ± 0.0067	-	0.0324 ± 0.0028	-	0.0316 ± 0.0043	-	0.0105 ± 0.0017	6.50E-05	***	0.0000 ± 0.0000	6.00E-06	***	0.0000 ± 0.0000	6.00E-06	***	0.0389 ± 0.0089	-			
	Total	0.1155 ± 0.0063	-	0.0928 ± 0.0341	-	0.0879 ± 0.0088	-	0.1080 ± 0.0125	-	0.0896 ± 0.0106	-	0.0423 ± 0.0082	1.10E-05	***	0.0026 ± 0.0019	1.00E-06	***	0.0016 ± 0.0025	1.00E-06	***	0.1115 ± 0.0212	-			
n-Alcohols	C22	0.0006 ± 0.0003	-	0.0010 ± 0.0006	-	0.0002 ± 0.0001	-	0.0007 ± 0.0001	-	0.0016 ± 0.0006	-	0.0006 ± 0.0002	-	0.0026 ± 0.0007	3.45E-03	**	0.0005 ± 0.0003	-	0.0002 ± 0.0001	-					
	C24	0.0027 ± 0.0033	-	0.0023 ± 0.0025	-	0.0019 ± 0.0038	-	0.0050 ± 0.0021	-	0.0010 ± 0.0002	-	0.0020 ± 0.0020	-	0.0004 ± 0.0002	-	0.0055 ± 0.0043	-	0.0018 ± 0.0018	-						
	C26	0.0011 ± 0.0006	-	0.0029 ± 0.0019	-	0.0019 ± 0.0004	-	0.0031 ± 0.0005	6.30E-03	**	0.0044 ± 0.0032	-	0.0036 ± 0.0017	-	0.0029 ± 0.0020	-	0.0009 ± 0.0010	-	0.0006 ± 0.0004	-					
	C28	0.0090 ± 0.0022	-	0.0109 ± 0.0046	-	0.0101 ± 0.0043	-	0.0209 ± 0.0052	-	0.0141 ± 0.0060	-	0.0120 ± 0.0055	-	0.0137 ± 0.0052	-	0.0022 ± 0.0016	4.07E-03	**	0.0047 ± 0.0012	-					
	C30	0.0239 ± 0.0067	-	0.0130 ± 0.0038	-	0.0228 ± 0.0063	-	0.0737 ± 0.0044	8.40E-05	***	0.0183 ± 0.0082	-	0.0218 ± 0.0097	-	0.0046 ± 0.0016	2.34E-03	**	0.0104 ± 0.0067	-	0.0129 ± 0.0060	-				
	C32	0.0247 ± 0.0044	-	0.0079 ± 0.0027	1.04E-03	**	0.0159 ± 0.0054	-	0.0170 ± 0.0035	-	0.0070 ± 0.0018	1.49E-03	**	0.0183 ± 0.0070	-	0.0065 ± 0.0024	5.00E-04	***	0.0086 ± 0.0068	-	0.0072 ± 0.0048	3.01E-03	**		
br. Alcohols	C34	0.0145 ± 0.0022	-	0.0031 ± 0.0014	1.74E-04	***	0.0071 ± 0.0030	-	0.0033 ± 0.0006	4.16E-04	***	0.0017 ± 0.0009	2.39E-04	***	0.0072 ± 0.0035	-	0.0004 ± 0.0004	2.00E-05	***	0.0032 ± 0.0025	8.32E-04	***	0.0030 ± 0.0011	1.20E-04	***
	Total	0.0765 ± 0.0185	-	0.0411 ± 0.0128	-	0.0596 ± 0.0153	-	0.1237 ± 0.0100	-	0.0482 ± 0.0192	-	0.0656 ± 0.0258	-	0.0310 ± 0.0095	7.76E-03	**	0.0312 ± 0.0213	-	0.0303 ± 0.0034	4.36E-03	**				
	C30	0.0239 ± 0.0063	-	0.0118 ± 0.0044	-	0.0159 ± 0.0045	-	0.0317 ± 0.0042	-	0.0143 ± 0.0024	-	0.0214 ± 0.0097	-	0.0066 ± 0.0054	9.77E-03	**	0.0084 ± 0.0060	-	0.0057 ± 0.0032	3.45E-03	**				
	C32	0.0514 ± 0.0183	-	0.0056 ± 0.0040	4.46E-03	**	0.0380 ± 0.0178	-	0.0608 ± 0.0113	-	0.0164 ± 0.0017	-	0.0393 ± 0.0215	-	0.0014 ± 0.0006	2.74E-03	**	0.0114 ± 0.0076	-	0.0177 ± 0.0056	-				
	C34	0.0018 ± 0.0007	-	0.0009 ± 0.0012	-	0.0011 ± 0.0008	-	0.0011 ± 0.0002	-	0.0021 ± 0.0002	-	0.0018 ± 0.0013	-	0.0007 ± 0.0005	-	0.0006 ± 0.0004	-	0.0004 ± 0.0004	-						
	Total	0.0771 ± 0.0251	-	0.0183 ± 0.0082	7.12E-03	**	0.055																		

4.4 Discussion

Our findings first confirmed that the Arabidopsis leaf wax alkenes have chain lengths C₃₃-C₃₉, much longer than the alkenes of other species and also longer than most other Arabidopsis wax compounds. To identify the mechanisms underlying their formation, we identified the Arabidopsis desaturase ADS4.2 introducing the double bond into acyl chains en route to the alkene products, based on detailed analyses of two *ads4.2* mutant alleles and corresponding complementation lines. Finally, we determined (i) the substrate chain length preferences of ADS4.2, (ii) its position on the pathway leading to the alkene products, and (iii) its specific role in leaf wax alkene formation. These three major characteristics of the desaturase will be discussed in the following sections.

4.4.1 Substrate chain length preferences of the desaturase ADS4.2

In terms of ADS4.2 substrates, our results first shed light on the overall range of acyl chain lengths the desaturase is interacting with. In this context, it must be noted that the enzyme was localized to the ER, the subcellular compartment of plant cells known to accumulate VLC acyl-CoAs, and the desaturase thus potentially has access to acyls with 20 or more carbons *in planta*. Furthermore, expression of ADS4.2 in different yeast strains showed that ADS4.2 is active on a wide range of VLC substrates from C₂₂ to C₃₄ acyl-CoAs. Therefore, almost all the VLC acyls accessible to ADS4.2 in the Arabidopsis ER qualify as potential substrates for desaturation.

Two of our findings also provide evidence for the preferences of ADS4.2 among acyls chains of different lengths. Firstly, empty-vector control yeast contained only small amounts of unsaturated VLC fatty acyls, and in all three yeast backgrounds the unsaturated VLC acyl pools were dominated by 20:1 regardless of the chain length distribution of accompanying saturated lipids. Thus, for example yeast wild type contained substantially more 26:0 than 20:0, but more 20:1 than 26:1 acyls, matching previous literature reports (Oh et al., 1997; Dittrich et al., 1998). Taken

together, these findings confirm previous reports that the endogenous yeast elongases have relatively low activities on unsaturated fatty acyls (Oh et al., 1997). Therefore, it seems unlikely that ADS4.2, when expressed in yeast, first desaturates relatively short acyls that then get elongated to the major 32:1 and 34:1 products found in the yeast transgenics. Instead, it is plausible that the yeast elongases provide saturated acyl-CoA up to 34:0, which ADS4.2 then used as substrates for desaturation.

Secondly, the relative chain length distributions of unsaturated fatty acyl-CoA pools in the three yeast backgrounds can be interpreted. Expression of ADS4.2 dramatically changed the relative distributions of unsaturated acyl chains from corresponding controls, increasing the amounts of all unsaturated acyl groups longer than C₂₂ but not of C₂₀. Consequently, the ratios of unsaturated:saturated C₂₂ and longer acyl chains increased in the presence of ADS4.2, while those of C₂₀ remained constant. The ratios were most drastically increased for C₃₂ and C₃₄ (between controls and ADS4.2 expressors), even to values greater than one implying that the majority of available acyl precursors with these extreme chain lengths were captured and turned over by the desaturase. Thus, given competing fatty acyl substrates, ADS4.2 has highest activity on those acyl-CoAs with hydrocarbon chains longer than C₃₂.

All our yeast results show that, among all the VLC acyl substrates available to ADS4.2 in the *Arabidopsis* epidermis ER, the enzyme strongly prefers those with 32 or more carbons. This desaturase is, therefore, clearly distinguished from all other ADSs characterized to date, including *Arabidopsis* ADS2 mainly forming 24:1 and 26:1 acyl-CoAs for membrane and seed storage lipids (Smith et al., 2013), and ADS4/CER17 yielding 26:1-30:1 acyls en route to unsaturated cuticular wax alcohols (Yang et al., 2017).

4.4.2 Position of ADS4.2 on the biosynthetic pathway leading to alkenes

Our findings on the characteristics of ADS4.2 and the composition of the wax alkenes, taken together, have implications for the pathway leading to the final products. The wax alkenes we identified in the wax mixture on expanding *Arabidopsis* rosette leaves have molecular structures resembling those of the accompanying alkanes, with particularly long hydrocarbon chains C_{33} - C_{39} dominated by odd-numbered homologs. Due to these similarities between alkenes and alkanes, it seems very likely that the enzyme machinery forming both compounds is similar, comprising elongation and head group modification stages. The biosynthetic pathway leading to alkenes, thus, likely involves FAEs synthesizing sets of acyl-CoA precursors with even-numbered chain lengths C_{34} – C_{40} similar to those en route to alkanes (but saturated or unsaturated). Ultimately, these elongated acyls must be converted into alkenes by removal of the carboxyl head group, leading to products each with one carbon less than the acyls. However, prior to this report it was not clear at which point of the pathway, relative to elongation and head group modification, the double bond is introduced into the hydrocarbon chain.

Our results that ADS4.2 has highest activity on fatty acyl substrates with 32 or more carbons implies that, among the acyl-CoAs available in the ER *in planta*, the enzyme mostly desaturates acyl-CoAs that have already been elongated to their final length. Desaturation thus occurs between elongation and head group modification to alkenes, and reactions on the alkene formation pathway occurring upstream of ADS4.2 (i.e., providing its substrates) must all be accomplished by FAE-like enzymes, while those downstream of ADS4.2 must involve a carboxyl group cleavage by CER3/CER1-like enzymes.

In *Arabidopsis*, one CER3 and two CER1 homologs have been characterized to date. Among them, CER1-like1 can form alkanes with chain lengths ranging from C_{25} to C_{35} , but contributing

relatively little to the synthesis of alkanes longer than C₂₉. Therefore, it is unlikely that this enzyme can handle the longer intermediates formed by ADS4.2 en route to the C₃₃ to C₃₇ alkenes. In contrast, CER3 and CER1 were known to be involved in formation of alkanes up to C₃₅ (Bourdenx et al., 2011; Pascal et al., 2019), and our results further showed that they are also synthesizing C₃₇ alkane. The mutants lacking the CER3 or CER1 enzymes had drastically reduced levels of the wax alkenes, showing that conversion of the unsaturated acyl-CoA products of ADS4.2 into the final products relies on these two enzymes. The same enzymes removing the carboxyl groups to form alkanes therefore act on all acyl-CoAs, regardless of the presence of a double bond in the hydrocarbon backbone. All enzymes catalyzing steps downstream of ADS4.2 in the alkene pathway are thus known.

It had previously been reported that mutants lacking the elongase enzyme KCS16 had substantially reduced levels of C₃₅ and C₃₇ alkenes (as well as alkanes), showing that FAEs containing this KCS are supplying precursors for alkene formation (Hegebarth et al., 2017). KCS16 is involved in elongation of C₃₂₊ up to C₃₈₊ acyls, which we now identified as the immediate substrates of ADS4.2. Thus, the steps directly upstream of the desaturase are also catalyzed by known enzymes. In contrast, none of the mutants lacking enzymes involved in preceding elongation rounds (CER6, CER2 and CER26) showed strong alkene phenotypes, indicating that additional, functionally redundant FAEs may be involved in forming C_{<32} acyls en route to the alkenes. In this context, it is interesting to note that the majority of the alkenes likely accumulates on trichomes and early during rosette leaf development, so the elongation machinery supplying substrates to the desaturase may be restricted to certain time points and cell types. It seems plausible that a trichome-specific set of FAEs generates a pool of acyl-CoAs that then serve as substrates for further elongation by KCS16 (which is highly expressed in trichomes) towards formation of

alkanes or alkenes. At least one such trichome-specific FAE may contain KCS5, an enzyme not fully characterized but thought to be similar to CER6 except for its trichome-specific expression (Haslam et al., 2015; Hegebarth et al., 2016; Busta et al., 2017).

Finally, the *Arabidopsis* mutant deficient in LACS1 also had strongly reduced levels of alkenes, implying that this enzyme too is involved in supplying precursors for alkene formation. However, the role of LACS1 in overall wax biosynthesis is somewhat enigmatic, since this enzyme is thought to catalyze the transformation of free fatty acids into acyl-CoA esters even though all known wax biosynthesis pathway intermediates already are CoA esters (Lü et al., 2009; Zhao et al., 2010; Bernard et al., 2012). Interestingly, LACS1 has higher activity on longer VLC acyls, pointing to its association with late elongation rounds (Lü et al., 2009). Our new findings on ADS4.2 and the alkene biosynthesis pathway now underscore this hypothesis, leading us to speculate that LACS1 may help maintain levels of CoA-activated acyls at least around FAEs containing KCS16 (but maybe also other KCSs). It will be interesting to determine the exact role of LACS1, which may be to (re-)activate either those substrates heading into the final rounds of elongation or those being transferred from elongation to desaturation and head group modification towards alkenes.

4.4.3 Role of ADS4.2 in formation of *Arabidopsis* leaf wax alkenes

Based on the biochemical characteristics of ADS4.2 and the alkene pathway, the overall role of this desaturase in the formation of the alkene products accumulating in the leaf wax can finally be assessed. As discussed above, our yeast results lead us to conclude that ADS4.2 desaturates fatty acyls after they have been elongated to their final chain lengths. Consequently, the *in planta* substrates of the enzyme are C₃₄-C₃₈ acyl-CoAs (towards formation of the C₃₃-C₃₇ alkene products), and in the epidermal ER the desaturase must compete for these substrates with several other enzymes such as the CER3/CER1 complex converting the saturated acyl-CoAs into alkanes.

However, we found that the same CER3/CER1 enzymes are also involved in forming alkenes from corresponding unsaturated acyl-CoAs, likely with similar activities as for saturated acyls. Therefore, the proportions of acyl substrate converted either directly to alkanes or via desaturation to alkenes can be taken as a proxy for the affinity of ADS4.2 for acyls with different chain lengths. Respective alkene:alkane ratios indicated that the desaturase turns over approximately 10% of the C₃₄ acyl-CoA available, more than 50% of the C₃₆, and nearly 75% of the C₃₈ substrate pools (Figure 4-2D). Our plant wax findings thus parallel the chain length specificity trends seen upon expression of ADS4.2 in *INVSUR4#* mutant yeast, together confirming that ADS4.2 is the key desaturase for formation of the 7-alkenes *in planta*. Overall, the elongation-desaturation-head group modification pathway leading to the characteristic 7-alkenes in Arabidopsis leaf wax is very different from the desaturation-elongation-head group modification pathways described before for wax alkene formation in other species.

The regio-specificity of ADS4.2 can be further assessed in the context of the protein tertiary structure. Since plant ADSs share relatively high sequence similarities with membrane-bound desaturases of other eukaryotes (Figure 4-14A), the three-dimensional structure of ADS4.2 can be modeled with fairly high confidence based on previously crystallized human or mouse homologs (Figure 4-14 B-D). The predicted ADS4.2 structure features three histidine clusters similar to those coordinating the two metal ion co-factors in the reference crystal structures (Bai et al., 2015), with almost identical spatial arrangement (Figure 4-14B,E). Site-directed mutagenesis of one histidine in each cluster of ADS4.2 (H77A, H114A, H246A) abolished the desaturase activity (Figure 4-15), confirming the functional importance of all three histidine clusters similar to those of comparable desaturases (Shanklin et al., 1994).

Since the active site of the enzyme is thus clearly defined, the substrate-binding cavities surrounding it can be inspected. The mouse and human desaturases have a hydrophobic tunnel extending from the active-site pocket and lined by a bundle of α -helices that also serve to anchor the protein in the ER membrane (Bai et al., 2015; Wang et al., 2015a). This tunnel accommodates the ω -tail of the acyl substrate, and the distance from the active site to the end of the tunnel hence determines the ω -regio-specificity of the desaturase. Most hydrophobic amino acids facing the tunnel surface are conserved between the mammalian ADSs and ADS4.2 (Figure 4-14A), and the tunnel is thus also well-defined in the (predicted) structure of the Arabidopsis desaturase (Figure 4-14C). However, ADS4.2 has a bulky phenylalanine (Figure 4-14A red arrow; Figure 4-14C) replacing the glycine residue (G291 in MsSCD1) near the bottom of the tunnel (formed by A292 in MsSCD1) of the mouse and human protein structures (Bai et al., 2015; Wang et al., 2015a). We predict that the phenylalanine side chain may block the tunnel, making it slightly shorter than those of the mammalian desaturases and explaining the ω -7 regio-specificity of the plant protein versus the ω -9 specificity of its mammalian counterparts (Figure 4-14D).

The mouse and human desaturases have a second tunnel connecting the active-site cavity to the surface of the proteins, and its length further determines the distance between the site of unsaturation and the Δ -end (carboxyl end) of the substrate along with the overall substrate chain length the enzymes can accept. However, the hydrophobic amino acids lining this tunnel are not well conserved in ADS4.2, and the position and length of this tunnel therefore cannot be predicted based on homology-based modelling alone. Further experiments aiming to co-crystallize ADS4.2 with VLC acyl-CoA (ideally C₃₄) are required to unravel the structural basis for the extreme substrate chain length preference of this enzyme.

A	ADS4.2MCDPIREDGSSNKRGAVS.KEKRP..YIHREWSWAIIRAITVINV.HFLCLLAPENYKWEALREGFVLVYALTSS	71
	ADS4MCDPTRDDGSSRSRVSTMQKRA..YFQRCWPLVIVVRASVVIV.HFLCLLAPENFKWEALREGVLVLFALTTS	72
	ADS1	MSLSASEKEENNKKMADKAEMGRKR..AMWERKWKRLIVKAFASLFV.HFLCLLAPENFTWFALRVALIVYTVGGIG	77
	ADS2	MSVTSTVEENHQKNPSTFAAVEEKKRRRWVWDRRWRRLYVKFASFTV.HSLALLAPFYFTWSALWVTFLEYTIGGIG	79
	ADS1.2MGDTTKDDGSSQSKAVR.GEKRA..FFFRKWTIRIARASAVGAV.HLLOLLAPENYKWEALREGVILAVTSS	71
	ADS1.3MSETTKDDGSSQKKSVR.KEKRA..YVLRKWTQFTVGRASTVGTV.HLLOLLAPENYKWEAFREGIILAILTNC	71
	ADS1.4MGDKNKDDSSSQSKAVR.KEKRA..FLFRKWTRVIVMRVSAVGAV.HLLOLLAPENYTWEAFRAAMVGISTNIS	71
	<i>S. cerevisiae</i> OLE1	NIDRLLEKDNCEKEEAKTKIHISEQPTLNNWHQHNLNLMVLVCGMPMIGWYFASGKVPLHINVFLESVFYAVGGVS	80
	<i>M. musculus</i> SCD1	VFLHLEEDIRFEMKEELIHPTYQDEEGPPPKLEYVWRNIILMVLHLHGGI.YGITLVP..SCKIYTCLEGFYYMTSAIG	77
	<i>M. musculus</i> SCD3	VFLYLEEDIRFEMKEELIYPTYQDEEGPPPKLEYVWRNIILMALIHVGAI.YGITLVP..SCKIYTCLEAFVYVVISIEG	77
	<i>H. sapiens</i> SCD1	MELYLEDIRFEDIKDIYPTYKYDKEGSPKVEYVWRNIILMSLIHLGAI.YGITLIP..TCKEYTWLGVYFYVFSALIG	77
	ADS4.2	ITFSYHRNLHRSFKLPKWLEYPLAYFAVFLQGEPLDWVSIHREHHQFTDSDRCPHSPIEGFWFSHVWVICDTRY.IKY	150
	ADS4	ITFSYHRNLHRSFKLPKWLEYPWASAVFALQGEPLDWVSIHREHHQFTDSDRCPHSPKEGLFESHIIWIFDTQY.IKY	151
	ADS1	ITVSYHRNLHRSFKVPKWLEYFFAYCGLLAIQGEPIIDVSTHRYHHQFTDSDRCPHSPNEGEWFSHLIWLFDITGY.LVE	156
	ADS2	ITVSYHRNLHRSFKVPKWLEYLLAYCALLAIQGEPIIDVSTHRYHHQFTDSERCPHSPKEGFWFSHLIWIYDSAY.LVS	158
	ADS1.2	ITFSYHRNLTHRSFKLPKWLEYPFAYSALFALQGHPIIDVSTHREHHQFTDSDRCPHSPIEGFWFSHVWIFDITSY.IRE	150
	ADS1.3	ITFSYHRNLTHRSFKLPKWLEYPFAYSALLALQGEPIIDVSIHREHHQFTDSDRCPHSPIEGFWFSHVWIFDITDY.IRE	150
	ADS1.4	ITFSYHRNLTHRSFKLPKWLEYPFAYSALFALQGHPIIDVSTHREHHQFTDSDRCPHSPIEGFWFSHVWIFDITSY.IRE	150
	<i>S. cerevisiae</i> OLE1	ITAGVHRLWSHRSYSAHWPLRLFYAIFGCASVEGSAKWGHSRHIRHYITDITLRFYDARRGWSHMGWMLLKP..P	157
	<i>M. musculus</i> SCD1	ITAGVHRLWSHRTYARLEIRIFLIANTMAFQNLVVEWARDHRAHKEFSETHALCPHNSRRGFEFSHVGLLVYKHFAVK	157
	<i>M. musculus</i> SCD3	ICAGVHRLWSHRTYARLEIRIFLIANTMAFQNLVVEWARDHRAHKEFSETHALCPHNSRRGFEFSHVGLLVYKHFAVK	157
	<i>H. sapiens</i> SCD1	ITAGVHRLWSHRSYARLEIRIFLIANTMAFQNLVVEWARDHRAHKEFSETHALCPHNSRRGFEFSHVGLLVYKHFAVK	157
	ADS4.2	KCGGRNVMDLRQQWFYFELRMTIGFHVLMFWTVI.....YLYGG..LFYLTCCGGVGVGIGVHYHVTWVNSACHIWGSR	222
	ADS4	KCGGRNVMDLRQQWFYFELRRTIAVHILMEWTII.....YLYGG..LFYLTCCGGVGIGIFIGVHYHVTWVNSACHIWGSR	223
	ADS1	KCGRRINVBDLRQWYYRBLQRTVLYHILTEGFLI.....YFEGG..LSFLTWMGIGVAMEHHVTCILNSLCHWVGSR	228
	ADS2	KCGRRANVEDLRQWFYFELCKTVLFHILIGGFFI.....FYLG..MSFVTWGMVGGALEVHVTCILNSLCHWVGSR	230
	ADS1.2	KCGGRNVMDLRQQWFYFELRNTIGIHILTFWTLV.....YLVGG..LFYLTCCGVVGGTIGYNGTWVNSACHIWGSR	222
	ADS1.3	KCGGRNVMDLRQQWFYFELKTLVLIHIIAEWTLI.....YLVGG..LFYLTWTVGFGVIGYHGTWVNSACHICCGSQ	222
	ADS1.4	KCGGRNVMDLRQQWFYFELCNTIGIHILTFEWTLV.....YLVGG..LFYLTWSVGVGGAIGYHATWVNSACHIWGSR	222
	<i>S. cerevisiae</i> OLE1	KYKARADITDMDTITIRFQHRHYIILMLLAFVIPTLIGYFEND.YMGGLIYAGFIRFVFIQCATECINSIAHYIGQ	236
	<i>M. musculus</i> SCD1	EKGKIDMSDLIAEKIVMEQRYYKFGILLMCFILPTLVFWYCWGETFVNSLFVSTFLRVTLVINATWVNSACHLYGYR	237
	<i>M. musculus</i> SCD3	EKGKIDMSDLIAEKIVMEQRYYKFGILLMCFILPTLVFWYCWGETFVNSLFVSTFLRVTLVINATWVNSACHLYGYR	237
	<i>H. sapiens</i> SCD1	EKGSTIDLSDLIAEKIVMEQRYYKFGILLMCFILPTLVFWYCWGETFVNSLFVSTFLRVTLVINATWVNSACHLYGYR	237
	ADS4.2	SWTKTITSRNWWLSIFFTMGESWNNHHAFAESSARQGLEWQIDITWYLIRLFEVIGIADVK.LPSEIQKQKIALT	298
	ADS4	SWNTKITSRNWWLSIFFTMGESWNNHHAFAESSARQGLEWQIDITWYLIRLFEVIGIADVK.LPSEIQKQKMAIV	299
	ADS1	TWKTNTITSRNWWLSVFSFGESWNNHHAFAESSARQGLEWQIDISWYINRFEIIGIADVK.LPSESQRRRMAMV	304
	ADS2	TWKTNTITSRNWWLSVFSFGESWNNHHAFAESSARQGLEWQIDISWYINRFEIIGIADVK.VPTEAQRRRMAIV	306
	ADS1.2	AWNTKITSRNIIWLGFFTMGESWNNHHAFAESARHGLEWYQVDITWYLICFFCAGIADVK.LPTDAQKRKIAFA	298
	ADS1.3	AWQNTITSRNWWIALLTMGESWNNHHAFAETSARHGLEWYQLDITWYLWFFCAGIADVK.LPTDAQKRKMAIR	298
	ADS1.4	AWNTKITSRNIIWLGFFTMGESWNNHHAFAESARHGLEWYQVDITWYLWFFCQVIGIADVK.LPTDAQKRKMSIA	298
	<i>S. cerevisiae</i> OLE1	PFDDRRTPRDNIITAIVTFGBGYHNFHEFFTDYRNAIKWYQYDFTKVITYLTSIVGLADLKFKFSQNAIEEALIQQ	313
	<i>M. musculus</i> SCD1	PYDKNIQSRNIIIVSISGAVGGEFHNHYHTFFEDYSASEYRWHINFTTFEFDCAAAIGIADRKVKSKATVIARIKRT	314
	<i>M. musculus</i> SCD3	PYDKNIDBRQNALVSISGSGGGEFHNHYHAFYDYSASEYRWHINFTTFEFDCAAAIGIADRKRVSKATVIARIKRT	314
	<i>H. sapiens</i> SCD1	PYDKNISPRENIIIVSISGAVGGEFHNHYHAFYDYSASEYRWHINFTTFEFDCAAAIGIADRKVKSKATVIARIKRT	314

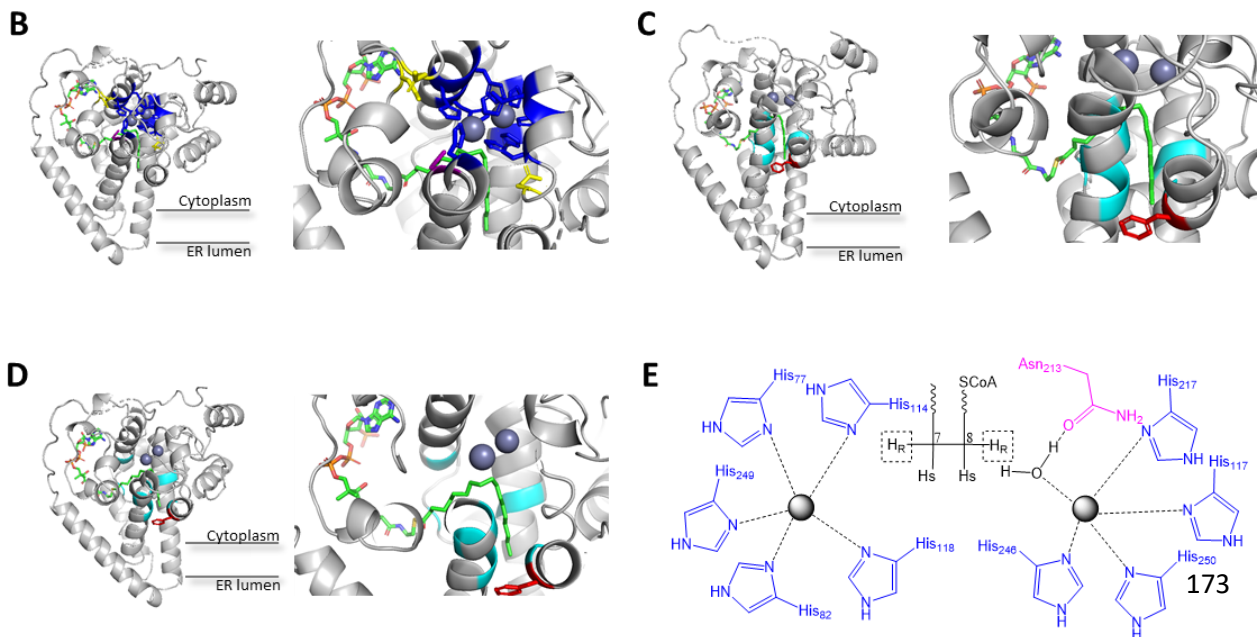


Figure 4-14: Structure analysis of ADS4.2 in comparison with other integral membrane desaturases

A) Sequence alignment of Arabidopsis ADS family members with other integral membrane desaturases. For sequences from yeast, mouse and human, only the region aligning to Arabidopsis ADS family members is included. The predicted transmembrane regions in ADS family members are underlined. The conserved Histidine clusters that coordinate the dimetal center are marked by red asterisks. The Asn coordinating a water molecule in the dimetal unit is labeled by a blue asterisk. The carboxylates bridge ligands in the secondary coordination of the dimetal center are marked by blue triangles. Acyl-chain binding sites are marked by black triangles. The acyl-CoA binding site in human and mouse SCDs are highlighted yellow. W258 in mammalian MsSCD1 forming a hydrogen bond with the acyl oxygen is highlighted blue. The Y104 and A108 in MsSCD1 reported to cap the substrate tunnel at the Δ -end of the acyl are marked by blue arrows. The Phe close to the ω -end of the acyl substrate is labeled by a red arrow. (B-D) ADS4.2 tertiary structure predicted based on the crystal structure of MsSCD1 (4YMK). The MsSCD1 substrate ω -9 16:1 fatty acyl-CoA is shown in green to illustrate the predicted protein-substrate interaction in ADS4.2; two horizontal lines depict the ER membrane to indicate the protein regions embedded in the bilayer and exposed to the cytoplasm or ER lumen. B) Overview and close-up view of the dimetal catalytic center. The gray balls represent the metal ions, the nine conserved histidine residues are shown in blue, the Asn residue in purple and the three carboxylate donors in yellow. C) Overview and close-up view of the ω -end of the substrate tunnel. D) Overview and close-up view of the Δ -end of the substrate tunnel. The conserved amino acid residues surrounding the ω -end of the acyl are shown in light blue and the Phe close to the end of the acyl tunnel is highlighted in red. E) 2D view of the ADS4.2 dimetal center. Protons HR are abstracted during desaturation to form a cis double bond at the ω -7 position of the acyl chain.

Our chemical analyses revealed the presence of several series of alkene regio-isomers, beside the dominant 7-alkenes formed by ADS4.2. Neither our yeast expression experiments nor the Arabidopsis mutant analyses provided evidence that these other alkene isomers might be formed by a side-activity of ADS4.2 (that would reflect limited product regio-specificity). It therefore appears likely that further desaturases, and possibly also specialized elongation systems, may be involved in the formation of the other alkene isomers found in Arabidopsis leaf wax, however their exact nature can only be speculated at this point. The second-most abundant series of alkenes, the 9-alkenes, could be either formed by an ADS enzyme similar to ADS4.2 but with ω -9 specificity,

or by elongation of plastidial Δ -9 (ω -9) 18:1 precursors similar to poplar. The former possibility seems unlikely, since we did not observe 9-alkene wax phenotypes for any of the ADS mutants we screened in this study, however it cannot be ruled out that several of the ADS enzymes have overlapping activities. The other minor series of isomers might also be formed by ADSs other than ADS4.2, and ADS1.3 and ADS4 are interesting candidates for this due to their relatively high expression in young rosette leaves and regio-specificities (Smith et al., 2013).

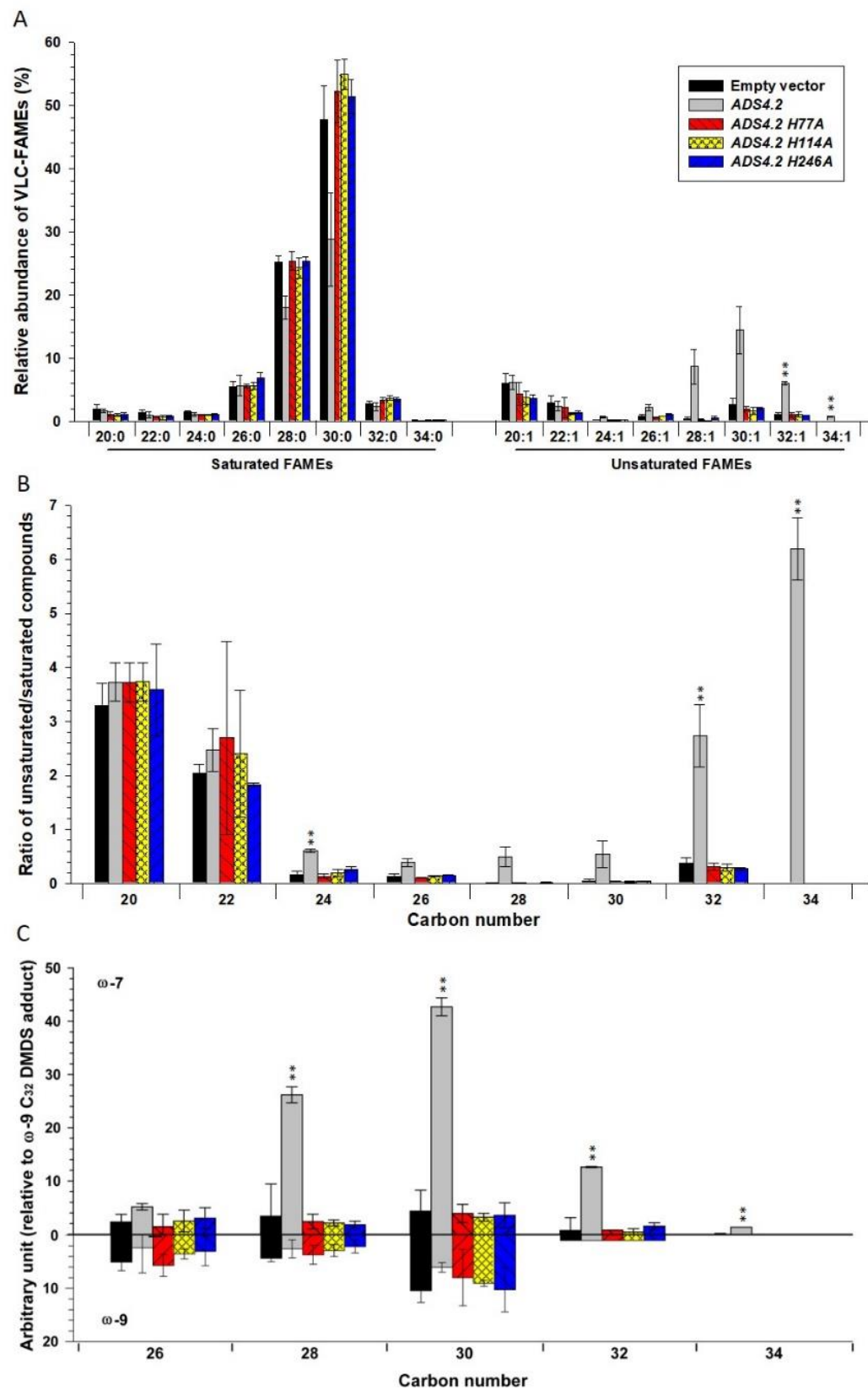


Figure 4-15: Activity of ADS4.2 histidine mutants

One histidine each in the three histidine clusters was mutated to alanine (H77A, H114A, H246A) and expressed in the yeast *INVSUR4#* mutant. A) Chain length distribution of saturated and unsaturated VLC FAMES of yeast expressing empty vector, native *ADS4.2* or one of the three *ADS4.2* mutant forms. B) Ratios of unsaturated FAME to the corresponding saturated FAME for each chain length in the five yeast lines. C) Chain length distributions of ω -7 and ω -9 monounsaturated FAMES in the five yeast lines. All data represent means of three independent yeast transformants, and error bars show standard deviations. All experiments were independently repeated twice with similar results. Asterisks indicate discovery of significant differences of coverage between control and yeast expressing each different *ADS4.2* based on Student's *t*-test (* $P < 0.05$, ** $P < 0.01$, *** $P < 0.001$).

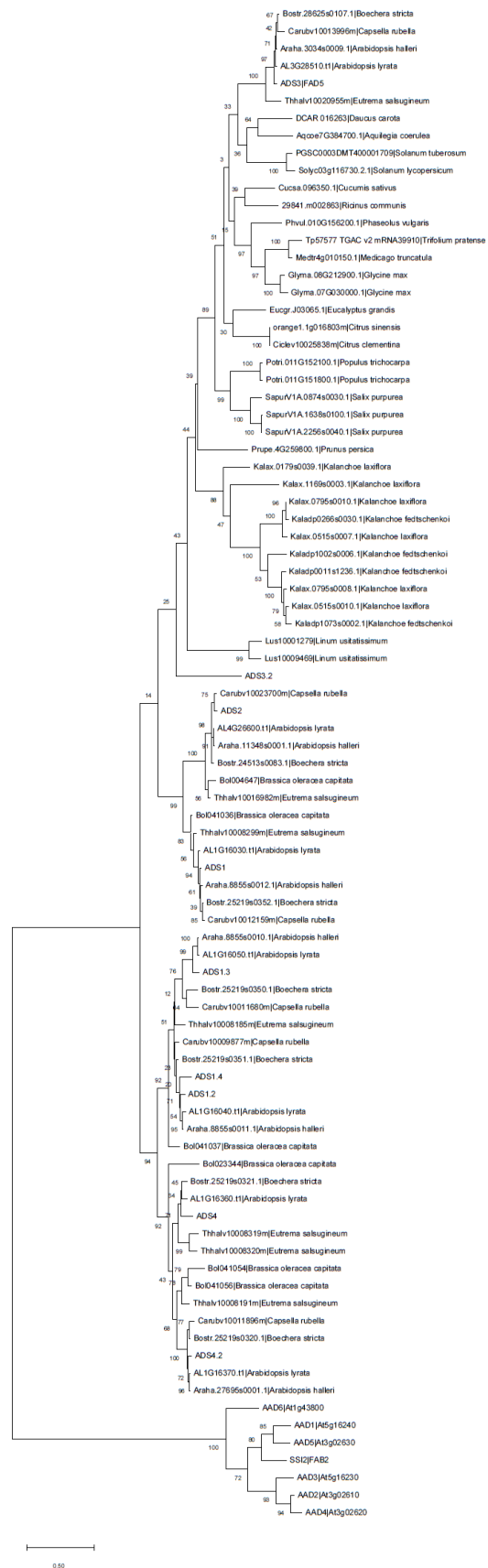
In this context, it should be noted that ADS 4.2 has relatively high primary sequence similarity with ADS4 as well as ADS1.2, 1.3 and 1.4 (Smith et al., 2013). Further sequence homology searches and phylogenetic analyses showed that the thus defined cluster of ADS proteins is shared by other Brassicaceae, but not by angiosperms in other families (Figure 4-16). Therefore, the pathway leading to wax alkenes is likely widespread in the Brassicaceae, but may be lacking in other clades. However, this analysis is severely limited by the number and family coverage of genomes sequenced to date, and future studies will have to explore in how far wax alkenes outside the Brassicaceae are formed by similar or different pathways. The scarce previous reports on double bond positions in wax alkenes and the underlying biochemistry of other angiosperms (including dicots and monocots) suggest that convergent pathways may use unsaturated plastidial fatty acids for elongation towards wax alkenes (Schlüter et al., 2011; Sedeek et al., 2016; Gonzales-Vigil et al., 2017).

Overall, we found that ADS4.2 acts as the key enzyme for formation of Arabidopsis wax alkenes with very characteristic chain lengths and double bond positions. This, together with the observation that both the enzyme and the alkene products are enriched in trichomes early on during

rosette leaf development, suggests that this desaturase is dedicated to forming these wax products mainly for trichome surface wax. It seems likely that the presence of these alkenes affects the physical properties of the cuticular wax mixtures, and that they, thus, may perform special ecophysiological roles even at relatively low concentrations. We hypothesize that trichomes, as single epidermal cells with high surface-to-volume ratios protruding from the leaf plane, may have special biomechanical and physiological requirements for wax sealing them against surface transpiration. The characteristic alkenes present in their cuticular waxes might influence the texture and fluidity (as a function of temperature) of their surface coating, and thus their barrier function (Small, 1984). It should also be noted that the alkenes in the trichomes and, to a lesser extent in epidermal pavement cells, co-occur with alkanes and likely aggregate with them on a molecular level. The physical properties of the mixture as well as its biological roles will depend on the chain length distributions of both compound classes, and we found that alkenes are dominated by C₃₅ and C₃₇ while the alkane series peaks around C₂₉-C₃₃. Our study revealed that this characteristic offset in chain length profiles between the closely related compound classes is due mainly to the characteristic substrate specificity of ADS4.2.

Figure 4-16: Phylogenetic analysis of protein sequences homologous to ADS4.2

ADS4.2-like protein sequences were retrieved from the Phytozome database (v12.1.5), aligned using the MUSCLE algorithm, and visualized in a phylogenetic tree by MEGA10.0 using the Maximum Likelihood method. Species names are indicated following each sequence ID.



Chapter 5: Major findings and future directions

5.1 Major findings

My PhD studies focused on both the ubiquitous and specialty wax components in crop species as well as *Arabidopsis*. This required clarification of the chemical structures of specialty and minor wax components as well as their homolog and isomer distributions. The knowledge of their chemical structures enabled further identification of non-canonical enzymes involved in wax biosynthesis, as well as clarification of these enzymes' biochemical function. In section 5.1.1 and 5.1.2, the work on ubiquitous wax components VLC alkanes and the specialty wax components β -diketones formation in crop species are summarized. In section 5.1.3, the findings on specialty wax components monounsaturated alkenes in *Arabidopsis* are discussed.

5.1.1 The alkane biosynthesis in bread wheat

In my first project, I aimed to understand wax VLC alkane biosynthesis in bread wheat and the potential roles of VLC alkanes in wheat development and adaptation. Here I summarize the major findings from this project (chapter 2).

5.1.1.1 The alkane profile in bread wheat

In this work, the alkane profiles from different tissues of bread wheat cv W87 have been investigated. The wax coverage of wheat leaf increased from vegetative stage to reproductive stage. Although primary alcohols are the predominant wax components in juvenile plants, alkanes and β -diketones are the major factors that drove the steady increase of cuticular wax coverage from juvenile to adult plants, especially in reproductive organ, the spikes and the major photosynthetic organs, the flag leaves. These findings match previous research showing that several wheat cultivars, despite otherwise different wax phenotypes, had alkane coverages

increasing steadily during wheat growth (Wang et al., 2015c). These results together indicate the importance of VLC alkanes in bread wheat growth and reproduction. The increased alkane coverages were accompanied by variations in chain length distributions within alkane compound class in different organs: the young leaf blades were covered by relatively longer alkanes with C₃₃ homolog predominant, while flag leaf blades and sheaths have similar alkane homolog profiles which followed approximately normal distribution and were dominated by the C₂₉ homolog. The spikes had the alkanes dominated by both C₂₉ and C₃₁ homologs. These results suggested differences of elongation and alkane-forming machineries were present in various wheat organs.

5.1.1.2 Characterization of *TaCER1-1A* in alkane biosynthesis in bread wheat

One of the core enzymes involved in alkane biosynthesis in bread wheat has been characterized in this study. The wheat *CER1* homologs analysis, combined with transcriptome analysis and wax chemical profiling from different organs enabled the identification of potential genes involved in alkane formation from the redundant hexaploid bread wheat genome, leading us to directly target *TaCER1-1A*.

In the following research, the biochemical function of *TaCER1-1A* was investigated. The difficulties in wheat transformation made it impossible to obtain the loss-of-function mutants or overexpression wheat lines easily, thus three other systems were used to characterize the function of *TaCER1-1A*. The wheat nullisomic-tetrasomic substitution line system is our first choice since it was the only system available to test the loss-of-function mutants in wheat quickly. The flag leaf blades wax from N1AT1B lines were analyzed. The reduced coverage of alkanes, mainly C₂₉ to C₃₃ homologs, but no differences in other wax compositions, suggested there was a locus (or loci) on chromosome 1A that strongly contributed to alkane formation. In the following

functional characterization, *TaCER1-1A* was heterologously expressed in Arabidopsis wild-type and *cer1* mutant plants. The enhanced accumulation of C₂₇ to C₃₅ alkanes in wild-type overexpression plants and C₂₉ to C₃₅ alkanes in *cer1* complementation plants suggested the function of *TaCER1-1A* in VLC alkane formation. The over accumulation of iso-alkanes in wild-type Arabidopsis overexpression lines further supported its function on iso-acyl precursors. Lastly, rice heterologous expression was used to further expand the knowledge of *TaCER1-1A*. The accumulation of alkanes ranging from C₂₅ to C₃₃ in rice overexpression lines again confirmed *TaCER1-1A* in VLC alkane formation with relatively broad substrate spectrum.

5.1.1.3 Alkane coverage and plant drought resistance

The correlation between alkane coverage and plant drought resistance is investigated in this study. The cuticle properties of rice and Arabidopsis with increased alkane coverage were tested in water loss assay and chlorophyll leaching assay. The lower water loss rates and reduced chlorophyll leaching rates of *TaCER1-1A* overexpression plants than wild-type plants suggested less permeable cuticles were present on plants with increased alkane coverage.

To directly test the relationship between wheat drought response and cuticular alkane coverage, wheat spikes, the organs that contained the highest proportion of alkanes were used in the following analysis. Three wheat cultivars with different wax characteristics all showed increased alkane coverage than the corresponding control after drought treatment, indicating the dynamic regulation and importance of alkane production in wheat drought response. Moreover, the upregulation of *TaCER1-1A* was detected in all the cultivars after drought response, indicating the contribution of *TaCER1-1A* to alkane production in bread wheat.

5.1.2 The β -diketone biosynthesis in barley

β -diketones are one of the major wax compound classes in barley and wheat at their reproductive stages. Although the gene cluster involved in β -diketone formation has been identified previously (Hen-Avivi et al., 2016; Schneider et al., 2016), the synthesis mechanisms and the biochemical function of each enzyme are still unclear. In the second project I aimed to comprehensively profile products from the β -diketone-forming pathway, analyze the biochemical functions of the core enzymes encoded by genes within the metabolic gene cluster and further test a revised model for the β -diketone-forming pathway in barley.

5.1.2.1 The biochemical function of DMH and DMP

The β -diketone-forming pathway has long been proposed based on the research in wheat and barley. In my research, three pieces of evidence have been provided to demonstrate that cuticular wax β -diketones are unlikely to be synthesized through the previously proposed direct sequential elongation (von Wettstein-Knowles, 2017). First, the novel even-carbon-numbered β -diketone isomers have been identified. The chemical structures of these isomers conflict with the C_2 -unit elongation rule of fatty acyl chain biosynthesis. Second, the isotope profiling of purified wax component reveals that the ^{13}C isotope abundance of C_{31} β -diketone is much higher than C_{31} alkane and does not follow the linear regression model built on 2-alkanol esters, 1-alkanol esters, and alkanes. Third, the barley wax FAE complex component mutant *cer6*, which showed deficiency on aliphatic wax elongation beyond C_{24} were used to investigate the β -diketone formation. The mutant showed no significant differences on any β -diketone related wax components compared to wild type, indicating at least the aliphatic wax elongation complex associated with CER6 does not participate in β -diketone formation.

We thus analyzed the biochemical function of DMH, the first enzyme on β -diketone formation pathway in both *E. coli* and yeast. These two systems possess different fatty acid *de novo* synthesis machineries. *E. coli* have type II FAS complexes, which are similar to plants, that contain four separable monofunctional catalytic elements, locate in the stroma of plastids. In contrast, yeast use type I FAS complexes that possess cytosol-located multifunctional proteins (Harwood and Murphy, 2005). The lipid profiling of *DMH* expressing *E. coli* showed an additional production of 2-ketones and 2-alkanols that were not detected in control, and enhanced accumulation of 3-hydroxy fatty acids, indicating that DMH functioned as a hydrolase or thioesterase that generate mainly 3-ketoacids with high preference for C₁₄ and C₁₆ substrates. The failure to produce any hydrolyzed products in yeast suggested DMH is compatible with type II but not type I FAS complexes.

The biochemical function of DMP was analyzed in *in vivo* and *in vitro* systems. The expression of DMP in yeast did not generate any products, indicating DMP alone is not enough to produce β -diketones. The feeding of 3-keto acids to DMP-expressing yeast led to the production of β -diketones, indicating 3-keto acids along with other substrates (likely malonyl-CoA in an elongation model) are enough for β -diketone production. As with previous studies, this data could be interpreted as both DMP and the FAE complex from yeast are required for β -diketone formation, however, *in vitro* testing of DMP supports an alternative model. β -Diketones were generated in the *in vitro* system containing DMP mixed with 3-keto acids and fatty acyl-CoA, indicating that DMP takes fatty acyl-CoA rather than malonyl-CoA as the other substrate. Moreover, FAE complexes are not required for β -diketone formation. We thus identified DMP as a unique plant PKS, using LC fatty acyl-CoAs as the starter, taking LC 3-keto acids as the extender, catalyzed the condensation leading to β -diketones.

5.1.2.2 The β -diketone-forming pathway in plants

The biochemical function of DMP have provided direct evidence that β -diketone is converted by the condensation between a molecule of 3-keto fatty acid and a molecule of fatty acyl-CoA in barley. This pathway includes at least three core enzymes to catalyze the intermediates and final wax products: the DMH hydrolase intercepts intermediates 3-keto fatty acids; DMP condenses 3-keto fatty acids with fatty acyl-CoAs to form the β -diketone carbon skeleton; and the DMC cytochrome P450 oxidizes β -diketone at a specific position to form hydroxy- β -diketone. With current data, we cannot rule out the possibility that the P450 may oxidize 3-keto fatty acids and the DMP could further condense the hydroxylated 3-keto fatty acids with fatty acyl-CoAs to form hydroxy- β -diketones. Additionally, how the 2-alkanol esters produced on β -diketone-forming pathway is still not clear. Whether specific decarboxylases and/or reductases are involved in the formation of 2-alkanols, and whether a specific wax synthase is required to produce 2-alkanol esters are all unknown. Further wax mutant characterization alongside the biochemical identification of wax synthesis related enzymes is required to test these hypotheses.

Since there is high genome synteny of the β -diketone metabolic gene cluster in the tribe Triticeae, barley, durum wheat and bread wheat likely share a similar pathway to form β -diketones with different enzyme substrate preferences. However, how β -diketones are synthesized in other Poaceae species or species outside of Poaceae family is still unknown. Wax studies from different species are required to clarify whether or not the convergent evolution of β -diketone formation is present in different plant species.

5.1.3 The alkene biosynthesis in Arabidopsis

In the last project, I aimed to understand the biosynthesis of minor wax components monounsaturated alkenes in Arabidopsis. In this study, the chemical structures of the unique

alkenes were clarified. Further targeted desaturase-deficient mutant analysis identified a non-canonical wax-forming enzyme, a desaturase in ADS family, ADS4.2. And a novel alkene biosynthesis pathway was demonstrated in plants.

5.1.3.1 The homolog/isomer profile of characteristic alkenes in Arabidopsis young leaves

As minor wax components, alkenes have previously been reported in Arabidopsis young leaves, however, without chemical structure clarification. The homolog as well as isomer profiling of characteristic alkenes were the first priority of this project. The TLC separation concentrated alkenes and further derivatization of the double-bonds by the DMDS reaction made the GC-MS characterization possible. From my analysis, Arabidopsis alkenes possessed extraordinary carbon chain length ranging from C₃₃ to C₃₉ and they are dominated by the C₃₅ homolog. Further DMDS-reaction-based isomer analysis identified five isomer series with 7- and 9- isomers domination. The 7- alkene series ranged from C₃₃ to C₃₉ and peaked at C₃₅ isomer; while 9- alkene isomers had the same chain length range but peaked at C₃₇ isomer. Similar results were obtained by OsO₄-reaction-based isomer analysis conducted by Dr. Hegebarth. The special alkenes are the hallmark of Arabidopsis since the alkenes with the extraordinary chain length and various isomer series have never been reported from other plant species. The chemical structure identification also paved the way to the clarification of alkene synthesis in Arabidopsis.

5.1.3.2 The characterization of ADS4.2 in Arabidopsis

The unusual isomer series in Arabidopsis alkenes indicated special desaturases were involved in their synthesis at one point. The regio-specificity of desaturases from different families were taken into consideration to screen the potential desaturases. The target desaturase ADS4.2 was identified by the phenotype analysis of loss-of-function mutant. Moreover, its involvement was

further confirmed in the second independent loss-of-function mutant as well as complementation assay.

The Arabidopsis transcriptome data showed the expression profile of *ADS4.2* was quite different from its homologs in ADS family. This was confirmed by both qRT-PCR results and GUS promoter activity analysis. The expression of *ADS4.2* was largely restricted in young leaves in qRT-PCR analysis. In GUS histochemical staining, the young leaf expression of *ADS4.2* was confirmed. In addition, the *ADS4.2* showed strong expression in young leaf trichomes and its expression was diminished during leaf maturation/expansion in GUS staining assay. The expression pattern of *ADS4.2* is corresponding to the previously reported accumulation pattern of characteristic alkene in Arabidopsis: the alkenes were detected only from young leaves and showed high association with trichomes but not pavement cells (Hegebarth et al., 2016). These results again suggested the direct involvement of *ADS4.2* in alkene formation.

5.1.3.3 The substrate preference of ADS4.2

The biochemical function of *ADS4.2* was analyzed in yeast system. *ADS4.2* showed ω -7 desaturase regio-specificity with broad substrate spectrum in our tested conditions. It accepted acyl-CoA substrates ranging from C₂₂ to C₃₄. But high turn-over rate was only found in substrates longer than C₃₂. These results clearly demonstrated that *ADS4.2* possessed the substrate preferences for acyl-CoAs longer than C₃₂. This specificity of *ADS4.2* also matched the alkene profile in Arabidopsis: the detected alkenes were all longer than C₃₃ (C₃₄ substrate). These results all indicate that *ADS4.2* takes elongated products *in planta*, which makes the Arabidopsis alkene synthesized through an elongation-desaturation pathway.

5.1.3.4 The alkene-forming pathway in Arabidopsis

The ubiquitous wax component synthesis machineries are well characterized in Arabidopsis. The corresponding mutants thus become powerful tools to test the participation as well as their position in the formation pathway of specialty wax components. The elongation, acyl-reduction, and decarbonylation core mutants were analyzed to test their participation as well as position in alkene synthesis. These analyses confirmed the LACS1, CER3 and CER1 played crucial roles in alkene formation, indicating the activation of VLC acyl-CoAs and decarbonylation are essential steps in alkene synthesis. However, the fatty acyl elongation complexes required to generate characteristic fatty acyls in alkene production are still not clear. KCS16 is the only enzyme that showed clear participation in alkene formation (Hegebarth et al., 2017). The redundancy of KCS family members as well as CER2-LIKEs in Arabidopsis make it difficult to identify the rest elongation machineries that participate in this process. *cer2 cer26* double mutant showed slight reduction of C₃₃ alkene coverage. The triple or even quadruple *CER2-LIKE* mutants are required to clarify the roles CER2-LIKEs play in alkene formation.

The substrate chain length specificity of ADS4.2 and ER-localization support its late position in alkene formation, which is after the acyl elongation, suggesting an elongation-desaturation-decarbonylation alkene synthesis pathway. This is different from all the other plants which use plastidial desaturases and follow a desaturation-elongation-decarbonylation alkene synthesis pathway (von Wettstein-Knowles, 2007; Gonzales-Vigil et al., 2017).

5.2 Future directions

In my PhD studies, I investigated the ubiquitous as well as specialty wax component synthesis. However, the contributions of these wax components to plant cuticle properties and overall plant adaptation is still ambiguous, especially the minor wax components. This is even worse in crop

species. I identified the core enzymes in specialty wax component formation and partly explored their biochemical function and found the homolog as well as isomer distribution of wax products were largely determined by the specificity of the participating enzymes. But the structural basis of these enzymes that led to the product specificity are barely explored so far. In the following section, I will focus on related questions that could be addressed in future studies based on my thesis work.

5.2.1 Specialty wax components and cuticle properties

Plant cuticle properties, to a great extent, are determined by the lipophilic components and their internal structural arrangement. The incorporation of specialty wax components, with special functional groups (e.g. double-bond, cyclic groups) and sometimes even with multiple polar functional groups assembled into a single molecule, are of particular interests. Cuticular waxes are enriched with lipophilic VLC fatty acyl tails and these molecules are proposed to arrange parallel with each other and build multilayered films (Koch et al., 2006; Wang et al., 2015c). Ubiquitous wax molecules that lack the in-chain functional groups interact with each other and stabilize the wax arrangement by weak intermolecular interactions (e.g. van der Waals). In contrast, the specialty wax molecules generally contain in-chain polar functional groups, which makes it impossible to have specialty wax molecules arrange the same way as the ubiquitous wax molecules. With the presence of specialty wax molecules, more hydrogen-bonds are introduced to the system, this will impact the weak intermolecular interactions between ubiquitous wax molecules. Therefore, the wax arrangement of mixed wax molecules is different from that of ubiquitous wax molecules alone. Thus, the functional groups of specialty wax components potentially influence the arrangement of wax molecules, which further influences cuticle properties. Although the direct evidence regarding to the wax molecule interactions

currently are still lacking, comparisons between phenotypes of plants with or without specialty wax components (likely due to changed cuticle properties) shed light on their function in cuticle arrangement. Evidence has been found that even minor specialty wax components have the potential to influence cuticle properties. For instance, in *Arabidopsis cer17* mutant, which lacks the minor wax component n-6 monounsaturated primary alcohols in their stem waxes, exhibited an increased cutin load and a thick and irregular-shaped cuticle structure (Yang et al., 2017), indicating an altered cutin-wax and wax-wax interaction after missing the specialty wax molecules. VLC monounsaturated primary alcohols comprise both hydroxy group and a special functional group in the double-bond, therefore they contain a strong polar group at one end of the hydrocarbon tail and a kink in the mid of the tail. These groups may enable their parallel arrangement with other VLC acyl molecules, and meanwhile push the surrounding molecules away to avoid tightly packing.

Minor wax component monounsaturated alkenes in *Arabidopsis* are different from other known wax components. Firstly, the extraordinary acyl chain length ranging from C₃₅ to C₃₉ is unusual in plant kingdom. Secondly, besides the major 7- and 9- isomer series, there are at least three more minor isomer series present. Monounsaturated alkenes accumulated highly in trichomes, the single-cell epidermal structure. This special chemical makeup may endow particular cuticle characteristics to the delicate trichomes. The double-bonds in the VLC acyls introduce kinks to molecules, which impacts the tightly packing of the cuticle and lower the overall melting point. As a consequence, they may enable more fluidity, imparting flexibility of trichome cuticle in cold conditions (Murata and Los, 1997; Gibbs, 2002).

Overall, how the structure of wax molecules influences the wax arrangement and cuticle properties at this moment is still far from clear. More research is required to figure out how the specialty wax components influence cuticle properties.

5.2.2 Metabolic gene clusters, their expression regulation and wax biosynthesis

The metabolic gene clusters have been widely reported in plant secondary (specialized) metabolite formation including the production of terpenes, alkaloids, cyanogenic glucosides and polyketides (Wilderman et al., 2004; Zhou et al., 2016; Nützmann et al., 2018). Metabolic gene clusters are common in bacteria and fungi that involved in the formation of both primary and secondary metabolites. However, these gene clusters identified from plants are unlikely to have originated from horizontal gene transfer from microbes, but rather through genomic duplication and neofunctionalization to recruit genes on the same metabolic pathway (Nützmann et al., 2018). The plant metabolic gene clusters are generally large: ranging from ca. 35 to several hundred kilobases in the genome (Nützmann et al., 2018). Unlike bacteria and fungi, the additional regulatory components and transporters that related to the metabolites are generally present outside the gene clusters in plants (Nützmann et al., 2018).

The metabolism of the wax β -diketones is determined by a typical metabolic gene cluster in barley and wheat. In wheat, two redundant metabolic gene clusters control its formation: the β -diketone forming loci *W1* and *W2* on chromosome 2B and 2D respectively (corresponding to *CER-CQU* locus in barley chromosome 2H) (Hen-Avivi et al., 2016; Schneider et al., 2016). At least three enzymes related to this process are tandemly arranged within the gene cluster (Hen-Avivi et al., 2016; Schneider et al., 2016). Additionally, there are two β -diketone forming regulatory components in wheat, the glaucous repressor loci *Iw1* and *Iw2* that locate on chromosome arms 2BS and 2DS respectively (Adamski et al., 2013; Huang et al., 2017). *Iw1* and

W1 have been mapped close to each other on the distal part of 2BS. While *W2* has been mapped to the proximal end of 2DS, which is far from *Iw2* that mapped to the distal end of 2DS (Tsunewaki and Ebana, 1999). Any of them is able to inhibit the formation of β -diketone. A recent study in durum wheat near-iso-genic lines has found that the *Iw1* locus encodes a miRNA precursor with the final product mediates the degradation of the *DMH* (*W1-COE*) transcript (Huang et al., 2017).

The studies of β -diketone in wheat showed that this wax compound class is far more dynamically regulated beyond these two loci. There is developmental stage-specific, tissue-specific production, drought and light induction, control of wheat β -diketone formation (Bi et al., 2017). However, the regulatory mechanisms behind this are still far from clear. The regulatory elements in the promoter region of β -diketone forming enzymes are of special interest to decipher the dynamic control of this compound in wheat.

Moreover, lots of specialty wax components in plants require multiple enzymes to form the backbone and finalize the decoration of the molecule. With the increasing availability of transcriptome data and genome information, more and more wax metabolic gene clusters will be identified from different plant species.

5.2.3 Wax composition and plant drought/pathogen resistance

Previous studies showed that cuticular waxes play important roles in plant survival. However, in crop species, how different wax compositions contribute to their stress resistance is barely explored. The modification of crop wax composition could be a feasible way to improve crop stress resistance and even crop yields.

Previous research on drought tolerance and cuticle properties on five bread wheat cultivars showed the elevated alkane coverage in all wheat cultivars after drought treatment (Bi et al., 2017). However, the limited cultivar population and variation of their genetic background made it hard to draw conclusions. Water use efficiency, gas exchange, photosynthesis and surface glaucousness study on isogenic wheat lines showed increased water use efficiency of glaucous wheat lines under drought condition comparing to their glossy counterparts (Richards et al., 1986). However, the details of wheat wax compositions were lacking in this study. In addition, the specific wax compositions have been shown to influence pathogen resistance of plants. The homogeneous coating of glass surfaces with leaf epicuticular waxes enabled the test of pathogen infection solely on the wax compositions. The surfaces reconstructed from wheat cuticular wax triggered the formation of appressoria, substomatal vesicles, and infection hyphae of wheat rust fungus, which could not be achieved in the uncoated or dental wax coated surfaces. Further experiments indicated that C₂₈ aldehyde was the major component that induced the infection structure formation (Reisigl et al., 2006).

The limited research proposed the huge potential to enhance crop drought and pathogen resistance by genetic modification of cuticular wax traits, which requires the guidance from basic research on the cuticular waxes of crops.

5.2.4 The substrate specificity of wax synthesis enzymes

In my PhD studies, three types of non-canonical wax-forming enzymes have been explored: acyl-CoA desaturase-like family member ADS4.2, the α/β hydrolase family member DMH and type III polyketide synthase DMP. All of these enzymes showed specificity for their substrates and thus lead to their peculiar product profiles.

ADS4.2 has strong affinity for fatty acyl-CoAs longer than C₃₂ in yeast expression assay, and its *in planta* products showed its activity on acyl-CoAs ranging from C₃₄ to C₄₀. Its close homolog ADS4 shares 81.3% amino acid identity with ADS4.2 and showed the activity towards fatty acyls ranging from C₂₆ to C₃₀ *in planta* (Yang et al., 2017). In contrast, the mouse counterpart MmSCD1 has a substrate preference for C₁₆ and C₁₈ fatty acyl-CoAs. The substrate specificity of ADS4.2 is unusual in the desaturase family and even in other hydrocarbon modification enzyme families. No enzymes have been reported to have strong activity on linear fatty acyl substrate within C₃₄ to C₄₀ chain length range. Experimental data on the 3D structure of ADS4.2 and ADS4 as well as the comparison with other desaturases, substrate pocket and substrate binding analyses are required to understand the structural basis of ADS4.2 substrate specificity. Further domain swapping and site-directed mutagenesis of ADS4.2 could be used to test the identified critical regions or amino acid residues that determine its specificity.

In β -diketone formation, the hydrolase DMH also showed strong substrate/product specificity to produce predominantly C₁₆ 3-keto fatty acid *in planta*. In *E. coli* expression, the monounsaturated C₁₆ 3-ketoacid was the major product, indicating that DMH may have a wide substrate pocket that has the potential to hydrolyze both straight-chain substrates and linear substrates with a mid-chain kink. The mechanism that DMH used to select its substrates is still unclear. There are two possibilities: 1) DMH determines its substrates by its channel specificity. It is possible that DMH has quite restricted pocket length/size and only recruits the free C₁₆ 3-keto acyl-ACP released by the FAS complex in stroma of plastids. 2) DMH recruits its substrates by interaction with other proteins. During the *de novo* fatty acid formation, the fatty acyls are associated with ACP which usually occurs as several isomers in plants. And in the elongation process, fatty acyl-ACPs interact with FAS complex components. In the loosely associated FAS

complex, KAS is the protein that determines the chain length specificity of the complex. It is possible that DMH interacts with KAS that is forming C₁₆ 3-keto fatty acyl-ACP and intercepts the substrate from the FAS complex, releasing the 3-keto fatty acid products. It is also possible that DMH interacts with specific ACP isomers which enables the specific interception of C₁₆ 3-keto fatty acyl-ACP and produce C₁₆ 3-keto fatty acid. It is equally possible that the interaction of DMH with other protein(s) and pocket size of DMH together endow the specificity of DMH. The interaction between FATB-type hydrolase/thioesterase and ACP isomers have been reported from several organisms (Blatti et al., 2012; Feng et al., 2017; Ziesack et al., 2018). Identification of the protein(s) interacting with DMH alongside the crystallization and structure analysis of DMH will provide insight on its product specificity.

As a polyketide synthase, DMP is unique because of the unusual extender substrate used during its reaction. Moreover, the C₁₆ fatty acyl-CoA as starter is also rare in the plant PKS family. The reaction mechanism of DMP is close to CURS from *Curcuma longa*. CURS mainly takes a molecule of feruloyl-CoA as starter and a molecule of feruloyl-diketide intermediate (likely hydrolyzed to acid form) as the extender to form curcumin *in planta*. And the feruloyl-diketide intermediates are synthesized by another PKS DKS, which takes a molecule of feruloyl-CoA as the starter and a unit of malonyl-CoA as extender (Katsuyama et al., 2009). The structure comparison of DMP and CURS may facilitate the substrate pocket identification thus finding the regions or amino acid residues that determine their substrate specificity.

All of the enzyme substrate specificity and catalytic mechanism knowledge will contribute to product-directed enzyme modification, which will assist in design and generation of desirable enzymes with high specificity and efficiency to produce the required metabolic products in cell factories.

References

- Aarts M, Keijzer CJ, Stiekema WJ and Pereira A** (1995) Molecular characterization of the *CER1* gene of Arabidopsis involved in epicuticular wax biosynthesis and pollen fertility. *The Plant Cell* **7**: 2115-2127
- Aarts MG, Hodge R, Kalantidis K, Florack D, Wilson ZA, Mulligan BJ, Stiekema WJ, Scott R and Pereira A** (1997) The Arabidopsis MALE STERILITY 2 protein shares similarity with reductases in elongation/condensation complexes. *The Plant Journal* **12**: 615-623
- Abdel-Latif A and Osman G** (2017) Comparison of three genomic DNA extraction methods to obtain high DNA quality from maize. *Plant Methods* **13**: 1-9
- Abe I and Morita H** (2010) Structure and function of the chalcone synthase superfamily of plant type III polyketide synthases. *Natural Product Reports* **27**: 809-838
- Abbràmoff MD, Magalhães PJ and Ram SJ** (2004) Image processing with ImageJ. *Biophotonics international* **11**: 36-42
- Adamski NM, Bush MS, Simmonds J, Turner AS, Mugford SG, Jones A, Findlay K, Pedentchouk N, von Wettstein-Knowles P and Uauy C** (2013) The *Inhibitor of wax 1* locus (*Iw1*) prevents formation of β - and OH- β -diketones in wheat cuticular waxes and maps to a sub-cM interval on chromosome arm 2 BS. *The Plant Journal* **74**: 989-1002
- Alexander LE, Okazaki Y, Schelling MA, Davis A, Zheng X, Rizhsky L, Yandea-Nelson MD, Saito K and Nikolau BJ** (2020) Maize *Glossy2* and *Glossy2*-like genes have overlapping and distinct functions in cuticular lipid deposition. *Plant Physiology* **183**: 840-853
- Andersson MX, Goksor M and Sandelius AS** (2007) Optical manipulation reveals strong attracting forces at membrane contact sites between endoplasmic reticulum and chloroplasts. *Journal of Biological Chemistry* **282**: 1170-1174
- Appels R, Eversole K, Stein N, Feuillet C, Keller B, Rogers J, Pozniak CJ, Choulet F, Distelfeld A, Poland J et al.** (2018) Shifting the limits in wheat research and breeding using a fully annotated reference genome. *Science* **361**
- Austin MB and Noel JP** (2003) The chalcone synthase superfamily of type III polyketide synthases. *Natural Product Reports* **20**: 79-110
- Bai Y, McCoy JG, Levin EJ, Sobrado P, Rajashankar KR, Fox BG and Zhou M** (2015) X-ray structure of a mammalian stearyl-CoA desaturase. *Nature* **524**: 252-256
- Barthlott W, Mail M, Bhushan B and Koch K** (2017) Plant Surfaces: structures and functions for biomimetic innovations. *Nano-Micro Letters* **9**: 23
- Bernard A, Domergue F, Pascal S, Jetter R, Renne C, Faure JD, Haslam RP, Napier JA, Lessire R and Joubès J** (2012) Reconstitution of plant alkane biosynthesis in yeast

demonstrates that *Arabidopsis* ECERIFERUM1 and ECERIFERUM3 are core components of a very-long-chain alkane synthesis complex. *The Plant Cell* **24**: 3106-3118

Bernard A and Joubès J (2013) *Arabidopsis* cuticular waxes: Advances in synthesis, export and regulation. *Progress in Lipid Research* **52**: 110-129

Bi H, Kovalchuk N, Langridge P, Tricker PJ, Lopato S and Borisjuk N (2017) The impact of drought on wheat leaf cuticle properties. *BMC Plant Biology* **17**: 85

Bi H, Shi J, Kovalchuk N, Luang S, Bazanova N, Chirkova L, Zhang D, Shavrukov Y, Stepanenko A and Tricker P (2018) Overexpression of the *TaSHN1* transcription factor in bread wheat leads to leaf surface modifications, improved drought tolerance, and no yield penalty under controlled growth conditions. *Plant, cell & environment* **41**: 2549-2566

Bi X, Sheng G, Liu X, Li C and Fu J (2005) Molecular and carbon and hydrogen isotopic composition of n-alkanes in plant leaf waxes. *Organic geochemistry* **36**: 1405-1417

Biedermann W, Lückner E, Pörschmann J, Lachhab S, Truyen U and Hensel A (2004) Structural characterization of some fatty acids from the brain as biomarkers of BSE risk material. *Analytical and bioanalytical chemistry* **379**: 1031-1038

Bird D, Beisson F, Brigham A, Shin J, Greer S, Jetter R, Kunst L, Wu XW, Yephremov A and Samuels L (2007) Characterization of *Arabidopsis* ABCG11/WBC11, an ATP binding cassette (ABC) transporter that is required for cuticular lipid secretion. *The Plant Journal* **52**: 485-498

Blatti JL, Beld J, Behnke CA, Mendez M, Mayfield SP and Burkart MD (2012) Manipulating fatty acid biosynthesis in microalgae for biofuel through protein-protein interactions. *PLoS One* **7**: e42949

Bourdenx B, Bernard A, Domergue F, Pascal S, Léger A, Roby D, Pervent M, Vile D, Haslam RP, Napier JA, Lessire R and Joubès J (2011) Overexpression of *Arabidopsis* *ECERIFERUM1* promotes wax very-long-chain alkane biosynthesis and influences plant response to biotic and abiotic stresses. *Plant physiology* **156**: 29-45

Bourgault R, Matschi S, Vasquez M, Qiao P, Sonntag A, Charlebois C, Mohammadi M, Scanlon MJ, Smith LG and Molina I (2019) Constructing functional cuticles: analysis of relationships between cuticle lipid composition, ultrastructure and water barrier function in developing adult maize leaves. *Annals of Botany* **125**: 79-91

Brinkerhoff RC, Tarazona HF, de Oliveira PM, Flores DC, D'Oca CDRM, Russowsky D and D'Oca MGM (2014) Synthesis of β -ketoesters from renewable resources and Meldrum's acid. *RSC Advances* **4**: 49556-49559

Brown AP, Affleck V, Fawcett T and Slabas AR (2006) Tandem affinity purification tagging of fatty acid biosynthetic enzymes in *Synechocystis* sp PCC6803 and *Arabidopsis thaliana*. *Journal of Experimental Botany* **57**: 1563-1571

- Bryant FM, Munoz-Azcarate O, Kelly AA, Beaudoin F, Kurup S and Eastmond PJ** (2016) ACYL-ACYL CARRIER PROTEIN DESATURASE2 and 3 are responsible for making ω -7 fatty acids in the Arabidopsis aleurone. *Plant physiology* **172**: 154-162
- Busta L, Budke JM and Jetter R** (2016) Identification of β -hydroxy fatty acid esters and primary, secondary-alkanediol esters in cuticular waxes of the moss *Funaria hygrometrica*. *Phytochemistry* **121**: 38-49
- Busta L, Hegebarth D, Kroc E and Jetter R** (2017) Changes in cuticular wax coverage and composition on developing Arabidopsis leaves are influenced by wax biosynthesis gene expression levels and trichome density. *Planta* **245**: 297-311
- Busta L and Jetter R** (2018) Moving beyond the ubiquitous: the diversity and biosynthesis of specialty compounds in plant cuticular waxes. *Phytochemistry Reviews* **17**: 1275-1304
- Busta L, Serra O, Kim OT, Molinas M, Peré-Fossoul I, Figueras M and Jetter R** (2020) Oxidosqualene cyclases involved in the biosynthesis of triterpenoids in *Quercus suber* cork. *Scientific reports* **10**: 1-12
- Chai G, Li C, Xu F, Li Y, Shi X, Wang Y and Wang Z** (2018) Three endoplasmic reticulum-associated fatty acyl-coenzyme A reductases were involved in the production of primary alcohols in hexaploid wheat (*Triticum aestivum* L.). *BMC plant biology* **18**: 1-16
- Chikaraishi Y and Naraoka H** (2007) $\delta^{13}\text{C}$ and δD relationships among three n-alkyl compound classes (n-alkanoic acid, n-alkane and n-alkanol) of terrestrial higher plants. *Organic Geochemistry* **38**: 198-215
- Choulet F, Alberti A, Theil S, Glover N, Barbe V, Daron J, Pingault L, Sourdille P, Couloux A, Paux E et al.** (2014) Structural and functional partitioning of bread wheat chromosome 3B. *Science* **345**
- Clarke J, McCaig T and DePauw R** (1993) Relationship of glaucousness and epicuticular wax quantity of wheat. *Canadian journal of plant science* **73**: 961-967
- Clough RC, Matthis AL, Barnum SR and Jaworski JG** (1992) Purification and Characterization of 3-Ketoacyl-Acyl Carrier Protein Synthase-III from Spinach - a condensing enzyme utilizing acetyl-Coenzyme-A to initiate fatty-acid synthesis. *Journal of Biological Chemistry* **267**: 20992-20998
- Clough SJ and Bent AF** (1998) Floral dip: a simplified method for Agrobacterium-mediated transformation of Arabidopsis thaliana. *The Plant Journal* **16**
- Collister JW, Rieley G, Stern B, Eglinton G and Fry B** (1994) Compound-specific $\delta^{13}\text{C}$ analyses of leaf lipids from plants with differing carbon dioxide metabolisms. *Organic geochemistry* **21**: 619-627

- DeBono A, Yeats TH, Rose JKC, Bird D, Jetter R, Kunst L and Samuels L** (2009) Arabidopsis LTPG is a Glycosylphosphatidylinositol-Anchored Lipid Transfer Protein required for export of lipids to the plant surface. *The Plant Cell* **21**: 1230-1238
- Denic V and Weissman JS** (2007) A molecular caliper mechanism for determining very long-chain fatty acid length. *Cell* **130**: 663-677
- Dennison T, Qin W, Loneman DM, Condon SG, Lauter N, Nikolau BJ and Yandea-Nelson MD** (2019) Genetic and environmental variation impact the cuticular hydrocarbon metabolome on the stigmatic surfaces of maize. *BMC plant biology* **19**: 430
- Devedjiev Y, Dauter Z, Kuznetsov SR, Jones TL and Derewenda ZS** (2000) Crystal structure of the human acyl protein thioesterase I from a single X-ray data set to 1.5 Å. *Structure* **8**: 1137-1146
- Dittrich F, Zajonc D, Hühne K, Hoja U, Ekici A, Greiner E, Klein H, Hofmann J, Bessoule JJ, Sperling P and Schweizer E** (1998) Fatty acid elongation in yeast: Biochemical characteristics of the enzyme system and isolation of elongation-defective mutants. *European Journal of Biochemistry* **252**: 477-485
- Dormann P, Voelker TA and Ohlrogge JB** (2000) Accumulation of palmitate in Arabidopsis mediated by the acyl-acyl carrier protein thioesterase FATB1. *Plant Physiology* **123**: 637-643
- Edgar RC** (2004) MUSCLE: multiple sequence alignment with high accuracy and high throughput. *Nucleic acids research* **32**: 1792-1797
- Equiza MA, Miravé JP and Tognetti JA** (2001) Morphological, anatomical and physiological responses related to differential shoot vs. root growth inhibition at low temperature in spring and winter wheat. *Annals of Botany* **87**: 67-76
- Eversole K and Director IE** (2008) The International Wheat Genome Sequencing Consortium. *In Plant and Animal Genome XXVI Conference* (January 13-17, 2018). PAG
- Feng Y and Cronan JE** (2009) *Escherichia coli* unsaturated fatty acid synthesis: complex transcription of the *fabA* gene and *in vivo* identification of the essential reaction catalyzed by FabB. *Journal of Biological Chemistry* **284**: 29526-29535
- Feng Y, Wang Y, Liu J, Liu Y, Cao X and Xue S** (2017) Structural insight into acyl-ACP thioesterase toward substrate specificity design. *ACS chemical biology* **12**: 2830-2836
- Fich EA, Segerson NA and Rose JKC** (2016) The Plant Polyester Cutin: Biosynthesis, structure, and biological roles. *Annual Review of Plant Biology*, Vol 67 **67**: 207-233
- Fiebig A, Mayfield JA, Miley NL, Chau S, Fischer RL and Preuss D** (2000) Alterations in *CER6*, a gene identical to *CUT1*, differentially affect long-chain lipid content on the surface of pollen and stems. *The Plant Cell* **12**: 2001-2008

Francis GW (1981) Alkylthiolation for the determination of double-bond position in unsaturated fatty acid esters. *Chemistry and Physics of Lipids* **29**: 369-374

Franke R, Hofer R, Briesen I, Emsermann M, Efremova N, Yephremov A and Schreiber L (2009) The *DAISY* gene from *Arabidopsis* encodes a fatty acid elongase condensing enzyme involved in the biosynthesis of aliphatic suberin in roots and the chalaza-micropyle region of seeds. *The Plant Journal* **57**: 80-95

Gibbs A and Pomonis JG (1995) Physical properties of insect cuticular hydrocarbons: the effects of chain length, methyl-branching and unsaturation. *Comparative Biochemistry and Physiology Part B: Biochemistry and Molecular Biology* **112**: 243-249

Gibbs AG (2002) Lipid melting and cuticular permeability: new insights into an old problem. *Journal of Insect Physiology* **48**: 391-400

Gietz RD and Woods RA (2002) Transformation of yeast by lithium acetate/single-stranded carrier DNA/polyethylene glycol method. *In Methods in enzymology*, Vol 350. Elsevier, pp 87-96

Gonzales-Vigil E, Hefer CA, von Loessl ME, La Mantia J and Mansfield SD (2017) Exploiting natural variation to uncover an alkene biosynthetic enzyme in poplar. *The Plant Cell* **29**: 2000-2015

Gonzales-Vigil E, vonLoessl ME, Chen JY, Li S, Haslam TM, Kunst L and Mansfield SD (2021) Understanding the role of *Populus* ECERIFERUM2-Likes in the Biosynthesis of very-long-chain fatty acids for cuticular waxes. *Plant and Cell Physiology*

Goodwin SM, Rashotte AM, Rahman M, Feldmann KA, Jenks MA (2005) Wax constituents on the inflorescence stems of double eceriferum mutants in *Arabidopsis* reveal complex gene interactions. *Phytochemistry* **66**: 771-780

Gorb E, Haas K, Henrich A, Enders S, Barbakadze N and Gorb S (2005) Composite structure of the crystalline epicuticular wax layer of the slippery zone in the pitchers of the carnivorous plant *Nepenthes alata* and its effect on insect attachment. *Journal of Experimental Biology* **208**: 4651-4662

Greer S, Wen M, Bird D, Wu X, Samuels L, Kunst L and Jetter R (2007) The cytochrome P450 enzyme CYP96A15 is the midchain alkane hydroxylase responsible for formation of secondary alcohols and ketones in stem cuticular wax of *Arabidopsis*. *Plant physiology* **145**: 653-667

Gülz P-G, Müller E, Schmitz K, Marner F-J and Güth S (1992) Chemical composition and surface structures of epicuticular leaf waxes of *Ginkgo biloba*, *Magnolia grandiflora* and *Liriodendron tulipifera*. *Zeitschrift für Naturforschung C* **47**: 516-526

Harwood J and Murphy D (2005) Plant lipids: biology, utilisation and manipulation. *In Fatty acid biosynthesis*. Blackwell Publishing

- Haslam TM, Haslam R, Thoraval D, Pascal S, Delude C, Domergue F, Fernandez AM, Beaudoin F, Napier JA, Kunst L and Joubès J** (2015) ECERIFERUM2-LIKE proteins have unique biochemical and physiological functions in very-long-chain fatty acid elongation. *Plant Physiology* **167**: 682-692
- Haslam TM and Kunst L** (2013) Extending the story of very-long-chain fatty acid elongation. *Plant Science* **210**: 93-107
- Haslam TM and Kunst L** (2020) Arabidopsis ECERIFERUM2-LIKEs are mediators of condensing enzyme function. *Plant and Cell Physiology* **61**: 2126-2138
- Haslam TM, Manas-Fernandez A, Zhao LF and Kunst L** (2012) Arabidopsis ECERIFERUM2 is a component of the Fatty Acid Elongation machinery required for fatty acid extension to exceptional lengths. *Plant Physiology* **160**: 1164-1174
- Hegebarth D, Buschhaus C, Joubès J, Thoraval D, Bird D and Jetter R** (2017) Arabidopsis ketoacyl-CoA synthase 16 (KCS16) forms C36/C38 acyl precursors for leaf trichome and pavement surface wax. *Plant, Cell and Environment* **40**: 1761-1776
- Hegebarth D, Buschhaus C, Wu M, Bird D and Jetter R** (2016) The composition of surface wax on trichomes of *Arabidopsis thaliana* differs from wax on other epidermal cells. *The Plant Journal* **88**: 762-774
- Hen-Avivi S, Savin O, Racovita RC, Lee W-S, Adamski NM, Malitsky S, Almekias-Siegl E, Levy M, Vautrin S, Bergès H, Friedlander G, Kartvelishvili E, Ben-Zvi G, Alkan N, Uauy C, Kanyuka K, Jetter R, Distelfeld A and Aharoni A** (2016) A metabolic gene cluster in the wheat *W1* and the barley *Cer-cqu* loci determines β -diketone biosynthesis and glaucousness. *The Plant Cell* **28**: 1440-1460
- Herbin G and Robins P** (1968) Studies on plant cuticular waxes I: The chemotaxonomy of alkanes and alkenes of the genus *Aloe* (Liliaceae). *Phytochemistry* **7**: 239-255
- Ho SN, Hunt HD, Horton RM, Pullen JK and Pease LR** (1989) Site-directed mutagenesis by overlap extension using the Polymerase Chain Reaction. *Gene* **77**: 51-59
- Holmquist M** (2000) α/β -hydrolase fold enzymes structures, functions and mechanisms. *Current Protein and Peptide Science* **1**: 209-235
- Hooker TS, Millar AA and Kunst L** (2002) Significance of the expression of the CER6 condensing enzyme for cuticular wax production in Arabidopsis. *Plant Physiology* **129**: 1568-1580
- Horn D and Lamberton J** (1962) Long-chain β -diketones from plant waxes. *Chem. Ind. (London)*, pp 2036-2037
- Horn D and Lamberton J** (1964) The occurrence of 11, 12-dehydrourosolic lactone acetate in *Eucalyptus* waxes. *Australian Journal of Chemistry* **17**: 477-480

- Huang D, Feurtado JA, Smith MA, Flatman LK, Koh C and Cutler AJ** (2017) Long noncoding miRNA gene represses wheat β -diketone waxes. *Proceedings of the National Academy of Sciences* **114**: E3149-E3158
- Huhtinen K, O'Byrne J, Lindquist PJ, Contreras JA and Alexson SE** (2002) The peroxisome proliferator-induced cytosolic type I acyl-CoA thioesterase (CTE-I) is a serine-histidine-aspartic acid α/β hydrolase. *Journal of Biological Chemistry* **277**: 3424-3432
- James DW, Lim E, Keller J, Plooy I, Ralston E and Dooner HK** (1995) Directed tagging of the *Arabidopsis Fatty Acid Elongation 1 (FAE1)* gene with the Maize Transposon activator. *The Plant Cell* **7**: 309-319
- Ji X and Jetter R** (2008) Very long chain alkylresorcinols accumulate in the intracuticular wax of rye (*Secale cereale* L.) leaves near the tissue surface. *Phytochemistry* **69**: 1197-1207
- Jing F, Zhao L, Yandeau-Nelson MD and Nikolau BJ** (2018) Two distinct domains contribute to the substrate acyl chain length selectivity of plant acyl-ACP thioesterase. *Nature Communications* **9**: 860
- World Health Organization and FAO/WHO Expert Committee** (2017) Evaluation of certain contaminants in food: eighty-third report of the Joint FAO/WHO Expert Committee on Food Additives. World Health Organization
- Jolad SD, Lantz RC, Solyom AM, Chen GJ, Bates RB and Timmermann BN** (2004) Fresh organically grown ginger (*Zingiber officinale*): composition and effects on LPS-induced PGE2 production. *Phytochemistry* **65**: 1937-1954
- Joubès J, Raffaele S, Bourdenx B, Garcia C, Laroche-Traineau J, Moreau P, Domergue F, and Lessire R** (2008) The VLCFA elongase gene family in *Arabidopsis thaliana*: phylogenetic analysis, 3D modelling and expression profiling. *Plant Molecular Biology* **67**: 547-566
- Jung K-H, Han M-J, Lee D-Y, Lee Y-S, Schreiber L, Franke R, Faust A, Yephremov A, Saedler H, and Kim Y-W** (2006) *Wax-deficient anther1* is involved in cuticle and wax production in rice anther walls and is required for pollen development. *The Plant Cell* **18**: 3015-3032
- Kachroo A, Lapchyk L, Fukushige H, Hildebrand D, Klessig D and Kachroo P** (2003) Plastidial fatty acid signaling modulates salicylic acid- and jasmonic acid-mediated defense pathways in the *Arabidopsis ssi2* mutant. *The Plant Cell* **15**: 2952-2965
- Kachroo A, Shanklin J, Whittle E, Lapchyk L, Hildebrand D and Kachroo P** (2007) The *Arabidopsis* stearyl-acyl carrier protein-desaturase family and the contribution of leaf isoforms to oleic acid synthesis. *Plant Molecular Biology* **63**
- Kachroo P, Shanklin J, Shah J, Whittle EJ and Klessig DF** (2001) A fatty acid desaturase modulates the activation of defense signaling pathways in plants. *Proceedings of the National Academy of Sciences* **98**: 9448-9453

Kalinger RS, Pulsifer IP, Hepworth SR and Rowland O (2020) Fatty acyl synthetases and thioesterases in plant lipid metabolism: diverse functions and biotechnological applications. *Lipids* **55**: 435-455

Katsuyama Y, Kita T, Funa N and Horinouchi S (2009) Curcuminoid biosynthesis by two type III polyketide synthases in the herb *Curcuma longa*. *Journal of Biological Chemistry* **284**: 11160-11170

Kelley LA, Mezulis S, Yates CM, Wass MN and Sternberg MJ (2015) The Phyre2 web portal for protein modeling, prediction and analysis. *Nature protocols* **10**: 845-858

Kim H, Lee SB, Kim HJ, Min MK, Hwang I and Suh MC (2012) Characterization of Glycosylphosphatidylinositol-Anchored Lipid Transfer Protein 2 (LTPG2) and overlapping function between LTPG/LTPG1 and LTPG2 in cuticular wax export or accumulation in *Arabidopsis thaliana*. *Plant and Cell Physiology* **53**: 1391-1403

Kim J, Jung JH, Lee SB, Go YS, Kim HJ, Cahoon R, Markham JE, Cahoon EB and Suh MC (2013) Arabidopsis 3-Ketoacyl-Coenzyme A Synthase 9 is involved in the synthesis of tetracosanoic acids as precursors of cuticular waxes, suberins, sphingolipids, and phospholipids. *Plant Physiology* **162**: 567-580

Klepikova AV, Kasianov AS, Gerasimov ES, Logacheva MD and Penin AA (2016) A high resolution map of the *Arabidopsis thaliana* developmental transcriptome based on RNA-seq profiling. *The Plant Journal* **88**: 1058-1070

Klinkenberg J, Faist H, Saupe S, Lambertz S, Krischke M, Stingl N, Fekete A, Mueller MJ, Feussner I, Hedrich R and Deeken R (2014) Two fatty acid desaturases, STEAROYL-ACYL CARRIER PROTEIN Δ^9 -DESATURASE6 and FATTY ACID DESATURASE3, are involved in drought and hypoxia stress signaling in Arabidopsis crown galls. *Plant Physiology* **164**: 570-583

Koch K, Hartmann KD, Schreiber L, Barthlott W and Neinhuis C (2006) Influences of air humidity during the cultivation of plants on wax chemical composition, morphology and leaf surface wettability. *Environmental and Experimental Botany* **56**: 1-9

Kosma DK, Bourdenx B, Bernard A, Parsons EP, Lu S, Joubès J and Jenks MA (2009) The impact of water deficiency on leaf cuticle lipids of Arabidopsis. *Plant physiology* **151**: 1918-1929

Kulkarni M, Soolanayakanahally R, Ogawa S, Uga Y, Selvaraj MG and Kagale S (2017) Drought response in wheat: key genes and regulatory mechanisms controlling root system architecture and transpiration efficiency. *Frontiers in chemistry* **5**: 106

Kumar S, Stecher G, Li M, Knyaz C and Tamura K (2018) MEGA X: molecular evolutionary genetics analysis across computing platforms. *Molecular biology and evolution* **35**: 1547-1549

Kunst L and Samuels AL (2003) Biosynthesis and secretion of plant cuticular wax. *Progress in Lipid Research* **42**: 51-80

Kunst L and Samuels L (2009) Plant cuticles shine: advances in wax biosynthesis and export. *Current Opinion in Plant Biology* **12**: 721-727

Kunst L, Taylor DC and Underhill EW (1992) Fatty-Acid Elongation in developing seeds of *Arabidopsis thaliana*. *Plant Physiology and Biochemistry* **30**: 425-434

Larkin JC, Young N, Prigge M and Marks MD (1996) The control of trichome spacing and number in *Arabidopsis*. *Development* **122**: 997-1005

Lee SB, Jung SJ, Go YS, Kim HU, Kim JK, Cho HJ, Park OK and Suh MC (2009) Two *Arabidopsis* 3-ketoacyl CoA synthase genes, *KCS20* and *KCS2/DAISY*, are functionally redundant in cuticular wax and root suberin biosynthesis, but differentially controlled by osmotic stress. *The Plant Journal* **60**: 462-475

Leide J, Hildebrandt U, Reussing K, Riederer M and Vogg G (2007) The developmental pattern of tomato fruit wax accumulation and its impact on cuticular transpiration barrier properties: effects of a deficiency in a β -ketoacyl-coenzyme A synthase (*LeCER6*). *Plant physiology* **144**: 1667-1679

Leide J, Hildebrandt U, Vogg G and Riederer M (2011) The *positional sterile* (*ps*) mutation affects cuticular transpiration and wax biosynthesis of tomato fruits. *Journal of Plant Physiology* **168**: 871-877

Lesk C, Rowhani P and Ramankutty N (2016) Influence of extreme weather disasters on global crop production. *Nature* **529**: 84-87

Li-Beisson Y, Pollard M, Sauveplane V, Pinot F, Ohlrogge J and Beisson F (2009) Nanoridges that characterize the surface morphology of flowers require the synthesis of cutin polyester. *Proceedings of the National Academy of Sciences* **106**: 22008-22013

Li-Beisson Y, Shorrosh B, Beisson F, Andersson MX, Arondel V, Bates PD, Baud S, Bird D, DeBono A, Durrett TP et al. (2013) Acyl-lipid metabolism. *The Arabidopsis Book* **11**: e0161

Li F, Wu X, Lam P, Bird D, Zheng H, Samuels L, Jetter R and Kunst L (2008) Identification of the wax ester synthase/acyl-coenzyme A: diacylglycerol acyltransferase WSD1 required for stem wax ester biosynthesis in *Arabidopsis*. *Plant physiology* **148**: 97-107

Li N, Gügel IL, Giavalisco P, Zeisler V, Schreiber L, Soll J and Philippar K (2015) FAX1, a novel membrane protein mediating plastid fatty acid export. *PLoS biology* **13**: e1002053

Li T, Sun Y, Liu T, Wu H, An P, Shui Z, Wang J, Zhu Y, Li C, Wang Y, Jetter R and Wang Z (2019) *TaCER1-1A* is involved in cuticular wax alkane biosynthesis in hexaploid wheat and responds to plant abiotic stresses. *Plant, Cell and Environment* **42**: 3077-3091

Liao P, Ray S, Boachon B, Lynch JH, Deshpande A, McAdam S, Morgan JA and Dudareva N (2021) Cuticle thickness affects dynamics of volatile emission from petunia flowers. *Nature Chemical Biology* **17**: 138-145

- Lim G-H, Liu H, Yu K, Liu R, Shine M, Fernandez J, Burch-Smith T, Mobley JK, McLetchie N and Kachroo A** (2020) The plant cuticle regulates apoplastic transport of salicylic acid during systemic acquired resistance. *Science Advances* **6**: eaaz0478
- Livak KJ and Schmittgen TD** (2001) Analysis of relative gene expression data using real-time quantitative PCR and the $2^{-\Delta\Delta CT}$ method. *Methods* **25**: 402-408
- Lobell DB and Gourdji SM** (2012) The influence of climate change on global crop productivity. *Plant Physiology* **160**: 1686-1697
- Lolle SJ, Hsu W, Pruitt RE** (1998) Genetic analysis of organ fusion in *Arabidopsis thaliana*. *Genetics* **149**: 607-619
- Lu P, Qin JX, Wang GX, Wang LL, Wang ZZ, Wu QH, Xie JZ, Liang Y, Wang Y, Zhang DY, Sun QX and Liu ZY** (2015) Comparative fine mapping of the *Wax 1* (*W1*) locus in hexaploid wheat. *Theoretical and Applied Genetics* **128**: 1595-1603
- Lü SY, Song T, Kosma DK, Parsons EP, Rowland O, Jenks MA** (2009) *Arabidopsis CER8* encodes LONG-CHAIN ACYL-COA SYNTHETASE 1 (*LACS1*) that has overlapping functions with *LACS2* in plant wax and cutin synthesis. *The Plant Journal* **59**: 553-564
- Luo B, Xue XY, Hu WL, Wang LJ and Chen XY** (2007) An ABC transporter gene of *Arabidopsis thaliana*, *AtWBC11*, is involved in cuticle development and prevention of organ fusion. *Plant and Cell Physiology* **48**: 1790-1802
- Lütz C and Güzl P-G** (1985) Comparative analysis of epicuticular waxes from some high alpine plant species. *Zeitschrift für Naturforschung C* **40**: 599-605
- Marks MD, Wenger JP, Gilding E, Jilk R and Dixon RA** (2009) Transcriptome analysis of *Arabidopsis* wild-type and *gl3-sst sim* trichomes identifies four additional genes required for trichome development. *Molecular plant* **2**: 803-822
- Matas AJ, Sanz MJ and Heredia A** (2003) Studies on the structure of the plant wax nonacosan-10-ol, the main component of epicuticular wax conifers. *International Journal of Biological Macromolecules* **33**: 31-35
- McFarlane HE, Shin JJH, Bird DA and Samuels AL** (2010) *Arabidopsis* ABCG Transporters, which are required for export of diverse cuticular lipids, dimerize in different combinations. *The Plant Cell* **22**: 3066-3075
- McFarlane HE, Watanabe Y, Yang WL, Huang Y, Ohlrogge J and Samuels AL** (2014) Golgi- and Trans-Golgi network-mediated vesicle trafficking is required for wax secretion from epidermal cells. *Plant Physiology* **164**: 1250-1260
- Mehrshahi P, Johnny C and DellaPenna D** (2014) Redefining the metabolic continuity of chloroplasts and ER. *Trends in Plant Science* **19**: 501-507

- Mehrshahi P, Stefano G, Andaloro JM, Brandizzi F, Froehlich JE and DellaPenna D** (2013) Transorganellar complementation redefines the biochemical continuity of endoplasmic reticulum and chloroplasts. *Proceedings of the National Academy of Sciences of the United States of America* **110**: 12126-12131
- Merah O, Deléens E, Souyris I and Monneveux P** (2000) Effect of glaucousness on carbon isotope discrimination and grain yield in durum wheat. *Journal of Agronomy and Crop Science* **185**: 259-265
- Mikkelsen JD** (1979) Structure and biosynthesis of β -diketones in barley spike epicuticular wax. *Carlsberg Research Communications* **44**: 133
- Mikkelsen JD** (1984) Biosynthesis of esterified alkan-2-ols and β -diketones in barley spike epicuticular wax: Synthesis of radioactive intermediates. *Carlsberg Research Communications* **49**: 391
- Mikkelsen JD and von Wettstein-Knowles P** (1978) Biosynthesis of β -diketones and hydrocarbons in barley spike epicuticular wax. *Archives of biochemistry and biophysics* **188**: 172-181
- Millar AA, Clemens S, Zachgo S, Giblin EM, Taylor DC and Kunst L** (1999) *CUT1*, an arabidopsis gene required for cuticular wax biosynthesis and pollen fertility, encodes a very-long-chain fatty acid condensing enzyme. *The Plant Cell* **11**: 825-838
- Monneveux P, Reynolds M, González-Santoyo H, Pena R, Mayr L and Zapata F** (2004) Relationships between grain yield, flag leaf morphology, carbon isotope discrimination and ash content in irrigated wheat. *Journal of Agronomy and Crop Science* **190**: 395-401
- Morita H, Wanibuchi K, Nii H, Kato R, Sugio S and Abe I** (2010) Structural basis for the one-pot formation of the diarylheptanoid scaffold by curcuminoid synthase from *Oryza sativa*. *Proceedings of the National Academy of Sciences* **107**: 19778-19783
- Moses T, Pollier J, Shen Q, Soetaert S, Reed J, Erffelinck M-L, Van Nieuwerburgh FC, Vanden Bossche R, Osbourn A, Thevelein JM, Deforce D, Tang K and Goossens A** (2015) OSC2 and CYP716A14v2 catalyze the biosynthesis of triterpenoids for the cuticle of aerial organs of *Artemisia annua*. *The Plant Cell* **27**: 286-301
- Murata N and Los DA** (1997) Membrane fluidity and temperature perception. *Plant physiology* **115**: 875
- Negruk V, Yang P, Subramanian M, McNevin JP and Lemieux B** (1996) Molecular cloning and characterization of the *CER2* gene of *Arabidopsis thaliana*. *The Plant Journal* **9**: 137-145
- Netting A and von Wettstein-Knowles P** (1976) Biosynthesis of the β -diketones of barley spike epicuticular wax. *Archives of biochemistry and biophysics* **174**: 613-621
- Nützmann H-W, Scazzocchio C and Osbourn A** (2018) Metabolic gene clusters in eukaryotes. *Annual review of genetics* **52**: 159-183

Oh C-S, Toke DA, Mandala S and Martin CE (1997) *ELO2* and *ELO3*, homologues of the *Saccharomyces cerevisiae ELO1* gene, function in fatty acid elongation and are required for sphingolipid formation. *Journal of Biological Chemistry* **272**: 17376-17384

Ohlrogge J and Browse J (1995) Lipid biosynthesis. *The Plant Cell* **7**: 957

Oyarce P, De Meester B, Fonseca F, de Vries L, Goeminne G, Pallidis A, De Rycke R, Tsuji Y, Li Y, Van den Bosch S, Sels B, Ralph J, Vanholme R and Boerjan W (2019) Introducing curcumin biosynthesis in *Arabidopsis* enhances lignocellulosic biomass processing. *Nature Plants* **5**: 225-237

Pascal S, Bernard A, Deslous P, Gronnier J, Fournier-Goss A, Domergue F, Rowland O and Joubès J (2019) *Arabidopsis* CER1-LIKE1 functions in a cuticular very-long-chain alkane-forming complex. *Plant Physiology* **179**: 415-432

Pascal S, Bernard A, Sorel M, Pervent M, Vile D, Haslam RP, Napier JA, Lessire R, Domergue F and Joubes J (2013) The *Arabidopsis cer26* mutant, like the *cer2* mutant, is specifically affected in the very long chain fatty acid elongation process. *The Plant Journal* **73**: 733-746

Perera MAD, Qin W, Yandeau-Nelson M, Fan L, Dixon P and Nikolau BJ (2010) Biological origins of normal-chain hydrocarbons: a pathway model based on cuticular wax analyses of maize silks. *The Plant Journal* **64**: 618-632

Pérez-Sancho J, Tilsner J, Samuels AL, Botella MA, Bayer EM and Rosado A (2016) Stitching Organelles: Organization and function of specialized membrane contact sites in plants. *Trends in Cell Biology* **26**: 705-717

Pérez-Sancho J, Vanneste S, Lee E, McFarlane HE, del Valle AE, Valpuesta V, Friml J, Botella MA and Rosado A (2015) The *Arabidopsis* Synaptotagmin1 is enriched in Endoplasmic Reticulum-plasma membrane contact sites and confers cellular resistance to mechanical stresses. *Plant Physiology* **168**: 132-U837

Pfeifer M, Kugler KG, Sandve SR, Zhan B, Rudi H, Hvidsten TR, Mayer KF, Olsen O-A, IWGS Consortium (2014) Genome interplay in the grain transcriptome of hexaploid bread wheat. *Science* **345**

Pighin JA, Zheng HQ, Balakshin LJ, Goodman IP, Western TL, Jetter R, Kunst L and Samuels AL (2004) Plant cuticular lipid export requires an ABC transporter. *Science* **306**: 702-704

Pillitteri LJ, Peterson KM, Horst RJ and Torii KU (2011) Molecular profiling of stomatal meristemoids reveals new component of asymmetric cell division and commonalities among stem cell populations in *Arabidopsis*. *The Plant Cell* **23**: 3260-3275

Preuss D, Lemieux B, Yen G and Davis R (1993) A conditional sterile mutation eliminates surface components from *Arabidopsis* pollen and disrupts cell signaling during fertilization. *Genes and development* **7**: 974-985

Pulsifer IP, Kluge S and Rowland O (2012) Arabidopsis LONG-CHAIN ACYL-COA SYNTHETASE 1 (LACS1), LACS2, and LACS3 facilitate fatty acid uptake in yeast. *Plant Physiology and Biochemistry* **51**: 31-39

Pulsifer IP, Lowe C, Narayanan SA, Busuttil AS, Vishwanath SJ, Domergue F and Rowland O (2014) Acyl-lipid thioesterase1-4 from Arabidopsis thaliana form a novel family of fatty acyl-acyl carrier protein thioesterases with divergent expression patterns and substrate specificities. *Plant Molecular Biology* **84**: 549-563

Qin B-X, Tang D, Huang J, Li M, Wu XR, Lu LL, Wang KJ, Yu HX, Chen JM, Gu MH and Cheng ZK (2011) Rice *OsGLI-1* is involved in leaf cuticular wax and cuticle membrane. *Molecular Plant* **4**: 985-995

Racovita RC, Hen-Avivi S, Fernandez-Moreno JP, Granell A, Aharoni A, Jetter R (2016) Composition of cuticular waxes coating flag leaf blades and peduncles of *Triticum aestivum* cv. Bethlehem. *Phytochemistry* **130**: 182-192

Racovita RC and Jetter R (2016a) Identification of in-chain-functionalized compounds and methyl-branched alkanes in cuticular waxes of *Triticum aestivum* cv. Bethlehem. *PloS one* **11**: e0165827

Racovita RC and Jetter R (2016b) Identification of polyketides in the cuticular waxes of *Triticum Aestivum* cv. Bethlehem. *Lipids* **51**: 1407-1420

Ramaroson-Raonizafinimanana B, Gaydou EM and Bombarda I (2000) Long-chain aliphatic β -diketones from epicuticular wax of Vanilla bean species. Synthesis of nervonoylacetone. *Journal of agricultural and food chemistry* **48**: 4739-4743

Reina-Pinto JJ and Yephremov A (2009) Surface lipids and plant defenses. *Plant Physiology and Biochemistry* **47**: 540-549

Reisige K, Gorzelanny C, Daniels U and Moerschbacher BM (2006) The C₂₈ aldehyde octacosanal is a morphogenetically active component involved in host plant recognition and infection structure differentiation in the wheat stem rust fungus. *Physiological and molecular plant pathology* **68**: 33-40

Richards R, Rawson H and Johnson D (1986) Glaucousness in wheat: Its development and effect on water-use efficiency, gas exchange and photosynthetic tissue temperatures. *Functional Plant Biology* **13**

Riederer M and Schreiber L (2001) Protecting against water loss: analysis of the barrier properties of plant cuticles. *Journal of experimental botany* **52**: 2023-2032

Rommerskirchen F, Eglinton G, Dupont L and Rullkötter J (2006) Glacial/interglacial changes in southern Africa: Compound-specific $\delta^{13}\text{C}$ land plant biomarker and pollen records from southeast Atlantic continental margin sediments. *Geochemistry, Geophysics, Geosystems* **7**

Rowland O, Zheng H, Hepworth SR, Lam P, Jetter R and Kunst L (2006) *CER4* encodes an alcohol-forming fatty acyl-coenzyme A reductase involved in cuticular wax production in Arabidopsis. *Plant physiology* **142**: 866-877

Samuels L, Kunst L and Jetter R (2008) Sealing plant surfaces: Cuticular wax formation by epidermal cells. *Annual Review of Plant Biology* **59**: 683-707

Samuels L and McFarlane HE (2012) Plant cell wall secretion and lipid traffic at membrane contact sites of the cell cortex. *Protoplasma* **249**: S19-S23

Sato D, Ando Y, Tsujimoto R and Kawasaki Ki (2001) Identification of novel nonmethylene-interrupted fatty acids, 7*E*, 13*E*-20: 2, 7*E*, 13*E*, 17*Z*-20: 3, 9*E*, 15*E*, 19*Z*-22: 3, and 4*Z*, 9*E*, 15*E*, 19*Z*-22: 4, in ophiuroidea (*Brittle star*) lipids. *Lipids* **36**: 1371-1375

Sayanova O, Haslam R, Caleron MV and Napier JA (2007) Cloning and characterization of unusual fatty acid desaturases from *Anemone leveillei*: identification of an acyl-coenzyme A C₂₀ Δ^5 -desaturase responsible for the synthesis of sciadonic acid. *Plant physiology* **144**: 455-467

Schiestl FP, Ayasse M, Paulus HF, Löfstedt C, Hansson BS, Ibarra F and Francke W (1999) Orchid pollination by sexual swindle. *Nature* **399**: 421-421

Schiestl FP and Cozzolino S (2008) Evolution of sexual mimicry in the orchid subtribe orchidinae: the role of preadaptations in the attraction of male bees as pollinators. *BMC Evolutionary Biology* **8**: 27

Schlüter PM, Xu S, Gagliardini V, Whittle E, Shanklin J, Grossniklaus U and Schiestl FP (2011) Stearoyl-acyl carrier protein desaturases are associated with floral isolation in sexually deceptive orchids. *Proceedings of the National Academy of Sciences* **108**: 5696-5701

Schneider LM, Adamski NM, Christensen CE, Stuart DB, Vautrin S, Hansson M, Uauy C, and von Wettstein-Knowles P (2016) The *Cer-cqu* gene cluster determines three key players in a β -diketone synthase polyketide pathway synthesizing aliphatics in epicuticular waxes. *Journal of experimental botany* **67**: 2715-2730

Schnurr J, Shockey J and Browse J (2004) The acyl-CoA synthetase encoded by *LACS2* is essential for normal cuticle development in Arabidopsis. *The Plant Cell* **16**: 629-642

Schondelmaier G FG and Jahoor A (1993) Linkage studies between morphological and RFLP markers in the barley genome. *Barley Genetics Newsletter* **22**: 57-62

Schönherr J (1976) Water permeability of isolated cuticular membranes: the effect of cuticular waxes on diffusion of water. *Planta* **131**: 159-164

Schulz S, Arsene C, Tauber M and McNeil JN (2000) Composition of lipids from sunflower pollen (*Helianthus annuus*). *Phytochemistry* **54**: 325-336

- Sedeek KE, Whittle E, Guthörl D, Grossniklaus U, Shanklin J and Schlüter PM** (2016) Amino acid change in an orchid desaturase enables mimicry of the pollinator's sex pheromone. *Current Biology* **26**: 1505-1511
- Shanklin J and Cahoon EB** (1998) Desaturation and related modifications of fatty acids. *Annual review of plant biology* **49**: 611-641
- Shanklin J, Whittle E and Fox BG** (1994) Eight histidine residues are catalytically essential in a membrane-associated iron enzyme, stearoyl-CoA desaturase, and are conserved in alkane hydroxylase and xylene monooxygenase. *Biochemistry* **33**: 12787-12794
- Shibahara A, Yamamoto K, Kinoshita A and Anderson BL** (2008) An improved method for preparing dimethyl disulfide adducts for GC/MS analysis. *Journal of the American Oil Chemists' Society* **85**: 93-94
- Shimakata T and Stumpf PK** (1982) Isolation and Function of Spinach Leaf β -Ketoacyl-[Acyl-Carrier-Protein] Synthases. *Proceedings of the National Academy of Sciences of the United States of America-Biological Sciences* **79**: 5808-5812
- Small DM** (1984) Lateral chain packing in lipids and membranes. *Journal of Lipid Research* **25**: 1490-1500
- Smith MA, Dauk M, Ramadan H, Yang H, Seamons LE, Haslam RP, Beaudoin F, Ramirez-Erosa I and Forseille L** (2013) Involvement of Arabidopsis ACYL-COENZYME A DESATURASE-LIKE2 (At2g31360) in the biosynthesis of the very-long-chain monounsaturated fatty acid components of membrane lipids. *Plant physiology* **161**: 81-96
- Soltis PS, Marchant DB, Van de Peer Y and Soltis DE** (2015) Polyploidy and genome evolution in plants. *Current opinion in genetics and development* **35**: 119-125
- Staehelin LA** (1997) The plant ER: A dynamic organelle composed of a large number of discrete functional domains. *The Plant Journal* **11**: 1151-1165
- Sun Y, Yao R, Ji X, Wu H, Luna A, Wang Z and Jetter R** (2020) Characterization of an alkylresorcinol synthase that forms phenolics accumulating in the cuticular wax on various organs of rye (*Secale cereale*). *The Plant Journal* **102**: 1294-1312
- Tamura K, Peterson D, Peterson N, Stecher G, Nei M and Kumar S** (2011) MEGA5: molecular evolutionary genetics analysis using maximum likelihood, evolutionary distance, and maximum parsimony methods. *Molecular biology and evolution* **28**: 2731-2739
- Tanaka K, Arita M, Sakurai H, Ono N and Tezuka Y** (2015) Analysis of chemical properties of edible and medicinal ginger by metabolomics approach. *BioMed Research International* **2015**
- Thimmappa R, Geisler K, Louveau T, O'Maille P and Osbourn A** (2014) Triterpene biosynthesis in plants. *Annual review of plant biology* **65**: 225-257

Thompson JD, Gibson TJ and Higgins DG (2003) Multiple sequence alignment using ClustalW and ClustalX. *Current protocols in bioinformatics*: 2.3. 1-2.3. 22

Todd J, Post-Beittenmiller D and Jaworski JG (1999) *KCS1* encodes a fatty acid elongase 3-ketoacyl-CoA synthase affecting wax biosynthesis in *Arabidopsis thaliana*. *The Plant Journal* **17**: 119-130

Trenkamp S, Martin W and Tietjen K (2004) Specific and differential inhibition of very-long-chain fatty acid elongases from *Arabidopsis thaliana* by different herbicides. *Proceedings of the National Academy of Sciences of the United States of America* **101**: 11903-11908

Trka A and Streibl M (1974) Mass spectra of long-chain aliphatic β -diketones and some of their derivatives. *Collection of Czechoslovak Chemical Communications* **39**: 468-474

Tsunewaki K and Ebana K (1999) Production of near-isogenic lines of common wheat for glaucousness and genetic basis of this trait clarified by their use. *Genes and Genetic Systems* **74**: 33-41

Tulloch A, Baum BR and Hoffman L (1980) A survey of epicuticular waxes among genera of Triticeae. 2. Chemistry. *Canadian Journal of Botany* **58**: 2602-2615

Tulloch AP and Hoffman LL (1976) Epicuticular wax of *Agropyron intermedium*. *Phytochemistry* **15**: 1145-1151

Vogg G, Fischer S, Leide J, Emmanuel E, Jetter R, Levy AA and Riederer M (2004) Tomato fruit cuticular waxes and their effects on transpiration barrier properties: functional characterization of a mutant deficient in a very-long-chain fatty acid β -ketoacyl-CoA synthase. *Journal of Experimental Biology* **55**

von Wettstein-Knowles P (2017) The polyketide components of waxes and the *Cer-cqu* gene cluster encoding a novel polyketide synthase, the β -diketone synthase, DKS. *Plants* **6**: 28

von Wettstein-Knowles P and Netting A (1976) Esterified alkan-1-ols and alkan-2-ols in barley epicuticular wax. *Lipids* **11**: 478-484

von Wettstein-Knowles P and Sogaard B (1980) The *cer-cqu* region in barley: Gene cluster or multifunctional gene. *Carlsberg Research Communications* **45**: 125

von Wettstein-Knowles P (2007) Analyses of barley spike mutant waxes identify alkenes, cyclopropanes and internally branched alkanes with dominating isomers at carbon 9. *The Plant Journal* **49**: 250-264

Waese J, Fan J, Pasha A, Yu H, Fucile G, Shi R, Cumming M, Kelley LA, Sternberg MJ, Krishnakumar V, et al. (2017) ePlant: visualizing and exploring multiple levels of data for hypothesis generation in plant biology. *The Plant Cell* **29**: 1806-1821

Wang A, Xia Q, Xie W, Dumonceaux T, Zou J, Datla R and Selvaraj G (2002) Male gametophyte development in bread wheat (*Triticum aestivum* L.): molecular, cellular, and

biochemical analyses of a sporophytic contribution to pollen wall ontogeny. *The Plant Journal* **30**: 613-623

Wang H, Klein MG, Zou H, Lane W, Snell G, Levin I, Li K and Sang BC (2015a) Crystal structure of human stearyl-coenzyme A desaturase in complex with substrate. *Nature structural and molecular biology* **22**: 581-585

Wang JJ, Zhang BR and Chen SL (2011) Oleaginous yeast *Yarrowia lipolytica* mutants with a disrupted fatty acyl-CoA synthetase gene accumulate saturated fatty acid. *Process Biochem* **46**

Wang M, Wang Y, Wu H, Xu J, Li T, Hegebarth D, Jetter R, Chen L and Wang Z (2016) Three *TaFAR* genes function in the biosynthesis of primary alcohols and the response to abiotic stresses in *Triticum aestivum*. *Scientific Reports* **6**: 1-14

Wang W, Zhang Y, Xu C, Ren J, Liu X, Black K, Gai X, Wang Q and Ren H (2015b) *Cucumber ECERIFERUM1 (CsCER1)*, which influences the cuticle properties and drought tolerance of cucumber, plays a key role in VLC alkanes biosynthesis. *Plant molecular biology* **87**: 219-233

Wang X, Guan Y, Zhang D, Dong X, Tian L and Qu LQ (2017) A β -ketoacyl-CoA synthase is involved in rice leaf cuticular wax synthesis and requires a CER2-LIKE protein as a cofactor. *Plant Physiology* **173**: 944-955

Wang Y, Wang J, Chai G, Li C, Hu Y, Chen X and Wang Z (2015c) Developmental changes in composition and morphology of cuticular waxes on leaves and spikes of glossy and glaucous wheat (*Triticum aestivum* L.). *PloS one* **10**: e0141239

Wang Y, Wang M, Sun Y, Hegebarth D, Li T, Jetter R and Wang Z (2015d) Molecular characterization of *TaFAR1* involved in primary alcohol biosynthesis of cuticular wax in hexaploid wheat. *Plant and Cell Physiology* **56**: 1944-1961

Wang Y, Wang M, Sun Y, Wang Y, Li T, Chai G, Jiang W, Shan L, Li C and Xiao E (2015e) FAR5, a fatty acyl-coenzyme A reductase, is involved in primary alcohol biosynthesis of the leaf blade cuticular wax in wheat (*Triticum aestivum* L.). *Journal of experimental botany* **66**: 1165-1178

Wang Z, Yeats T, Han H and Jetter R (2010) Cloning and characterization of oxidosqualene cyclases from *Kalanchoe daigremontiana*: enzymes catalyzing up to 10 rearrangement steps yielding friedelin and other triterpenoids. *Journal of Biological Chemistry* **285**: 29703-29712

Weidenbach D, Jansen M, Franke RB, Hensel G, Weissgerber W, Ulferts S, Jansen I, Schreiber L, Korzun V and Pontzen R, et al. (2014) Evolutionary conserved function of barley and Arabidopsis 3-KETOACYL-CoA SYNTHASES in providing wax signals for germination of powdery mildew fungi. *Plant physiology* **166**: 1621-1633

Wen M, Buschhaus C and Jetter R (2006) Nanotubules on plant surfaces: chemical composition of epicuticular wax crystals on needles of *Taxus baccata* L. *Phytochemistry* **67**: 1808-1817

Wilderman PR, Xu M, Jin Y, Coates RM and Peters RJ (2004) Identification of Syn-pimara-7, 15-diene synthase reveals functional clustering of terpene synthases involved in rice phytoalexin/allelochemical biosynthesis. *Plant physiology* **135**: 2098-2105

Winter D, Vinegar B, Nahal H, Ammar R, Wilson GV and Provart NJ (2007) An “Electronic Fluorescent Pictograph” browser for exploring and analyzing large-scale biological data sets. *PloS one* **2**: e718

Wollrab V (1968) Über Naturwachse VIII. Olefine und Paraffine aus den Wachsen einiger Pflanzen der Familie *Rosaceae*. *Collection of Czechoslovak Chemical Communications* **33**: 1584-1600

Xia YJ, Nicolau BJ and Schnable PS (1996) Cloning and characterization of *CER2*, an Arabidopsis gene that affects cuticular wax accumulation. *The Plant Cell* **8**: 1291-1304

Yang C, Zhao L, Zhang H, Yang Z, Wang H, Wen S, Zhang C, Rustgi S, von Wettstein D and Liu B (2014) Evolution of physiological responses to salt stress in hexaploid wheat. *Proceedings of the National Academy of Sciences* **111**: 11882-11887

Yang X, Wang Z, Feng T, Li J, Huang L, Yang B, Zhao H, Jenks MA, Yang P and Lü S (2018) Evolutionarily conserved function of the sacred lotus (*Nelumbo nucifera* Gaertn.) *CER2-LIKE* family in very-long-chain fatty acid elongation. *Planta* **248**: 715-727

Yang X, Zhao H, Kosma DK, Tomasi P, Dyer JM, Li R, Liu X, Wang Z, Parsons EP, Jenks MA and Lü S (2017) The acyl desaturase *CER17* is involved in producing wax unsaturated primary alcohols and cutin monomers. *Plant Physiology* **173**: 1109-1124

Yeats TH and Rose JKC (2013) The formation and function of plant cuticles. *Plant Physiology* **163**: 5-20

Yoo S-D, Cho Y-H and Sheen J (2007) Arabidopsis mesophyll protoplasts: a versatile cell system for transient gene expression analysis. *Nature protocols* **2**: 1565-1572

Yu G, Nguyen TT, Guo Y, Schauvinhold I, Auldrige ME, Bhuiyan N, Ben-Israel I, Iijima Y, Fridman E and Noel JP (2010) Enzymatic functions of wild tomato methylketone synthases 1 and 2. *Plant physiology* **154**: 67-77

Zampieri M, Ceglar A, Dentener F, Toreti A (2017) Wheat yield loss attributable to heat waves, drought and water excess at the global, national and subnational scales. *Environmental Research Letters* **12**: 064008

Zhang D, Beverly EJ, Levin NE, Vidal E, Matia Y, Feakins SJ (2021) Carbon isotopic composition of plant waxes, bulk organics and carbonates from soils of the Serengeti grasslands. *Geochimica et Cosmochimica Acta*

Zhang D, Yang H, Wang X, Qiu Y, Tian L, Qi X and Qu LQ (2020) Cytochrome P450 family member CYP96B5 hydroxylates alkanes to primary alcohols and is involved in rice leaf cuticular wax synthesis. *New Phytologist* **225**: 2094-2107

Zhang Z, Wang W and Li W (2013) Genetic interactions underlying the biosynthesis and inhibition of β -diketones in wheat and their impact on glaucousness and cuticle permeability. *PloS one* **8**: e54129

Zhang Z, Wei W, Zhu H, Challa GS, Bi C, Trick HN, Li W (2015) *W3* is a new wax locus that is essential for biosynthesis of β -diketone, development of glaucousness, and reduction of cuticle permeability in common wheat. *PloS one* **10**: e0140524

Zhao LF, Katavic V, Li FL, Haughn GW and Kunst L (2010) Insertional mutant analysis reveals that long-chain acyl-CoA synthetase 1 (*LACS1*), but not *LACS8*, functionally overlaps with *LACS9* in Arabidopsis seed oil biosynthesis. *The Plant Journal* **64**: 1048-1058

Zhou L, Ni E, Yang J, Zhou H, Liang H, Li J, Jiang D, Wang Z, Liu Z and Zhuang C (2013) Rice *OsGL1-6* is involved in leaf cuticular wax accumulation and drought resistance. *PloS one* **8**: e65139

Zhou Y, Ma Y, Zeng J, Duan L, Xue X, Wang H, Lin T, Liu Z, et al. (2016) Convergence and divergence of bitterness biosynthesis and regulation in *Cucurbitaceae*. *Nature Plants* **2**: 16183

Ziesack M, Rollins N, Shah A, Dusel B, Webster G, Silver PA and Way JC (2018) Chimeric fatty acyl-acyl carrier protein thioesterases provide mechanistic insight into enzyme specificity and expression. *Applied and environmental microbiology* **84**: e02868-02817